Doctoral Dissertations   Graduate School

8-2003

Shear and effective elongational rheology and polymer molecular characteristics

Xiaoling Wei

Follow this and additional works at: https://trace.tennessee.edu/utk_graddiss

Recommended Citation

To the Graduate Council:

I am submitting herewith a dissertation written by Xiaoling Wei entitled "Shear and effective elongational rheology and polymer molecular characteristics." I have examined the final electronic copy of this dissertation for form and content and recommend that it be accepted in partial fulfillment of the requirements for the degree of Doctor of Philosophy, with a major in Polymer Engineering.

John R. Collier, Major Professor

We have read this dissertation and recommend its acceptance:
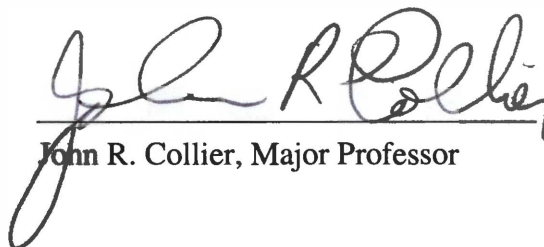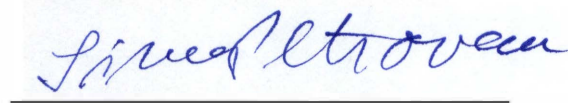
Accepted for the Council:

Carolyn R. Hodges

Vice Provost and Dean of the Graduate School

(Original signatures are on file with official student records.)

To the Graduate Council:

I am submitting herewith a dissertation written by Xiaoling Wei entitled "Shear and Effective Elongational Rheology and Polymer Molecular Characteristics." I have examined the final paper copy of this dissertation for form and content and recommend that it be accepted in partial fulfillment of the requirements for the degree of Doctor of Philosophy, with a major in Polymer Engineering.

_____
John R. Collier, Major Professor

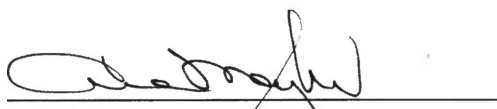We have read this dissertation
and recommend its acceptance:

_____
Billie J. Collier

_____
Joseph E. Sprunell

_____
Simioan Petrovan

Accepted for the Council:

_____
Vice Provost and Dean of
Graduate Studies

SHEAR AND EFFECTIVE ELONGATIONAL RHEOLOGY AND

POLYMER MOLECULAR CHARACTERISTICS

A Dissertation

Presented for the

Doctor of Philosophy

Degree

The University of Tennessee, Knoxville

Xiaoling Wei

August 2003

DEDICATION

This dissertation is dedicated to my parents, Chixuan Wei and Ying'e Wu, and my sister, Qiaoling Wei, and my brother, Zhaohui Wei, and my husband, Derong Gu, and the rest of the family, for always believing in me, inspiring me, and encouraging me to achieve my goals.

ACKNOWLEDGEMENTS

ABSTRACT

Extensional deformations play a significant role in many processing operations which involve a rapid change of shape such as fiber spinning, film blowing, blow molding, and nonwoven melt processing. To develop real time, on-line process and quality control analysis in these operations, knowledge of the molecular weight (MW) and molecular weight distribution (MWD), effects of molecular characteristics and processing conditions on the elongational rheology, and orientation of polymeric materials in these operations is essential.

In this work, shear rheology of six polyethylenes (PE), one polyisobutylene (PIB), and five cellulose solutions was measured at different temperatures using a rotational rheometer. Effective elongational viscosity of polyethylenes and polyisobutylene was also measured at different Hencky strains and temperatures using a capillary rheometer by replacing the capillary cylindrical die with a hyperbolic converging die. The hyperbolic shape of the dies establishes a purely elongational flow field at a constant elongational strain rate throughout the die.

The effect of molecular characteristics such as MW, MWD, and long chain branches and the processing conditions such as temperature and Hencky strain on the elongational rheology of PE and PIB samples was studied. The results from the hyperbolic dies were compared with results from other techniques, namely Rheometrics Extensional Rheometer (RER) and Elongational Rheometer for Melts (RME). Good master curves were generated for the temperature and Hencky strain shifting, and simultaneous shifting with respect to both temperature and Hencky

strain. The enthalpy and entropy changes were calculated from the effective elongational and shear viscosities to investigate flow induced orientation of the polymer melts in hyperbolic dies. The enthalpy and entropy changes increase in magnitude with higher elongational strain rate and higher Hencky strain. The storage and loss moduli were used to determine and test the three parameters needed to predict the MW and MWD.

TABLE OF CONTENTS

LIST OF TABLES

LIST OF FIGURES

xix

NOMENCLATURE AND ABBREVIATIONS

Nomenclature

a_H	Hencky strain shift factor
a_T	temperature shift factor
$\underline{b}$	internal body force
n	power-law exponent
$\underline{q}$	heat flux
r	radius of the flow channel
t	time
z	z direction (Ch. 2), axial flow direction (Ch. 3)
A	geometry-defined constant
B	geometry-defined constant
DP_w	weight-average degree of polymerization
$F(M,t)$	monodisperse relaxation function
$G(t)$	relaxation modulus
G'	storage modulus
G''	loss modulus
G_N^0, G_N	plateau modulus
$H(\lambda)$	relaxation spectrum
$\hat{H}$	enthalpy per unit mass
K_λ	front factor
L	centerline length of the die
M	molecular weight
M_n	number-average molecular weight
M_w	weight-average molecular weight
M_z	z-average molecular weight
P	pressure

R	universal constant
R^2	coefficient of determination
T	temperature
T_0	reference temperature
TR	effective Trouton ratio (Ch. 5)
T_R	Trouton ratio (Ch. 1)
$W(M)$	weight based MWD
α	relaxation time exponent
$\dot{\gamma}$	shear rate
ε_H, H	Hencky strain
ε_{H_0}, H_0	reference Hencky strain
$\dot{\varepsilon}$	elongational strain rate
$\dot{\varepsilon}_r$	reduced elongational strain rate
η, η_s	shear viscosity
η_0	zero-shear-rate viscosity
η_e	(uniaxial) elongational viscosity
η_{eb}	biaxial elongational viscosity
η_{eff}	effective (uniaxial) elongational viscosity
$(\eta_{eff})_r$	reduced effective (uniaxial) elongational viscosity
η_{ep}	planar elongational viscosity
η^*	complex viscosity
η_r^*	reduced complex viscosity
λ	time constant
$\lambda(M)$	characteristic relaxation time for the monodisperse system
$\underline{v}$	velocity vector
v_0	initial velocity
v_r	velocity component in r direction

v_x	velocity component in x direction
v_y	velocity component in y direction
v_z	velocity component in z direction
ρ	density
$\underline{\underline{\tau}}$	stress tensor
τ_{zz}	axial normal component of the stress tensor
τ_{rr}	transverse normal component of the stress tensor
Φ	potential function
Ψ	stream function
ω	angular frequency
ω_r	reduced angular frequency
ΔE_α	activation energy of flow
ΔH	enthalpy change
ΔG	Gibbs free energy
ΔP	pressure drop
ΔS	entropy change

Abbreviations

ACER	Advanced Capillary Extrusion Rheometer
ARES	Advanced Rheometric Expansion System
DP	degree of polymerization
DSC	differential scanning calorimetry
GPC	gel permeation chromatography
HDPE	high-density polyethylene
LCB	long chain branches
LDPE	low-density polyethylene
LLDPE	linear low-density polyethylene
MI	melt index

MW	molecular weight
MWD	molecular weight distribution
PE	polyethylene
PI	polydispersity index
PIB	polyisobutylene
RER	Rheometrics Extensional Rheometer
RME	Elongational Rheometer for Melts
UTK	University of Tennessee, Knoxville
VPI	Virginia Polytechnic Institute

Chapter 1

Introduction

§1.1 RHEOLOGY: SHEAR AND ELONGATION

Rheology can be defined as the science of the flow and deformation of materials as a result of an applied stress. In polymer processing operations, materials are subject to different modes of flow, among which shear flow and elongational flow (also called extensional flow) are two primary modes. Figure 1.1 illustrates the difference between shear deformation and elongational deformation. In shear flow, material particles on different streamlines are dislocated relative to each other. In elongational flow, the deformation of a material occurs along the streamline so that the distance between material planes that are perpendicular to the flow direction changes with time. In shear flow the velocity gradient is perpendicular to the flow direction, whereas in elongational flow the velocity gradient is parallel to the flow direction.

Elongational flow received scant attention until the mid 1960s, when the importance of elongational flows in polymer processing operations was realized. For example, in the film blowing process it is well established that bubble instability, melt extensibility, and film thickness uniformity are dictated by the elongational rheology behavior of the polymer melt (1). Very often in polymer processing the deformation of the melt before solidification is elongational, and this has a pronounced influence on the molecular orientation of the final product, in other words, the anisotropy of the end-use properties.

(a) Simple shear
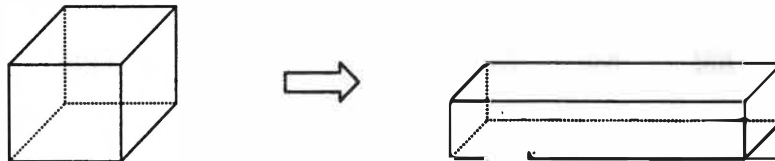
(b) Uniaxial elongational

Figure 1.1. Comparison of shear and elongational deformation: (a) Simple shear deformation; (b) Uniaxial elongational deformation.

Elongational flow is dominant when a rapid change of shape such as stretching is involved in the operation. Typical examples of elongational flow are fiber spinning, film blowing, extrusion through converging profiles, injection, and blow molding (2-4). The flow characteristics of such processes cannot be predicted on the basis of shear rheology alone. Knowledge of the elongational viscosity of the processing material and its variation with the strain rate is necessary.

Polymer melts show rheological properties such as complex shear viscosity behavior, elastic properties, normal stress phenomena, and tensile (elongational, or extensional) viscosity. Viscosity is the ratio of two quantities: stress and rate of strain. The concept of elongational viscosity was first introduced by Trouton (5) in 1906 in a study of pitch, tar, and similar substances descending under their own

4

weight. Later, Ballman (6) carried out elongational tests for rubbery polystyrene and found a constant elongational viscosity.

There were some problems with elongational experiments for polymer melts, i.e. the difficulty of conducting large strain and constant strain rate experiments; large gravitational effects on tension; the question of clamping the melt without necking. The work of Meissner (3, 7, 8) was pioneering in overcoming these problems. In his instrument, two pairs of toothed wheels used as rotating clamps at a constant distance from each other were used to homogeneously elongate the rodlike samples. Elongational viscosity has been measured for polymer melts using a variety of techniques, including extension, fiber spinning, and converging flow method.

For the last two decades, uniaxial elongational viscosity has been investigated for various homogeneous polymers such as high-density polyethylene (9), low-density polyethylene (10), linear low-density polyethylene (1, 11, 12), polypropylene (13, 14), polystyrene (15), and polybutylene-1 (16). In these polymers, the increase of the viscosity with time can be divided into two stages. In the first stage, which appears at small strain, the viscosity is independent of strain rate and increases slowly with time, until a critical time is reached. The viscosity data at various strain rates are superposed and almost coincide with the linear viscoelastic curve, i.e. the curve shows the elongational viscosity to be three times the shear viscosity at very low shear strain rate. In the second state, which appears at large strain, the viscosity depends on the strain rate. Beyond the critical time, the viscosity curves deviate from

5

the first state and rapidly increase. This behavior is called the strain hardening phenomenon.

The elongational properties of the resin are affected by a number of factors, such as temperature (17), miscibility and blend ratio in the case of polymer blends (18, 19), and molecular characteristics. More generally, molecular characteristics refer to molecular weight, molecular weight distribution, and degree of branching in the resin. A number of studies (1, 9-11, 13-15, 20-31) on the elongational flow of homogeneous polymer melts have been directed toward understanding the effect of polymer macromolecular characteristics. These studies have shown that the strain hardening phenomenon of homogeneous polymers is closely related to the long-time relaxation caused by the existence of the long chain branching or a small amount of extremely high molecular weight chains (32). The elongational viscosity reacts much more sensitively to high-molecular-weight components than does the shear viscosity. Whereas in the case of shear, correlations between rheological properties and molecular characteristics are well-established, only little is known in this aspect in the field of stretching flows, where the molecular characteristics of polymers influence their elongational properties in a complex way, partially due to the lack of reliable experimental equipment.

§1.2 ELONGATIONAL FLOW: THEORETICAL CONSIDERATION

Figure 1.2 shows three different types of elongational flow fields typically occurring in polymer processing operations, i.e. uniaxial, biaxial, and planar
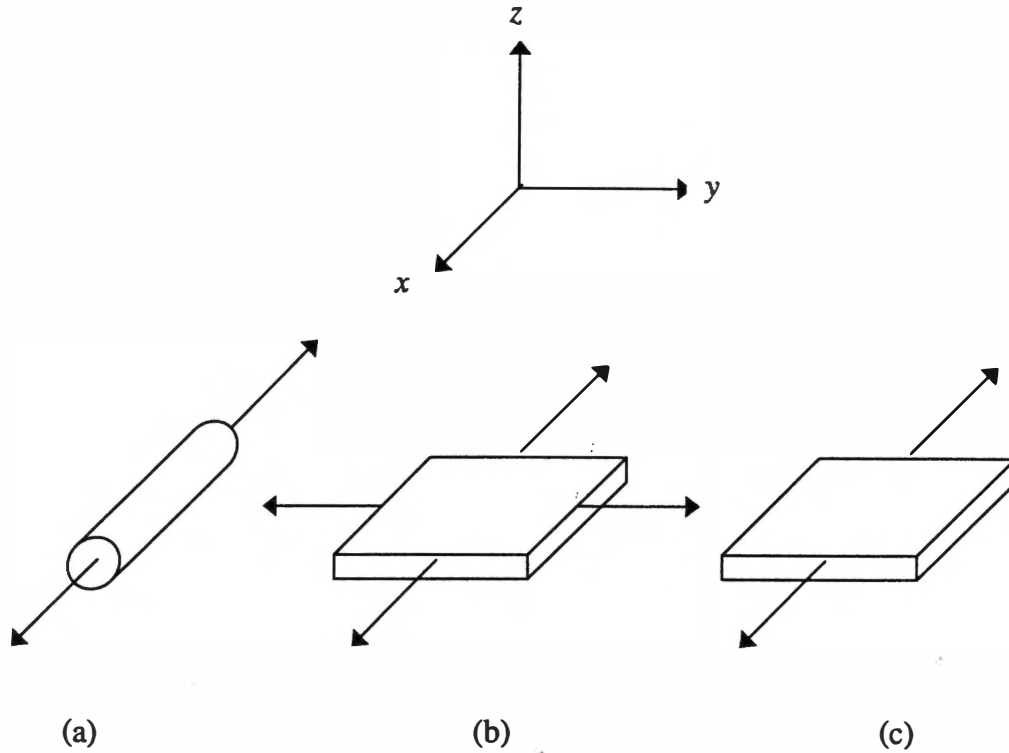
Figure 1.2. Three different types of elongational flow fields shown by the arrows: (a) Uniaxial; (b) Biaxial; (c) Planar.

extension. In the proposed work, attention is focused on the uniaxial elongational flow. The velocity field and stress field for these three different types of elongational flow are shown in Table 1.1, where $\dot{\varepsilon}$ is a constant elongational strain rate, v_x, v_y, and v_z are the velocity components in x, y, and z directions, respectively, η_e, η_{eb} and η_{ep} are the uniaxial, biaxial, and planar elongational viscosities, respectively. In general, the elongational viscosity is a function of the elongational strain rate $\dot{\varepsilon}$, just as the shear viscosity η is a function of shear rate $\dot{\gamma}$. The relationship between the uniaxial and biaxial elongational viscosities can be shown as follows (2)

$$\eta_{eb}(\dot{\varepsilon}) = 2\eta_e(-2\dot{\varepsilon}) \tag{1.1}$$

7

Table 1.1. Comparison of the three different types of elongational flow fields. [Source: H.A.Barnes, J.F.Hutton, and K.Walters. *An Introduction to Rheology*. Elsevier Science Publishers B.V., Amsterdam. 1989.]

Type of elongational flow	Velocity field	Stress field
Uniaxial extension	$v_x = \dot{\varepsilon}x, \quad v_y = -\dot{\varepsilon}y/2,$ $v_z = -\dot{\varepsilon}z/2$	$\sigma_{xx} - \sigma_{yy} = \sigma_{xx} - \sigma_{zz} = \dot{\varepsilon}\eta_e(\dot{\varepsilon}),$ $\sigma_{xy} = \sigma_{xz} = \sigma_{yz} = 0$
Biaxial extension	$v_x = \dot{\varepsilon}x, \quad v_y = \dot{\varepsilon}y,$ $v_z = -2\dot{\varepsilon}z$	$\sigma_{zz} - \sigma_{xx} = \sigma_{zz} - \sigma_{yy} = -\dot{\varepsilon}\eta_{eb}(\dot{\varepsilon}),$ $\sigma_{xy} = \sigma_{xz} = \sigma_{yz} = 0$
Planar extension	$v_x = \dot{\varepsilon}x, \quad v_y = 0,$ $v_z = -\dot{\varepsilon}z$	$\sigma_{xx} - \sigma_{zz} = \dot{\varepsilon}\eta_{ep}(\dot{\varepsilon}),$ $\sigma_{xy} = \sigma_{xz} = \sigma_{yz} = 0$

The uniaxial extension is equivalent to stretching a thin and narrow sheet of material in one direction, with a corresponding contraction in its thickness and in the width of the sheet or a fiber in the axial direction with a corresponding, volume conserving, reduction in radius. The biaxial extension is equivalent to stretching a thin sheet of material in two orthogonal directions simultaneously, with a corresponding decrease in the sheet thickness. The two-dimensional planar flow extension is equivalent to stretching a thin flat sheet of material in one direction only (the x direction), with a corresponding contraction in its thickness in the z direction, but with no change in the width of the sheet.

A fluid for which η_e increases with increasing $\dot{\varepsilon}$ is said to be tension thickening. If η_e decreases with increasing $\dot{\varepsilon}$, it is said to be tension thinning. Experimentally, the steady state implied in the velocity field and stress field is often

difficult to reach. Therefore, a transient elongational viscosity $\bar{\eta}_e(t, \dot{\varepsilon})$, which is a function of t and $\dot{\varepsilon}$, is defined. The transient elongational viscosity can still show the rheological properties of polymer melts.

For non-Newtonian fluids, the following limiting relations between elongational and shear viscosities are true (33, 34)

$$\eta_e(\dot{\varepsilon})\big|_{\dot{\varepsilon}\to 0} = 3\eta(\dot{\gamma})\big|_{\dot{\gamma}\to 0} \tag{1.2}$$

This relationship is valid for all values of $\dot{\varepsilon}$ and $\dot{\gamma}$ in the case of Newtonian fluids, obtained by Trouton (5) as early as 1906. Accordingly, rheologists have introduced the concept of the 'Trouton ratio' T_R defined as the ratio of the steady-state uniaxial extensional viscosity to the steady-state shear viscosity shown as follows

$$T_R = \frac{\eta_e(\dot{\varepsilon})}{\eta(\dot{\gamma})} \tag{1.3}$$

where $\dot{\gamma} = \dot{\varepsilon}$ or $\dot{\gamma} = \sqrt{3}\dot{\varepsilon}$ (2). The Trouton ratio for Newtonian liquids is equal to 3. Elastic liquids are noted for having high Trouton ratios.

§1.3 ELONGATIONAL RHEOLOGY OF LDPE AND LLDPE

Polyethylenes are largely crystalline with their chains in a zig-zag conformation. They are produced by different polymerization processes. Polyethylenes may be divided into three categories, high-density polyethylene (HDPE), low-density polyethylene (LDPE), and linear low-density polyethylene (LLDPE), where density represents the level of crystallinity. HDPE possesses largely linear chains with little branching or co-monomer while LDPE is long-chain

9

branched. LLDPE is low-density polyethylene with linear chains. In LDPE the crystallinity is disrupted by the occurrence of branching during polymerization. In LLDPE the crystallinity is disrupted by copolymerization of ethylene with small amounts of a second monomer such as butene-1, hexene-1, octene-1, or 4-methyl pentene-1. LDPE is generally used in film, molded products, and insulation. HDPE is mostly applied for blow-molded bottles, injection-molded products, and pipes (35).

The relationship between molecular characteristics and rheological properties particularly in elongation is a very complex one in the case of polyethylenes. The elongational flow, where elastic deformation is predominant, is more strongly influenced by long chain branches (20, 36) than shear deformation. LDPEs exhibit unique rheological properties, especially elongational rheology, compared with linear polyethylenes, such as HDPEs and LLDPEs, because of the presence of long chain branching in LDPE. For example, LDPE shows larger flow activation energy (20), and marked stronger strain hardening characteristics in elongational viscosity (30, 36-39) than that observed for LLDPE. Strain hardening increased with increasing branching. The elongational viscosity function of long chain branched LDPE melts and also of high molecular weight HDPE melts may show a pronounced maximum versus strain rate or tensile stress (20). Long chain branching as in LDPE is much more effective than molecular weight distribution in producing the pronounced maximum (20). The height of the maximum also increases with the degree of branching. Münstedt and Laun (22) found that for LDPEs the maximum of

10

the steady-state elongational viscosity increased if the molecular weight distribution was broadened by the addition of high molecular weight components. A variation of the weight-average molecular weight did shift the elongation viscosity curve but left its shape unchanged. For polystyrenes the molecular weight distribution is the determining quantity for the shape of the elongational viscosity curve (15). In the case of polyethylenes the degree of branching is an additional molecular parameter which can be expected to determine the shape of the elongational viscosity curve.

The LLDPE generally responds as linear chain polyethylenes and their behavior is directly comparable to the HDPE (23). Indeed their rheological properties are quite similar to HDPEs of about the same molecular weight distribution (23). It is well known that the poor processability of LLDPE in processes where elongation prevails over shear can be greatly improved by adding a small quantity of LDPE to the LLDPE. The poor performance of LLDPE is thought to be related to its lack of shear thinning whereas LDPE exhibits an onset of shear thinning at very low shear rates (12).

§1.4 MOTIVATION FOR THE PRESENTED WORK

Extensional deformations play a significant role in many processing operations. For example, fiber spinning, thermoforming, film blowing, blow molding, nonwoven melt processing, and foam production are all essentially extensional deformations. Flow in converging or diverging regions of dies and molds as well as flow at the moving front during mold filling may have large extensional

11

components. Extensional flows strongly orient polymer molecules and asymmetric particles, which has significant effects on the melt flow behavior and can be measured in terms of elongational viscosity and changes in entropy and enthalpy. Because of the orientation development, regions of extensional flow in a particular process may have a strong effect on the final product's mechanical and bulk properties such as resistance to stresses, toughness and degree of crystallinity. Knowledge of a polymeric material's elongational melt flow behavior is useful information in terms of selecting an adequate polymer grade for a particular application when expecting desired product properties. Moreover, the ability to quantitatively assess the forces that result in the orientation development opens the possibility for on-line process control with fast process parameter adjustments.

The uniqueness of a polymer is most frequently measured and expressed in terms of molecular weight, molecular weight distribution, degree of branching, and degree of crystallinity. Besides the knowledge of the dependence of the elongational behavior on external parameters like strain rate, strain, and temperature, it is necessary to get some insight into the relationship between elongational properties and molecular characteristics mentioned above if possible.

There are several different types of elongational rheometers for obtaining the elongational viscosity of polymer melts and solutions. As will be discussed in Chapter 2, most of the existing elongational rheometers measure the elongational viscosity of polymers just beyond their melting points. In addition, the measurements are done at elongational strain rates at least an order of magnitude lower than

processing strain rates. Previous research done by Collier and his research group (40-42) has shown that an essentially pure elongational flow of polymer melts can be generated using hyperbolic convergent dies in a capillary rheometer. An experimental technique for measuring elongational viscosity was developed (41-43) that can measure the elongational viscosity of polymer melts and solutions at processing strain rates and temperatures.

The knowledge of molecular weight (MW) and molecular weight distribution (MWD) is very important in selecting a proper polymer for a specific polymer processing operation. Currently, the most widely used method for the direct determination of MW and MWD is gel permeation chromatography (GPC). It is however, a time consuming and labor intensive method, with the accuracy of the results depending strongly on the skills and experience of the operator. It has long been realized that the linear viscoelastic rheological properties of polymer melts and concentrated solutions are strong functions of molecular weight and its distribution (44). It is in principle possible to invert that relationship and determine the MW and MWD by measuring the linear viscoelastic rheological properties of polymeric materials (45-48). Rheological measurements are quick, easy, and inexpensive thus providing an opportunity to develop real time, on-line process and quality control analysis of polymer properties in industrial equipments.

In this research, shear rheology of polyethylenes, polyisobutylene, and cellulose solutions was measured at different temperatures. Elongational viscosity of polyethylenes and polyisobutylene was measured at different Hencky strains and

13

temperatures. The objective is to study the effect of both molecular characteristics and processing conditions on the elongational rheology of the mentioned polymers. Methods to determine and test the parameters needed to predict the MW and MWD of polyethylene and cellulose (in dissolving pulp concentrated solution) samples from their shear rheological data are presented.

Chapter 2

Literature Review

§2.1 TECHNIQUES TO MEASURE ELONGATIONAL RHEOLOGY

Despite the obvious importance of elongational rheological data as an aid in polymer characterization, in production control, and as an excellent indicator for processability (49), it is shear viscosity to which is paid more attention compared with elongational viscosity. The main reason is that it is much easier to measure shear viscosity than to measure elongational viscosity.

Elongational viscosity is very difficult to assess. In order to obtain reliable elongational viscosity data, the following problems should be solved. First, pure elongational flow should be obtained. Only elongational flow with free boundaries is pure elongational flow. But without boundaries it is difficult to control the deformation. The flow in the tubes whose diameter changes or the entrance flow in abrupt convergence consists of shear flow and elongational flow because of the boundaries. In the meantime, it is difficult to measure the shear effects. Second, it is difficult to reach a steady state with a stable gradient of velocity. Another problem with elongational viscosity measurement is that large strains are difficult to reach. In shear flows, large strains can be achieved by going to long residence time since the streamlines are parallel. In extensional flows, the streamlines diverge (or converge) so that a sample must become very thin in at least one direction to achieve large strain. This becomes self-evident when it is realized that the Hencky strain of 7 in uniaxial extension corresponds to stretching the sample to 1100 times its original length.

Many different methods have been tried to solve these problems and measure the extensional viscosity. Extension, fiber spinning, and converging flow are among the most successful methods. The following is an informative review discussing the mode of operation, advantages, and limitations for each of these methods.

§2.1.1 Simple Extension

The simplest way to generate uniaxial extension is to grab a rod of fluid on each end and pull on it, as shown in Figure 2.1. The sample cross section is not necessarily circular. In order to attain a constant elongational strain rate in the sample, the length of the sample or the velocity of the sample end must increase exponentially with time (50).

A number of methods for holding the ends of the sample have been tried. One method is to bond the ends of the sample to a metal clip (translating clamp, or movable clamp, or end loading). Such instruments were originally applied for creep measurements only, as by Cogswell (4). The improvement and further development of the apparatus performed by Münstedt (51) now allows small samples to be extended not only with constant stress but also with constant strain rate to a
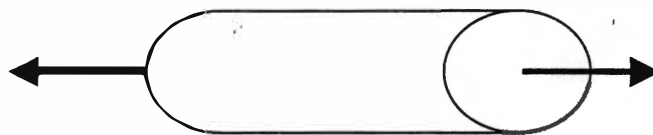
Figure 2.1. Schematic diagram of the simple extension method to generate an elongational flow.

18

maximum total Hencky strain of approximately 4. In the Cogswell-Münstedt-type instrument (51), cylindrically shaped samples, glued at their ends to metal pieces, are immersed in an oil of matched density and are vertically stretched at a constant tensile stress.

The rotating clamp, developed by Meissner (7) and further improved by Meissner and co-workers (3, 8, 21), is an alternate method for pulling samples. In Meissner's apparatus, two pairs of toothed wheels used as rotating clamps at a constant distance from each other are used to homogeneously elongate the rodlike samples. These wheels rotate with constant angular velocity. The molten samples are heated to the test temperature by floating on a silicon oil bath when they are stretched at a constant strain rate, as indicated in Figure 2.2 (2). The oil bath
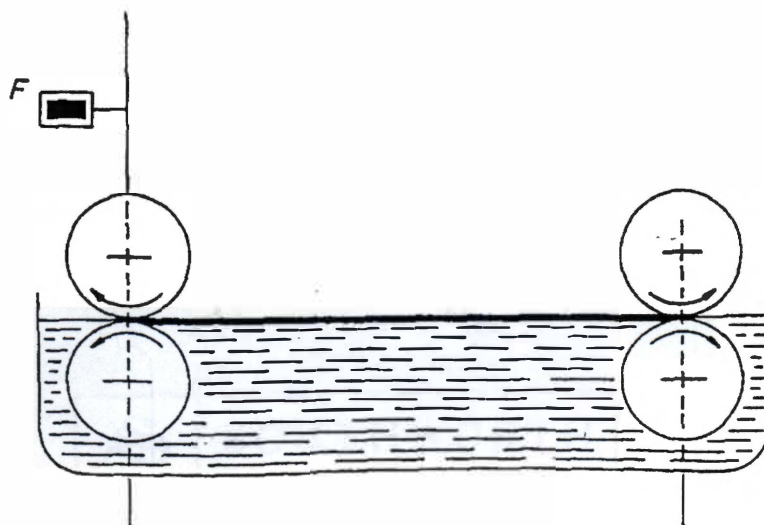
Figure 2.2. Schematic diagram of the Meissner's apparatus.
[Source: H.A.Barnes, J.F.Hutton, and K.Walters. *An Introduction to Rheology*. Elsevier Science Publishers B.V., Amsterdam. 1989.]

19

compensates for the inertia of the sample by buoyancy. The stress is measured by the deflection of a spring, associated with one pair of rollers. Using this method, Meissner (37) was able to reach Hencky strains up to 7 for a low-density polyethylene melt, where Hencky strain is the natural logarithm of area reduction during the elongation.

As mentioned above, the sample is pulled by two pairs of rotating clamps in Meissner's apparatus. A simpler alternative is to fix one end of the sample while the free end is pulled between rotating gears or wrapped around a rotating rod (9, 13, 50, 52, 53). One of these modified designs was made by Laun and Münstedt (53). Figure 2.3 (53) shows the schematic of the apparatus designed by Laun and Münstedt. The sample is stretched by only one pair of toothed wheels acting on one end of the rod. The other end of the sample is glued to a metal sheet (M) which is fastened to a hook

Figure 2.3. Schematic drawing of the simplified constant stretching apparatus designed by Laun and Münstedt.
[Source: H.M.Laun and H.Münstedt. *Rheologica Acta* **17**, 415 (1978).]

on the leaf spring (LS). According to the authors, the leaf spring and the use of a Linear Voltage Differential Transformer (LVDT) overcame some of the experimental difficulties caused by the combination of fo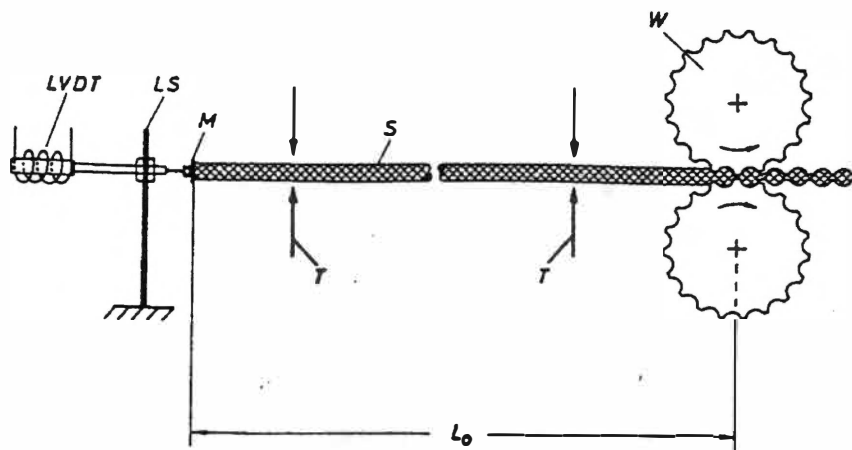rce measurement and drawing in Meissner's design. And the separation of the force measurement from the driving system considerably simplified the whole system and made possible the elongational viscosity measurement at strain rates smaller than 10^{-4} s^{-1}. It was also found that the homogeneity of sample deformation was still satisfied compared with the results of the experiments using two pairs of rotating clamps.

Using the Meissner-type device, elongational viscosity measurements have been performed on polyethylene (8, 20, 32, 36), blends of LDPE and linear low density polyethylene (LLDPE) (54, 55), polypropylene (13, 16), polybutene-1 (16), thermotropic liquid crystalline polymers (LCP) (56-58), talc-thermoplastic compounds (59), polystyrene (PS), and polymethylmethacrylate (PMMA) (60).

Comparing the rotating clamp with the translating clamp technique, it is much easier to achieve a constant extension rate with the rotating clamp than with the translating clamp. And the overall apparatus can be shorter for the rotating clamp. The polymer melt within the rotating clamps is continuously transported outside the basis length L_0 so that no necking zone usually develops in the sample near the clamp. On the contrary, necking of the sample occurs at the moving clamps. Other advantages of using rotary clamps are that a very homogeneous deformation and very large total strain can be obtained. Disadvantages of rotating clamps relative to translating clamps are that tests other than constant rate are more difficult and

21

longer samples are required. Another problem with rotating clamps is slip at the clamp surface.

The major advantage of the extension method is that the flow is homogeneous. There are some limitations with this method, for example, temperature gradients, low strain rate, density mismatch with surrounding fluid, uptake of buoyancy fluid, surface tension at low strain rate, end effects which include necking at the bonded clamp for moving clamps or slip for rotating clamps, and sample inhomogeneity. In summary, the major problems are buoyancy, clamping, and sample preparation (50). The extension method is restricted to high-viscosity materials and generally near the melting point of the materials.

§2.1.2 Fiber Spinning

With lower viscosity liquids, $\eta < 10^3$ Pa·s, it is impossible to grab and pull such fluids as is done with the melts in the extension method (50). Gravity, surface tension, and air drag all work against the desired extensional flow (50). Fiber spinning is one of the approximate extensional methods for lower viscosity samples.

Figure 2.4 (2) shows the basic features of this fiber spinning method. The sample is continuously extruded from a reservoir and stretched by a rotating wheel or vacuum suction. It is self-evident that fiber spinning involves a significant elongational flow component. It is relatively easy to perform, the general kinematics can be determined with relative ease, and a suitable stress variable can be obtained from force measurement on the reservoir or the take-up device (61-63). The fiber
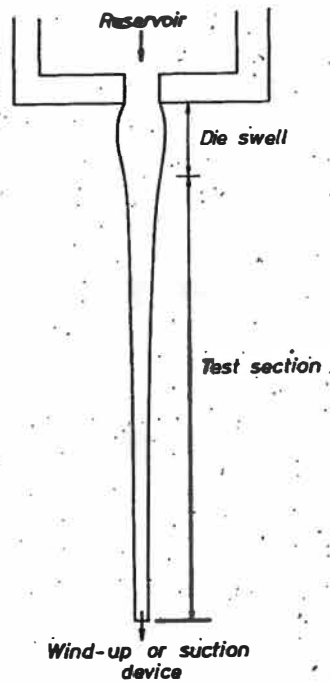
22

Figure 2.4. Schematic diagram of the spin-line rheometer.
[Source: H.A.Barnes, J.F.Hutton, and K.Walters. *An Introduction to Rheology*. Elsevier Science Publishers B.V., Amsterdam. 1989.]

diameter is measured as a function of distance along the fiber, either photographically or by a video camera. The extension rate can be determined from measurements of fiber diameter and flow rate. At the same time, it is extremely difficult to interpret the data unambiguously in terms of the elongational viscosity. Although the velocity at a fixed distance down the threadline does not vary with time, the strain rate experienced by a given fluid element will generally change as it moves along the threadline (2). Also, a change of conditions in the spinneret can significantly affect the response along the threadline.

The spinning technique can be used for polymer melts (20) and for low viscosity fluids (62). The major problem associated with this method is that typically the strain rate is not constant. For this reason, the fiber spinning method is not a true rheometer, but gives only an apparent uniaxial extensional viscosity. Other disadvantages include effect of shear history in feed die, extrudate swell, unstable flow, solvent evaporation, nonisothermal flow for polymer melts, and uncertainty in diameter due to vibration. Strain is not usually constant. Gravity can be significant for low viscosity fluids.

§2.1.3 Converging Flow

As the fluid flows from a large cross section tube into a small cross section tube, the streamlines converge, shown in Figure 2.5 (50). The fluid dissipates extra energy, which is expressed as the entrance pressure drop, to overcome this reduction
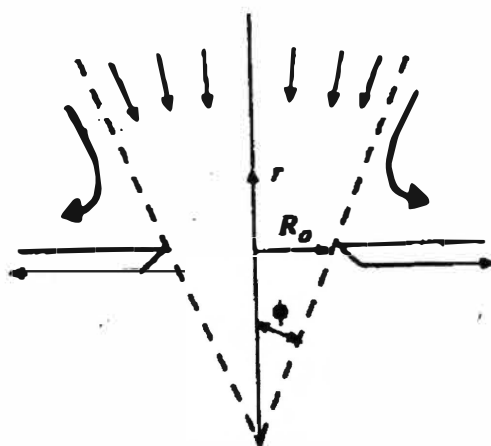

Figure 2.5. Streamlines showing the entrance flow into an orifice.
[Source: C.W.Macosko. *Rheology: Principles, Measurements, and Applications*. VCH Publishers, Inc., New York. 1994.]

24

in the cross-sectional area and continue to flow. The existence of the extensional flow is indicated by the converging streamlines. However, a shear component is imparted to the flow because of the walls along the contraction. Everage and Ballman (52) and Winter *et al.* (64) attempted to minimize the shear component by lubricating the tube walls. Several different analyses have been developed to estimate the extensional viscosity from the entrance pressure drop measurements. The three major approaches are sink flow analysis by Metzner and Metzner (65), Cogswell's analysis (66, 67), and Binding's analysis (68).

In the sink flow analysis, Metzner and Metzner (65) assumed a purely extensional flow in which the shear components are negligible. For an axisymmetric contraction, the flow into the orifice is analogous to a point sink. For a planar contraction flow, the analogy is with a line sink (69).

Cogswell (66, 67) proposed that the converging flow field could be interpreted as an extensional deformation superposed onto a simple shear flow. The shearing component and the extensional component can be treated separately and added to give the total flow. With the knowledge of shear viscosity data, Cogswell's equations result in a very convenient way for quickly ranking fluids by simply measuring the pressure drop and volume flow rate.

Binding's analysis (68) is based on the assumption that the flow field is the one of least resistance; it includes both shear and extension in its formulation. By applying variational principles to minimize the overall energy consumption, the extensional viscosity is calculated as a function of the entrance pressure drop, the

25

power law parameters of the shear and extensional viscosities, shear rate, and the contraction ratio. The result of Binding's analysis is a more comprehensive analysis that relates the entry pressure and flow rate to the elongational flow properties for a converging flow field. Tremblay (70) compared sink flow analysis, Cogswell's analysis, and Binding's analysis for polyethylene melts. He found that for LLDPE the sink flow and Binding predictions were reasonably close, while the Cogswell prediction was considerably larger in magnitude.

The converging flow is an indirect method for the measurement of elongational viscosity of polymer melts. It can overcome the difficulties and the limitations of the direct measurement method such as temperature control and clamp design in the simple extension. The major advantage of the converging flow is that it is the easiest extensional flow to generate and measure because it primarily involves forcing the fluid through an orifice and measuring the pressure drop. It can be especially useful in quickly ranking the extensional effects. It can also cover a wide range of viscosity and flow rates. The limitation of this method is that there remains the question of interpretation since it is a complex flow.

§2.1.4 Other Techniques

Many other techniques have been suggested for studying the elongational behavior of polymeric liquids and solutions. These include compression and stagnation flow (71-74). The compression method, like extension, can give homogeneous, purely extensional deformations. They do not result in the same

26

material functions since the normal stress difference needed to generate uniaxial compression is not merely the negative of the stresses needed to generate unaxial extension (50). Extension and compression methods have only been used successfully with higher viscosity samples since the edges of a sample should be held during experiment. The stagnation flow, like fiber spinning and converging flow, is used with lower viscosity liquids (50). Impinging two liquid streams can generate a stagnation flow, which can create steady extensional deformations. This flow is not homogeneous. A material element near the central part of the flow will experience much higher strain than one further out. The opposed-nozzle technique (71-73) in which a stagnation flow is created is relatively new and is applicable for the measurement of elongational viscosity of low viscosity polymer melts and dilute solutions.

As discussed in Chapter 1 the elongational viscosity of polymers is affected by the molecular characteristics of the resin and the processing conditions. The magnitude of the elongational viscosity strongly affects its processing behavior. As concluded from the above literature review, there is a need for a technique to characterize the elongational flow behavior of both polymer melts and solutions at temperatures and elongational strain rates typically used in industrial polymer processing operations. Previous research in this group has resulted in the development of a rheometer that can achieve these objectives. The theoretical background of this work will be briefly discussed in Chapter 3. The experimental details of this technique will be discussed in Chapter 4. One objective of this work is

to study the effect of molecular characteristics and processing conditions on the elongational rheology of polymer melts measured by hyperbolic convergent dies. A set of PE resins and one PIB samples are studied in this work. The experimental results of the elongational viscosity measurements of these polymers will be discussed in Chapter 5.

The other objective of this work is to study the feasibility of using the rheological method to determine the molecular weight and molecular weight distribution. In the next section, methods to determine the molecular weight and molecular weight distribution will be reviewed.

§2.2 METHODS TO DETERMINE MOLECULAR WEIGHT AND MOLECULAR WEIGHT DISTRIBUTION

Molecular weight (MW) is one of the most important properties of a molecule. It can be used to distinguish different molecule species. A polymeric molecule is a large molecule built up by the repetition of small, simple structural or monomeric units. It is also called macromolecule because of its high molecular weight. The molecular weights of polymers are also characterized by their molecular weight distributions (MWD), since molecular chains of polymers consist of different number of monomeric units after polymerization.

The MW and MWD of polymer materials have a considerable effect on their properties, such as melting point, heat capacity, yield stress (75), adherence, toughness, brittleness, tensile strength, environmental stress-crack resistance, fatigue

resistance, gas permeability, and processibility, etc. The MW and MWD are also important for polymer processing (76) such as extrusion, fiber spinning and melt blowing.

It is much more difficult to measure the molecular weights of polymers, as compared to low molecular weight compounds because the molecular weights are much larger. Furthermore, the distribution of molecular weights must also be considered. Therefore, average molecular weights and some other measures of distribution should be used to describe the molecular weights of polymers. There are a number of ways to define an average molecular weight. The most common two are number-average molecular weight, M_n, and weight-average molecular weight, M_w. Assuming that M_i and N_i are the molecular weight and number of moles of chain length of i, respectively, $M_n = \sum M_i N_i / \sum N_i$ and $M_w = \sum M_i^2 N_i / \sum M_i N_i$. Polydispersity index ($PI = M_w / M_n$) can be conveniently used to describe the breadth or dispersion of the molecular weight distribution or the polydispersity of polymers.

There are a number of techniques for experimentally determining the number-average molecular weights of polymers, such as end-group analysis through chemical methods, or physical methods such as infrared vibrational spectroscopy, and NMR spectroscopy, boiling point elevation (ebulliometry), vapor pressure osmometry (VPO), and freezing point depression (cryoscopy), while light scattering

(low-angle laser light-scattering LALLS), ultracentrifugation, etc., measure the weight-average molecular weight.

The solution viscosity method is the most simple and convenient method to measure MW of polymeric material. But it is not an absolute method. In polydisperse systems, the solution viscosity method does not give the simple average molecular weight such as M_n and M_w. Instead, it gives a viscosity-average molecular weight.

Gel permeation chromatography (GPC) or size exclusion chromatography, is, in fact, a new form of liquid chromatography (77). The polymer solution is injected into a continuous stream of solvent that is passing through gel particles in a column. Polymer molecules diffuse into the pores, are eluted, and pass out of the column as more of the solvent passes through the system. The larger molecules are eluted first and the smallest ones last. The advantages of this method are: simple manipulation, short time period, reliable data, and good reproducibility (78). So, GPC became a breakthrough in determining molecular weight and molecular weight distribution. It is one of the most popular techniques for MWD determination. It can be widely used in biochemistry, polymer chemistry, and organic chemistry. If appropriate liquid-solid elution columns are used, it is possible to determine molecular weights ranging from 2 to 100 million (79).

GPC is not an absolute method to determine molecular weight because it uses a calibration curve to convert experimental data into molecular weight. Each chromatography column should be calibrated with monodisperse standards of the same composition as that of the polymers under investigation. If the Mark-Houwink

30

parameters for the polymers are known, universal calibration curve can be used. But possibly universal calibration will produce erroneous results. However, if a low-angle laser light-scattering detector, which can determine the absolute molecular weights, is used together with GPC, absolute molecular weights can be achieved without any standards for calibration or Mark-Houwink parameters. Many references (80-85) are dealing with the determination of molecular weight and molecular weight distribution using GPC-LALLS technique.

There are some disadvantages in applying this method. It takes a long time and exchanging the columns to use different solvents is difficult. Solvents are used. The rheological technique shows many advantages in determining MW and MWD.

It has been long realized that the viscoelastic rheological properties of polymer melts and concentrated solutions are related to molecular motions (86, 87) and are very sensitive to molecular weight (44), especially the high end tail of the molecular weight distribution. Therefore, rheological data can be used to measure the molecular weight and its distribution (45-48).

There has been a considerable amount of work reported on relating the rheology of molten polymers to MW and MWD. Recent reviews on the subject have been offered by Pearson (88), Tuminello (89), Shaw and Tuminello (90), and Mead (91). Zeichner and Macosko (92) succeeded in correlating the polydispersity ratios with the crossover point of the dynamic moduli curves for the terminal relaxation zone. The sensitivity of dynamic measurements to changes in polydispersity ratio and MW was documented by Mobil (93). Ninomiya and Fujita (94) first attempted to

31

calculate the MWD from rheological data. Then, Menefee and Peticolas (46, 95, 96) developed an expression relating the MWD to the stress relaxation modulus, assuming that the melt chains obey Rouse dynamics. Bersted (47) derived a method to determine MWD from viscosity curves. Wu (97) determined MW and MWD from the storage modulus $G'(\omega)$ using approximations derived from the description of chain dynamics by the Doi-Edwards constitutive model (98), which is based on the tube and reptation concept of de Gennes (99). Tuminello (100) developed a method for determining MWD using the dynamic elastic modulus (G') and plateau modulus (G_N^0). This technique has been successfully used on polystyrene (101), poly (tetrafluorethylene) and its copolymers (102-104). Mead (91) inverted des Cloizaux's double reptation mixing rule (105-107), which has achieved considerable success in modeling polydisperse systems, to obtain the MW and MWD. Braun, Eckstein, Fuchs and Friedrich (108) compared different rheological methods using different rheological properties related to molecular weight.

There are many advantages in applying the rheological methods over traditional techniques for determining molecular weight. First, "the sensitivity of the rheological method is such that materials with ostensibly identical GPC traces can show markedly different rheological properties" (91). The molecular weight scaling and sensitivity of various methods of discriminating linear flexible polymers on the basis of molecular weight are shown in Table 2.1 (91). Second, the rheological

32

Table 2.1. Molecular weight scaling of various methods of discriminating linear flexible polymers on the basis of molecular weight. Sensitivity is defined as the derivative of the measurable property with respect to molecular weight.
[Source: D.W.Mead. *Journal of Rheology* **38**, 1797 (1994).]

Method	Discrimination scaling	Sensitivity scaling	Comments
GPC	$M^{1/2}$	$M^{-1/2}$	Size exclusion, insensitive to high MW
Intrinsic viscosity	$M^{0.6}$	$M^{-0.4}$	Hydrodynamic size method, insensitive to high MW
Light scattering	M^1	M^0	Good sensitivity to high MW
Osmotic pressure	M^{-1}	M^{-2}	Good indicator of *number-average* MW for low MW polymers
Zero shear viscosity	$M^{3.4}$	$M^{2.4}$	Principally a function of the *weight-average* MW for systems with similarly shaped distributions
Recoverable compliance	$(M_z/M_w)^{-3.5}$	---	Indicative of the *dispersion* in the MWD. Insensitive to the absolute value of MW

method is applicable to insoluble polymers such as fluoropolymers, melt anisotropic (rigid-rod) polymers, and polyimides as well as soluble polymers, while traditional methods such as light scattering, osmometry, and gel permeation chromatography require that the polymer is soluble in a suitable solvent. Third, the rheological method is a technique which can be used to develop on-line process and quality control analysis in polymer processing operations. Fourth, the rheological method is more economical due to a small sample use, and low cost for its simple operation.

Besides many fundamental contributions in the literature, numerical methods have been developed to calculate the MW and MWD from rheological data. Some commercial software programs have been developed and applied, such as Polysoft (109, 110) by Haake, and ^{RSI}Orchestrator^{TM} by Rheometric Scientific^{TM} (now TA Instruments) in which two functions are used to calculate MW and MWD: "Synthesize Molecular Weight Function" and "Calculate Molecular Weight Distribution Function". One advantage of the former over the latter is that it does not require a master curve that covers the range of viscoelasticity from the rubbery region all the way down into the terminal region (111).

The normal GPC technique is not sufficient for a clear characterization of cellulose in the N-methyl-morpholine oxide monohydrate (NMMO·H_2O). The flow of the NMMO cellulose solution is strongly influenced by the existence of high molecular cellulose fractions (112). When heated, the cellulose solutions in NMMO·H_2O are subject to the same rules as those of the viscoelastic polymer melts

34

(112, 113). The MW and MWD of cellulose from dissolving pulps concentrated solutions can be determined by rheological data.

It can be concluded from the above discussion the linear viscoelastic rheological properties of polymer melts and concentrated solutions are strong functions of molecular weight and its distribution (44). It is in principle possible to invert that relationship and determine the MW and MWD by measuring the linear viscoelastic rheological properties of polymeric materials (45-48). Rheological measurements are quick, easy, friendly, and inexpensive, thus providing an opportunity to develop real time, on-line process and quality control analysis in polymer processing operations. The determination and test of the parameters needed to predict the MW and MWD of polyethylene and cellulose (in dissolving pulp concentrated solution) samples from their shear rheological data will be presented in Chapter 5.

Chapter 3

Theoretical Background for Data Acquisition

§3.1   PREVIOUS RESEARCH

§3.2   THEORETICAL BASIS FOR THE EFFECTIVE
        ELONGATIONAL VISCOSITY

§3.1 PREVIOUS RESEARCH

In prior studies accomplished by this research group, a unique technique for characterizing the elongational rheology of polymer melts at processing strain rates was developed (40, 42). It was demonstrated that use of lubricated skin/core flow and a hyperbolic shaped converging die resulted in essentially pure elongational flow at a constant elongational strain rate in the core layer. The viscosity ratio of the core polymer used was at least 100 times that of the skin and the converging flow channel must have a specific hyperbolic shape. The high viscosity ratio (core-to-skin) caused the skin layer to act as a lubricating layer. A Dowex low-density polyethylene was used as the skin and a Marlex polypropylene was used as the core. A series of skin/core layered flows were first modeled: power-law rectangular channel shearing flow; Newtonian fluid converging channel elongational flow; and power-law fluid converging channel elongational flow. Experimental measurements using tracer particles and an image analysis then confirmed the predicted behavior and demonstrated the ability to achieve essentially pure elongational flow at a constant elongational strain rate in the core layer. The constant elongational strain rate was controlled by the volumetric flow rate and the die geometry.

One of the limitations of this technique was that appropriate lubricant or skin had to be chosen (42). In attempting to develop a correction factor for skinless measurements, Collier *et al.* (41) showed that the apparent orientation effect of the melt dominated the flow so strongly that shearing gradients near the wall were

39

insignificant, eliminating the need for the lubrication to achieve an essentially pure elongational flow. Elongational rheology of polymer melts and solutions may be measured using a nonlubricated flow through a hyperbolic converging die. Elongational strain rates up to 733 s^{-1} have been achieved using hyperbolic dies which have Hencky strains up to 7. This strain rate range includes the processing rates encountered in typical industrial processes (41, 114).

§3.2 THEORETICAL BASIS FOR THE EFFECTIVE ELONGATIONAL VISCOSITY

The theoretical foundation for the hyperbolic die technique to characterize the elongational rheology of polymer melts and solutions was established previously in this group (41). In order to provide the reader a better understanding of those concepts underlying the data acquisition, the theoretical development is sketched out here.

Hyperbolic convergent dies were designed for the melt or solution to generate a constant elongational strain rate throughout the core. This is accomplished by describing the flow channel surface area with the equation $r^2(z) = A/(z+B)$, where z is the axial flow direction, r is the radius of the flow channel, A and B are geometry-defined constants. Four hyperbolic dies used in this research had Hencky strain, ε_H, of 4, 5, 6, and 7. The Hencky strain is defined as the natural logarithm of the ratio of die entrance area to exit area. The flow channel surfaces of these four dies are shown in Figure 3.1. A sketch of a die appears in Figure 3.2 (42).

40
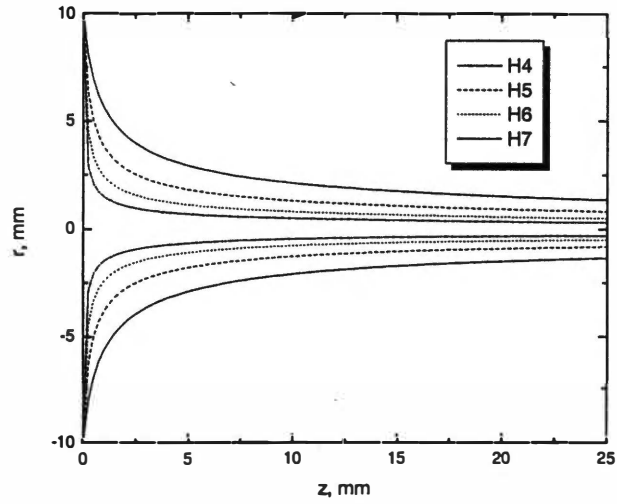
Figure 3.1. Flow channel surfaces of four hyperbolic convergent dies with Hencky strains of 4, 5, 6, and 7.
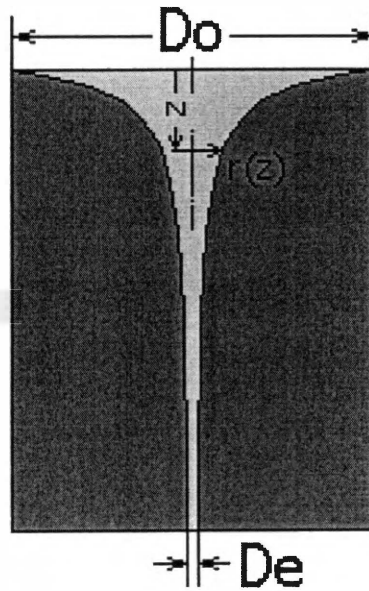
Figure 3.2. Schematic diagram of a hyperbolic convergent die.
[Source: J.R.Collier. *Lubricated Flow Elongational Rheometer*. [5,357,784]. 1994. U.S. Ref Type: Patent.]

When the melt flows through the hyperbolic channel, it assumes the interface between the polymer melt or solution and the die wall may be viewed as a set of streamlines experiencing the same conditions. These streamlines can be described by the stream function, Ψ, which is defined to satisfy the continuity equation. The potential function, Φ, which is related to velocity components in shear free flows, must be orthogonal to Ψ and satisfy the irrotationality equation. In shear free flows, constant values of the potential function should define constant pressure surfaces. For the axisymmetric die geometry cylindrical coordinates seem most appropriate, for which the stream function is defined as

$$\Psi = -\frac{\dot{\varepsilon}}{2}r^2 z \tag{3.1}$$

and the potential function is given as

$$\Phi = \dot{\varepsilon}\left(\frac{r^2}{4} - \frac{z^2}{2}\right) \tag{3.2}$$

The pressure, P, is directly proportional to $\rho\dot{\varepsilon}\Phi$, where $\dot{\varepsilon}$ is the elongational strain rate, and ρ is density. The velocity components are

$$v_z = -\frac{1}{r}\frac{\partial\Psi}{\partial r} = -\frac{\partial\Phi}{\partial z} = \dot{\varepsilon}z \tag{3.3}$$

$$v_r = \frac{1}{r}\frac{\partial\Psi}{\partial z} = -\frac{\partial\Phi}{\partial r} = -\frac{\dot{\varepsilon}}{2}r \tag{3.4}$$

and the non-zero velocity gradients are

$$\frac{\partial v_z}{\partial z} = \dot{\varepsilon}, \quad \frac{1}{r}\frac{\partial(rv_r)}{\partial r} = -\dot{\varepsilon}, \quad \frac{\partial v_r}{\partial r} = -\frac{\dot{\varepsilon}}{2} \tag{3.5}$$

42

The basic equations describing the flow are the equation of continuity (conservation of mass), conservation of momentum, conservation of energy, expressed in terms of enthalpy per unit mass, $\hat{H}$, and the irrotationality equation for the potential flow. Mass, momentum and energy balances are conserved separately.

Mass balance

$$\frac{D\rho}{Dt} = -\rho(\underline{\nabla} \cdot \underline{v})$$ (3.6)

Momentum balance

$$\rho\frac{D}{Dt}\underline{v} = -(\underline{\nabla}P) + [\underline{\nabla} \cdot \underline{\underline{\tau}}] + \rho\underline{b}$$ (3.7)

Energy balance

$$\rho\frac{D\hat{H}}{Dt} = -(\underline{\nabla} \cdot \underline{q}) + (\underline{\underline{\tau}} : \underline{\nabla v}) + \frac{DP}{Dt}$$ (3.8)

Irrotationality equation

$$\underline{\nabla} \times \underline{v} = 0$$ (3.9)

where $\underline{\underline{\tau}}$ is the second-order stress tensor, $\underline{q}$ is the heat flux, $\underline{v}$ is the velocity vector, and $\underline{b}$ is an internal body force term that represents the force necessary for orientation development of the polymer melt.

As mentioned earlier, the hyperbolic shape is one that provides a constant elongational strain rate. The flow is therefore at constant acceleration as shown by the velocity gradient equations. Because of the constant elongational strain rate and strong dominance of the orientation development, the flow through the

43

hyperbolically converging die is expected to be essentially purely elongational. The only velocity gradients are in the flow and transverse directions; hence, the only non-zero components of the deformation rate tensor are the normal components.

Besides what has been mentioned up to this point, the basic assumptions and the related implications in the theoretical development are as follows:

1. The strain rate state determines the stress state; i.e., the flow is homogeneous. The die geometry dictates that in the essentially shear free flow region the only non-zero deformation rate components are the normal components and these components are not a function of position; therefore, the only non-zero stress components are the normal components, and the stress components are not a function of position. Namely, the axial and transverse normal components of the stress tensor, τ_{zz} and τ_{rr}, are constant. Their values depend on the strain rate. Therefore, $\underline{\nabla} \cdot \underline{\underline{\tau}} = 0$.

2. The fluid is incompressible; therefore, $\underline{\nabla} \cdot \underline{v} = 0$.

3. The system is isothermal; therefore, $\underline{\nabla} \cdot \underline{q} = 0$.

4. The inertial terms are negligible; therefore, $\underline{v} \cdot \underline{\nabla} \cdot \underline{v} = 0$, and $\underline{\nabla} \left(\dfrac{v_z}{2} \right) = 0$.

5. The flow is steady; therefore, $\dfrac{\partial}{\partial t} = 0$.

Using the above assumptions and implications 1 and 5, the solution to momentum balance reveals that the pressure gradient, $\underline{\nabla} P$, is equal to the body force term. Furthermore, since

44

$$v_z = \dot{\varepsilon} z \tag{3.10}$$

and

$$\varepsilon_H = \ln\left(\frac{r_0^2}{r_e^2}\right) \tag{3.11}$$

The energy balance can be integrated from the entrance to exit. Therefore, the stress component in cylindrical coordinates is

$$\tau_{zz} = \frac{2}{3}\frac{\Delta P}{\varepsilon_H} + \frac{2}{3}\frac{\rho\Delta\hat{H}}{\varepsilon_H} = \frac{2}{3}\frac{\Delta P}{\varepsilon_H} + \frac{2}{3}\frac{\Delta H}{\varepsilon_H} \tag{3.12}$$

where ΔP is defined as entrance minus exit pressure and ΔH is defined as exit minus entrance enthalpy per unit volume. The elongational viscosity, η_e, in cylindrical coordinates is defined and results in this geometry as follows:

$$\eta_e = \frac{\tau_{zz} - \tau_{rr}}{\dot{\varepsilon}} = \frac{3}{2}\frac{\tau_{zz}}{\dot{\varepsilon}} \tag{3.13}$$

Therefore, the elongational viscosity is

$$\eta_e = \frac{\Delta P}{\dot{\varepsilon}\varepsilon_H} + \frac{\rho\Delta\hat{H}}{\dot{\varepsilon}\varepsilon_H} = \frac{\Delta P}{\dot{\varepsilon}\varepsilon_H} + \frac{\Delta H}{\dot{\varepsilon}\varepsilon_H} \tag{3.14}$$

The enthalpy term represents either a real or apparent phase change that may be induced by the imposed orientation on the polymer melt or solution. Therefore, an effective elongational viscosity is defined and is related to η_e as follows:

$$\eta_{eff} \equiv \frac{\Delta P}{\dot{\varepsilon}\varepsilon_H} \tag{3.15}$$

and

45

$$\eta_e = \eta_{eff} + \frac{\Delta H}{\dot{\varepsilon}\varepsilon_H} \qquad (3.16)$$

This definition of effective elongational viscosity assumes that any enthalpy change is included in this. The elongational strain rate is defined as

$$\dot{\varepsilon} = (v_0/L)(\exp \varepsilon_H - 1) \qquad (3.17)$$

where ε_H is the Hencky strain as defined previously, L is the centerline length of the die, and v_0 is the initial velocity.

The enthalpy change associated with the orientation development in the melt can be estimated as follows. Making the assumption that the non-Newtonian character of the melt in excess of that reflected in the shear viscosity, η_s, at an equal value of shear rate is due to the resistance towards orientation, the actual Trouton ratio would be $\eta_e / \eta_s = 3$. Hence,

$$\Delta H = -\dot{\varepsilon}\varepsilon_H \left(\eta_{eff} - 3\eta_s \right) \qquad (3.18)$$

The entropy change, ΔS, is an indicator as to what extent orientation develops. It can be determined using $\Delta G = \Delta H - T\Delta S$, where ΔG is the Gibbs free energy and T is the absolute temperature. Assuming that ΔG is due to the flow-induced orientation and the flow reaches a quasi or transient steady state equilibrium, $\Delta G = 0$ and $\Delta S = \Delta H/T$. Therefore,

$$\Delta S = -\dot{\varepsilon}\varepsilon_H \left(\eta_{eff} - 3\eta_s \right)/T \qquad (3.19)$$

46

Chapter 4

Materials and Instruments

§4.1 MATERIALS

Four metallocene polyethylenes (PE), one conventional low-density polyethylene (LDPE), one conventional linear low-density polyethylene (LLDPE), one polyisobutylene (PIB), and five cellulose solutions (lyocell) are studied in this research. The PIB sample was provided by Dr. Hudson of the University of Strathclyde and has been characterized by a number of European rheologists. The polyethylene samples have different molecular characteristics. Details of polyethylenes and cellulose solutions are given in the following two sub-sections.

§4.1.1 Polyethylene Samples

The sample source, melt index (MI), density, weight-average molecular weight, polydispersity index (PI), and long chain branches (LCB) of the PE samples are given in Table 4.1. These PE samples and their molecular characteristics were supplied to us by Dr. Donald Baird of Virginia Polytechnic Institute (VPI) in order to measure elongational viscosity and compare our results with theirs. PE samples PE-1, PE-2, PE-3, and PE-4 are metallocene-catalyzed resins and have narrow molecular weight distributions (PI $\approx$ 2). PE-5 is a conventional LDPE resin, whereas, PE-6 is a conventional LLDPE. PE-1, PE-2, PE-3, PE-4, and PE-6 have similar melt flow indexes. PE-1, PE-2, and PE-4 are branched copolymers of ethylene and octene-1 with controlled sparse long chain branches (LCB). PE-3 and PE-6 are copolymers of ethylene and hexene with no LCB. All of these six PE samples are blown film grades.

49

Table 4.1. Molecular characteristics of PE samples.

Sample ID	Sample source	MI (g/10 min)	Density (g/cm³)	M_w	PI	M_z	LCB* (1/10⁴C)
PE-1	Dow Affinity PL 1840	1.0	0.909	87,400	2.43	160200	0.57
PE-2	Exxon Exact 0201	1.1	0.902	88,700	2.14	158900	0.79
PE-3	Exxon Exact 3132	1.2	0.900	111,000	2.04	180400	N/A**
PE-4	Dow Affinity PL 1880	1.0	0.902	115,800	2.12	183700	0.18
PE-5	Equistar NA 952	2.0	0.919	116,000	9.1	***	***
PE-6	Mobil NTX 101	0.9	0.917	122,700	3.44	319700	N/A**

*: long chain branches
**: not applicable (PE-3 and PE-6 are linear PE resins with no long chain branches.)
***: not available

§4.1.2 Cellulose Solution Samples

The cellulose sources studied include softwood Southern pine dissolving pulps of weight-average degree of polymerization (DP_w) of 670 and 1720. The DP 932, 1195, and 1457 samples were prepared by blending appropriate amounts of DP 670 and 1720 dissolving pulps. The 50% N-methyl-morpholine oxide aqueous solution was distilled under continuous mixing and vacuum in a water bath, using a Deluxe Model VE 50 GD rotary vacuum evaporator (Rinco Instrument Company, Inc.), until the monohydrate (NMMO·H2O) was obtained. The dissolving pulps were dissolved in the NMMO monohydrate and n-propyl gallate (at 1% of dissolving pulps) was added as an antioxidant into the cellulose solutions. Fourteen percent

cellulose solutions for dissolving pulps of DP 670, 932, 1195, 1457 and 1720 were prepared at high shear mixing in a C. W. Brabender Type-6 mixer (C. W. Brabender Instruments, Inc.) and optically observed for solution using an Olympus Optical Microscope between crossed polarizers.

§4.2 INSTRUMENTS AND DATA ACQUISITION

Elongational viscosity measurements were done using the Advanced Capillary Extrusion Rheometer (ACER) (TA Instruments). Measurements of shear rheology were done using the Advanced Rheometric Expansion System (ARES) rheometer (TA Instruments).

§4.2.1 Advanced Capillary Extrusion Rheometer (ACER)

A schematic of the ACER is shown in Figure 4.1. The capillary cylindrical die was replaced with a hyperbolic converging axisymmetric die (42). In this research four hyperbolic convergent dies of Hencky stains of 4, 5, 6, and 7 were used. The PE samples were tested at temperatures of 135, 150, 165, and 180°C. These temperatures were chosen because the research group at VPI has done the extensional measurements using a Rheometrics Extensional Rheometer (RER 9000) at temperatures of 135 and 150°C. The PIB sample was tested at temperatures of 210, 220, 230, and 240°C.

The experimental procedure is as follows. The hyperbolic die was attached to the barrel. The pellets of the polymer sample were loaded into the preheated barrel and allowed to melt and attain the desired steady state temperature. When the barrel
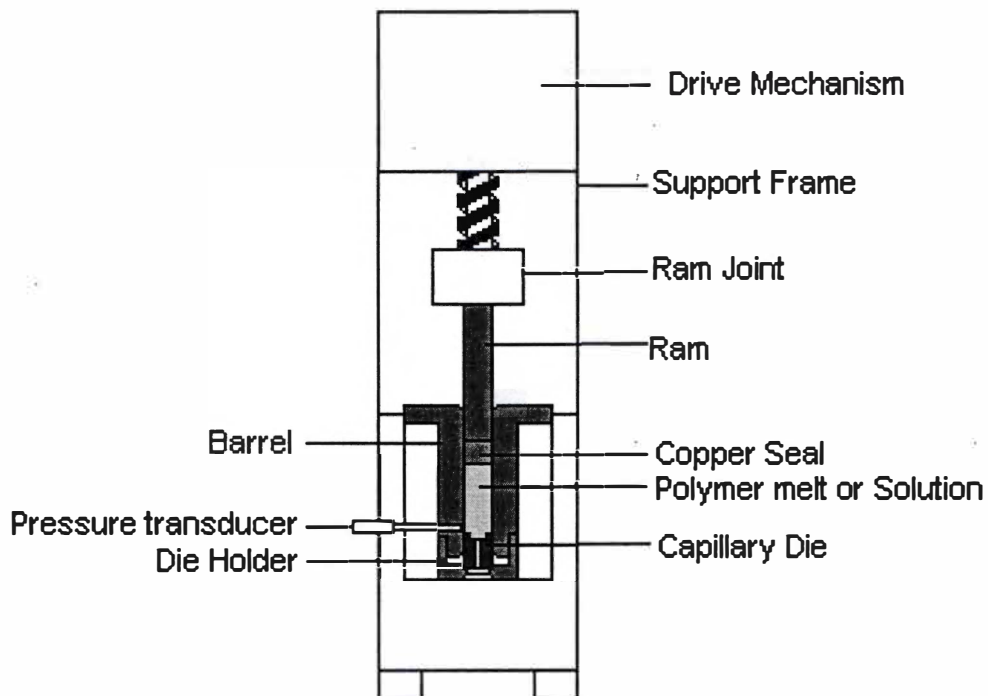
Figure 4.1. Schematic diagram of the Advanced Capillary Extrusion Rheometer (ACER).
[Source: John R.Collier, Ovidiu Romanoschi, and Simioan Petrovan. *Journal of Applied Polymer Science* **69**, 2357 (1998).]

temperature reached the set testing temperature and remained stable within ±1°C, the force transducer and pressure transducer were calibrated, where the pressure transducer is positioned right above the die entrance. The measurement was then performed by pushing the ram, at a constant speed corresponding to a constant chosen elongational strain rate, through the barrel that was filled with the sample under test. From the barrel, the sample was further forced through the die of known Hencky strain. From the knowledge of the elongational strain rate, Hencky strain, and measured steady state pressure, the effective elongational viscosity was then calculated as (41)

$$\eta_{\it eff} \equiv \frac{\Delta P}{\dot{\varepsilon}\varepsilon_H} \tag{4.1}$$

By sweeping the chosen elongational strain rates until a steady state of pressure (or stress) for each strain rate was accomplished, a flow curve of effective elongational viscosity versus elongational strain rate was constructed.

§4.2.2 Advanced Rheometric Expansion System (ARES)

A simplified schematic of the ARES rheometer with parallel plate geometry is shown in Figure 4.2. Circular disks of polyethylene specimens were prepared by compression molding at 200°C. Flat sheets of PIB samples were also prepared by compression molding at 50°C. The geometry used was parallel plates with diameter 25 mm. The gap was set at 1 mm. The experimental temperatures were the same as those in the elongational measurements for the PE and PIB samples. The PE samples

53
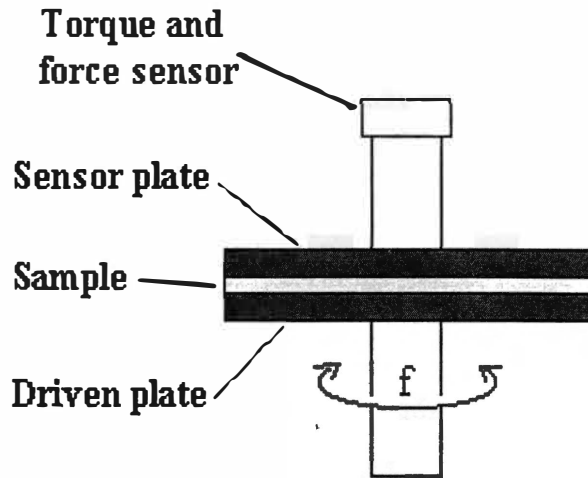
Figure 4.2. Simplified schematic of the Advanced Rheometric Expansion System (ARES).

were tested at 175°C as well so that data of two conventional LDPE samples in prior studies accomplished by this research group (115) could be incorporated into the MW and MWD calculation. For the cellulose solutions, the experimental temperature was 90°C.

The lower plate of the ARES rheometer is attached to a motor that can rotate in both steady and oscillatory modes. The upper plate is attached to the torque and force transducers. There are two transducers with different torque ranges (but same normal force range). During a test, the lower range transducer can be switched to the higher range transducer automatically, if needed. The plates of the rheometer are enclosed in a forced air convection oven to heat the sample. Two resistive heaters are mounted in the oven to control the temperature of the heating gas. Compressed air

was used during all tests. The temperature of the lower plate is also controlled by a platinum resistive thermometer (PRT).

The procedure of the rheological measurement using the ARES is as follows:

a. Dynamic strain sweep. Under a constant dynamic frequency of 1 rad/s, storage modulus G', loss modulus G'', and complex viscosity η^* as a function of strain were measured over the strain range of 0.1 to 100%. This was done to determine the range of strain for linear viscoelasticity.

b. Dynamic frequency sweep. Under a constant strain of 1% which was in the linear viscoelastic range, G', G'', and η^* were measured by the small amplitude oscillatory testing mode over angular frequency range of 0.1 to 100 rad/s.

c. Step rate test. By choosing a shear rate, the shear viscosity and first normal stress difference were measured as a function of time.

Chapter 5

Results and Discussions

§5.1 EFFECT OF MOLECULAR CHARACTERISTICS ON THE ELONGATIONAL RHEOLOGY OF POLYMER MELTS

The molecular characteristics of the polyethylene samples studied in this work were introduced in Chapter 4. This section will discuss how these molecular parameters affect the elongational rheology measured using hyperbolic converging dies. The effect of the processing conditions on the elongational rheology will be discussed in the next section.

The effect of molecular characteristics on the elongational rheology needs to be studied using a series of samples with different molecular characteristics. The six PE samples studied in this work pretty well fit this. As mentioned in Chapter 4, PE samples PE-1, PE-2, PE-3, and PE-4 are metallocene-catalyzed resins and have narrow molecular weight distributions (PI $\approx$ 2). PE-5 is a conventional LDPE resin, whereas, PE-6 is a conventional LLDPE. PE-1, PE-2, PE-3, PE-4, and PE-6 have similar melt flow indexes. PE-1, PE-2, and PE-4 are branched copolymers of ethylene and octene-1 with controlled sparse long chain branches (LCB). PE-3 and PE-6 are copolymers of ethylene and hexene with no LCB.

The effect of weight-average molecular weight, molecular weight distribution, and long chain branches on the elongational viscosity of PE samples measured at 135°C and four Hencky strains is shown in Figure 5.1. The effective elongational viscosity of different samples at the same Hencky strain converge at high strain rate except PE-5. The effective elongational viscosity of different
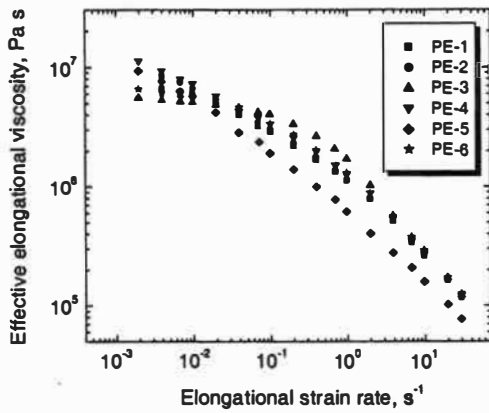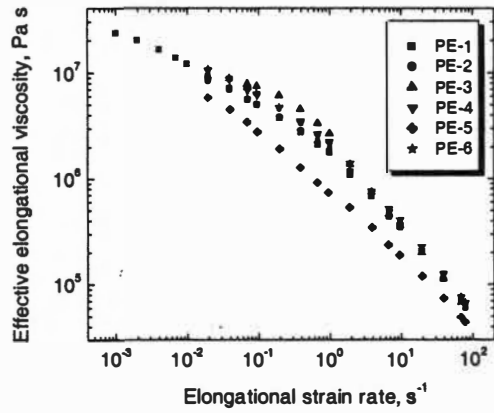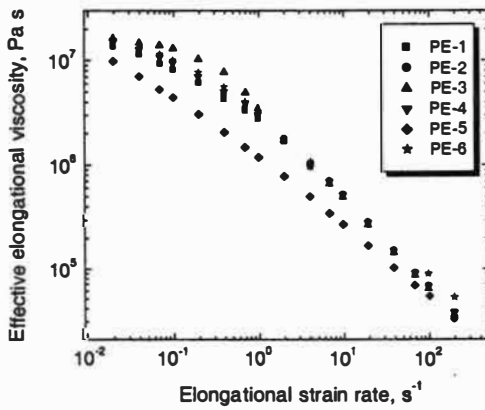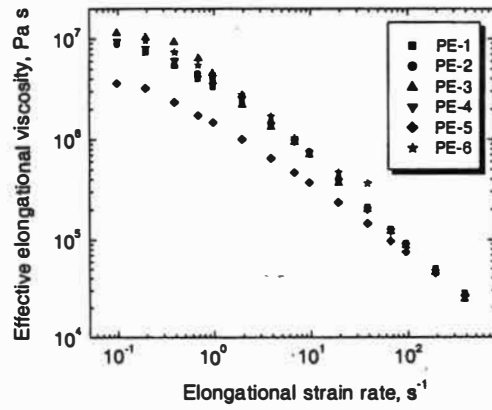
Figure 5.1. Effective elongational viscosity of different PE samples at 135°C.

samples flatten out differently at low strain rates. Compared with other figures in Figure 5.1, Figure 5.1(a) has lower starting strain rate and obviously shows that the elongational viscosity curves of all samples cross over each other at different low strain rates. It can be deduced that the onset of strain rate thinning has the order of PE-5 < PE-2 < PE-1 < PE-6 < PE-3. The strain rate thinning might be caused by the MWD and / or LCB. Comparison of PE-3 and PE-6 having no LCB shows that the broader MWD promotes the strain rate thinning since the onset of strain rate thinning is at a lower elongational strain rate for PE-6 which has higher PI. Keeping this in mind, comparison of PE-1 and PE-2, or PE-2 and PE-6, or PE-1 and PE-6 shows that the LCB also promotes the strain rate thinning.

The above explains that the onset of strain rate thinning is at a lower strain rate for PE-5, which is a conventional LDPE with higher PI and LCB. Hence, PE-5 shows a different shape of elongational viscosity curve and lower elongational viscosity when the elongational strain rate is higher than 0.02 s^{-1}. Comparison of PE-3 and PE-6 having no LCB at strain rate higher than 0.07 s^{-1} shows that broadening the molecular weight distribution seems to decrease the elongational viscosity, because despite the fact that PE-3 has a lower MW, its viscosity is higher than that of PE-6 at the same strain rate. PE-2 has higher MW and LCB but lower PI than PE-1. PE-1 and PE-2 have almost the same elongational viscosity at strain rate higher than 0.04 s^{-1}. Hence, the effect of LCB is to decrease the elongational viscosity. Figures 5.2 through 5.4 show similar observations at different Hencky strains and temperatures.
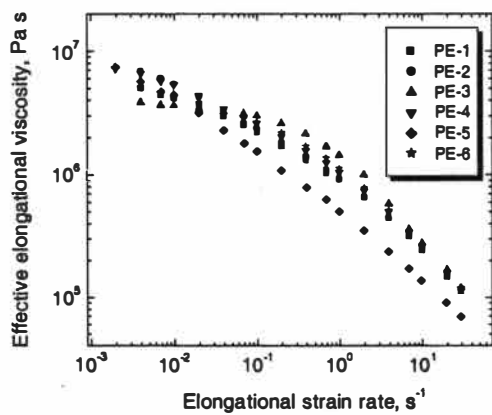
(a) Hencky 4
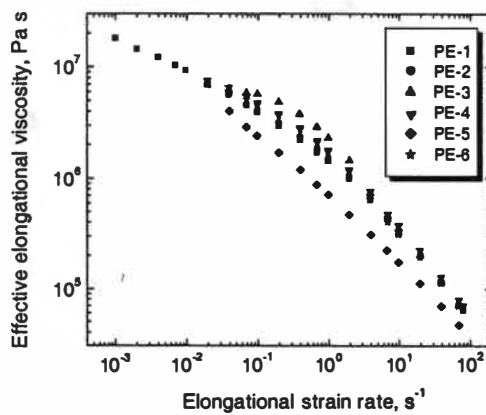
(b) Hencky 5
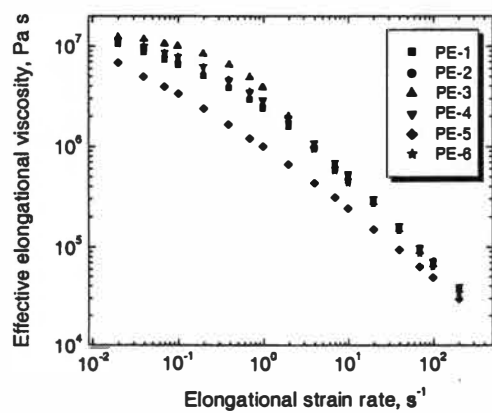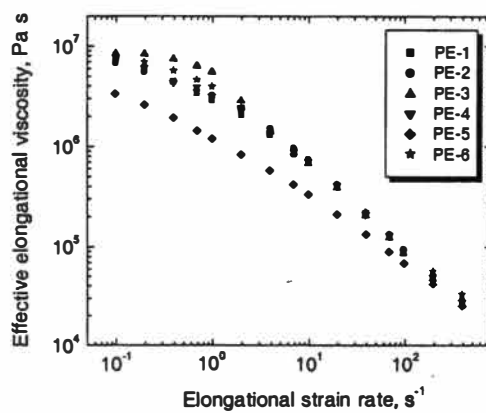
(c) Hencky 6

(d) Hencky 7

Figure 5.2. Effective elongational viscosity of different PE samples at 150°C.
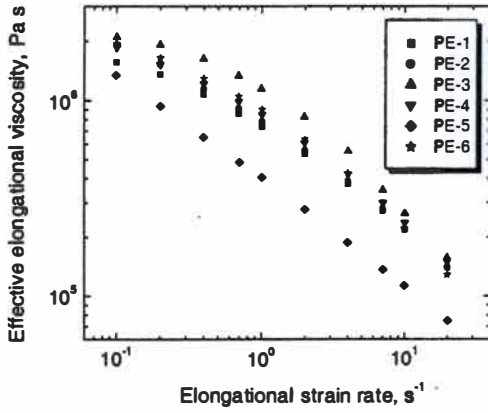
(a) Hencky 4
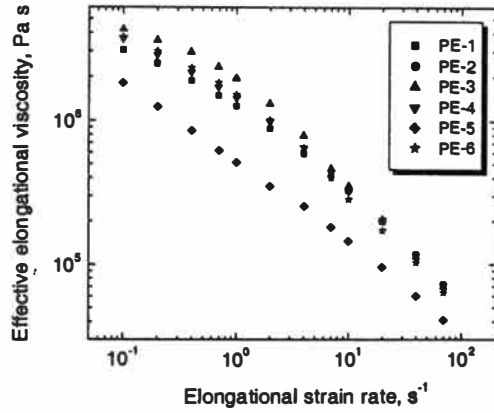
(b) Hencky 5
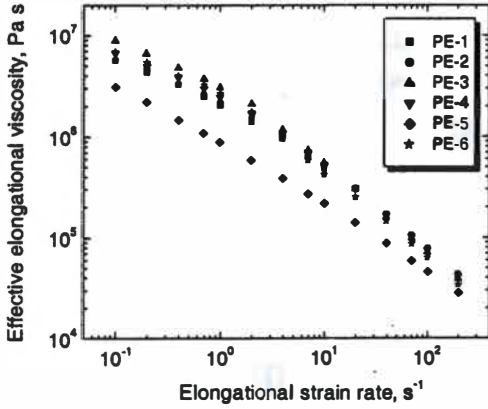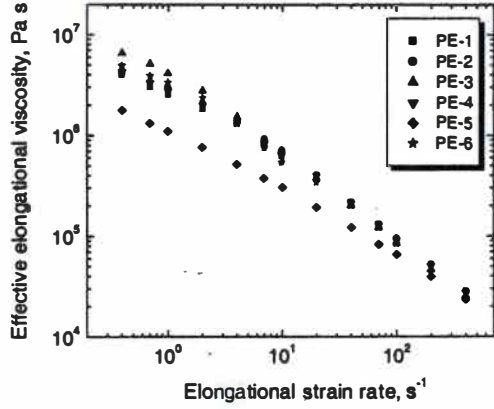
(c) Hencky 6

(d) Hencky 7

Figure 5.3. Effective elongational viscosity of different PE samples at 165°C.
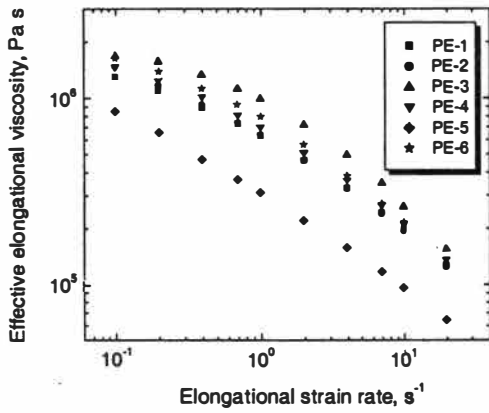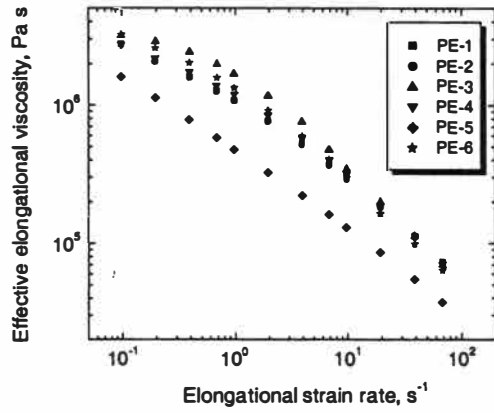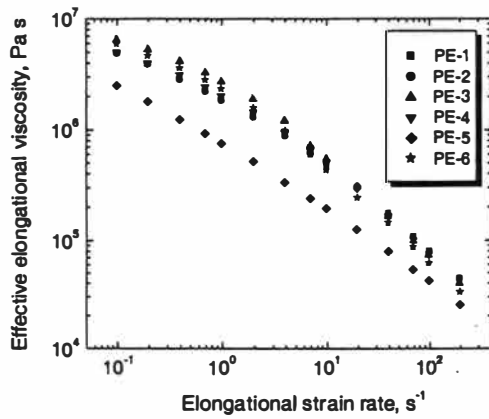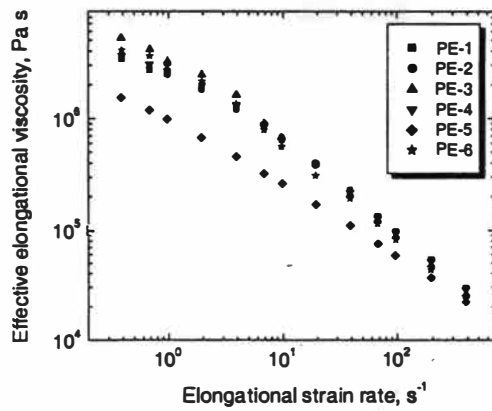
Figure 5.4. Effective elongational viscosity of different PE samples at 180°C.

Using our data, the effect of molecular characteristics on the strain hardening (described in Chapter 1) of PE samples can be discussed here. However, one should keep in mind that the strain hardening reported in the literature is a transient phenomenon observed in Meissner type devices. The strain hardening reported here is for the steady state behavior of polymer molecules in a converging elongational flow. The elongational flow in our technique is in a Eulerian steady state but not in a Lagrangian steady state, whereas, the elongational flow in Meissner type devices exhibits neither steady states. The data in Figures 5.1 through 5.4 is replotted as effective elongational viscosity at 0.1 and 1 s^{-1} vs. Hencky strain in Figures 5.5 and 5.6 for different PE samples. These two figures show that all PE samples show similar patterns of strain hardening. The effect of temperature on the patterns of strain hardening of these samples is not considerable. This is also illustrated by the strain hardening of PIB sample at strain rates of 0.1 and 1 s^{-1}, shown in Figures 5.7(a) and 5.7(b), respectively.

Using a Rheometrics Extensional Rheometer (RER 9000), constant extension rate uniaxial elongational tests were performed on these PE samples at 150°C by Dr. Donald Baird's group at Virginia Polytechnic Institute. From these measurements, elongational viscosity at Hencky strains of 1, 2, and 3 was obtained and plotted in Figures 5.5(b) and 5.6(b) along with our data measured by using the hyperbolic converging dies. Both figures show good agreement for the conventional low-density polyethylene (PE-5). But for other PE samples there is not good agreement. The data measured with RER show that the LDPE (PE-5), which is highly branched, exhibits

65
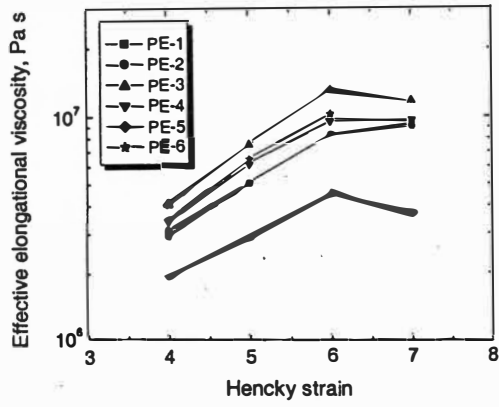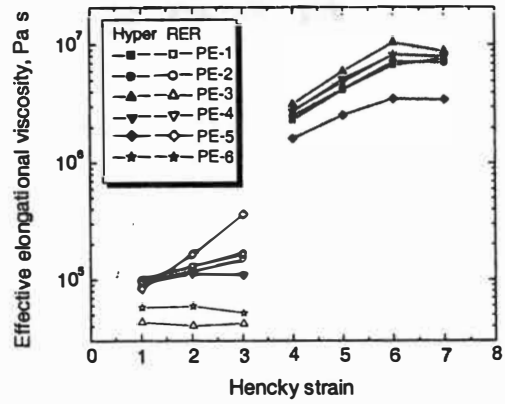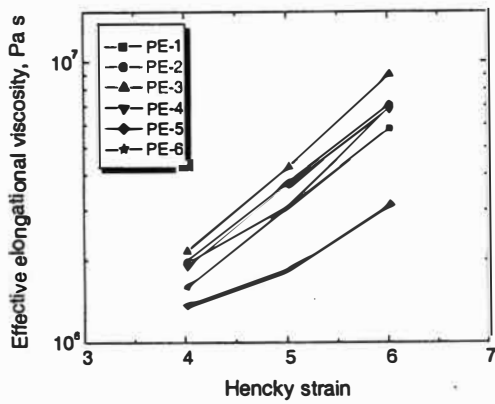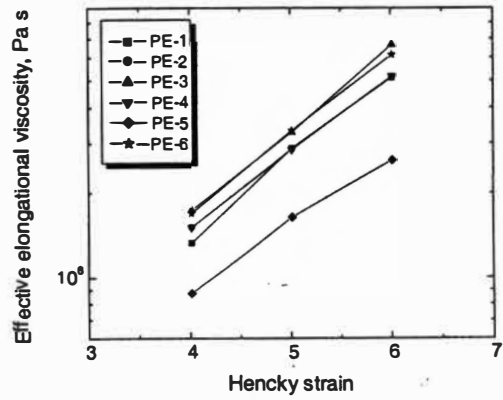
Figure 5.5. Strain hardening of PE samples at 0.1 s^{-1}.
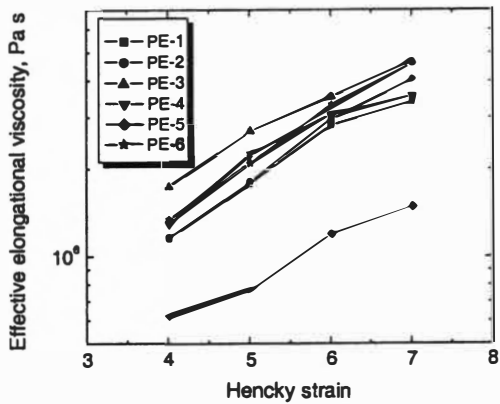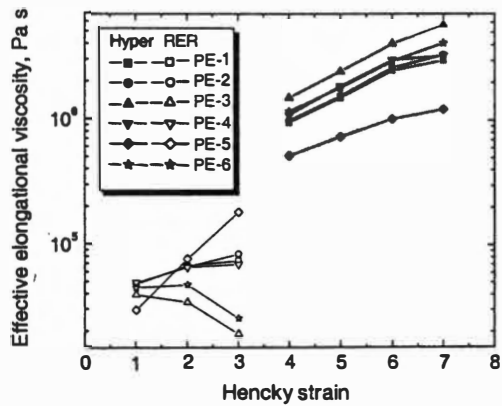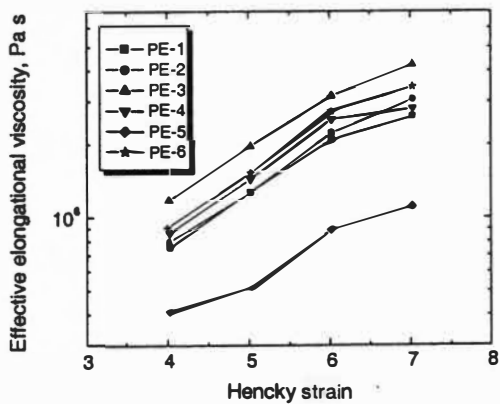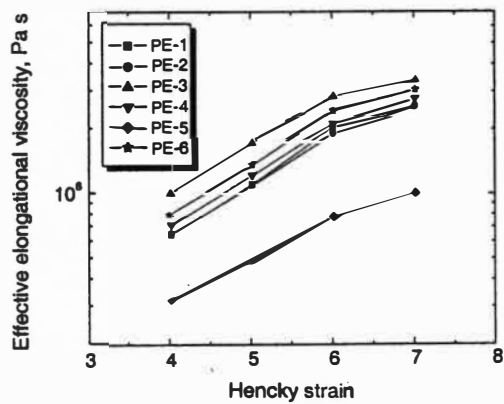
Figure 5.6. Strain hardening of PE samples at 1 s^{-1}.
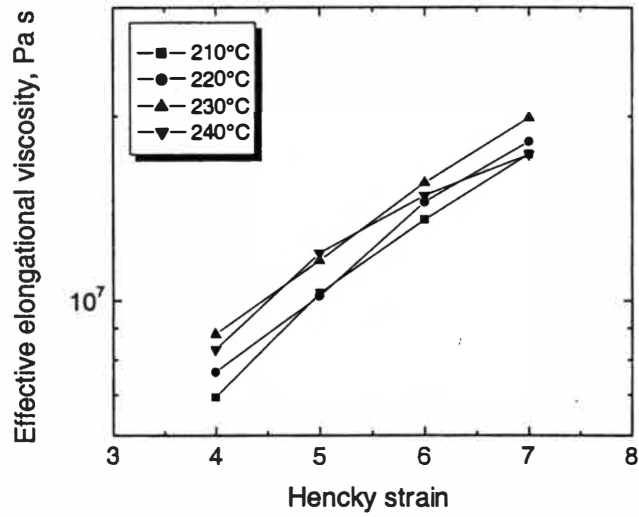
(a) Strain rate = 0.1 s^{-1}
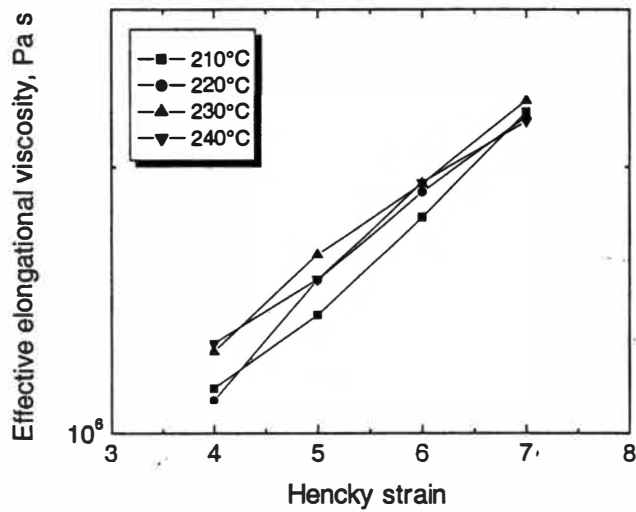
(b) Strain rate = 1 s^{-1}

Figure 5.7. Strain hardening of PIB sample.

a significant degree of strain hardening. Linear PEs (PE-3 and PE-6) do not show any strain hardening while other metallocene PEs (PE-1, PE-2, and PE-4), with some long chain branches, exhibit some degree of strain hardening.

The residence time of the fluid particles in the region of constant elongational strain rate can be defined as Hencky strain over strain rate. Figures 5.8 through 5.13 show the effective elongational viscosity measured using the hyperbolic dies and the shear viscosity as a function of the residence time for PE samples. All PE samples show similar patterns to each other, from which the strain hardening effect is evident, according to the relationship between shear viscosity and elongational viscosity measured from Meissner-type extensional rheometer. Figure 5.12(b) shows very good agreement between the RER and hyperbolic die techniques. It also shows strain hardening. The factorized Rivlin-Sawyers constitutive equation (116) has been used to calculate the elongational viscosity of some other PE samples by Dr. Brian Edwards' research group at the University of Tennessee, Knoxville. Good agreement is found between the calculated values and the experimental data. The calculated results also show the relationship between shear and elongational viscosities measured by using the Meissner-type extensional rheometer (117). It is concluded that the measured effective elongational viscosity is a good approximation to the material's true elongational viscosity.

Figure 5.14 illustrates the effective elongational viscosity as a function of the transient time for PIB sample. It is obvious that PIB and PE samples have different
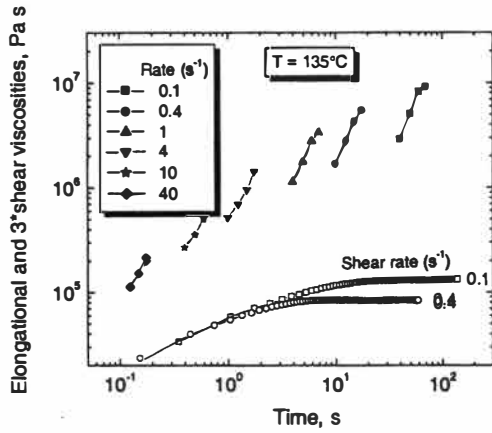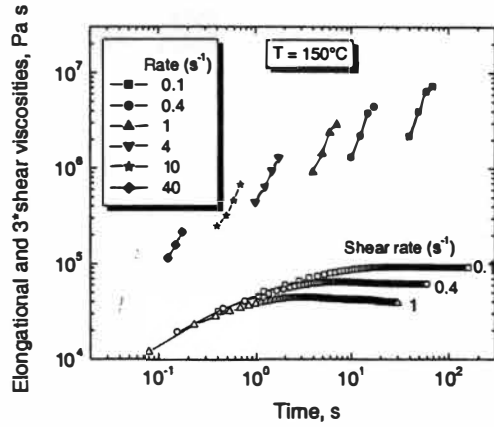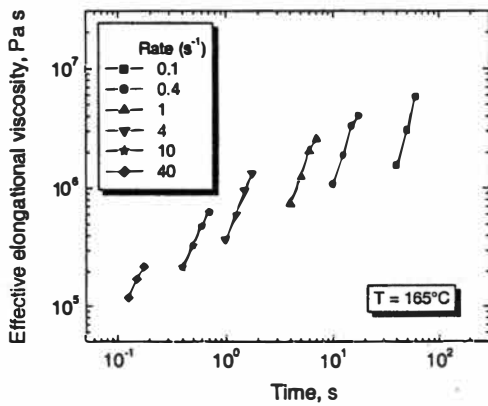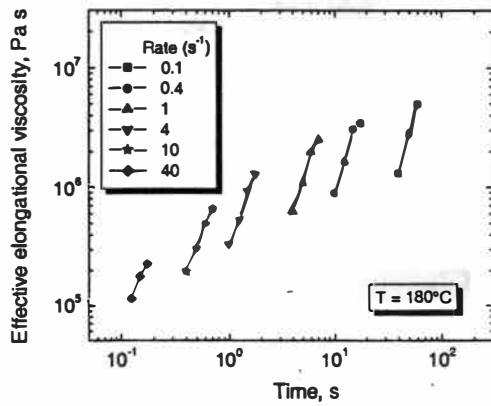
Figure 5.8. Effective elongational viscosity vs. time for PE-1.
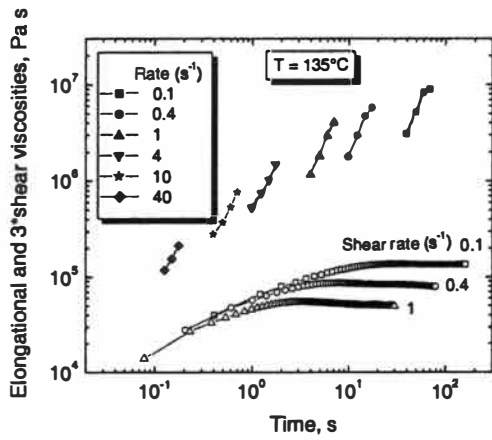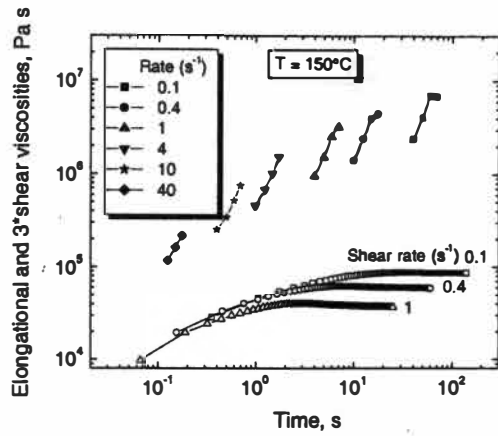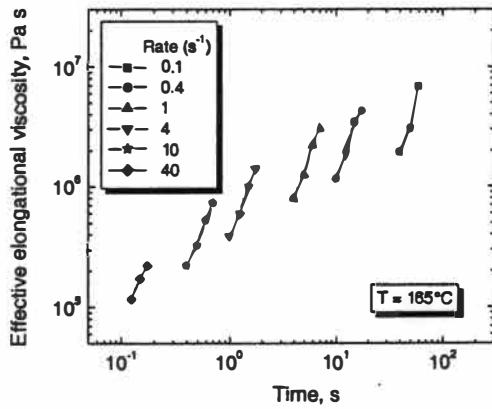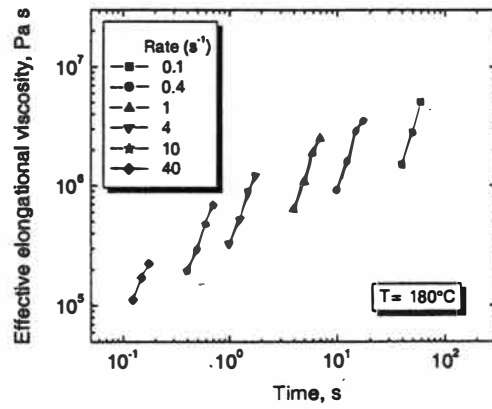
Figure 5.9. Effective elongational viscosity vs. time for PE-2.
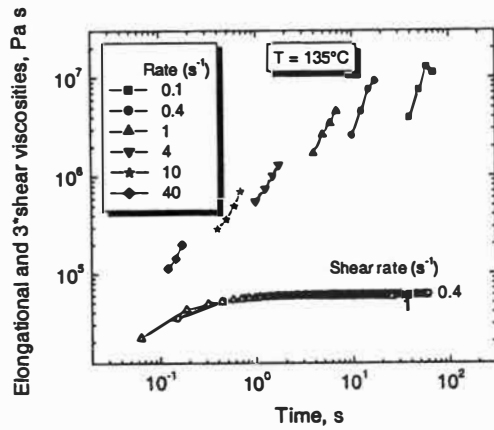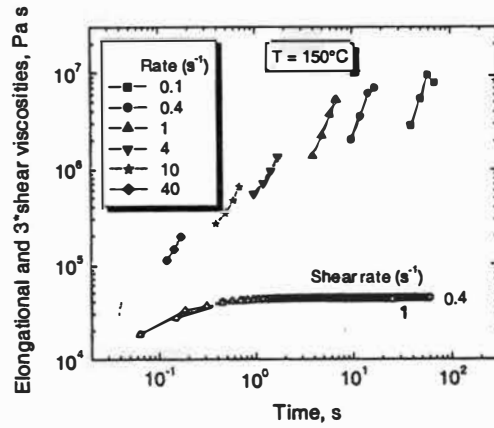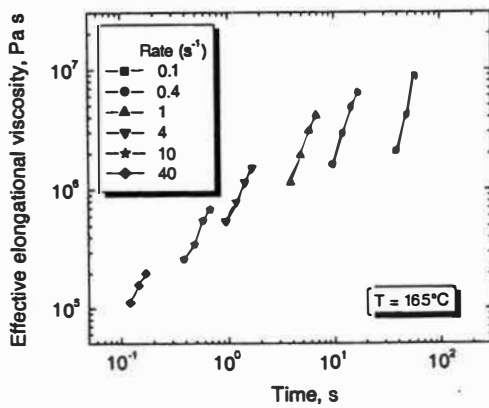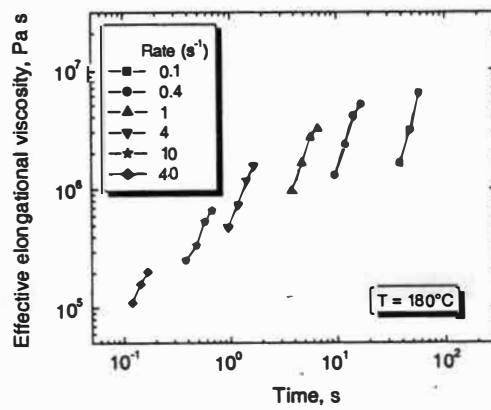
Figure 5.10. Effective elongational viscosity vs. time for PE-3.

(a) 135°C

(b) 150°C

(c) 165°C

(d) 180°C

72
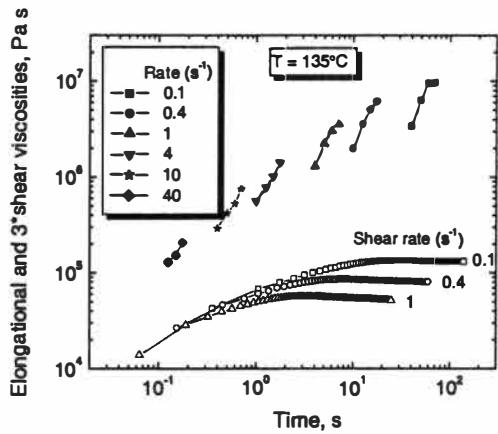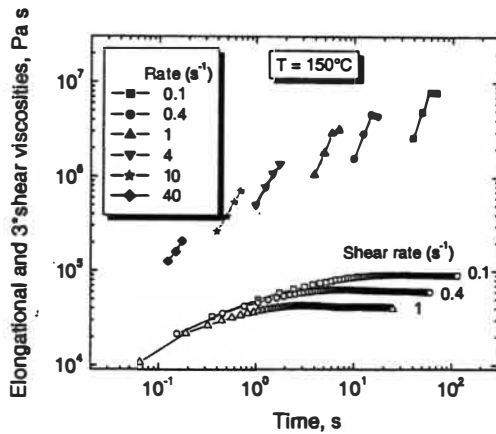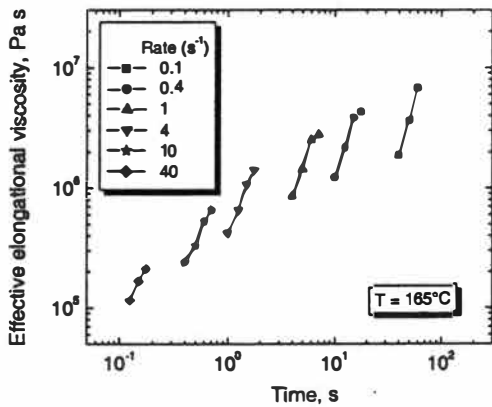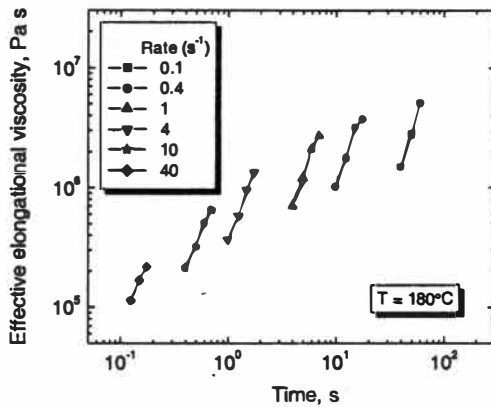
(a) 135°C

(b) 150°C

(c) 165°C

(d) 180°C

Figure 5.11. Effective elongational viscosity vs. time for PE-4.
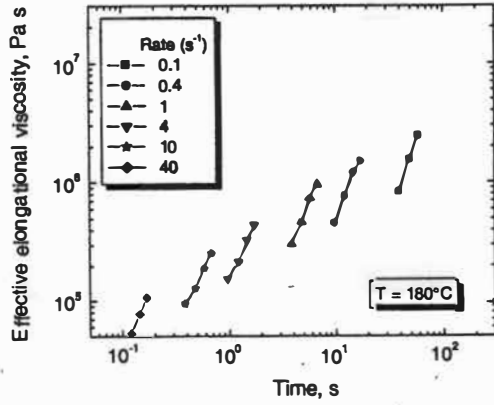
Figure 5.12. Effective elongational viscosity vs. time for PE-5.
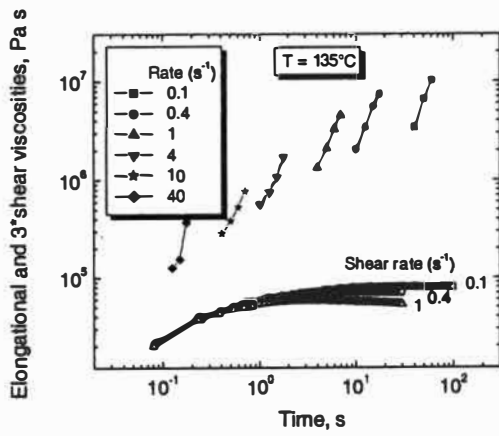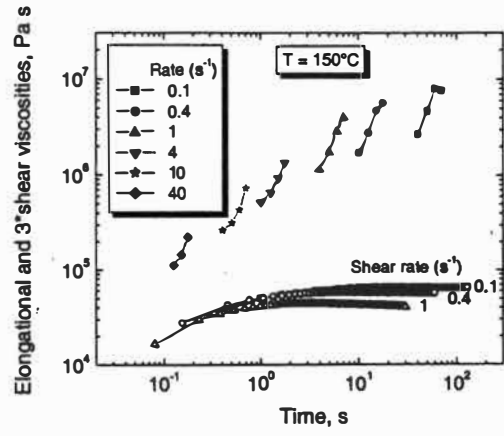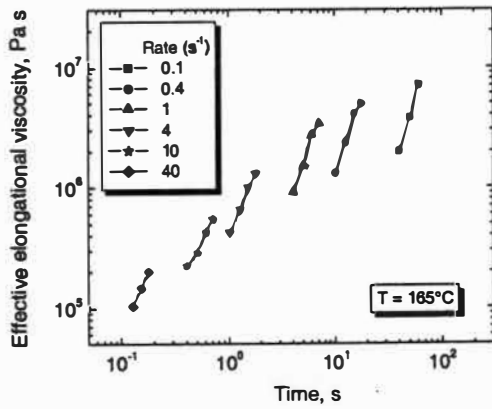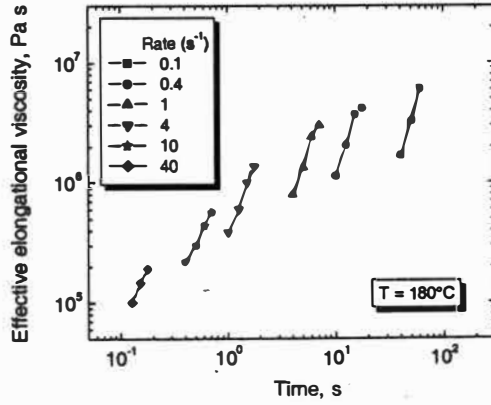
Figure 5.13. Effective elongational viscosity vs. time for PE-6.
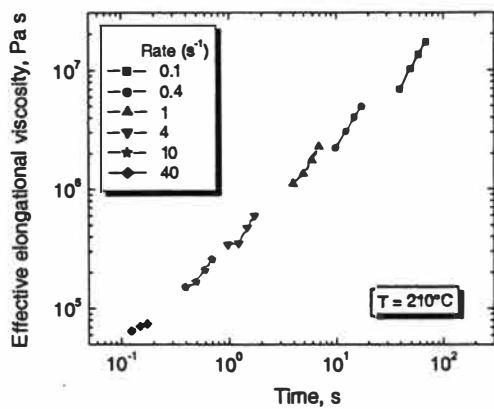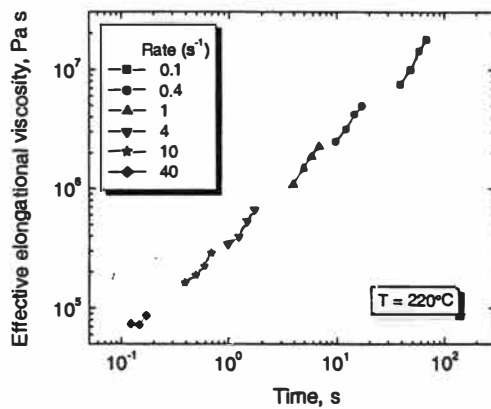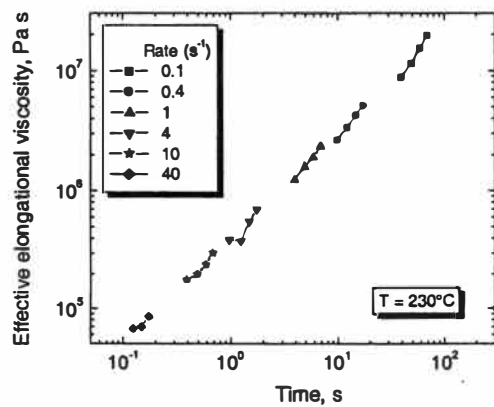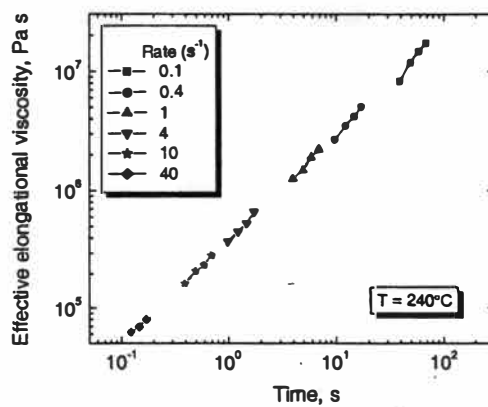
Figure 5.14. Effective elongational viscosity vs. time for PIB sample.

patterns. Figure 5.15 gives the comparison between the elongational viscosity measured by the hyperbolic die technique at 210°C and the Elongational Rheometer for Melts (RME) at 100°C or 120°C. The data from RME were performed by Meissner on his prototype RME seven years ago. It is seen that the data from two techniques show similar patterns. The values obtained in our work are close to those from RME. Considering the very small effect of temperature on the elongational viscosity which will be discussed in the next section, the result shown in Figure 5.15 again indicates that the measured effective elongational viscosity is a good approximation to the material's true elongational viscosity.
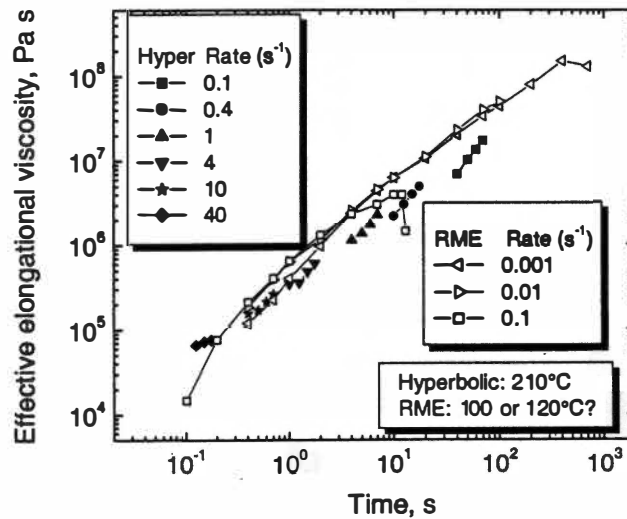
Figure 5.15. Elongational viscosity vs. time for PIB sample measured by hyperbolic dies and RME.

§5.2 EFFECT OF PROCESSING CONDITIONS ON THE ELONGATIONAL RHEOLOGY OF POLYMER MELTS

Besides the molecular parameters discussed above, rheological properties can be affected by the processing conditions as well. The most important processing parameters that affect elongational viscosity of a polymer include temperature, strain, and strain rate. The effective elongational viscosity of polymer melts increases by decreasing the temperature and increasing Hencky strain. In the next two sub-sections, quantitative relations are developed to shift the effective elongational viscosity curves at any temperature or Hencky strain to a reference curve at a reference temperature or Hencky strain.

§5.2.1 Temperature Shifting of Effective Elongational Viscosity

§5.2.1.1 Theoretical Background

The method of reduced variables predicts that a single master curve for the shear viscosity curves taken at different temperatures of a sample can be obtained by plotting reduced complex viscosity η_r^* vs. reduced angular frequency ω_r by using a shift factor (118). In the following, equations for the temperature shifting of shear viscosity are presented. It will be shown that these equations can also be applied for the temperature shifting of elongational viscosity curves.

In this work, two temperature shift factors are defined by

$$(a_T)_1 = \frac{\eta_0(T)}{\eta_0(T_0)} \tag{5.1}$$

78

and

$$(a_T)_2 = \frac{\eta_0(T)T_0}{\eta_0(T_0)T} \tag{5.2}$$

where $\eta_0(T)$ and $\eta_0(T_0)$ are zero-shear-rate viscosities of the melts at temperature T and reference temperature T_0, respectively. Thus, the method of reduced variables predicts that a single master curve can be obtained by plotting reduced complex viscosity η_r^* vs. reduced angular frequency ω_r where they are defined by

$$\eta_r^* = \eta^*(\omega,T)\frac{\eta_0(T_0)}{\eta_0(T)} \tag{5.3}$$

$$\omega_r = \omega a_T \tag{5.4}$$

Assuming that the Cox-Merz rule applies to PE and PIB samples, viscosity models are used to predict the zero-shear-rate viscosity of polymer melts from the complex viscosity data. Two such models are considered in this work: the three-parameter Cross model and the three-parameter Carreau model. The three-parameter Cross viscosity model is given by

$$\eta = \frac{\eta_0}{1+(\lambda\dot\gamma)^{1-n}} \tag{5.5}$$

and the three-parameter Carreau viscosity model given by

$$\eta = \eta_0\left[1+(\lambda\dot\gamma)^2\right]^{(n-1)/2} \tag{5.6}$$

where λ is a time constant and n is the power-law exponent. In general, the three-parameter Cross model tends to overpredict the zero-shear-rate viscosity, whereas the three-parameter Carreau model tends to slightly underpredict the zero-shear-rate

79

viscosity (119). A scouting study reveals that Eq. (5.1) is appropriate to generate a master curve for the complex viscosity when the three-parameter Cross model is used to predict the zero-shear-rate viscosity, whereas Eq. (5.2) is appropriate when the three-parameter Carreau model is used.

The temperature dependence of a_T is often found to be an "Arrhenius dependence" of the following form (118)

$$a_T = \exp\left[\frac{\Delta E_a}{R}\left(\frac{1}{T} - \frac{1}{T_0}\right)\right]$$

(5.7)

where ΔE_α is the activation energy of flow and R is the universal constant.

The relaxation time is a unique characteristic for a polymer at a given temperature and does not depend on the type of deformation. Hence, the dependence of relaxation time on temperature should be the same for both shear flow and elongational flow. The temperature shift factor is the ratio of relaxation times of polymers at two temperatures (120). Thus, the same temperature shift factors can be used to shift both shear and elongational viscosities (120). This could also be supported by Münstedt's finding (28). Münstedt calculated the activation energies for both shear and elongational flow from the zero-shear-rate viscosity and the elongational viscosity at very low strain rates, respectively. He found that the values were identical. Data on the temperature shifting of effective elongational viscosity of the PE and PIB samples are presented in the next two sub-sections.

§5.2.1.2 Results on Polyethylene Samples

The complex viscosity of PE-1 at four different temperatures is shown in Figure 5.16(a). Data from this figure show that changing the temperature does not affect very much the functional dependence of η^* on ω; it merely alters the zero-shear-rate viscosity and the angular frequency at which the transition from constant complex viscosity to power-law behavior occurs. This similarity provides the basis for the method of reduced variables.

The three-parameter Cross model mentioned above was used to fit the complex viscosity curves of PE-1 at each temperature. The fitted complex viscosity data are given as the solid lines in Figure 5.16(a). The parameters in the Cross model are also obtained and shown in the legend of Figure 5.16(a), together with the shift factors calculated using Eq. (5.1) by choosing 150°C as the reference temperature. A master curve of the complex viscosity of PE-1 was created and is shown in Figure 5.16(b). Similarly, master curves of dynamic moduli of PE-1 were also created and shown in Figure 5.16(c) using the same shift factors. The Arrhenius plot of $ln(a_T)$ vs. $1/T$ is shown in Figure 5.16(d). From the slope of the linear fit, the activation energy of PE-1 was calculated.

The three-parameter Carreau model mentioned above was also used to fit the complex viscosity curves of PE-1 at each temperature. The shift factors were calculated using Eq. (5.2). The fitted results are presented in Figure 5.17 in the same way as the results from the Cross model.
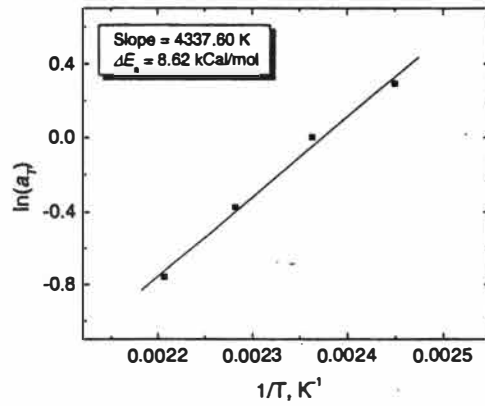
81
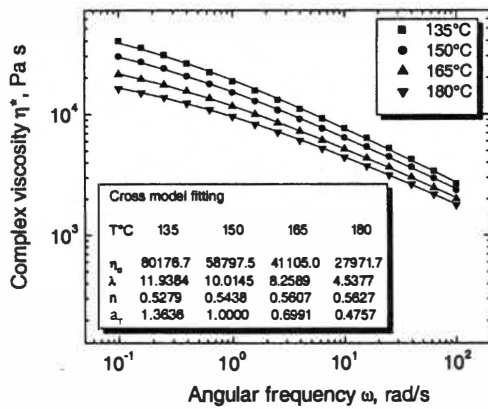
(a) Original curves
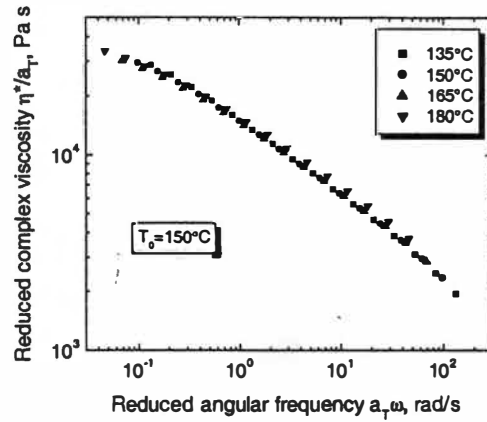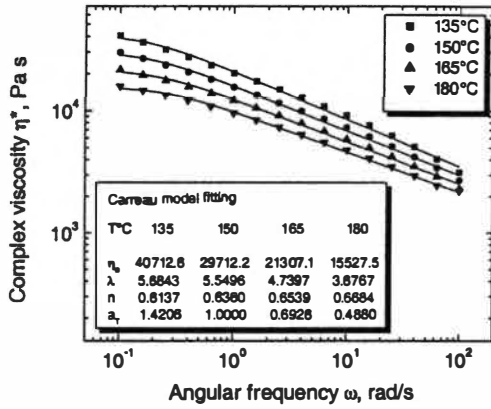
(b) Master curve for η^*
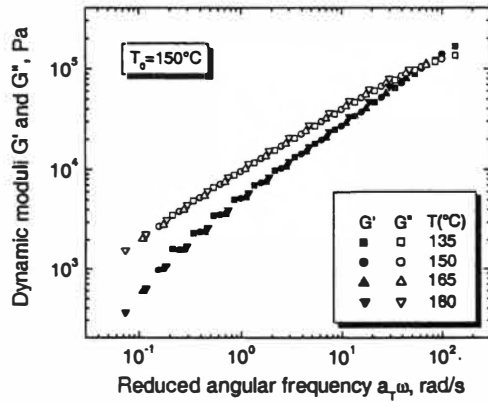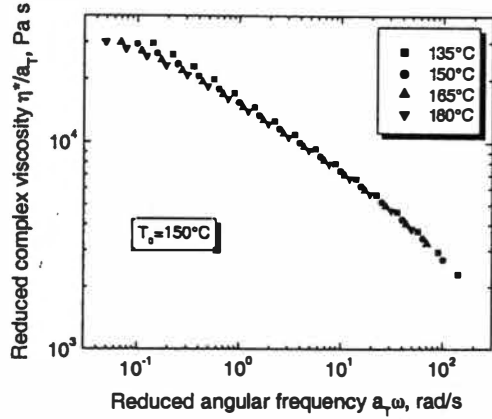
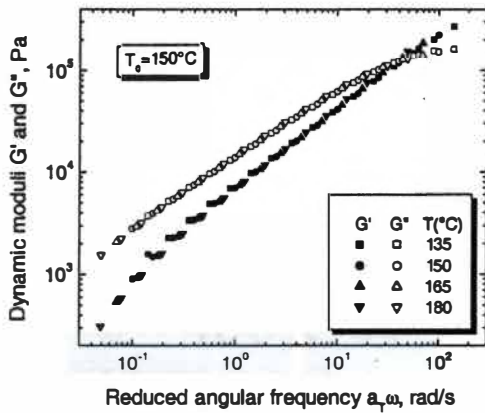(c) Master curves for G'& G"
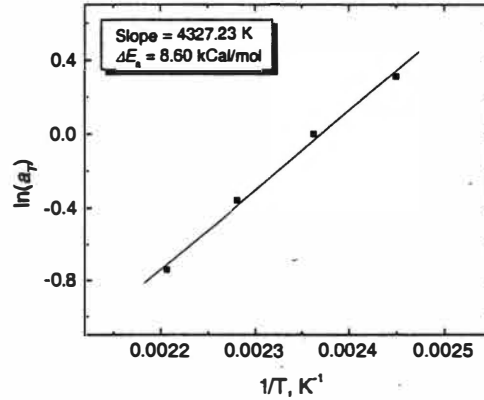
(d) $ln(a_T)$ vs. $1/T$

Figure 5.16. Temperature shifting of shear rheology data of PE-1 using Cross model.

82
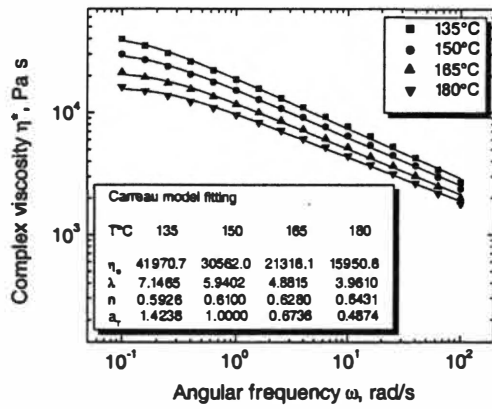
(a) Original curves
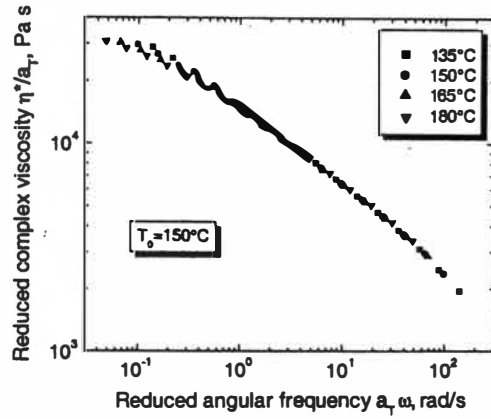
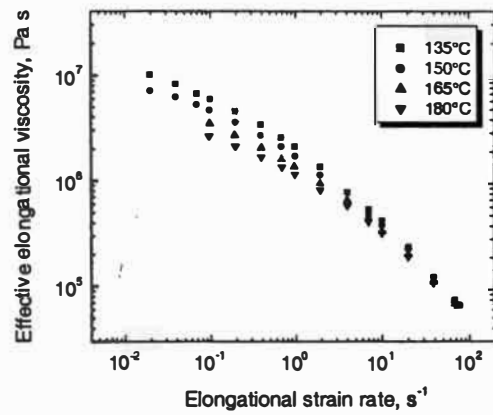(b) Master curve for η^*
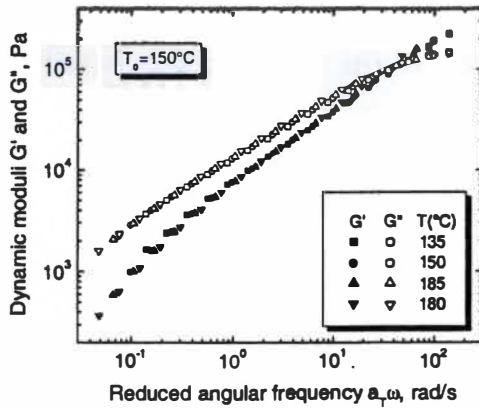
(c) Master curves for G' & G"
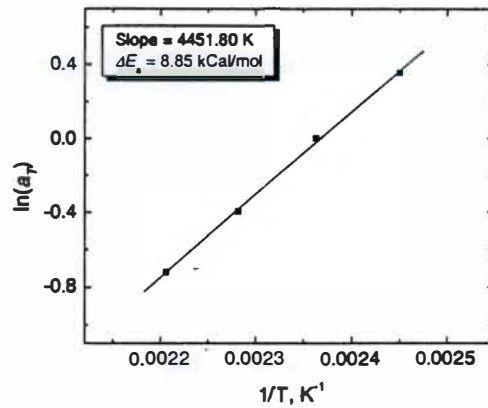
(d) $ln(a_T)$ vs. $1/T$

Figure 5.17. Temperature shifting of shear rheology data of PE-1 using Carreau model.

Figure 5.18 shows the effect of temperature on the effective elongational viscosity of PE-1 measured at different Hencky strains. The temperature master curves generated using the shift factors derived from the Cross and Carreau models are shown in Figures 5.19 and 5.20 for PE-1, respectively. Shifting results for the remaining PE samples are shown in Figures 5.21 through 5.45.

It can be seen that elongational viscosity decreases with increasing temperature. This is because increasing the temperature increases the mobility of molecular chains. With increasing strain rate, the viscosity differences at different temperatures appear to diminish since the lines converge at higher strain rate.

It can be observed that both Cross and Carreau models yield good master curves for the complex viscosity, dynamic moduli, and effective elongational viscosity. This can also be shown by the high coefficient of determination (R^2) values (higher than 0.988) for the polynomial fits of complex viscosity and temperature master curves, given in Tables 5.1 and 5.2, respectively. The elongational viscosity data measured at very low strain rates fell nicely on the master curves, indicating these data are probably accurate although the resulting pressure drop values in the measurements are somewhat low. The elongational viscosity of PE-6 does not show consistent convergence at high strain rates when measured at 135°C and Hencky strains of 6 and 7. This explains some obvious data points away from the corresponding master curves shown in Figures 5.44 and 5.45. Considering the much better master curve of complex viscosity for PE-5 using the Cross model,
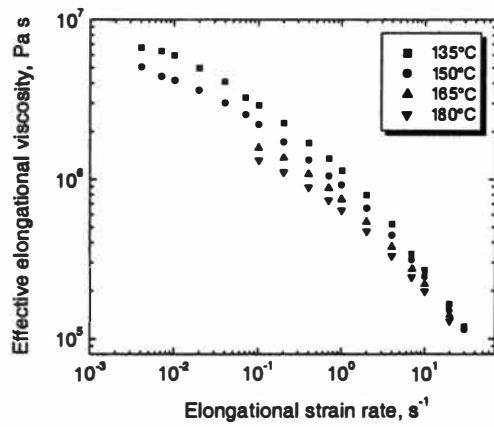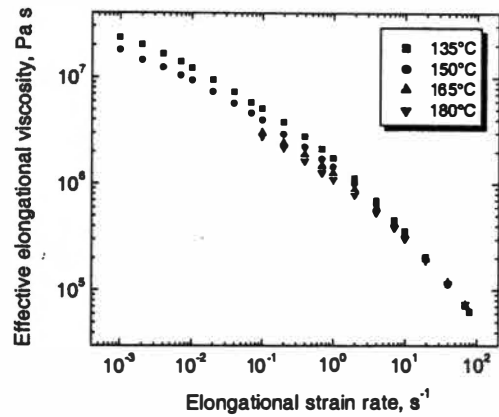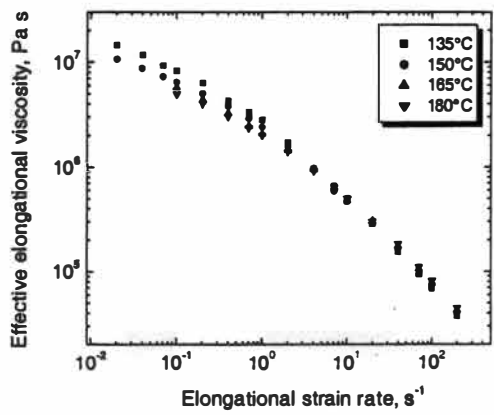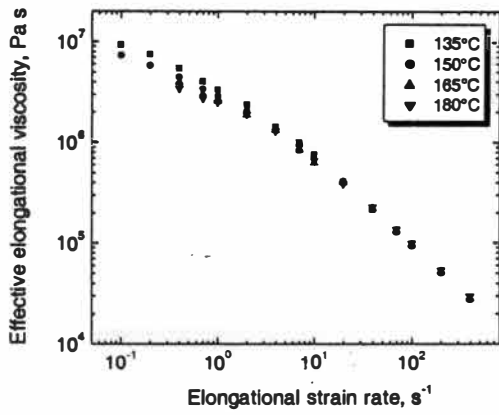
Figure 5.18. Effect of temperature on effective elongational viscosity of PE-1 at different Hencky strains.
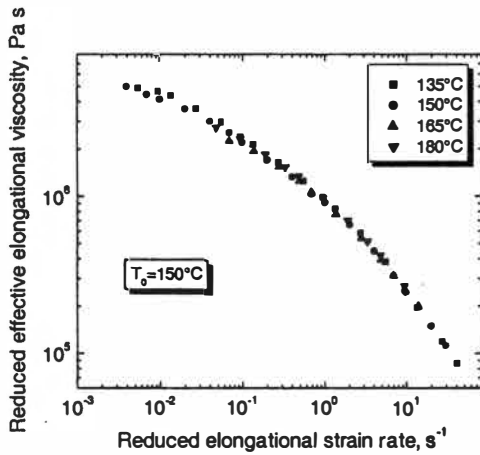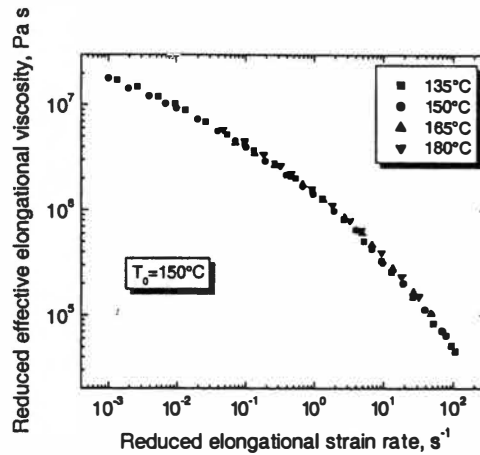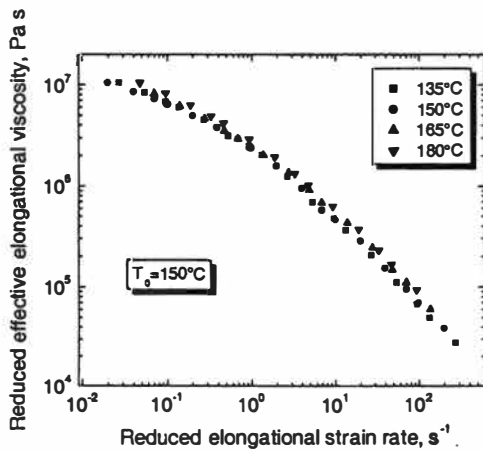
(a) Hencky 4
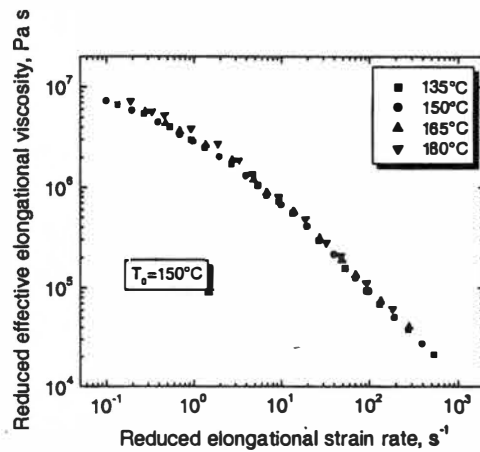
(b) Hencky 5

(c) Hencky 6

(d) Hencky 7

Figure 5.19. Temperature master curves of effective elongational viscosity of PE-1 at different Hencky strains using Cross model.
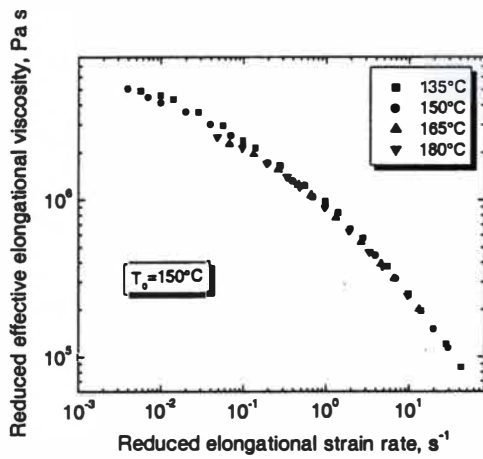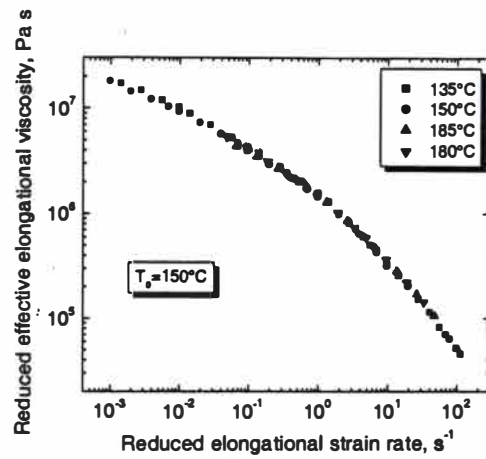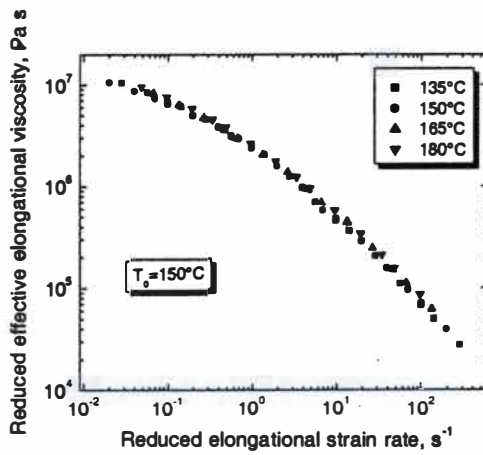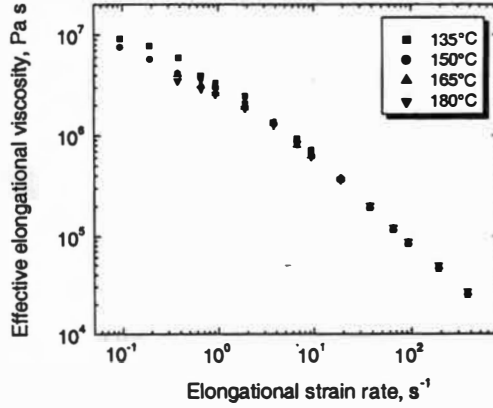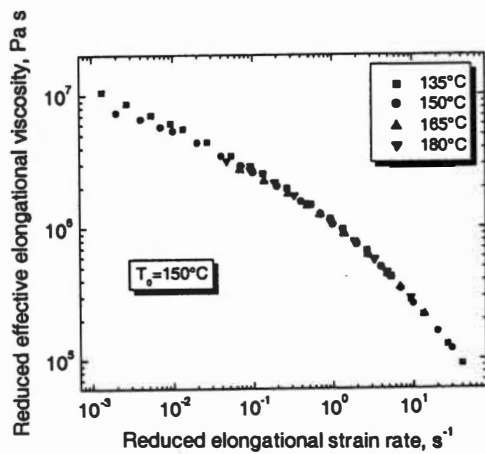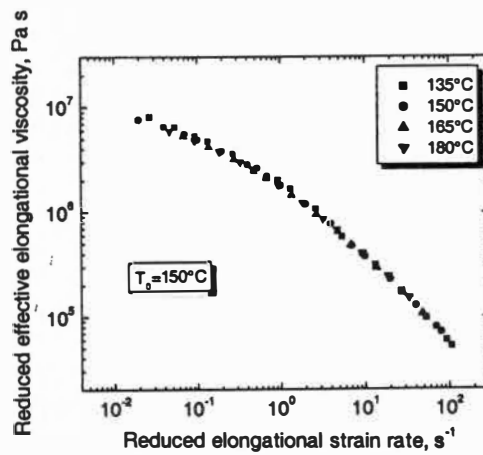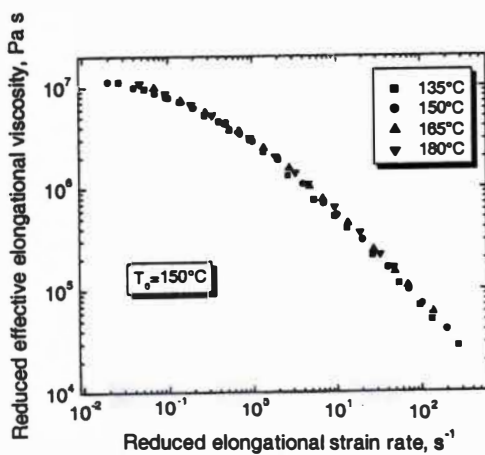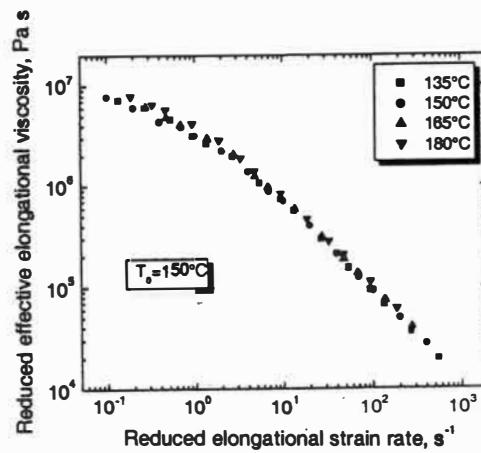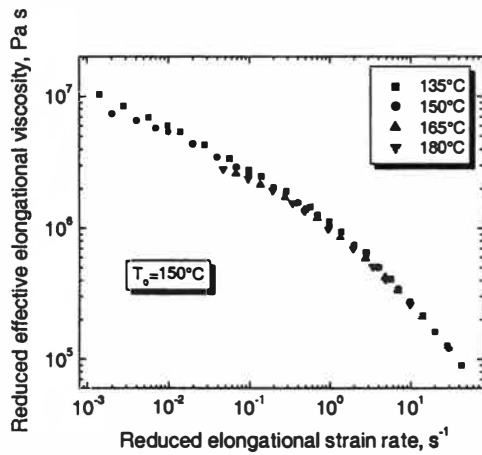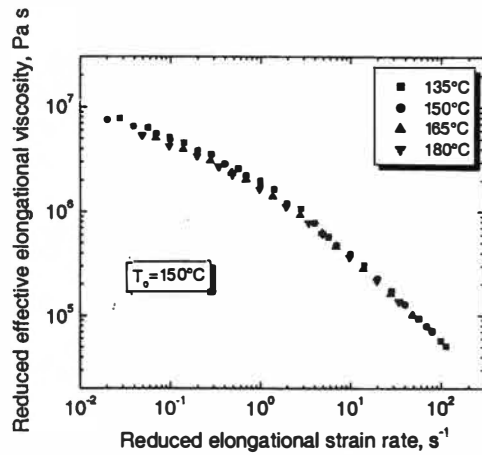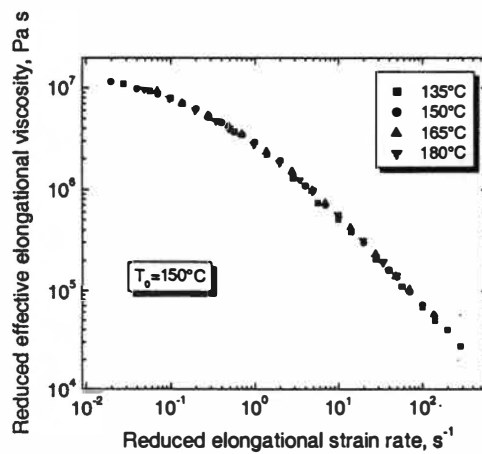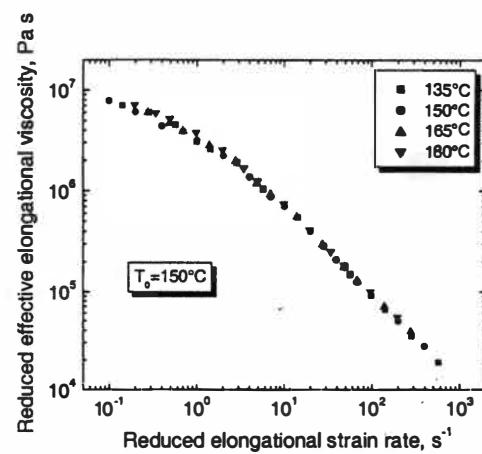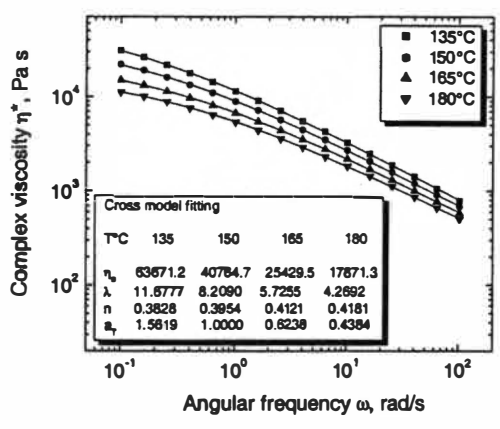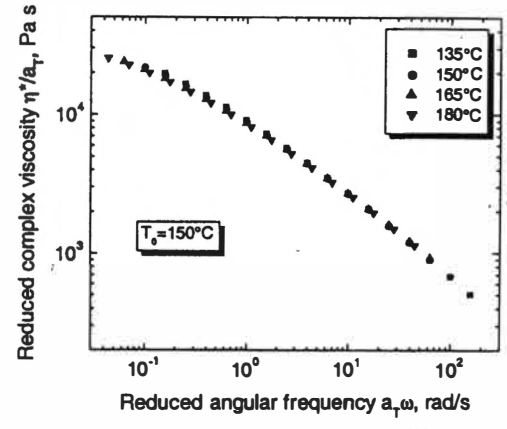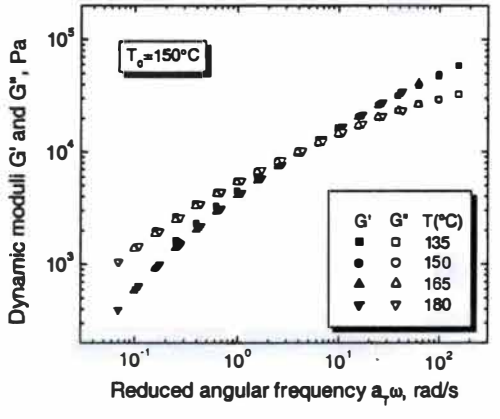
(a) Hencky 4
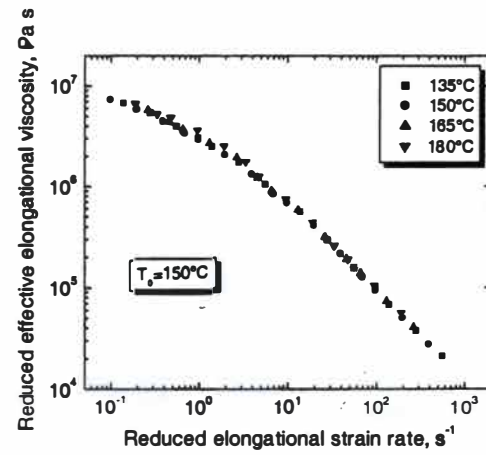
(b) Hencky 5

(c) Hencky 6

(d) Hencky 7

Figure 5.20. Temperature master curves of effective elongational viscosity of PE-1 at different Hencky strains using Carreau model.
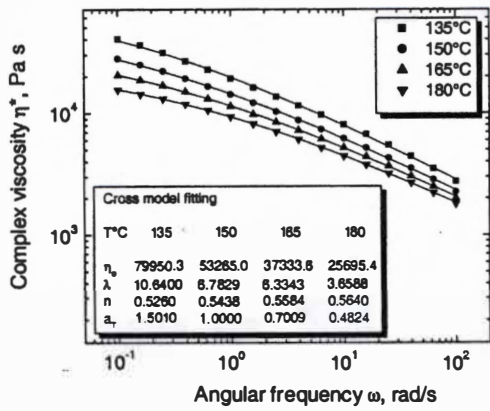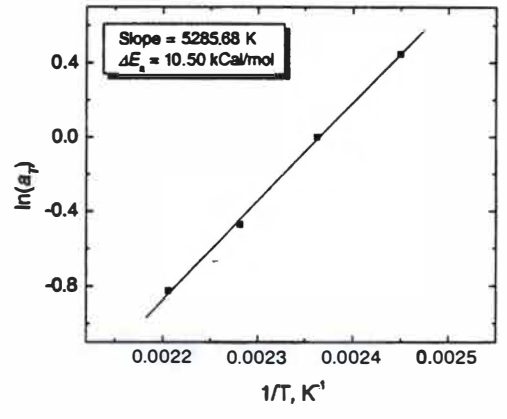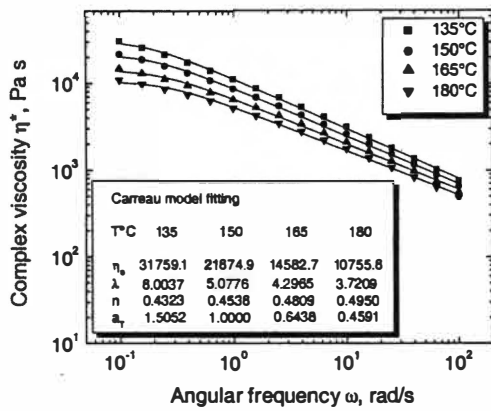
(a) Original curves
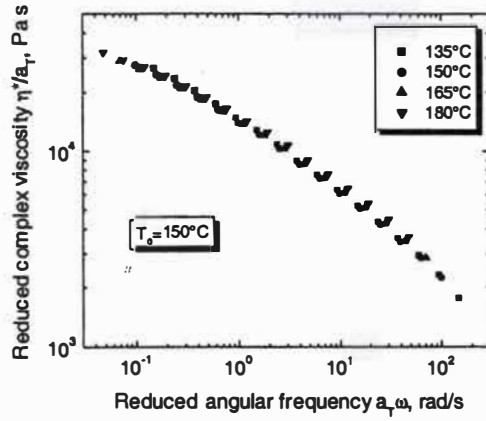
(b) Master curve for η^*
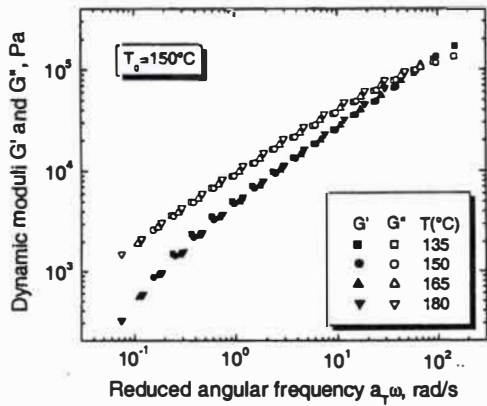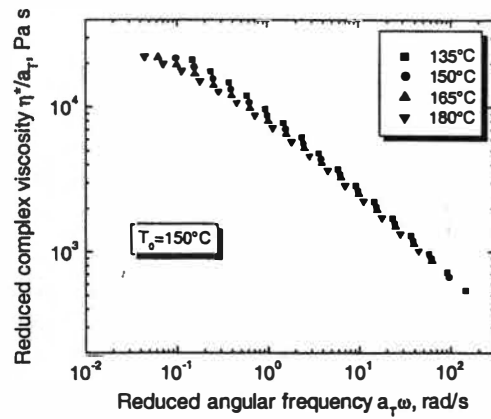
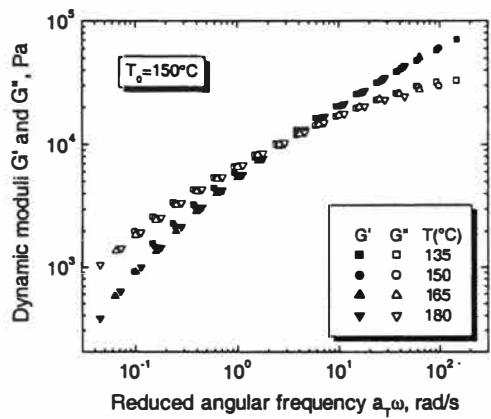(c) Master curves for G' & G''
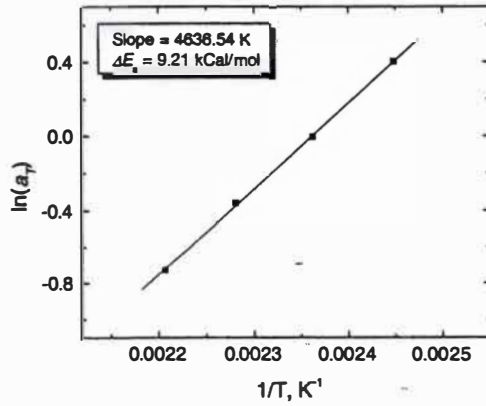
(d) $ln(a_T)$ vs. $1/T$

Figure 5.21. Temperature shifting of shear rheology data of PE-2 using Cross model.
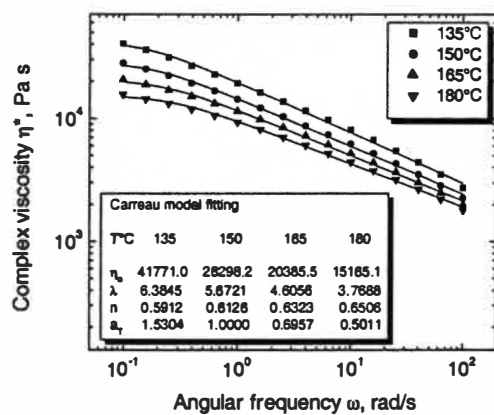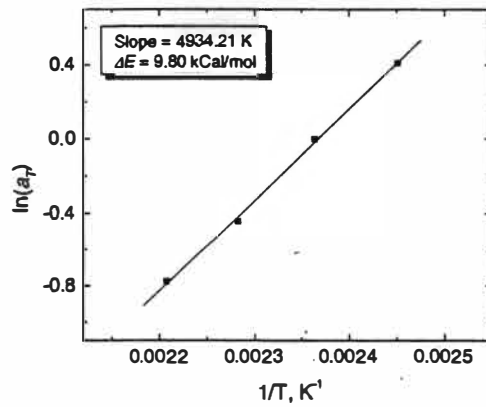
(a) Original curves
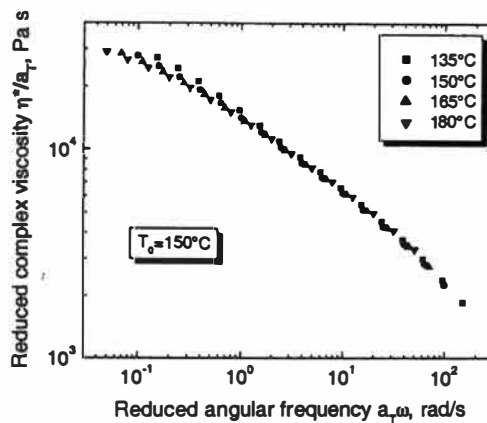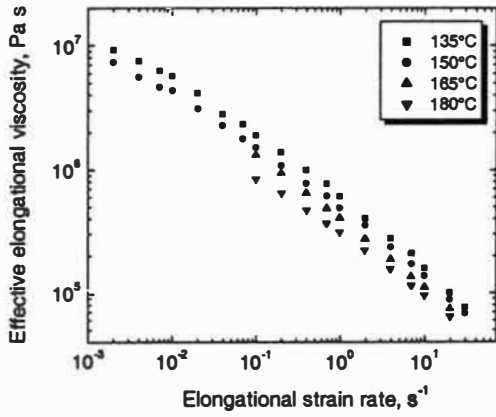
(b) Master curve for η^*
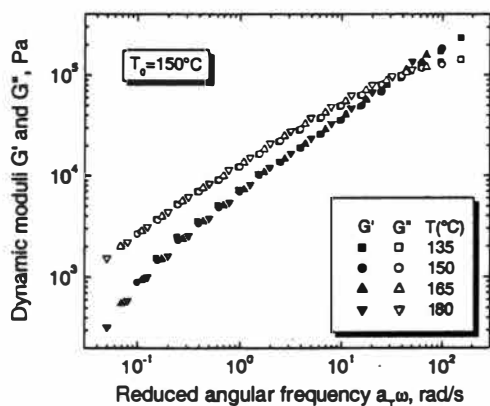
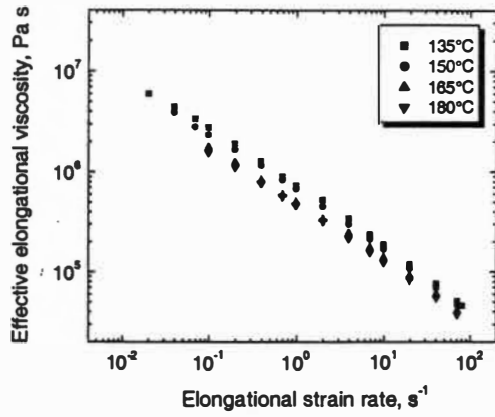(c) Master curves for G' & G"
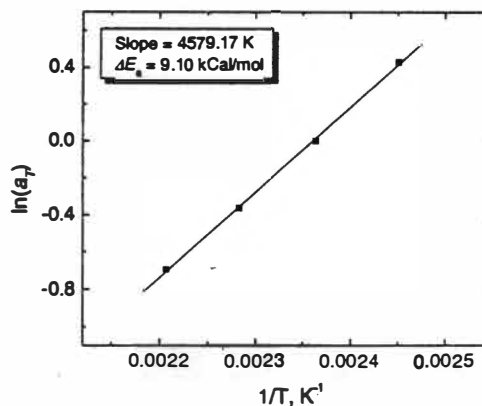
·(d) $ln(a_T)$ vs. $1/T$

Figure 5.22. Temperature shifting of shear rheology data of PE-2 using Carreau model.
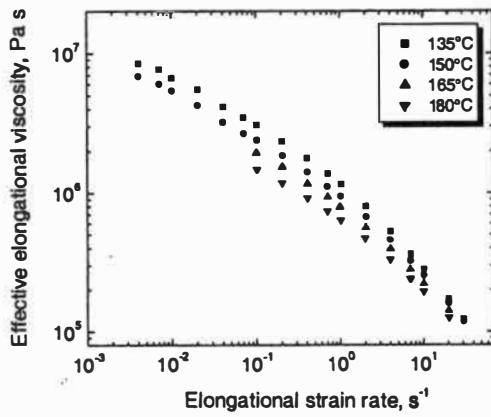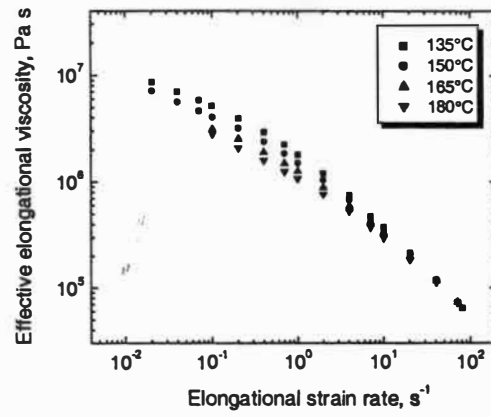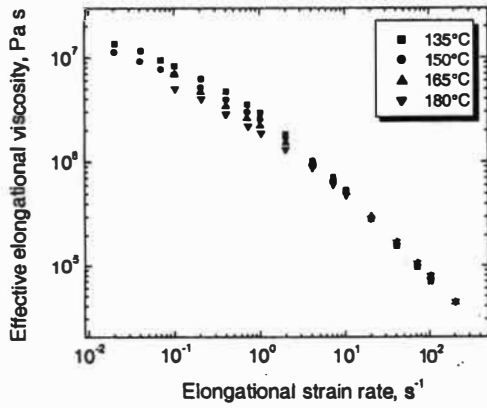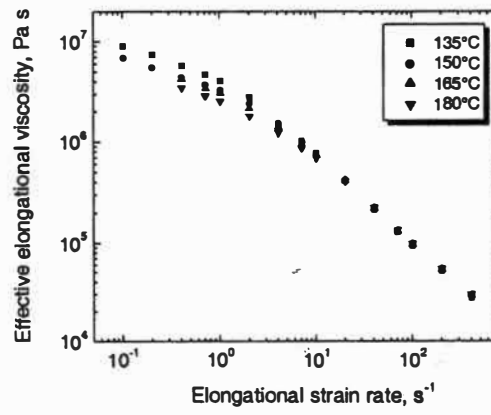
Figure 5.23. Effect of temperature on effective elongational viscosity of PE-2 at different Hencky strains.
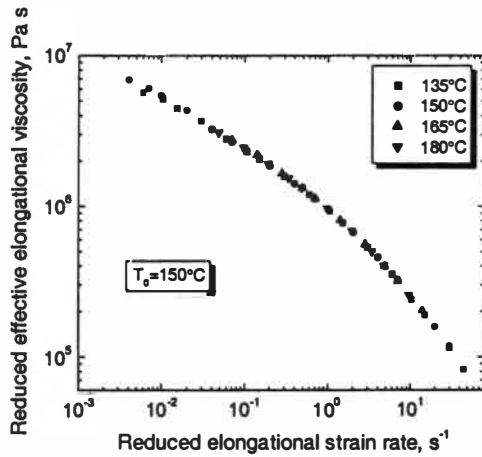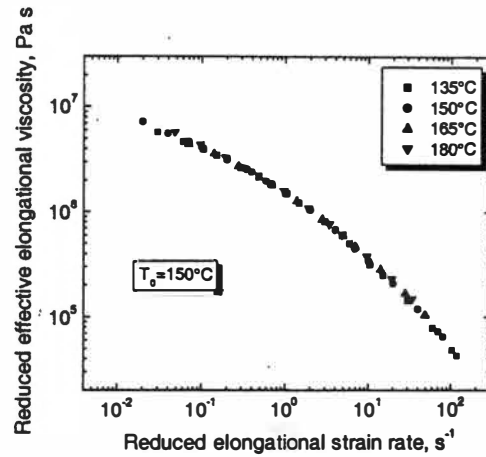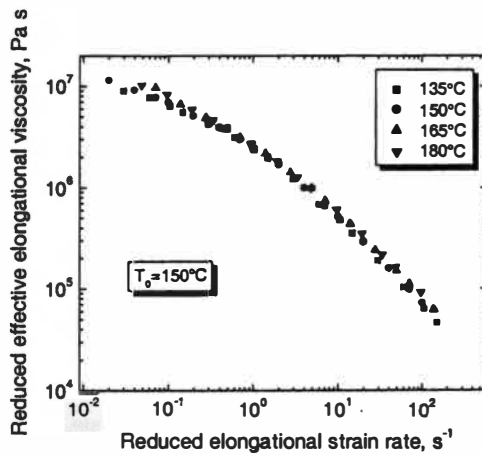
(a) Hencky 4
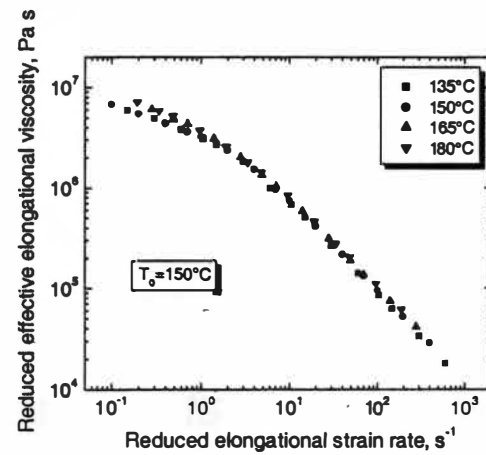
(b) Hencky 5

(c) Hencky 6

(d) Hencky 7

Figure 5.24. Temperature master curves of effective elongational viscosity of PE-2 at different Hencky strains using Cross model.
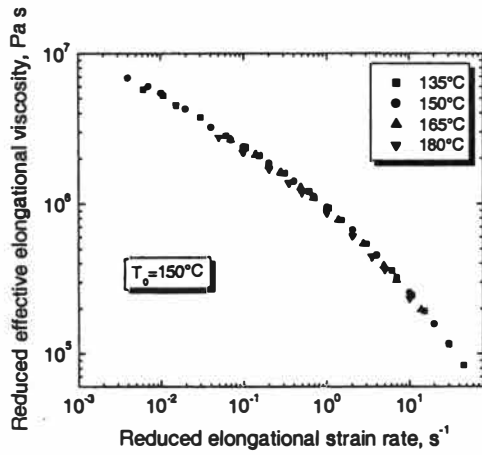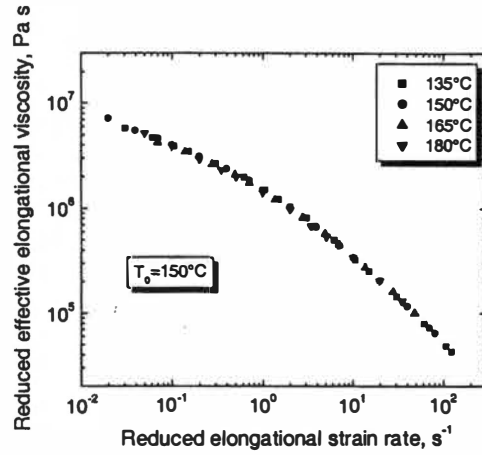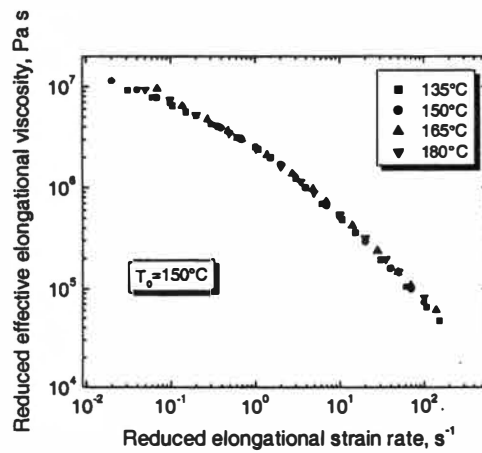
(a) Hencky 4
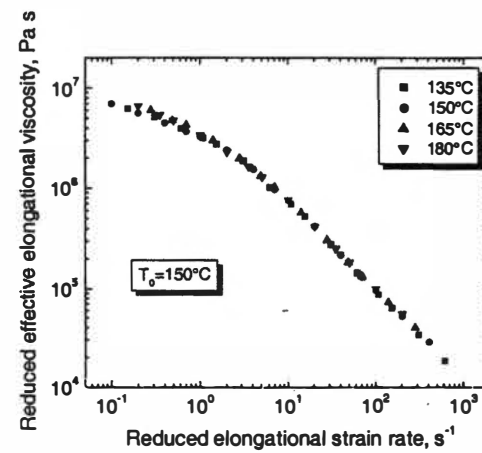
(b) Hencky 5

(c) Hencky 6

(d) Hencky 7

Figure 5.25. Temperature master curves of effective elongational viscosity of PE-2 at different Hencky strains using Carreau model.
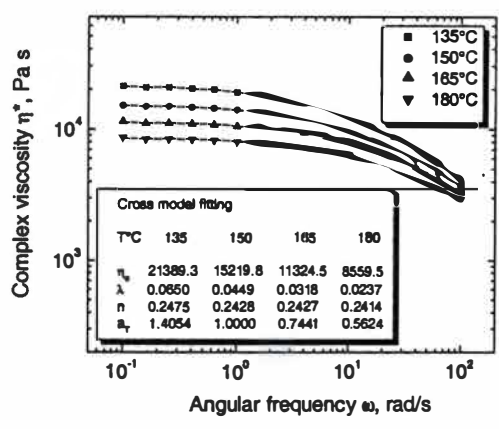
(a) Original curves
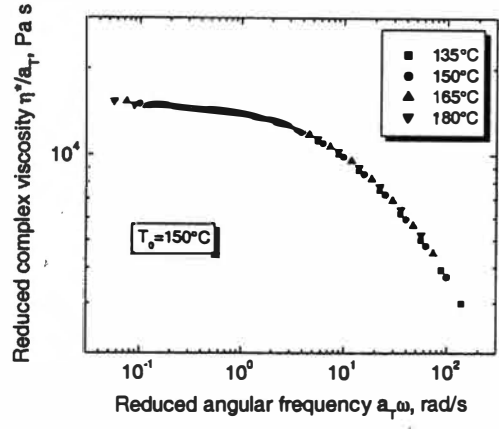
(b) Master curve for η^*
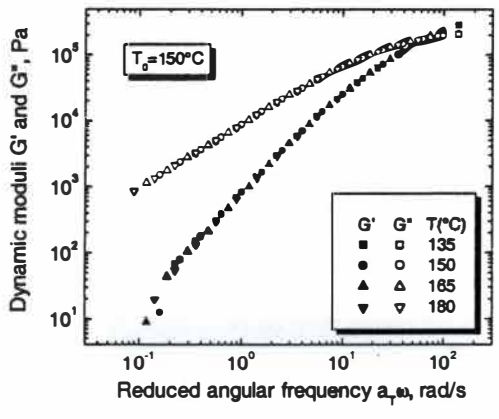
(c) Master curves for G'& G"
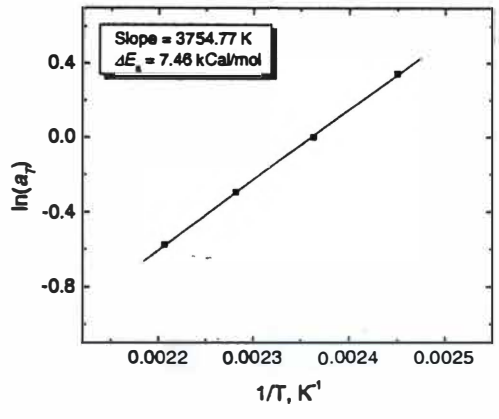
(d) $ln(a_T)$ vs. $1/T$

Figure 5.26. Temperature shifting of shear rheology data of PE-3 using Cross model.

93
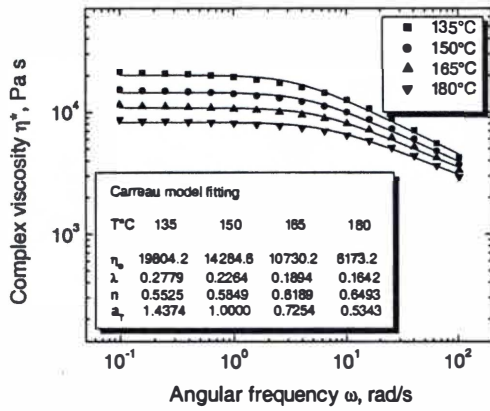
(a) Original curves
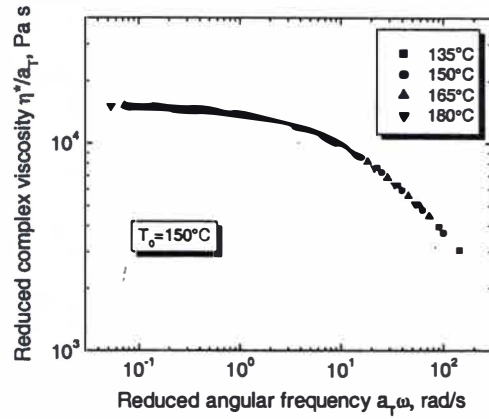
(b) Master curve for η^*
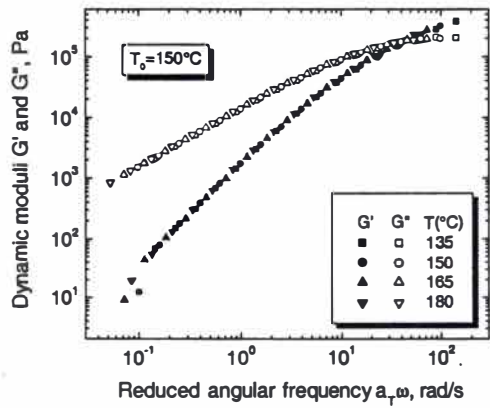
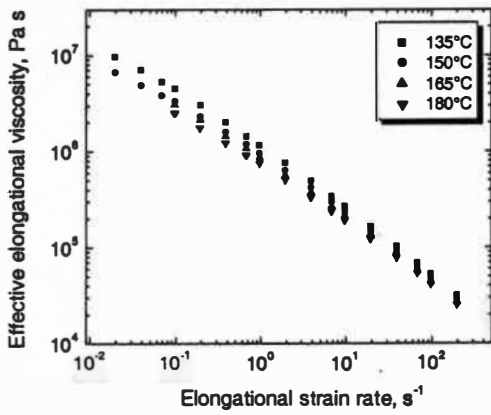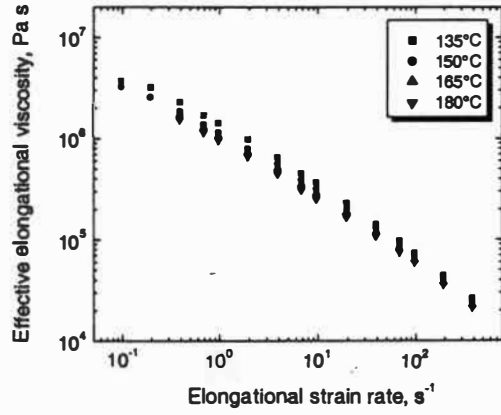(c) Master curves for G' & G"
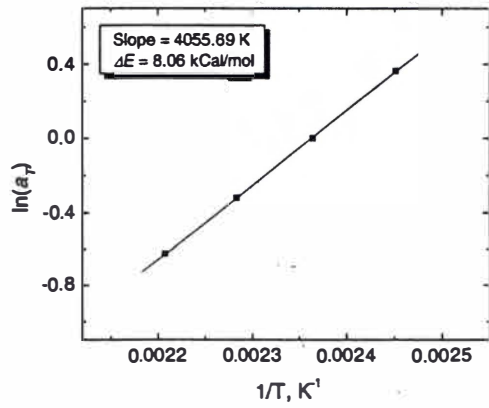
(d) $ln(a_T)$ vs. $1/T$

Figure 5.27. Temperature shifting of shear rheology data of PE-3 using Carreau model.
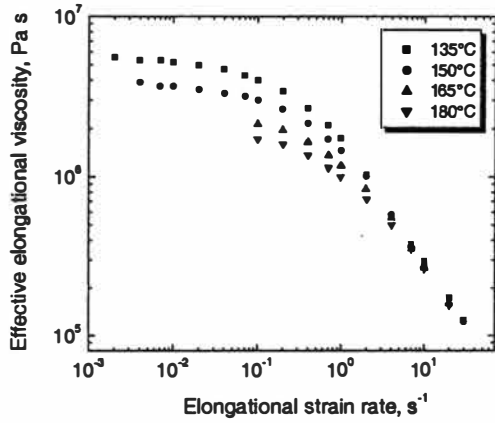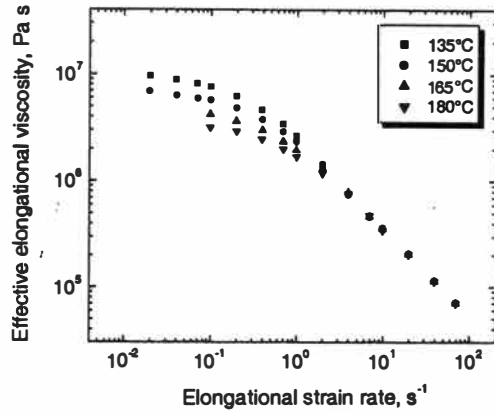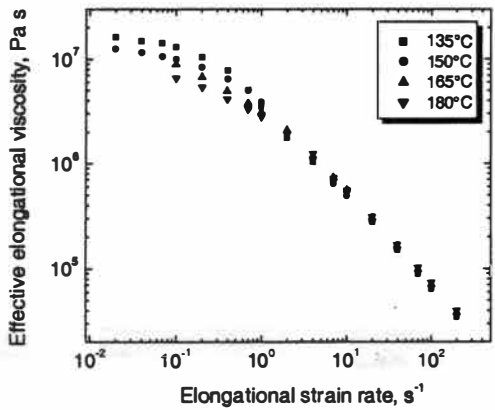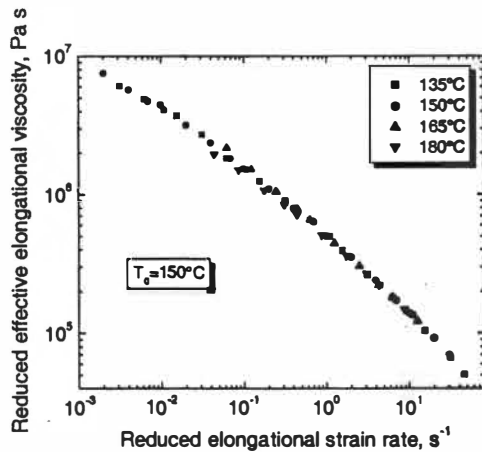
(a) Hencky 4
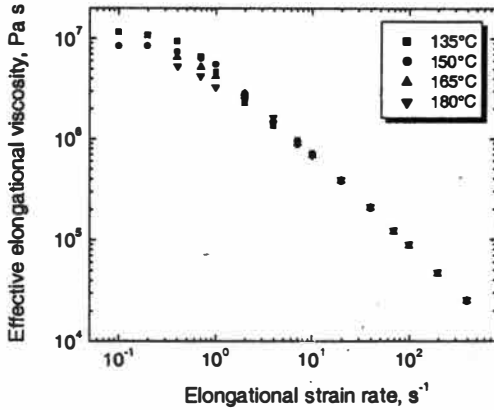
(b) Hencky 5

(c) Hencky 6

(d) Hencky 7

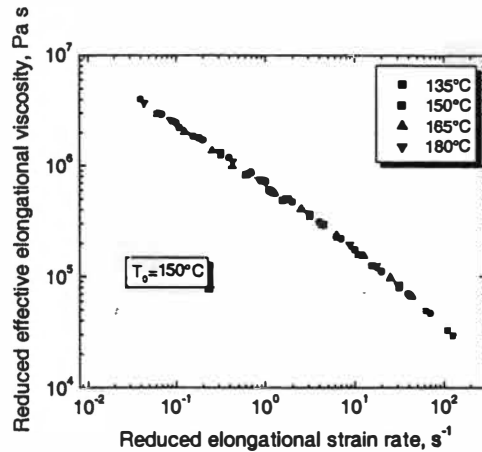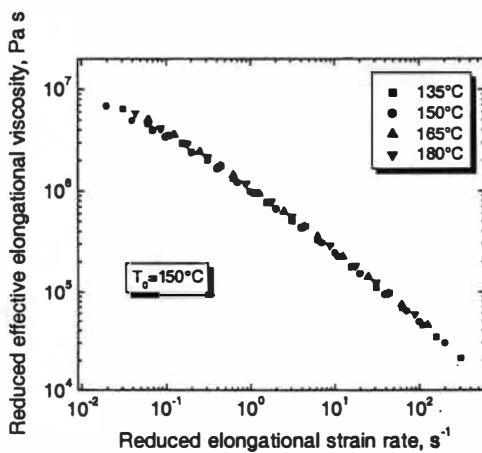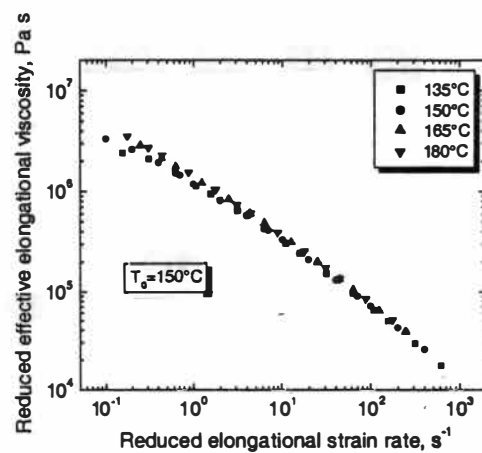**Figure 5.28.** Effect of temperature on effective elongational viscosity of PE-3 at different Hencky strains.
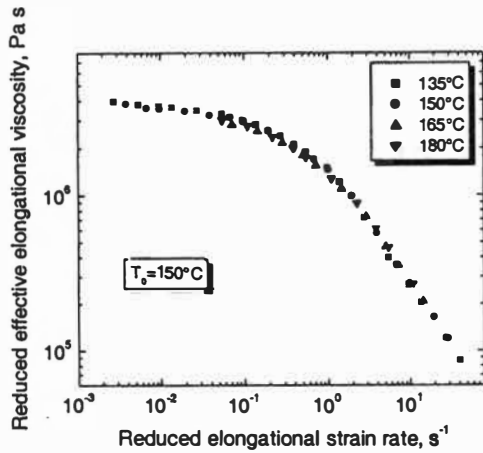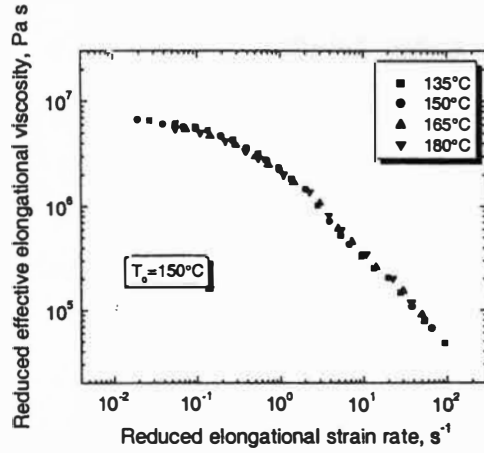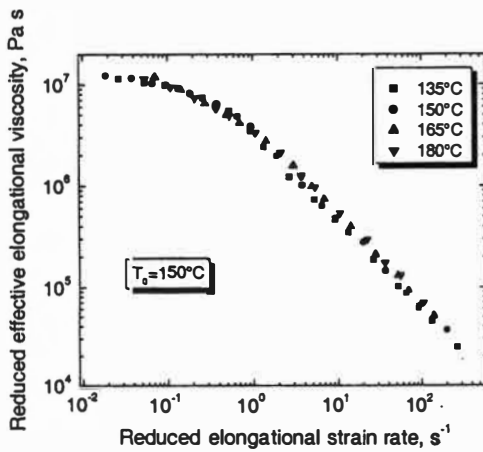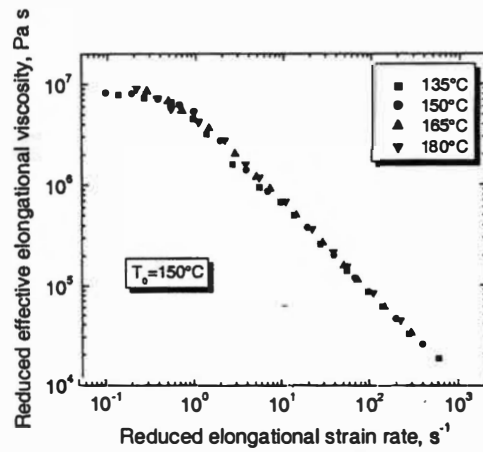
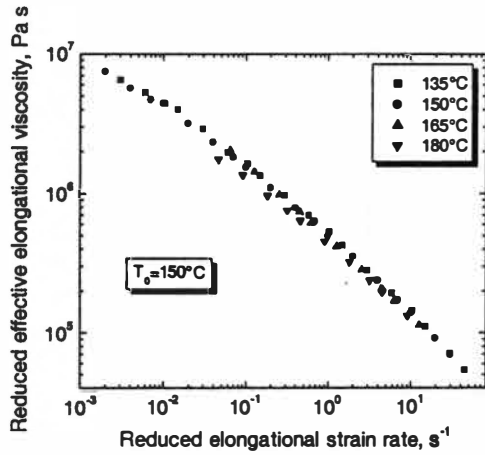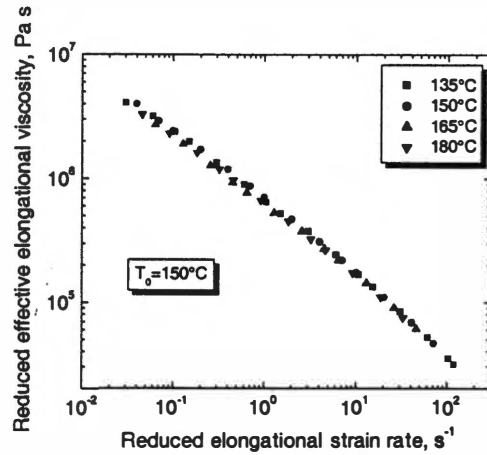**Figure 5.29.** Temperature master curves of effective elongational viscosity of PE-3 at different Hencky strains using Cross model.
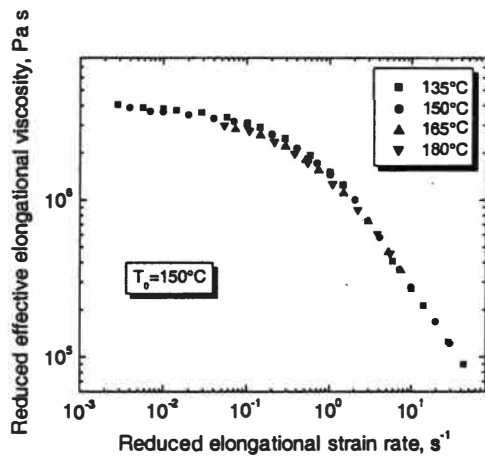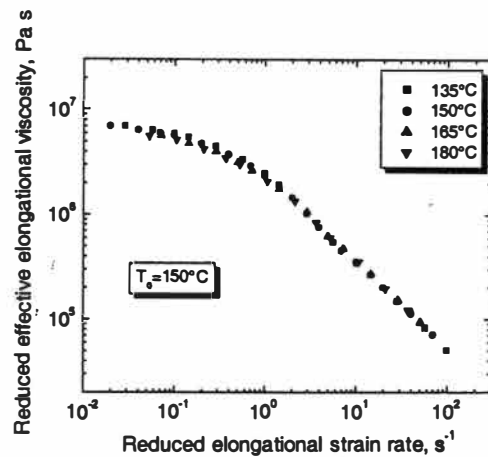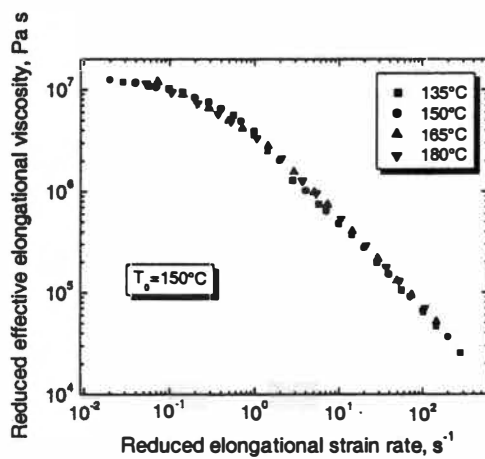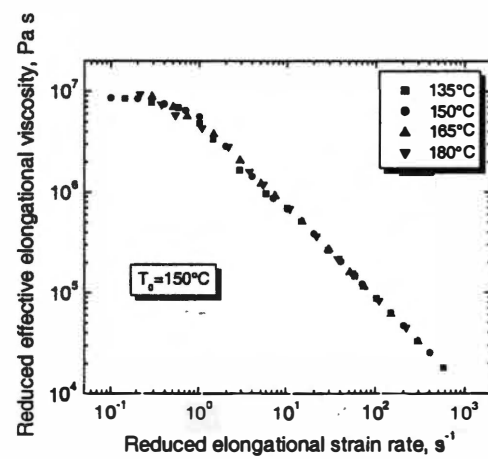
Figure 5.30. Temperature master curves of effective elongational viscosity of PE-3 at different Hencky strains using Carreau model.

97
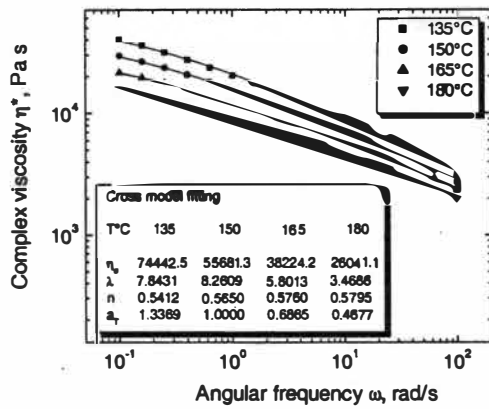
(a) Original curves
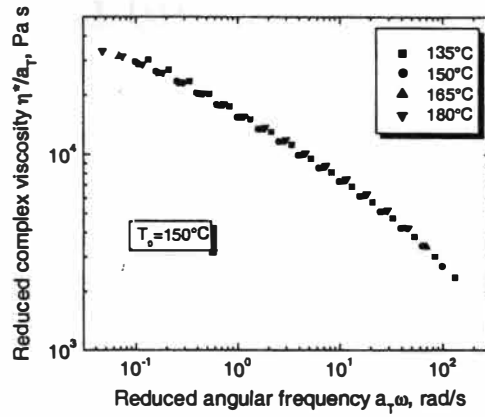
(b) Master curve for η^*
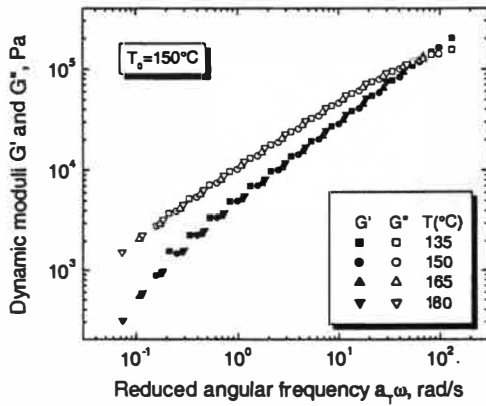
(c) Master curves for G' & G"

(d) $ln(a_T)$ vs. $1/T$

Figure 5.31. Temperature shifting of shear rheology data of PE-4 using Cross model.

(a) Original curves   (b) Master curve for η^*
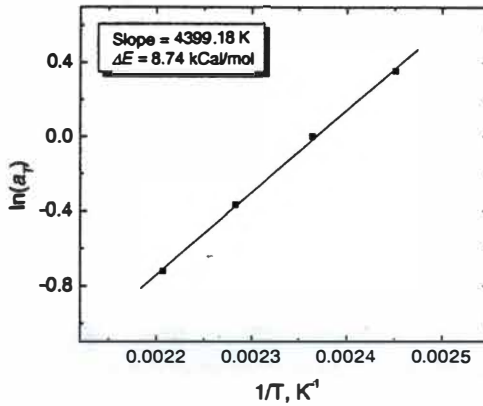
(c) Master curves for G'& G"   (d) $ln(a_T)$ vs. $1/T$

Figure 5.32. Temperature shifting of shear rheology data of PE-4 using Carreau model.

99
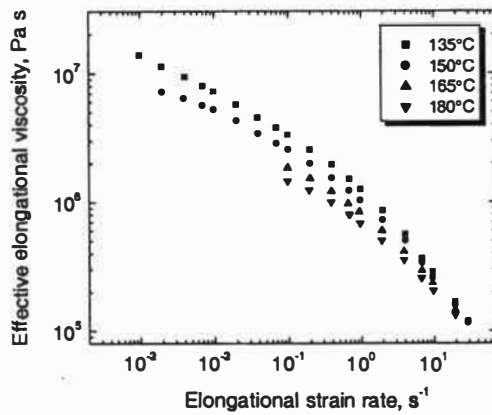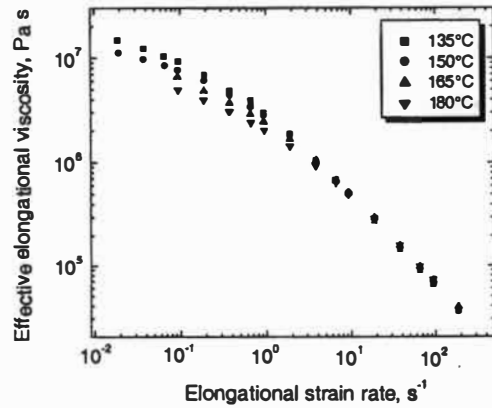
(a) Hencky 4

(b) Hencky 5

(c) Hencky 6

(d) Hencky 7

Figure 5.33. Effect of temperature on effective elongational viscosity of PE-4 at different Hencky strains.
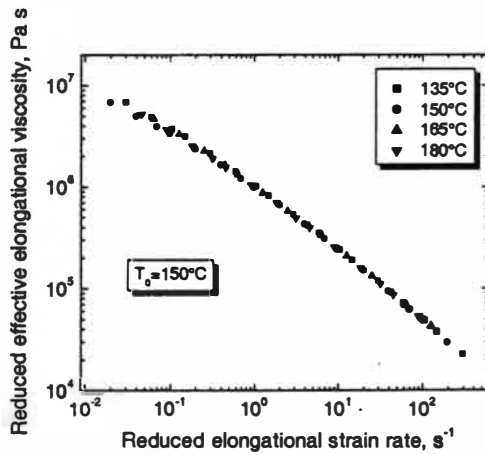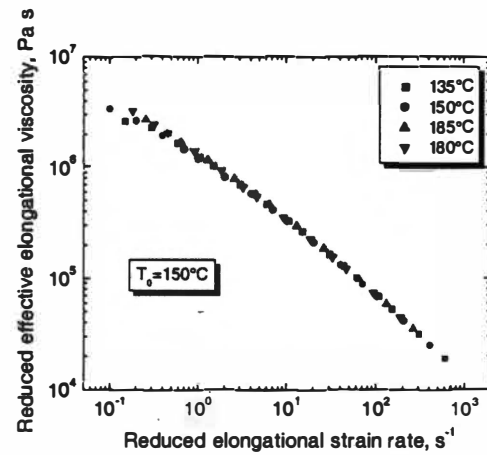
100

(a) Hencky 4

(b) Hencky 5
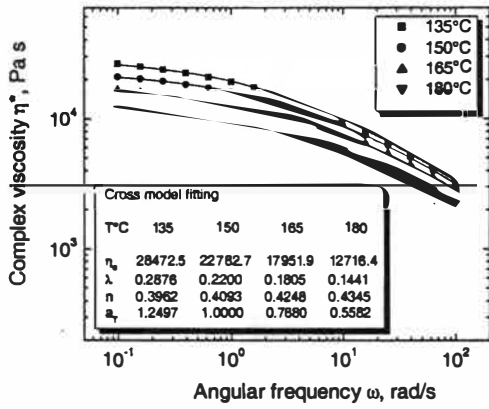
(c) Hencky 6

(d) Hencky 7

Figure 5.34. Temperature master curves of effective elongational viscosity of PE-4 at different Hencky strains using Cross model.
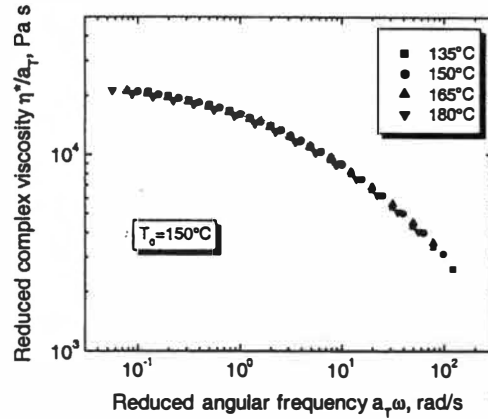
101

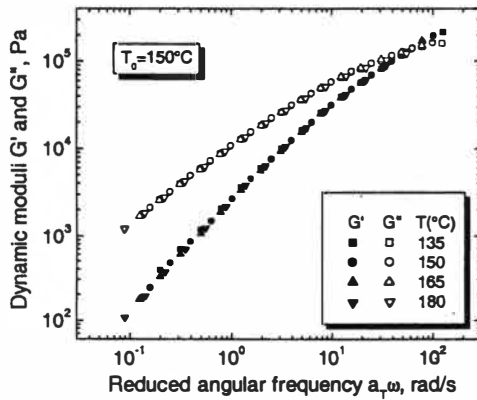(a) Hencky 4

(b) Hencky 5

(c) Hencky 6

(d) Hencky 7

Figure 5.35. Temperature master curves of effective elongational viscosity of PE-4 at different Hencky strains using Carreau model.
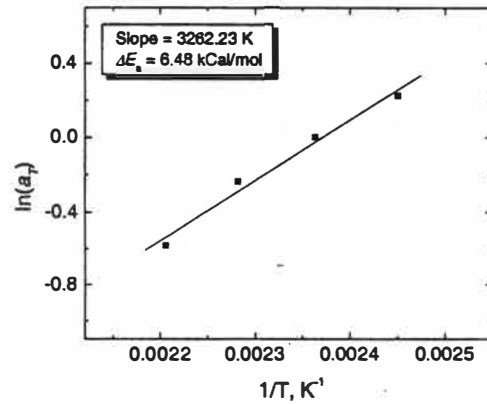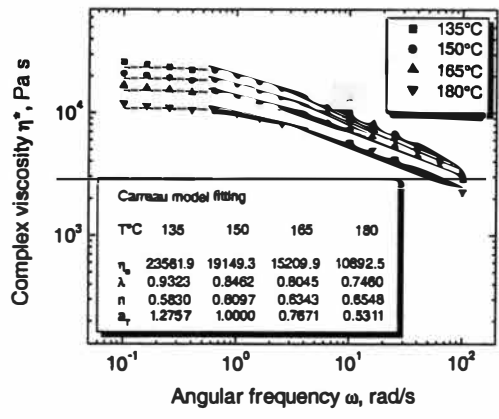
(a) Original curves

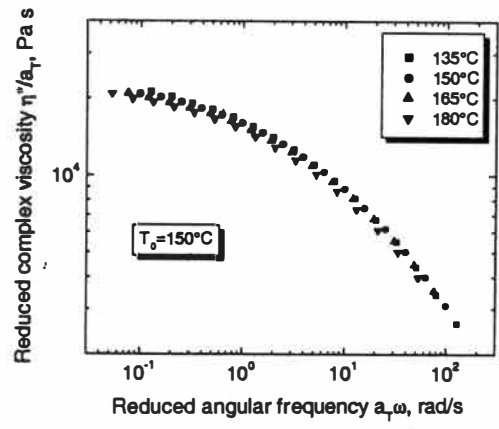(b) Master curve for η^*

(c) Master curves for G'& G"

(d) $ln(a_T)$ vs. $1/T$

Figure 5.36. Temperature shifting of shear rheology data of PE-5 using Cross model.

Carreau model fitting

T°C	135	150	165	180
η_0	31759.1	21874.9	14582.7	10755.8
λ	8.0037	5.0776	4.2965	3.7209
n	0.4323	0.4538	0.4809	0.4950
a_T	1.5052	1.0000	0.6438	0.4591

(a) Original curves

(b) Master curve for η^*
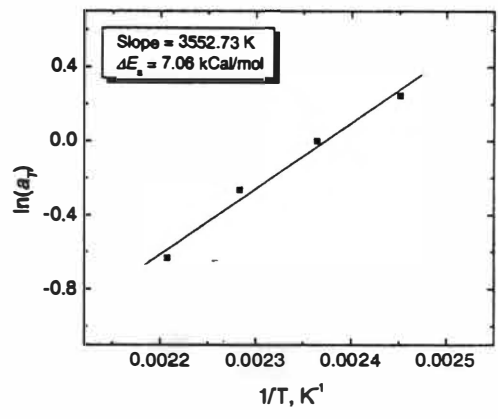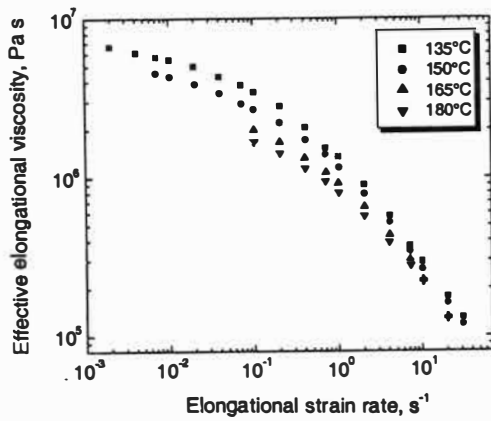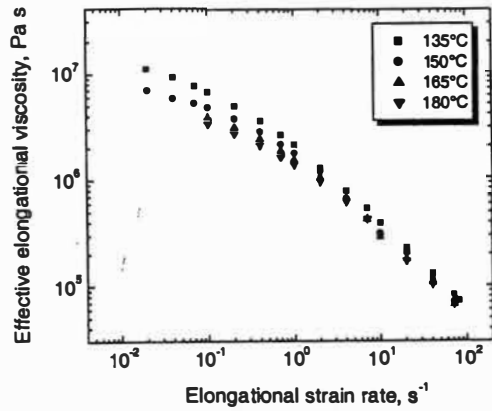
(c) Master curves for G' & G"

(d) $ln(a_T)$ vs. $1/T$

Figure 5.37. Temperature shifting of shear rheology data of PE-5 using Carreau model.

104

Figure 5.38. Effect of temperature on effective elongational viscosity of PE-5 at different Hencky strains.

Figure 5.39. Temperature master curves of effective elongational viscosity of PE-5 at different Hencky strains using Cross model.

(a) Hencky 4

(b) Hencky 5

(c) Hencky 6

(d) Hencky 7

Figure 5.40. Temperature master curves of effective elongational viscosity of PE-5 at different Hencky strains using Carreau model.

(a) Original curves

(b) Master curve for η^*
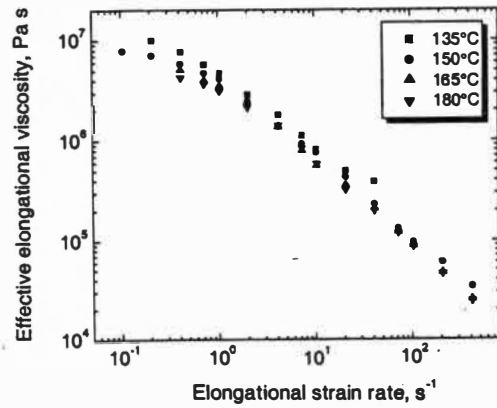
(c) Master curves for G' & G"

(d) $ln(a_T)$ vs. $1/T$

Figure 5.41. Temperature shifting of shear rheology data of PE-6 using Cross model.

(a) Original curves

(b) Master curve for η*
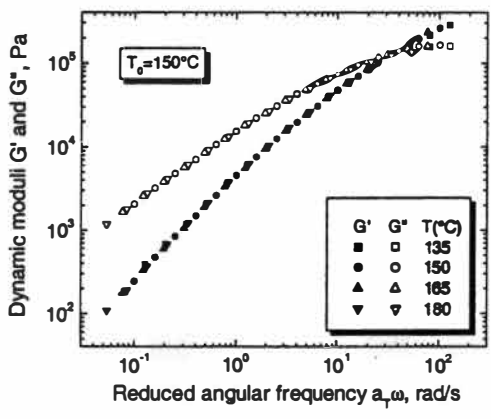
(c) Master curves for G' & G"

(d) $ln(a_T)$ vs. $1/T$

Figure 5.42. Temperature shifting of shear rheology data of PE-6 using Carreau model.
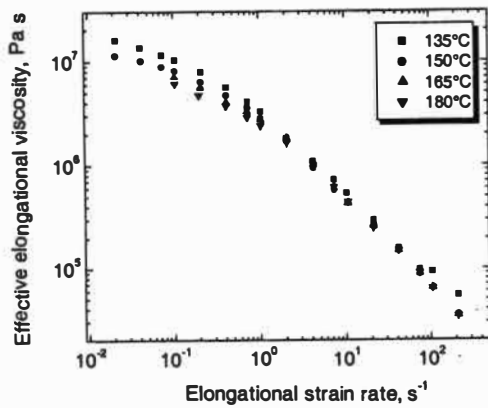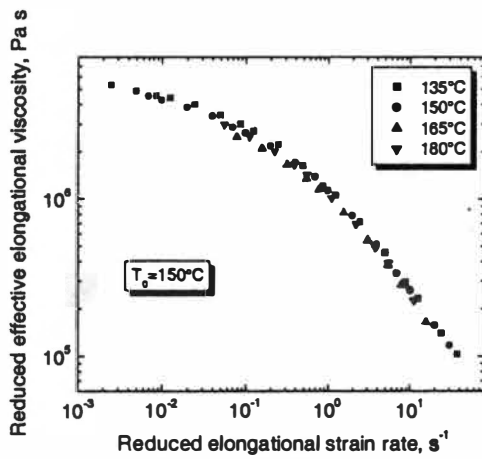
(a) Hencky 4
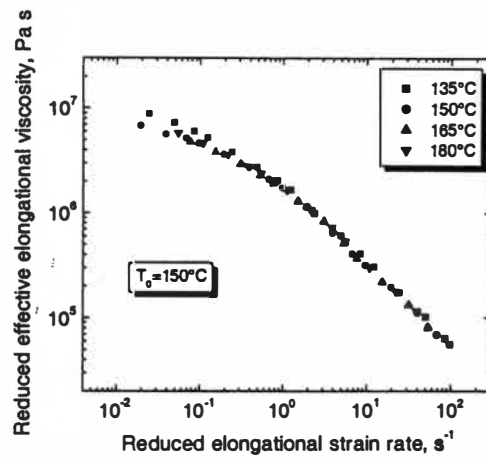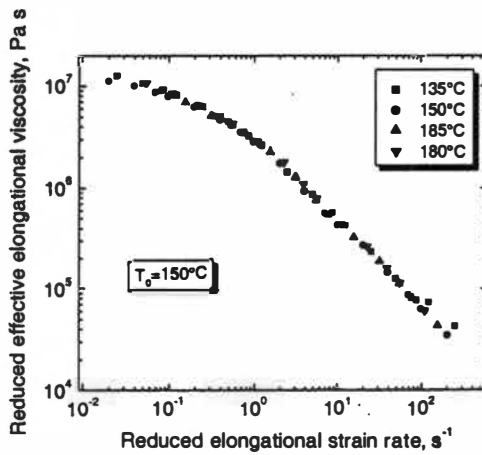
(b) Hencky 5

(c) Hencky 6

(d) Hencky 7

Figure 5.43. Effect of temperature on effective elongational viscosity of PE-6 at different Hencky strains.
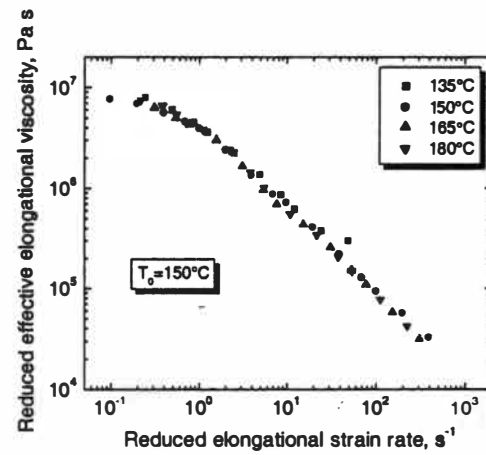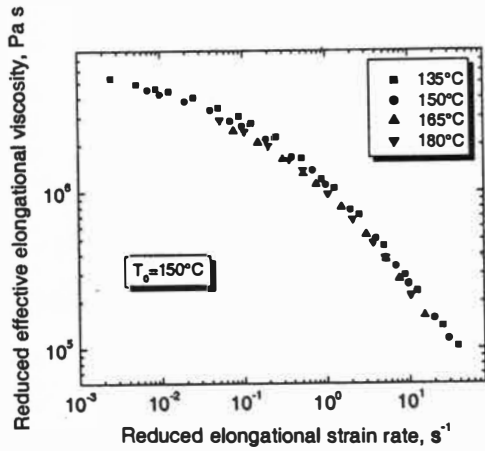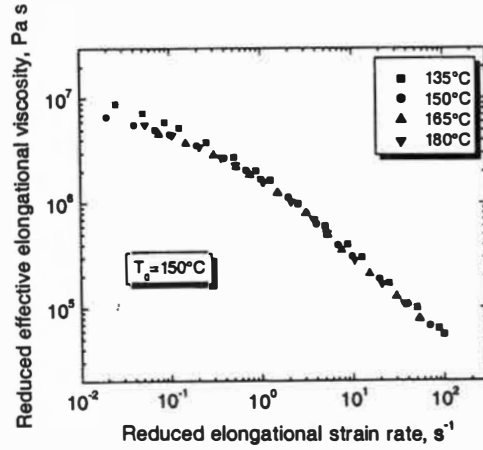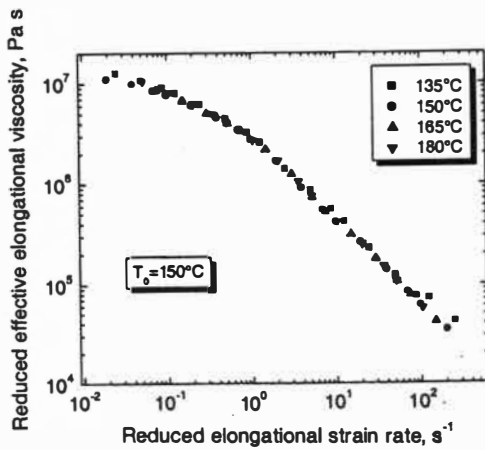
(a) Hencky 4

(b) Hencky 5

(c) Hencky 6

(d) Hencky 7

Figure 5.44. Temperature master curves of effective elongational viscosity of PE-6 at different Hencky strains using Cross model.
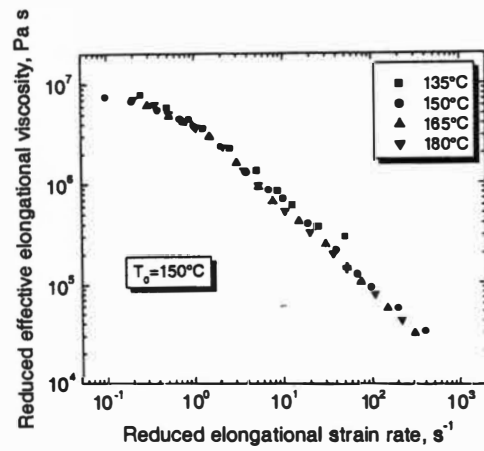
111

Figure 5.45. Temperature master curves of effective elongational viscosity of PE-6 at different Hencky strains using Carreau model.

Table 5.1. Coefficient of determination, R^2, values for the polynomial fits of complex viscosity master curves of PE samples.

Model	PE-1	PE-2	PE-3	PE-4	PE-5	PE-6
Cross	0.9975	0.9968	0.9883	0.9976	0.9994	0.9985
Carreau	0.9983	0.9978	0.9897	0.9969	0.9952	0.9970

Table 5.2. Coefficient of determination, R^2, values for the polynomial fits of temperature master curves of PE samples.

	Coefficient of determination, R^2, at Hencky strain							
	H4		H5		H6		H7	
Sample	Cross	Carreau	Cross	Carreau	Cross	Carreau	Cross	Carreau
PE-1	0.9980	0.9976	0.9976	0.9983	0.9965	0.9983	0.9971	0.9983
PE-2	0.9986	0.9981	0.9992	0.9995	0.9972	0.9988	0.9967	0.9977
PE-3	0.9958	0.9951	0.9959	0.9957	0.9947	0.9954	0.9940	0.9944
PE-4	0.9962	0.9957	0.9991	0.9978	0.9981	0.9989	0.9968	0.9980
PE-5	0.9989	0.9968	0.9990	0.9987	0.9989	0.9995	0.9968	0.9989
PE-6	0.9968	0.9948	0.9964	0.9949	0.9955	0.9949	0.9928	0.9910

the Cross model is chosen for the simultaneous temperature and Hencky strain shifting, and the calculation of enthalpy and entropy changes.

The shift factors show good Arrhenius dependence. From the slope of the Arrhenius plots, the activation energy of flow was calculated for each PE sample. The results are summarized in Table 5.3. Both Cross and Carreau models show that there are no discernable differences between activation energies of PE-1 and PE-4, which is in good agreement with the results shown in the literature (12). In addition,

113

Table 5.3. Molecular data and activation energies of flow for PE samples.

Sample	M_w	PI	LCB* $(1/10^4 C)$	ΔE_a (kCal/mol) Cross	Carreau
PE-1	87,400	2.43	0.57	8.60	8.85
PE-2	88,700	2.14	0.79	9.21	9.10
PE-3	111,000	2.04	N/A**	7.46	8.06
PE-4	115,800	2.12	0.18	8.62	8.74
PE-5	116,000	9.1	***	10.50	9.80
PE-6	122,700	3.44	N/A**	6.48	7.06

*: long chain branches
**: not applicable (PE-3 and PE-6 are linear PE resins with no long chain branches.)
***: not available

both models give the same order of activation energies which is PE-6 < PE-3 < PE-1 ~ PE-4 < PE-2 < PE-5. Conventional LDPE (PE-5) has larger activation energy, whereas linear PEs (PE-3 and PE-6) have smaller activation energies. Hence, the presence of long chain branches increases the flow activation energy of PE, which is also in agreement with data from literature (12, 121-123).

§5.2.1.3 Results on Polyisobutylene Samples

The complex viscosity, storage and loss moduli, and effective elongational viscosity of polyisobutylene were measured at four temperatures, namely 210, 220, 230, and 240°C. The reference temperature was taken as 220°C. These results are

analyzed and presented in Figures 5.46 through 5.50, similar to the PE results.

It is interesting to see that the temperature has a weak effect on the elongational viscosity of the PIB sample (Figure 5.48). Increasing the temperature brings about a slight increase of the mobility of molecular chains. This might be because PIB is a rubber. The dynamic moduli data show that the storage modulus is much higher than the loss modulus on almost the entire range of experimental angular frequency. Hence, the elasticity dominates for PIB sample, as compared with PE samples, where the viscidity dominates.

It can be observed that both Cross and Carreau models yield good master curves for the complex viscosity, dynamic moduli, and effective elongational viscosity of PIB sample. The coefficient of determination (R^2) values for the polynomial fits of complex viscosity and temperature master curves are all larger than 0.9970.

§5.2.2 Hencky Strain Shifting of Effective Elongational Viscosity

§5.2.2.1 *Theoretical Background*

The dependence of the effective elongational viscosity on the Hencky strain, is a result of the orientation developing in the polymeric fluid as it is being attenuated. Two methods (124) have been developed to calculate the Hencky strain shift factors and thus reduced effective elongational viscosity and reduced elongational strain rate. Method 1 is based upon an orientation ratio being equal to the relaxation ratio. The shift factor, reduced effective elongational viscosity, and
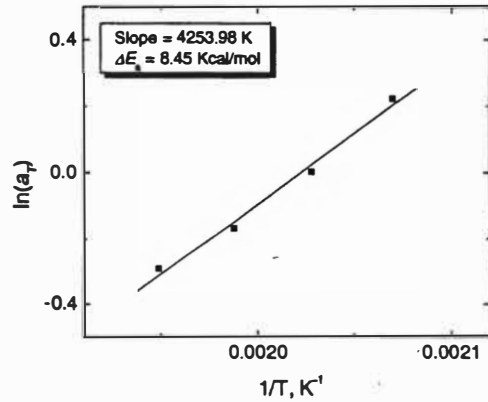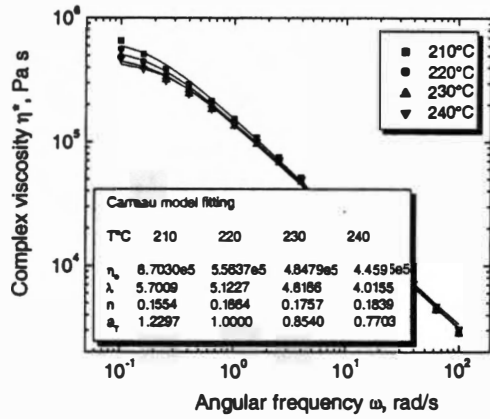
115
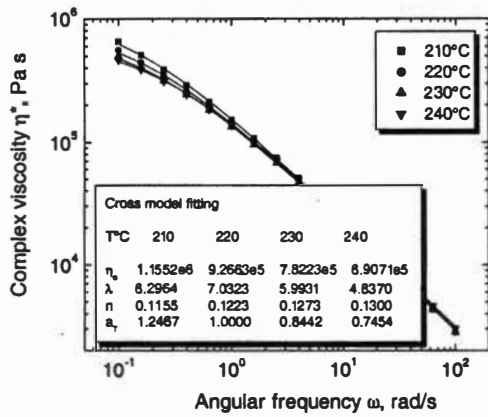
(a) Original curves
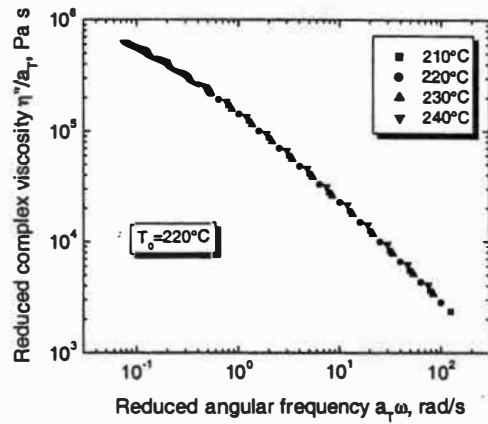
(b) Master curve for η^*
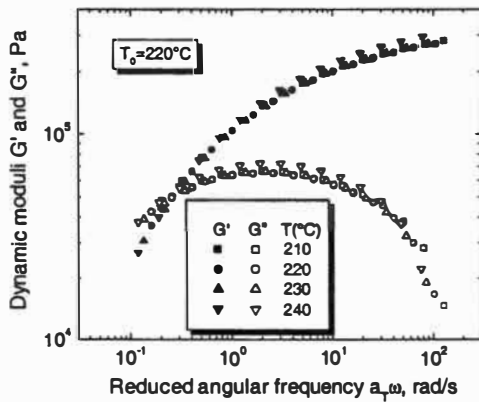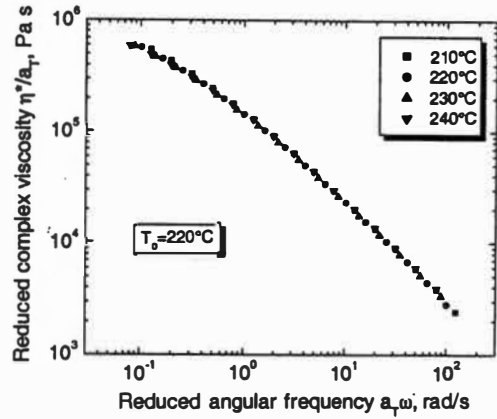
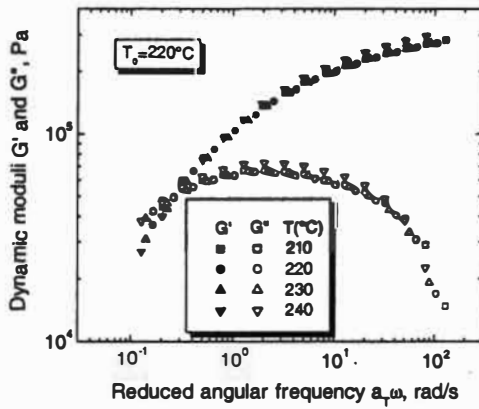(c) Master curves for G' & G"

(d) $ln(a_T)$ vs. $1/T$

Figure 5.46. Temperature shifting of shear rheology data of PIB using Cross model.

116
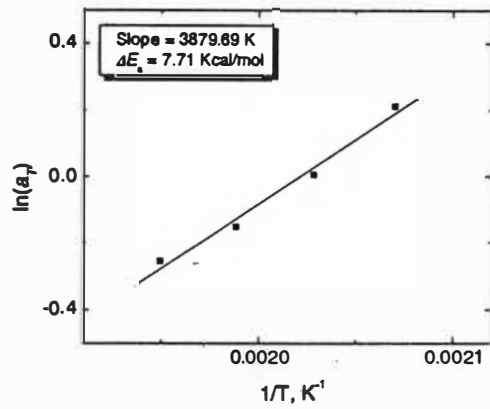
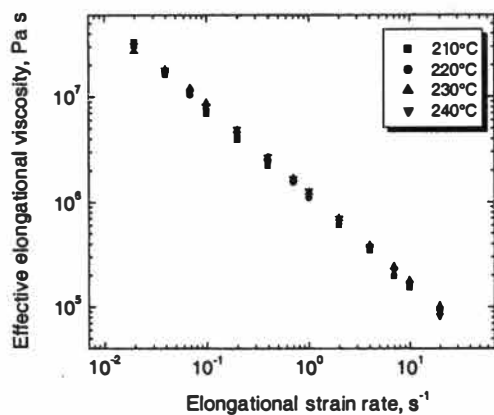(a) Original curves

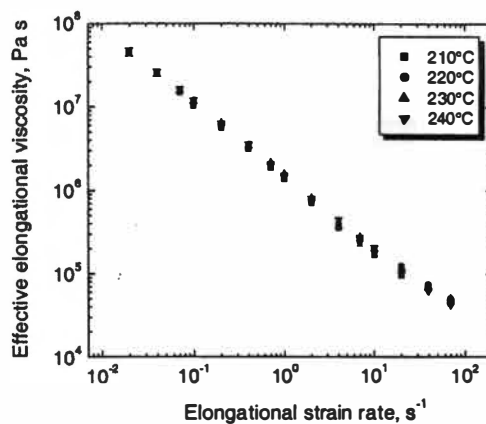(b) Master curve for η^*

(c) Master curves for G'& G"

(d) $ln(a_T)$ vs. $1/T$

Figure 5.47. Temperature shifting of shear rheology data of PIB using Carreau model.
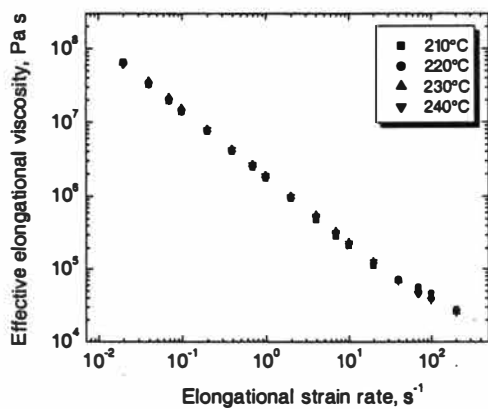
117

Figure 5.48. Effect of temperature on effective elongational viscosity of PIB at different Hencky strains.
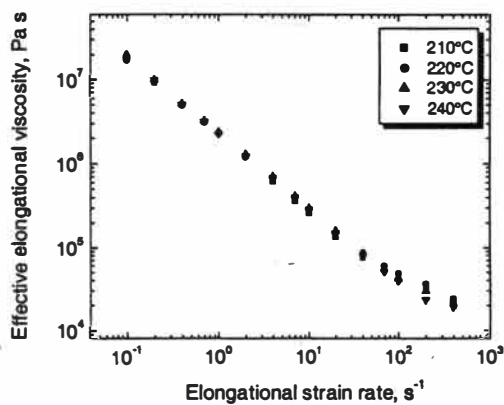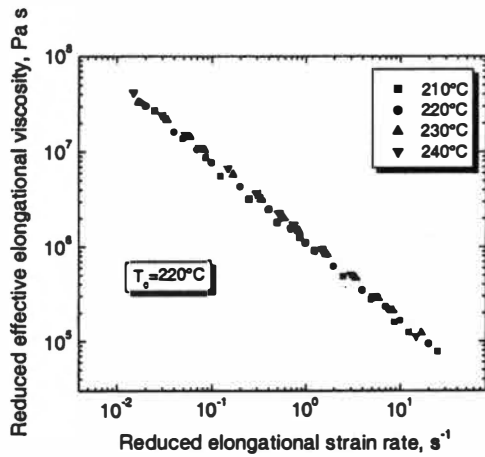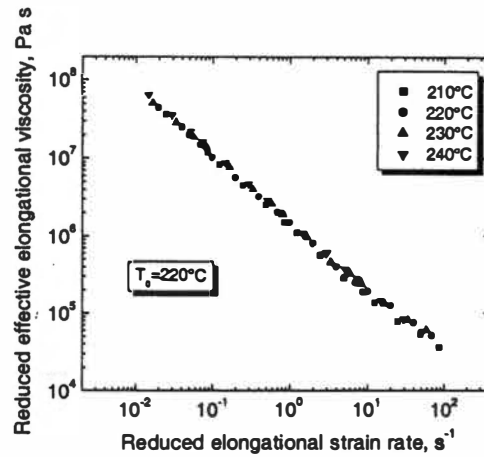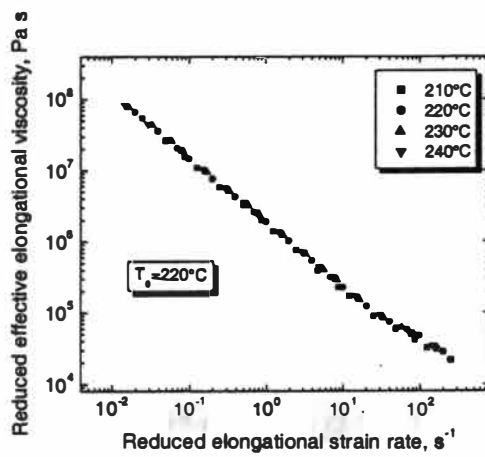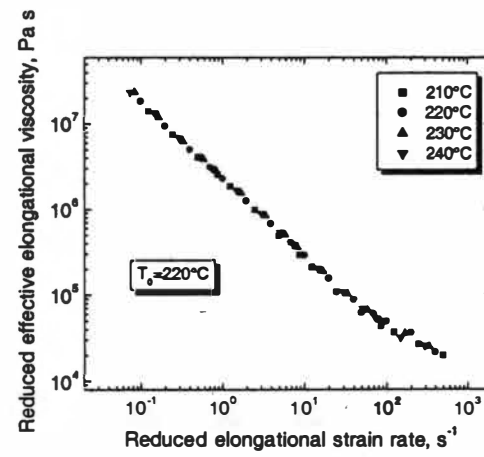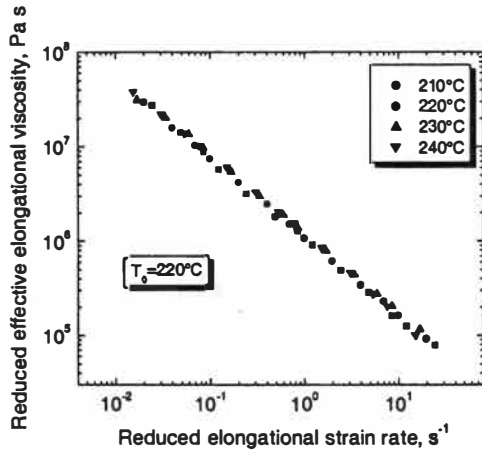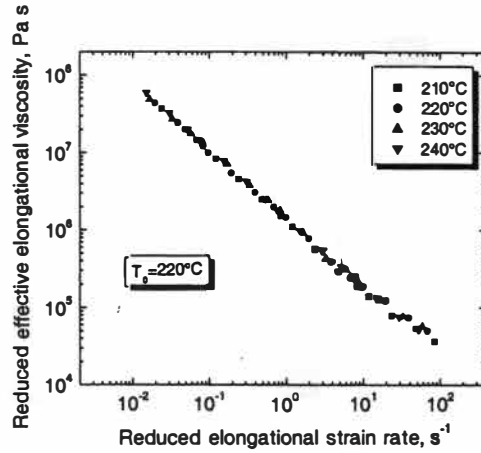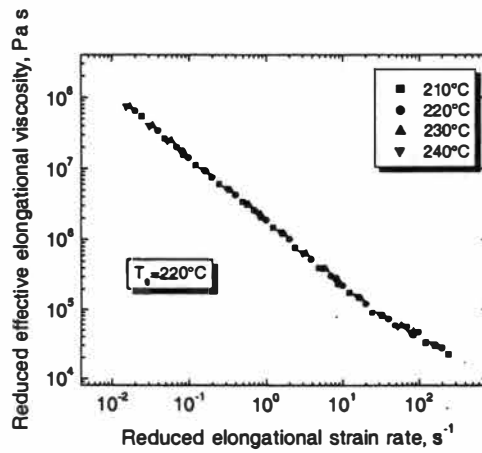
(a) Hencky 4

(b) Hencky 5

(c) Hencky 6

(d) Hencky 7

Figure 5.49. Temperature master curves of effective elongational viscosity of PIB at different Hencky strains using Cross model.
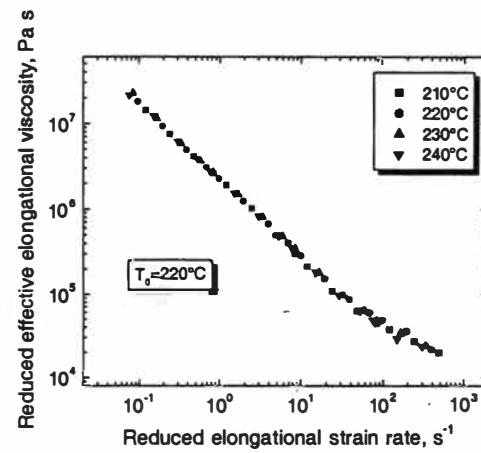
119

Figure 5.50. Temperature master curves of effective elongational viscosity of PIB at different Hencky strains using Carreau model.

reduced elongational strain rate are defined by (124)

$$(a_H)_1 = \frac{[TR-3]\varepsilon_{H_0}}{[TR-3]_0\,\varepsilon_H} \tag{5.8}$$

$$[\eta_{eff}(\dot{\varepsilon},\varepsilon_H)]_{r1} = \frac{\eta_{eff}(\dot{\varepsilon},\varepsilon_H)}{[(a_H)_1]^2} \tag{5.9}$$

$$(\dot{\varepsilon}_r)_1 = (a_H)_1\,\dot{\varepsilon} \tag{5.10}$$

where $(a_H)_1$ is a Hencky strain shift factor defined by Method 1, TR is the effective Trouton ratio, η_{eff}/η_s, η_{eff} and η_s are the effective elongational viscosity and shear viscosity, respectively, ε_H is Hencky strain, and $\dot{\varepsilon}$ is the elongational strain rate. The subscript "0" indicates the value of the variable at the reference state, e.g. the Hencky strain to which the data is being shifted, and the reference shear rate and reference elongational strain rate (for example 1 s^{-1}). Method 2 is based upon an "orientational viscosity ratio". The shift factor, reduced effective elongational viscosity, and reduced elongational strain rate are defined by (124)

$$(a_H)_2 = \frac{\eta_{eff}(\dot{\varepsilon}_0,\varepsilon_H)-3\eta_s}{\eta_{eff}(\dot{\varepsilon}_0,\varepsilon_{H_0})-3\eta_s} \tag{5.11}$$

$$[\eta_{eff}(\dot{\varepsilon},\varepsilon_H)]_{r2} = \eta_{eff}(\dot{\varepsilon},\varepsilon_H)[\frac{\varepsilon_{H_0}}{(a_H)_2\,\varepsilon_H}] \tag{5.12}$$

$$(\dot{\varepsilon}_r)_2 = (a_H)_2\,\dot{\varepsilon} \tag{5.13}$$

Data on the Hencky strain shifting of effective elongational viscosity of the PE and PIB samples are presented in the next two sub-sections.

§5.2.2.2 Results on Polyethylene Samples

The effective elongational viscosity of PE samples was measured at four different temperatures, 135, 150, 165, and 180°C; and at four Hencky strains, 4, 5, 6, and 7 for each temperature. The effect of Hencky strain on the elongational viscosity of PE-1 measured at four different termperatures is shown in Figure 5.51. By increasing the Hencky strain, a higher degree of orientation is imparted to the molecular chains, which results in a higher elongational stress leading to a higher elongational viscosity. The elongational viscosity curves have similar shapes at the different Hencky strains. This similarity provides the basis for the "method of reduced variables", for combining data taken at different Hencky strains into one master curve for the sample.

In order to calculate the shift factors for Hencky strain shifting, the reference Hencky strain was taken as 5. The Cox-Merz rule was assumed to apply to the PE and PIB samples so that the shear viscosity at the shear rate of 1 s^{-1} is equal to the complex viscosity at the angular frequency of 1 rad/s. The reference shear rate (angular frequency) and elongational strain rate were taken as 1 s^{-1}. At each temperature, the effective elongational viscosity curves of PE-1 were shifted to a master curve. These master curves are shown in Figure 5.52 and 5.53 using Method 1 and 2 of Hencky strain shifting mentioned above, respectively. Figures 5.54 through 5.68 show the results of Hencky strain shifting of the remaining PE samples. Both methods seem to fit the data very well for all PE samples except PE-3 at 135°C using Method 1 and PE-5 using Method 1. This is also shown by the coefficient of
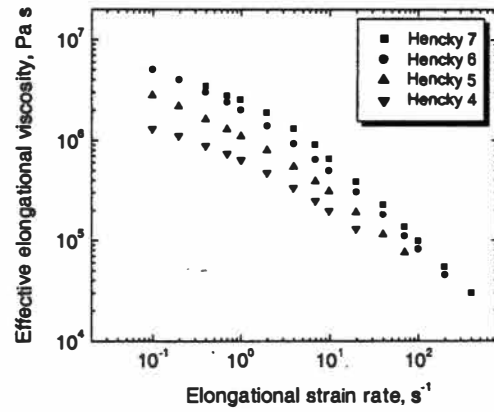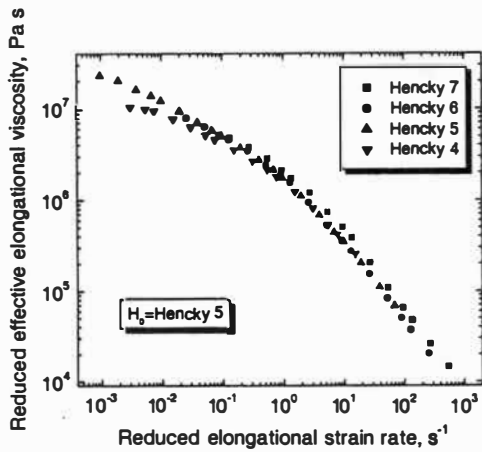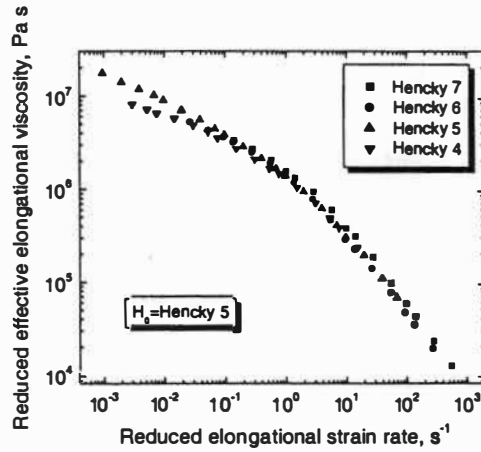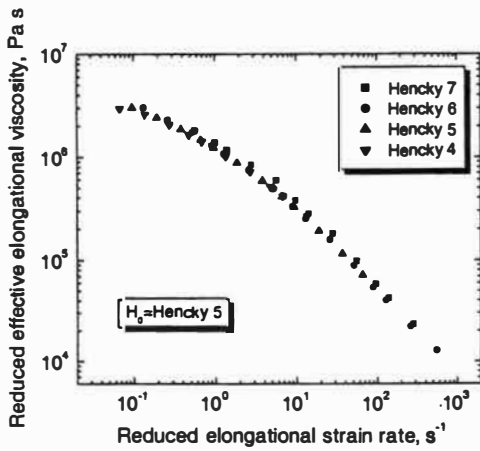
122
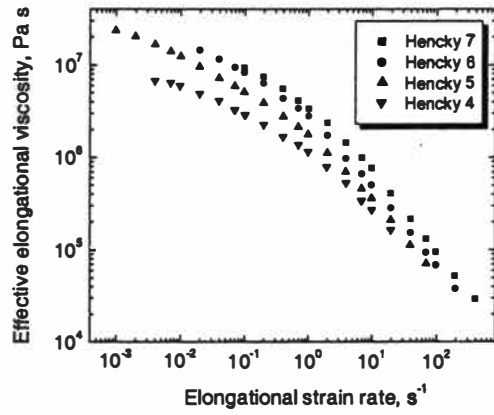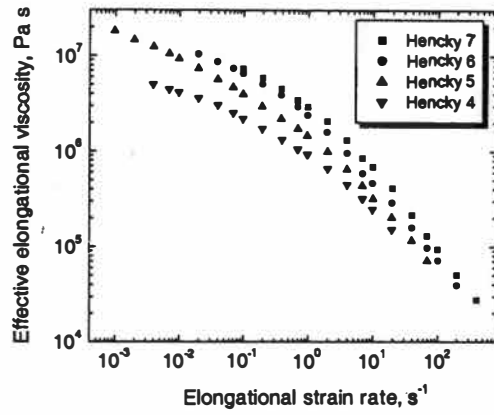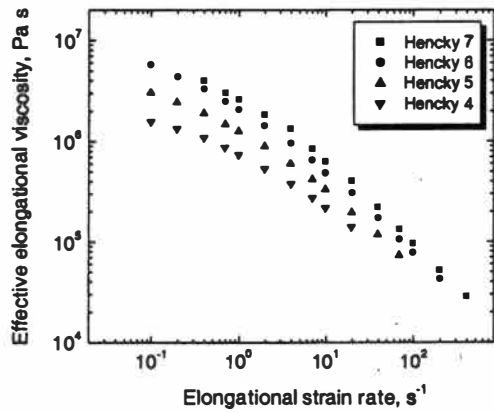
(a) 135°C

(b) 150°C

(c) 165°C

(d) 180°C

Figure 5.51. Effect of Hencky strain on effective elongational viscosity of PE-1 at different temperatures.

Figure 5.52. Hencky strain master curves of effective elongational viscosity of PE-1 at different temperatures created using Method 1.
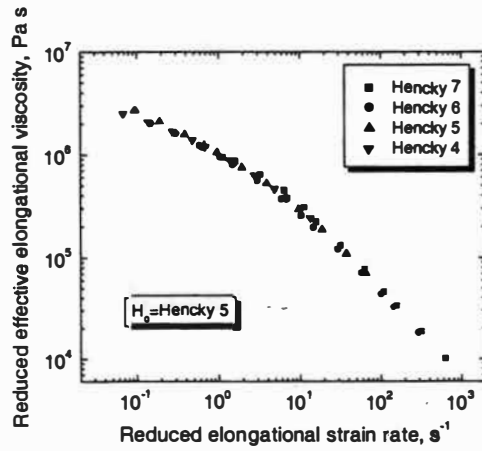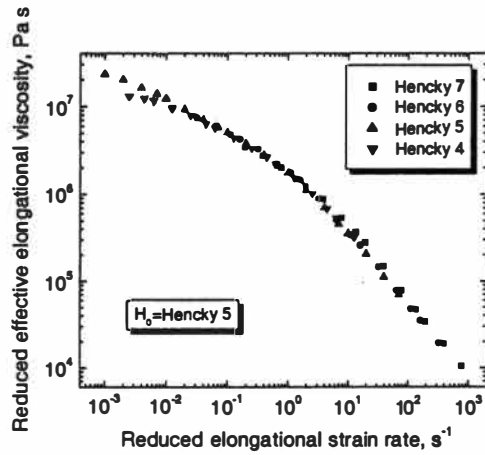
124

(a) 135°C

(b) 150°C

(c) 165°C

(d) 180°C

Figure 5.53. Hencky strain master curves of effective elongational viscosity of PE-1 at different temperatures created using Method 2.

Figure 5.54. Effect of Hencky strain on effective elongational viscosity of PE-2 at different temperatures.

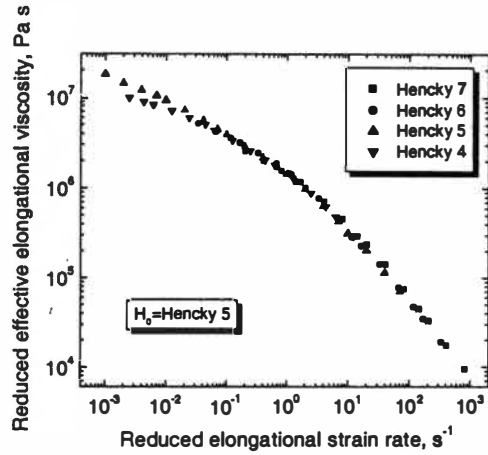**Figure 5.55.** Hencky strain master curves of effective elongational viscosity of PE-2 at different temperatures created using Method 1.

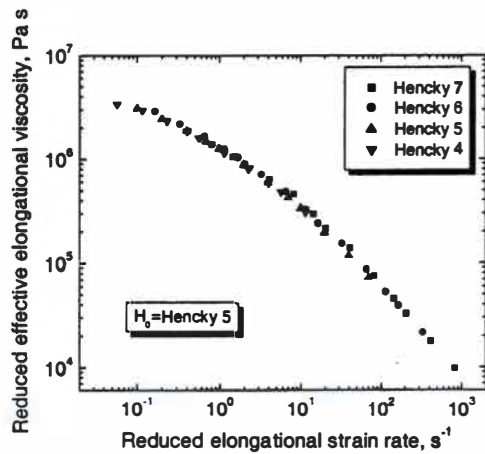**Figure 5.56.** Hencky strain master curves of effective elongational viscosity of PE-2 at different temperatures created using Method 2.

128

Figure 5.57. Effect of Hencky strain on effective elongational viscosity of PE-3 at different temperatures.
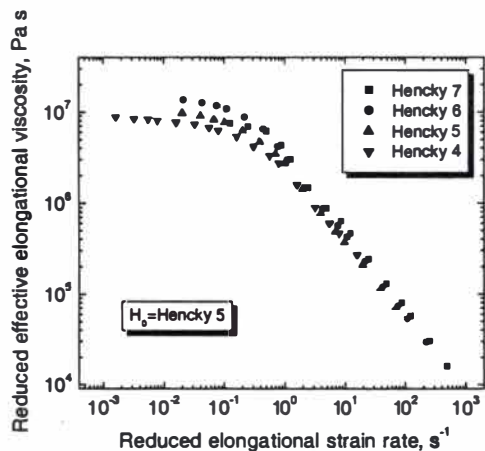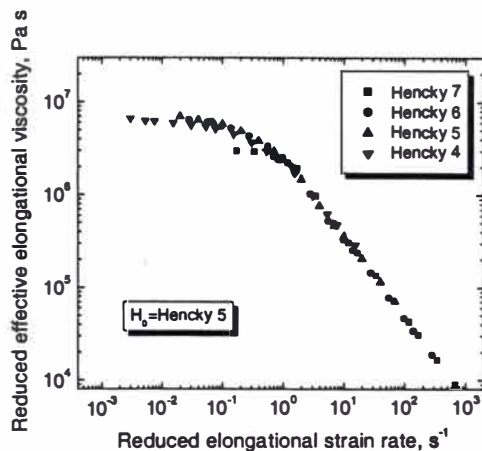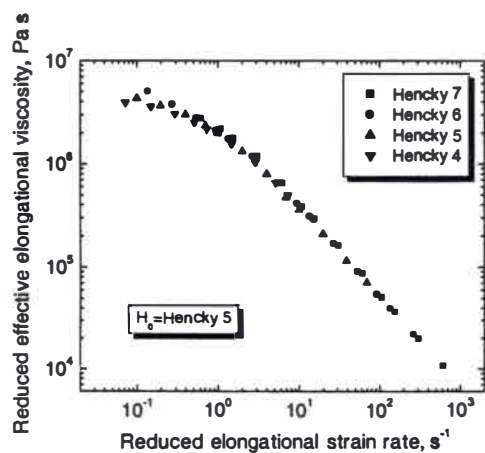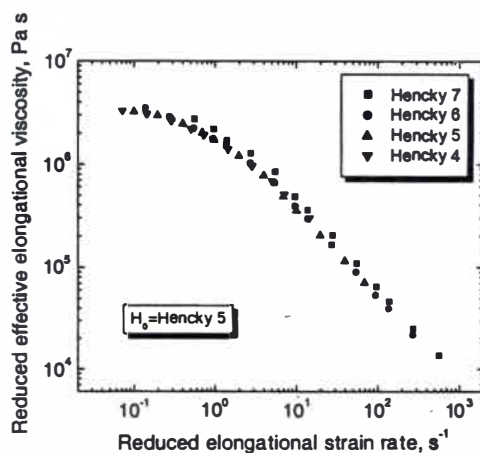
Figure 5.58. Hencky strain master curves of effective elongational viscosity of PE-3 at different temperatures created using Method 1.
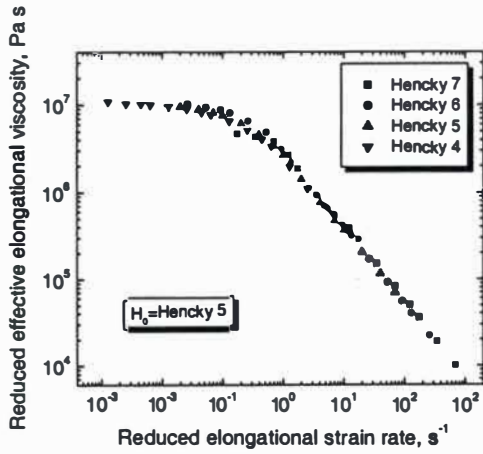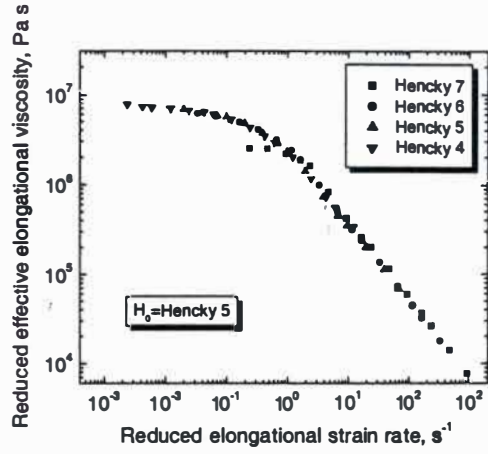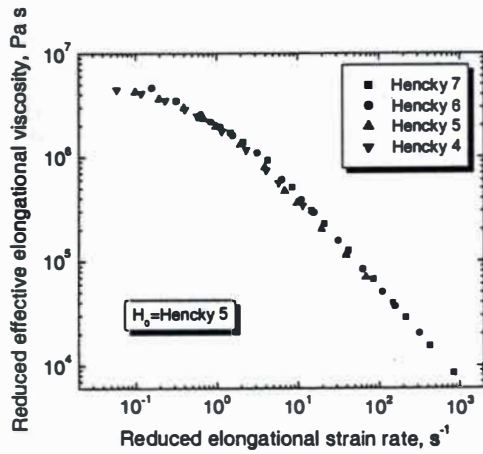
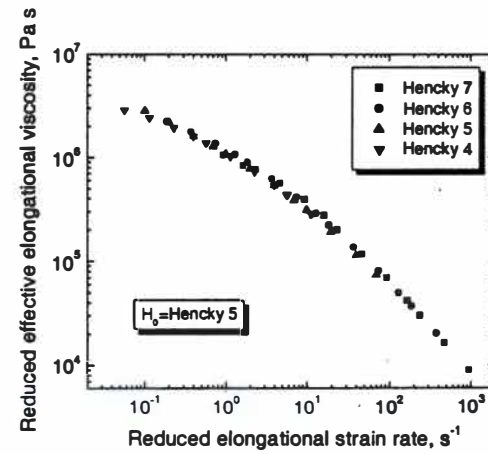**Figure 5.59.** Hencky strain master curves of effective elongational viscosity of PE-3 at different temperatures created using Method 2.

131

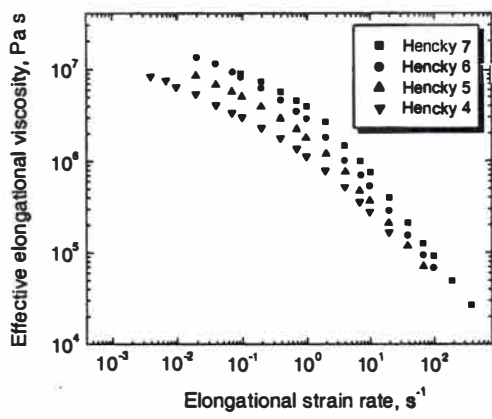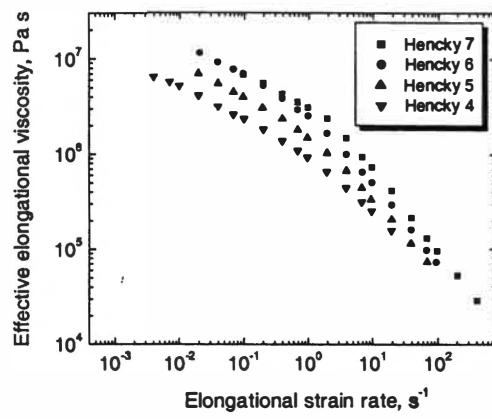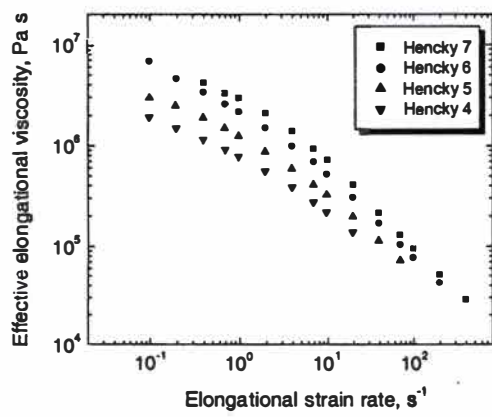**Figure 5.60.** Effect of Hencky strain on effective elongational viscosity of PE-4 at different temperatures.

132

Figure 5.61. Hencky strain master curves of effective elongational viscosity of PE-4 at different temperatures created using Method 1.

133
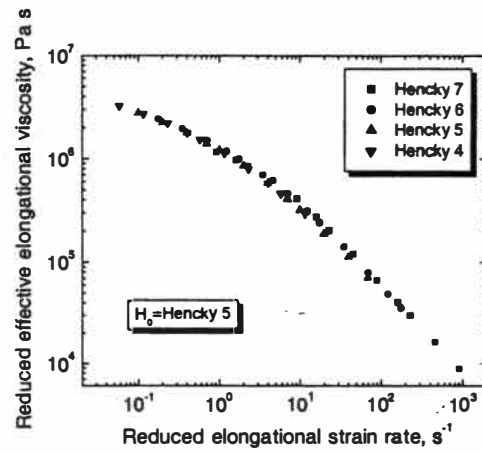
Figure 5.62. Hencky strain master curves of effective elongational viscosity of PE-4 at different temperatures created using Method 2.

134
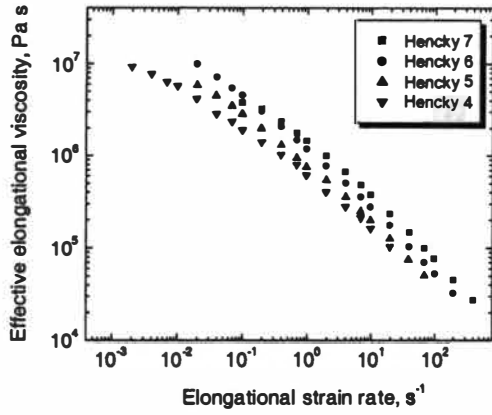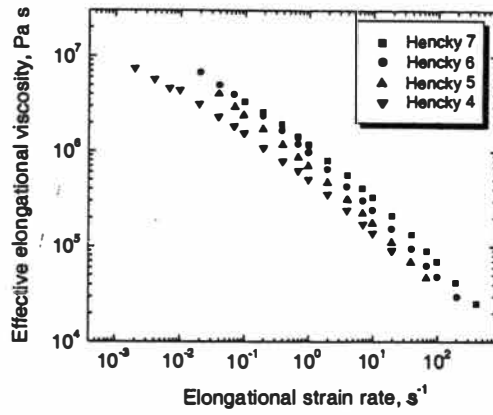
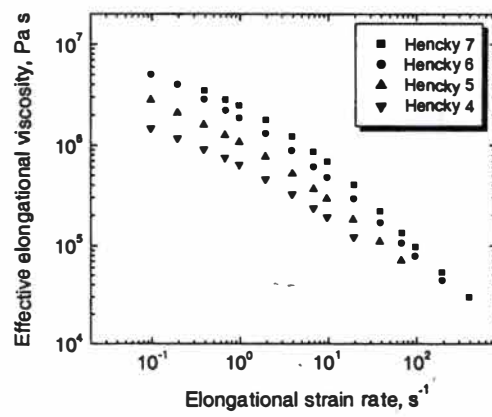**Figure 5.63.** Effect of Hencky strain on effective elongational viscosity of PE-5 at different temperatures.

135
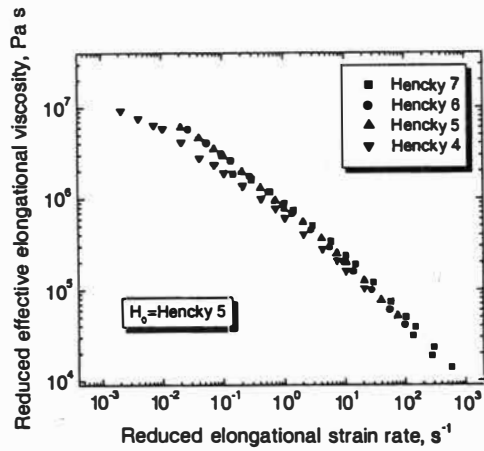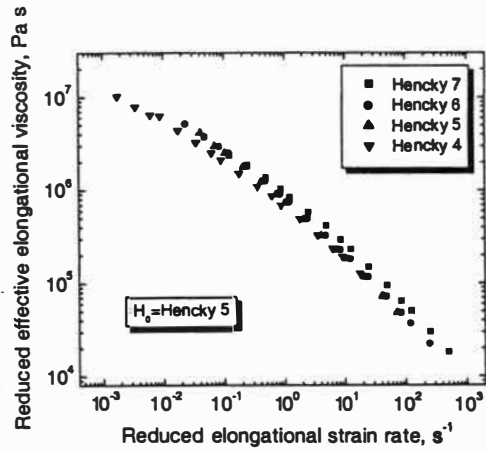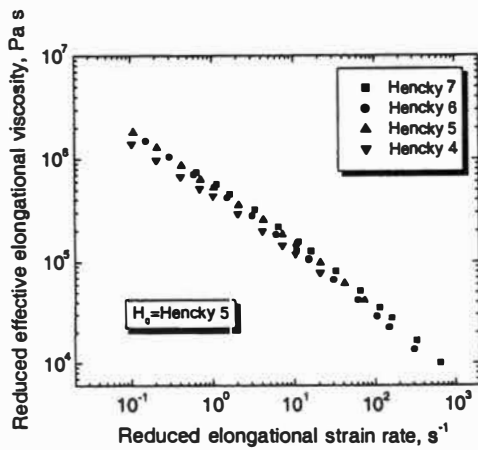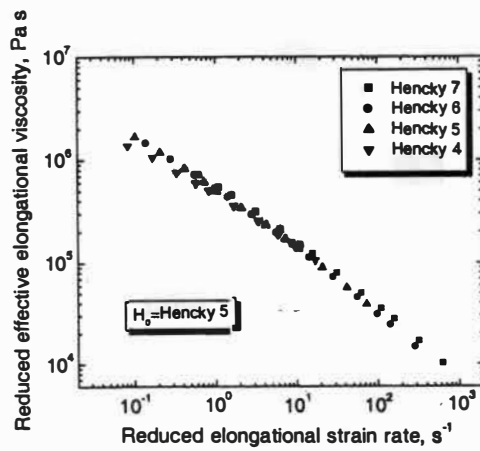
Figure 5.64. Hencky strain master curves of effective elongational viscosity of PE-5 at different temperatures created using Method 1.

136
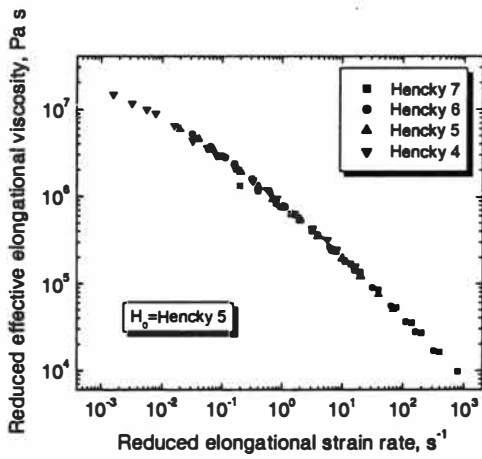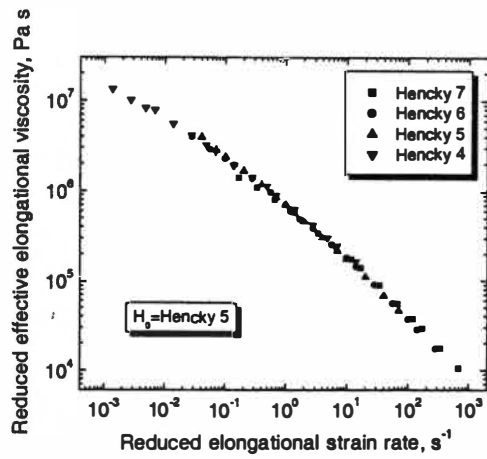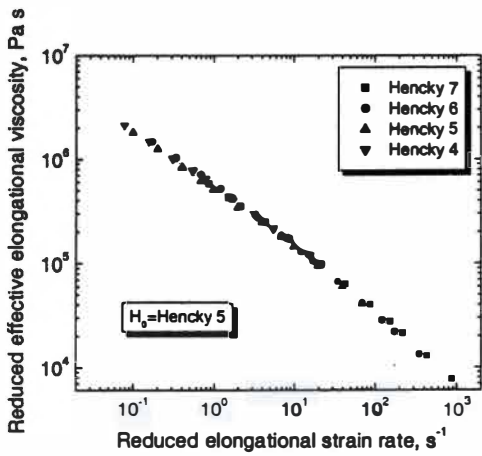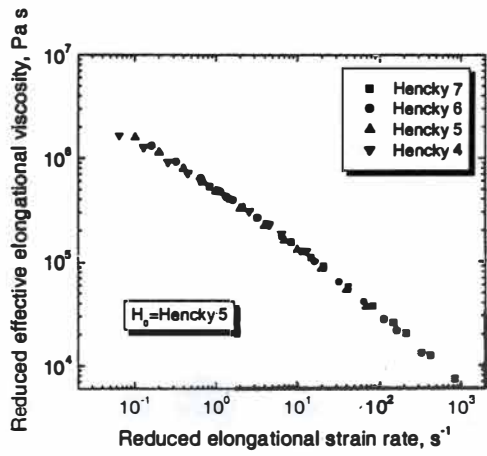
Figure 5.65. Hencky strain master curves of effective elongational viscosity of PE-5 at different temperatures created using Method 2.
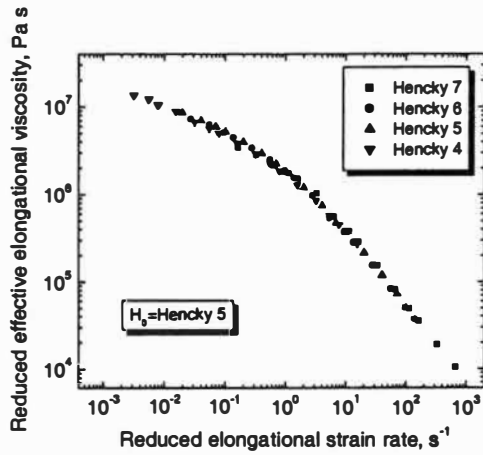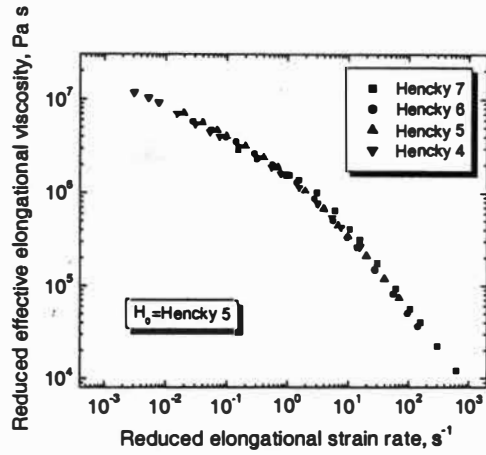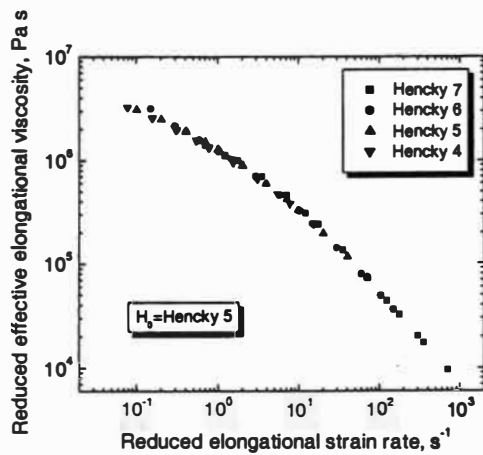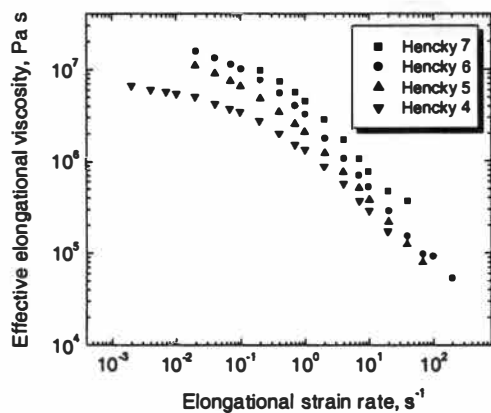
(a) 135°C
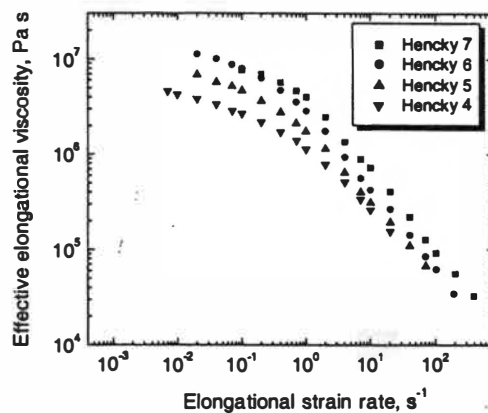
(b) 150°C
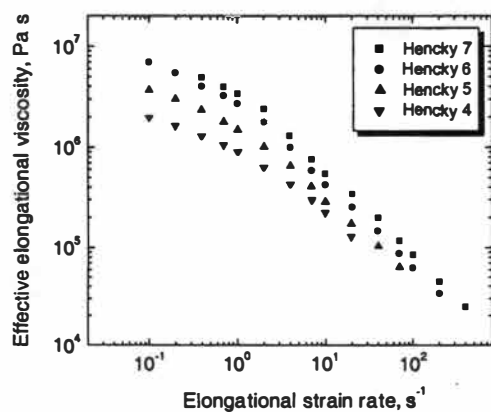
(c) 165°C
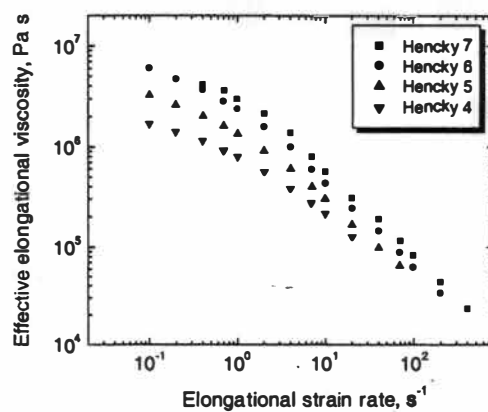
(d) 180°C

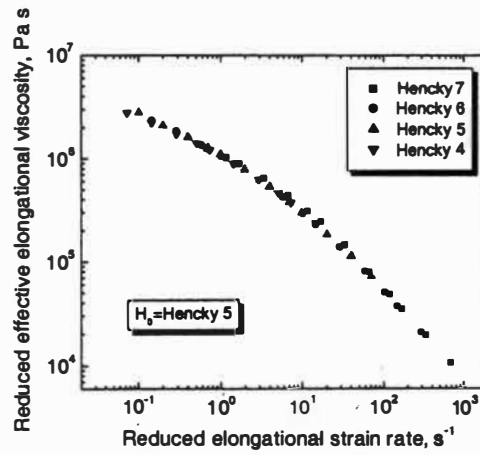**Figure 5.66.** Effect of Hencky strain on effective elongational viscosity of PE-6 at different temperatures.

138
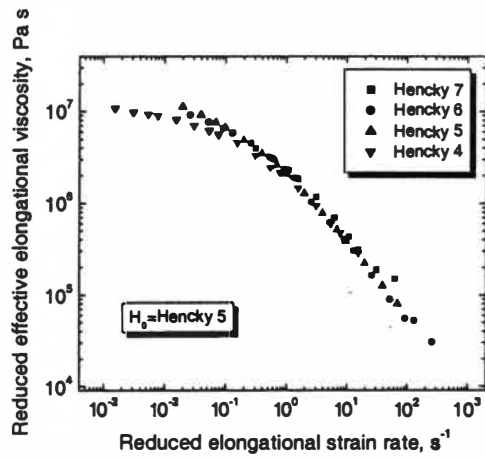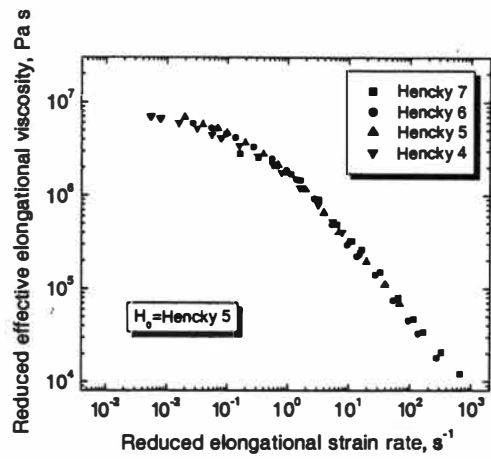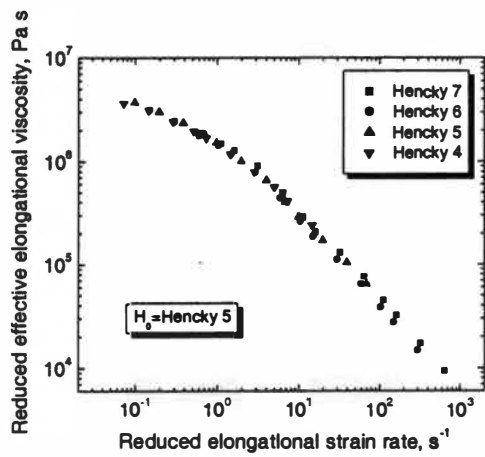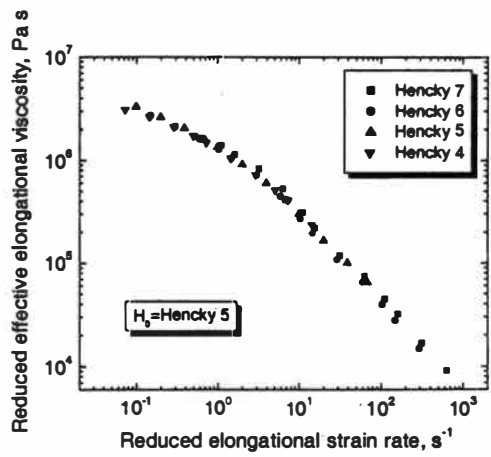
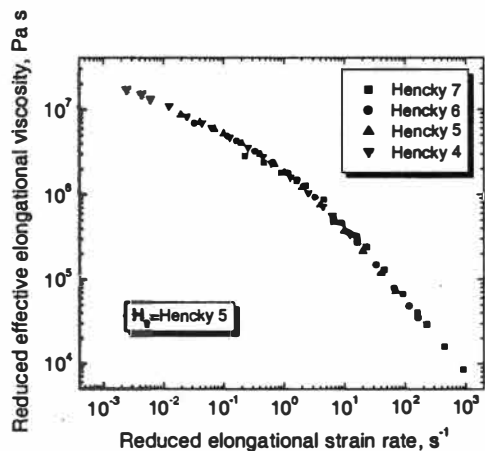**Figure 5.67.** Hencky strain master curves of effective elongational viscosity of PE-6 at different temperatures created using Method 1.
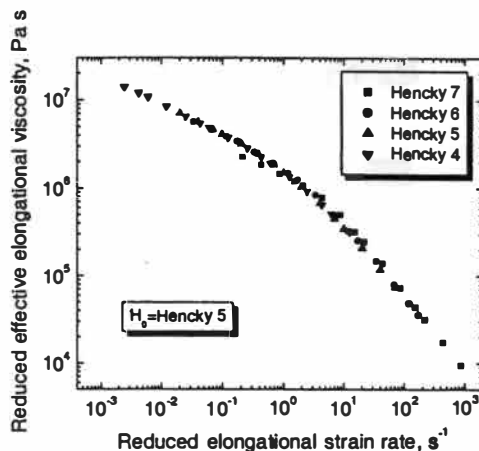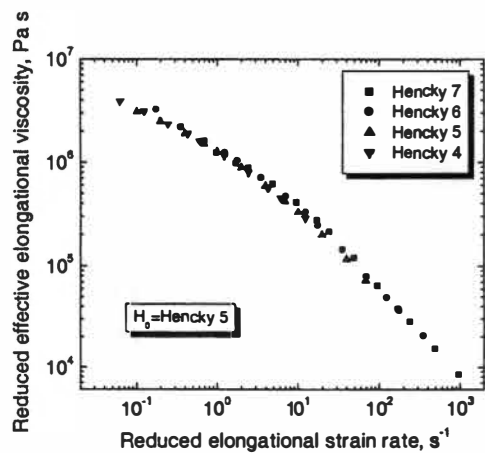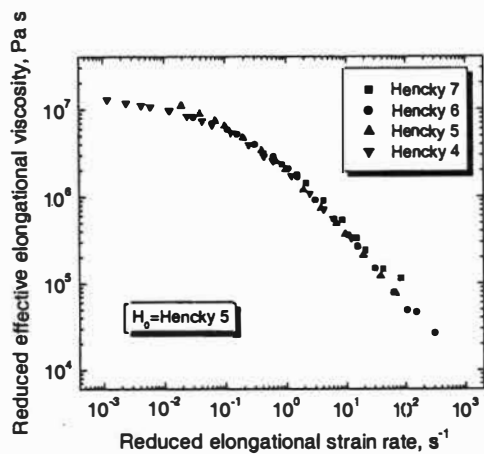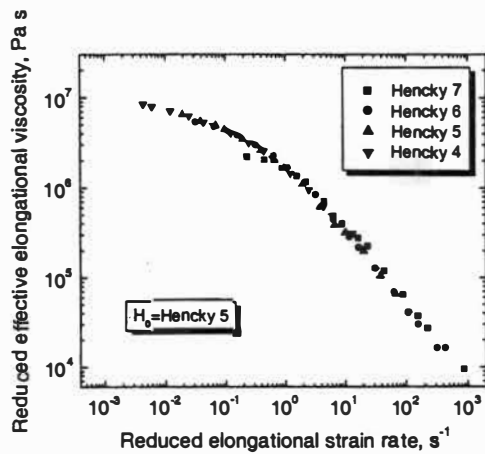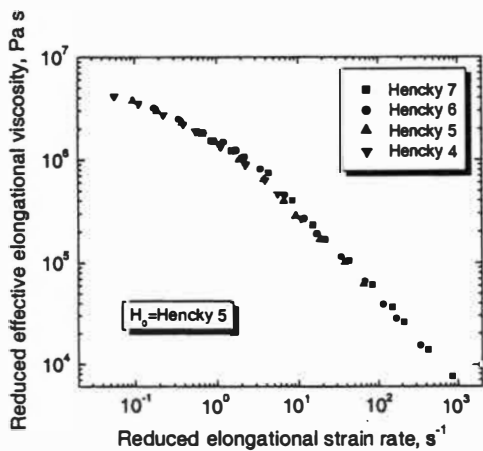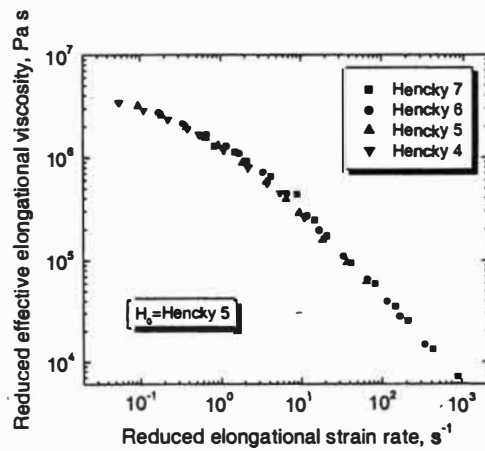
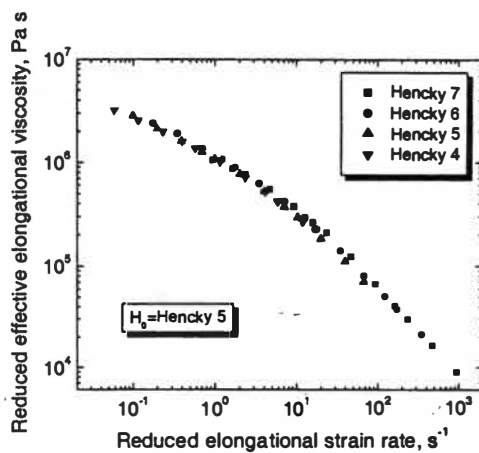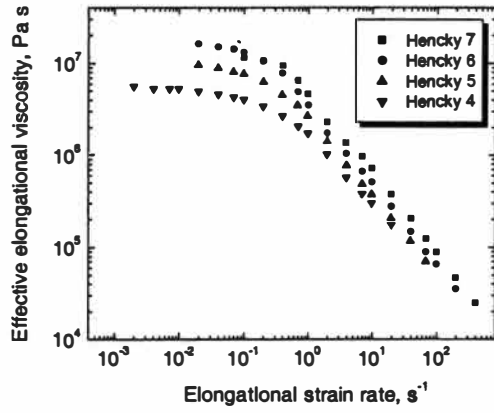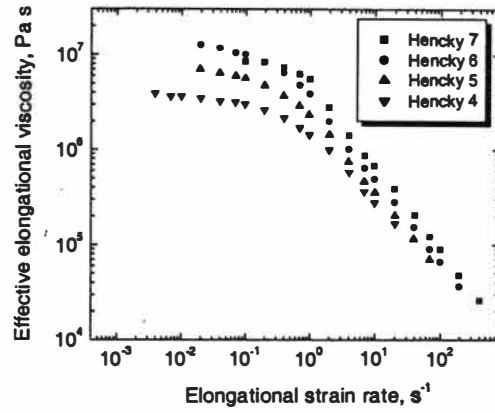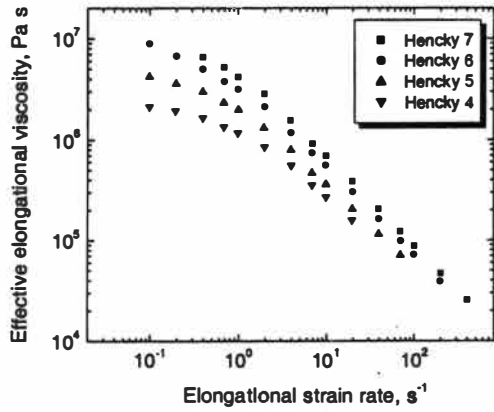**Figure 5.68.** Hencky strain master curves of effective elongational viscosity of PE-6 at different temperatures created using Method 2.
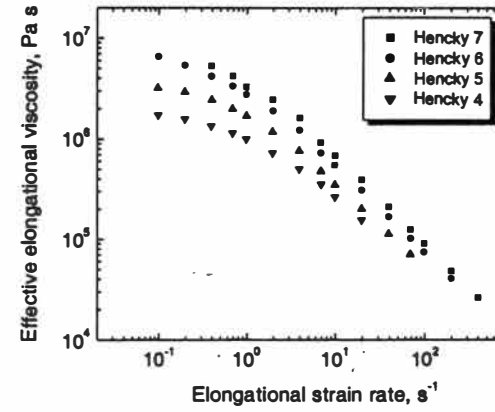
determination (R^2) values for the second order polynomial fits of Hencky strain master curves, given in Table 5.4. Except for PE-3, for which Method 1 gave poorer R^2 value of 0.9812 at 135°C, R^2 values for all PE samples are higher than 0.99 for both methods, indicating that good master curves can be created using these methods for PE samples. But, generally speaking, both visual inspection and the coefficient of determination (R^2) values show that Method 2 gives slightly better results than Method 1. This was also found in prior studies for Nylon samples accomplished by this research group (115).

§5.2.2.3 *Results on Polyisobutylene Samples*

Effective elongational viscosity of PIB was measured at four different temperatures, 210, 220, 230, and 240°C; and at four Hencky strains, 4, 5, 6, and 7 for each temperature. The reference Hencky was taken as 5. The Hencky strain shifting

Table 5.4. Coefficient of determination, R^2, values for the polynomial fits of Hencky strain master curves of PE samples.

	Coefficient of determination, R^2, at temperature							
	135°C		150°C		165°C		180°C	
Sample	M1	M2	M1	M2	M1	M2	M1	M2
PE-1	0.9935	0.9975	0.9940	0.9973	0.9973	0.9988	0.9979	0.9983
PE-2	0.9979	0.9976	0.9965	0.9968	0.9989	0.9980	0.9988	0.9982
PE-3	0.9812	0.9915	0.9924	0.9922	0.9950	0.9956	0.9928	0.9963
PE-4	0.9930	0.9979	0.9949	0.9979	0.9945	0.9983	0.9984	0.9983
PE-5	0.9919	0.9984	0.9918	0.9987	0.9917	0.9989	0.9959	0.9990
PE-6	0.9927	0.9944	0.9949	0.9949	0.9955	0.9963	0.9964	0.9971

141

master curves of the effective elongational viscosity of this sample using both methods described earlier are shown in Figures 5.69 through 5.71. The results also show that Method 2 gives slightly better results than Method 1.

§5.2.3 Simultaneous Temperature and Hencky Strain Shifting of Effective Elongational Viscosity

According to the results shown above, the elongational viscosity curves taken at different temperatures can be generated into a single master curve. The elongational viscosity curves taken at different Hencky strains can be generated into a single master curve as well. Therefore, by combining these two shifting operations, i.e. shifting with respect to temperature, and shifting with respect to Hencky strain, and using the appropriate shift factors, a generalized master curve could be obtained and the elongational strain rate range of the experimental geometry extended. One of the long-term objectives of this research group is to design an on-line elongational rheology sensor for polymer processing processes involving elongational flow. A generalized master curve and the shift factors associated would be very useful tool in developing such a sensor.

The reduced variables are defined by

$$[(\eta_{eff})_{r_{TH}}]_1 = \frac{\eta_{eff}}{(a_T)_1[(a_H)_1]^2} \tag{5.14}$$

$$(\dot{\varepsilon}_{r_{TH}})_1 = (a_T)_1(a_H)_1\dot{\varepsilon} \tag{5.15}$$

for Method 1 and

142
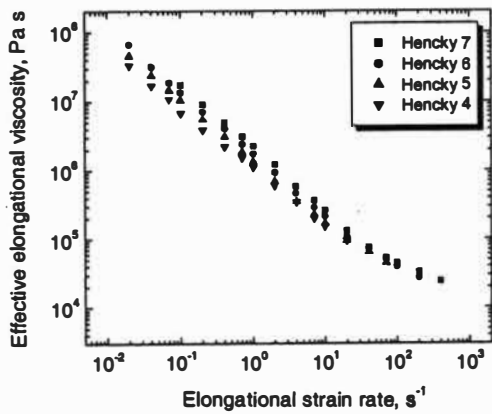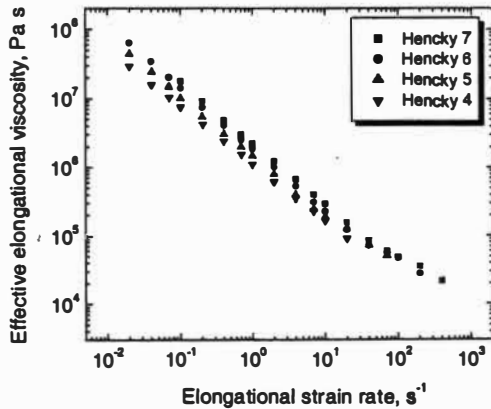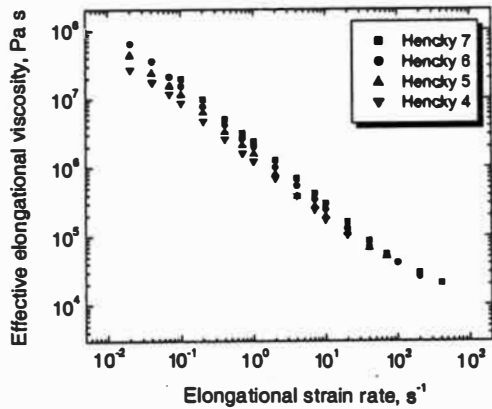
(a) 210°C

(b) 220°C

(c) 230°C

(d) 240°C

Figure 5.69. Effect of Hencky strain on effective elongational viscosity of PIB at different temperatures.

143
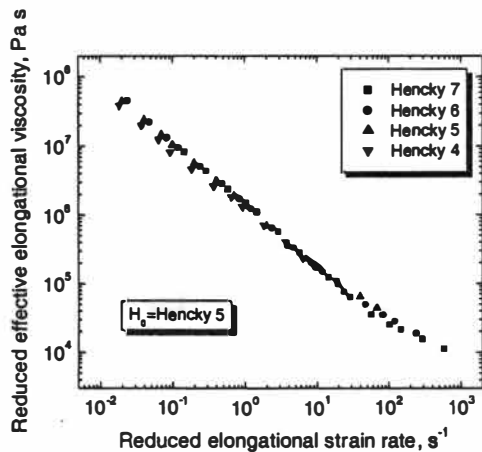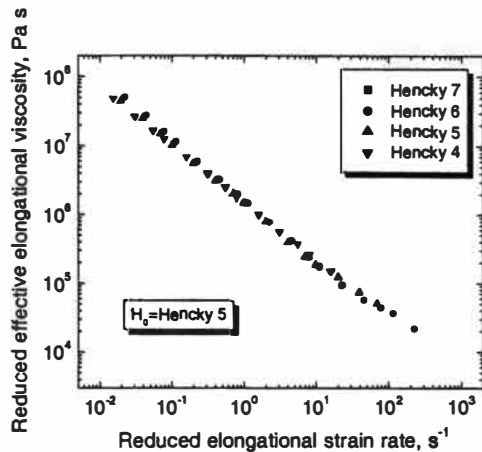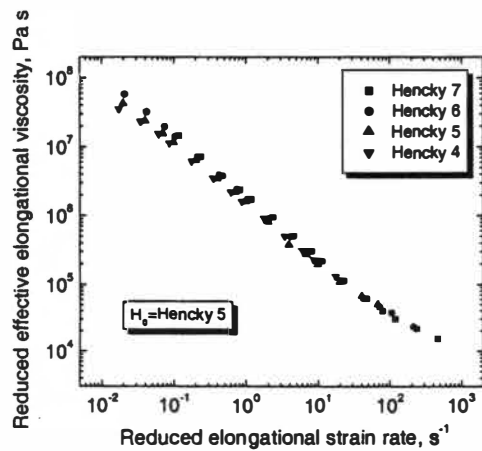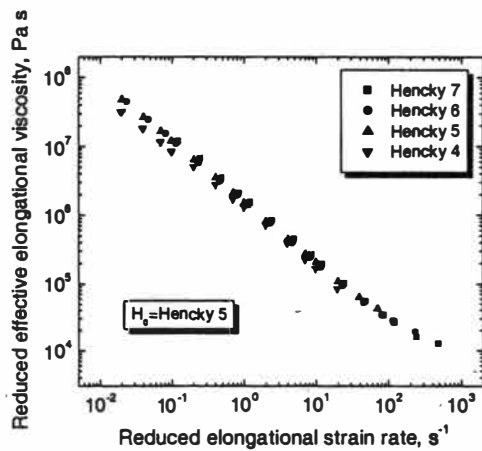
Figure 5.70. Hencky strain master curves of effective elongational viscosity of PIB at different temperatures created using Method 1.

144
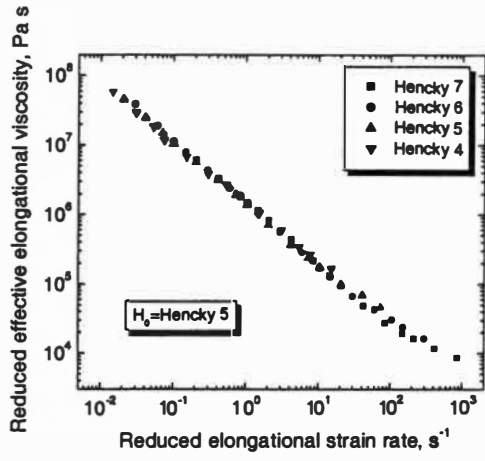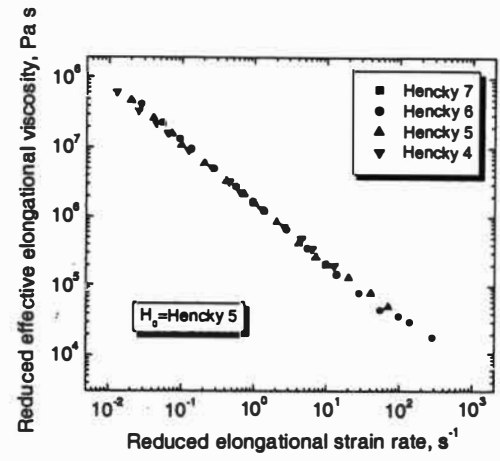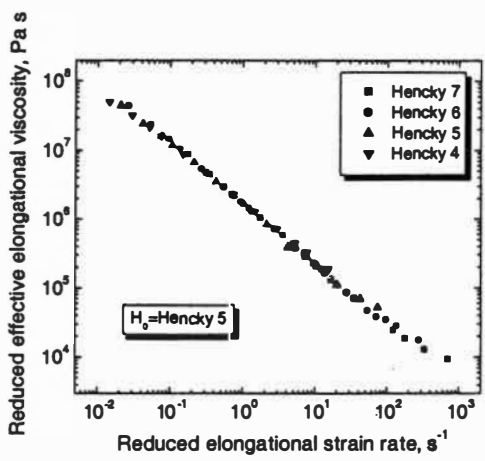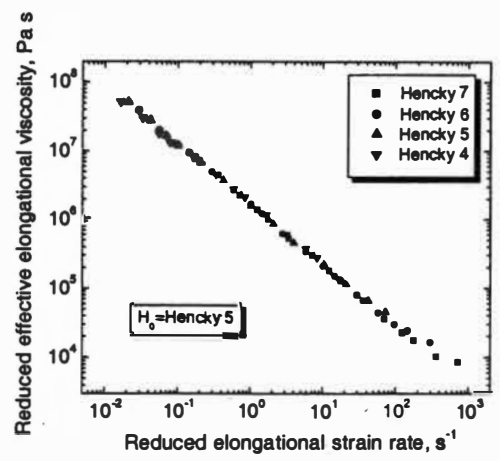
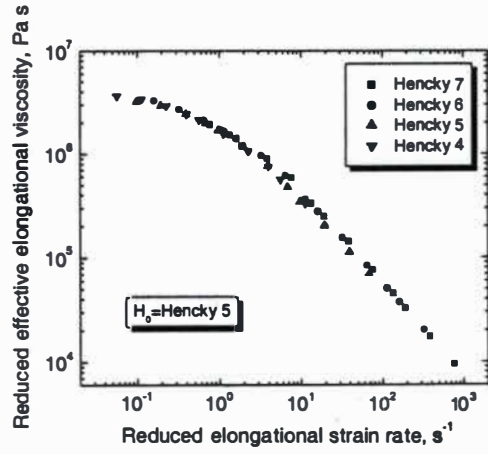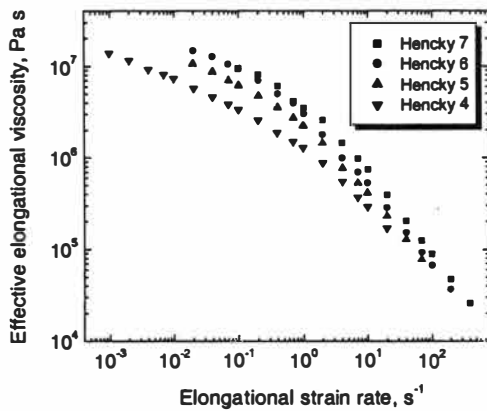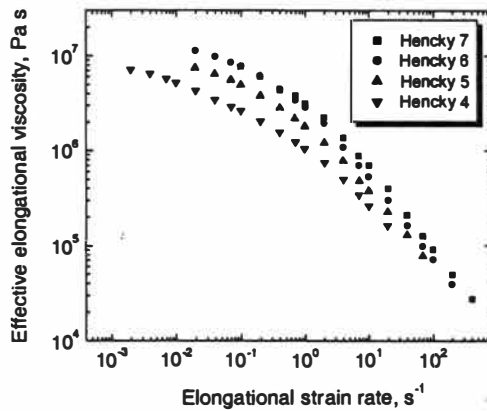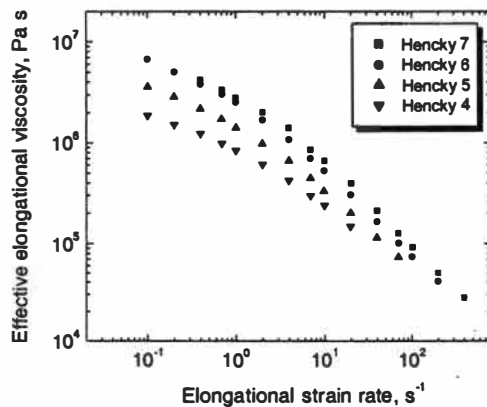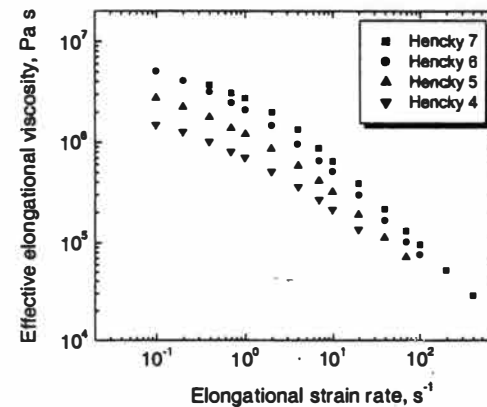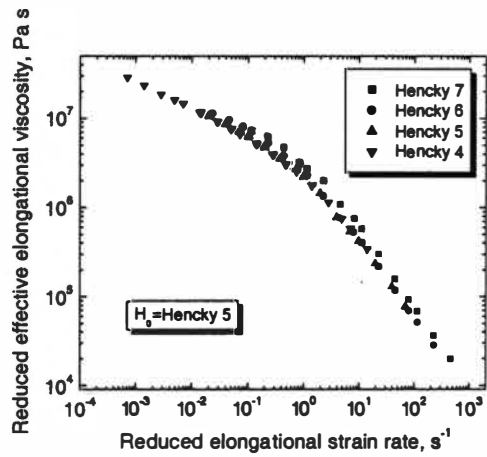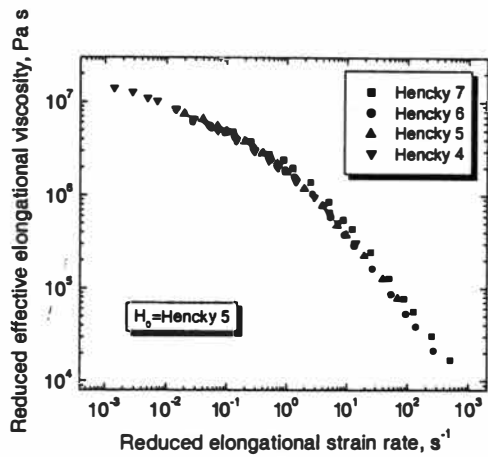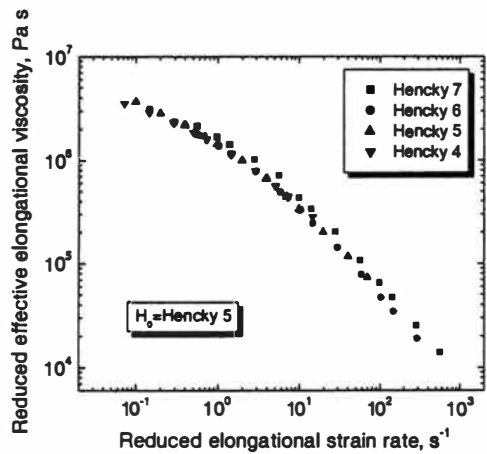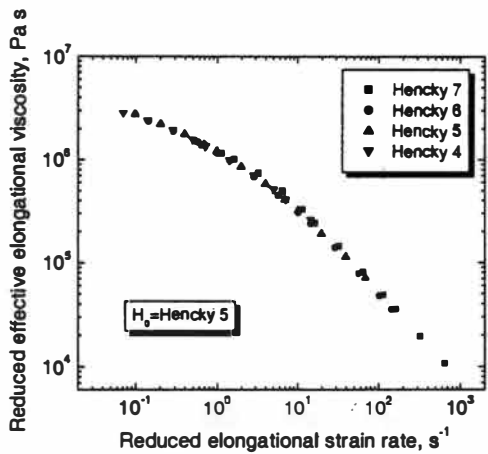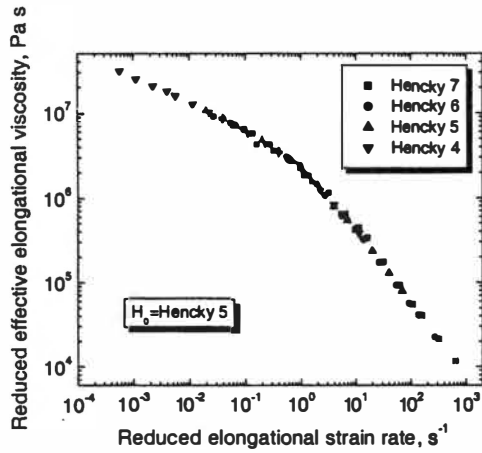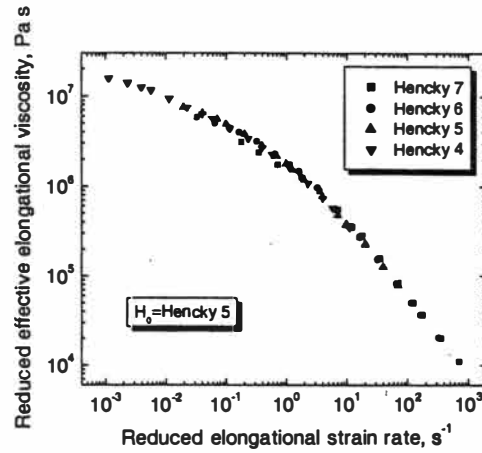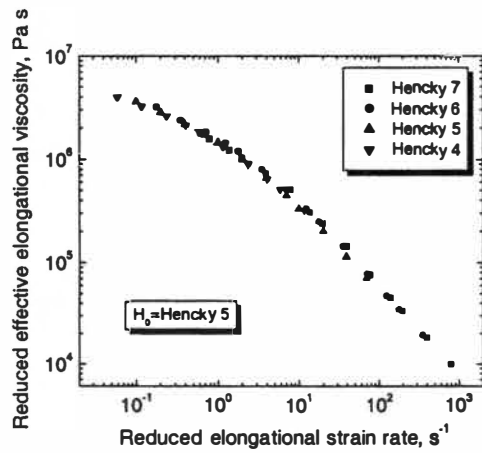**Figure 5.71.** Hencky strain master curves of effective elongational viscosity of PIB at different temperatures created using Method 2.

145

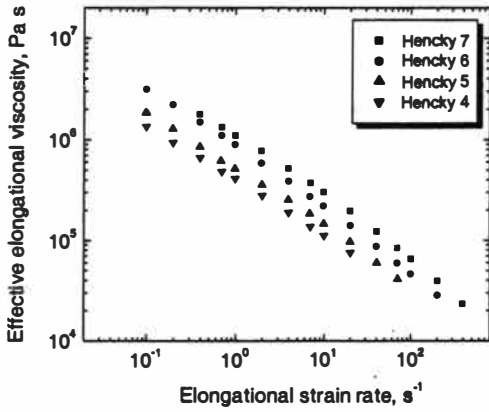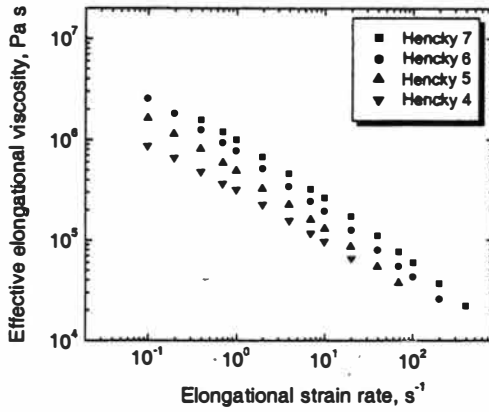$$[(\eta_{eff})_{r_{TH}}]_2 = \frac{\eta_{eff}}{(a_T)_1} \frac{\varepsilon_{H_0}}{(a_H)_2 \varepsilon_H} \qquad (5.16)$$

$$(\dot{\varepsilon}_{r_{TH}})_2 = (a_T)_1 (a_H)_2 \dot{\varepsilon} \qquad (5.17)$$

for Method 2, respectively.

The resulting general master curves for PE samples using both methods are presented in Figures 5.72 to 5.77. The reference temperature is 150°C and the reference Hencky strain is 5. Figure 5.78 gives the general master curves for PIB sample using both methods, for which the reference temperature is 220°C and the reference Hencky strain is 5. The coefficient of determination (R^2) values are shown in Table 5.5 for all samples. Except for PE-3 and PE-5 for which Method 1 gave poorer R^2 values of 0.9882 and 0.9897, respectively, at 135°C, R^2 values for all PE samples and PIB are higher than 0.99 for both method, indicating that good master curves can be created using these methods. But, generally speaking, both visual inspection and the coefficient of determination (R^2) values show that Method 2 gives slightly better results than Method 1.

§5.3 ENTHALPY AND ENTROPY CHANGES

The good results from Hencky strain shifting show the orientational viscosity, $\eta_{eff} - 3\eta_s$, is reasonable. This further verified that enthalpy and entropy changes can be calculated based on the Eqs. (3.18) and (3.19), presented in Chapter 3, assuming the Cox-Merz rule applies to PE and PIB samples. The enthalpy and entropy changes for all PE samples and PIB at four die geometries and different temperatures are

146
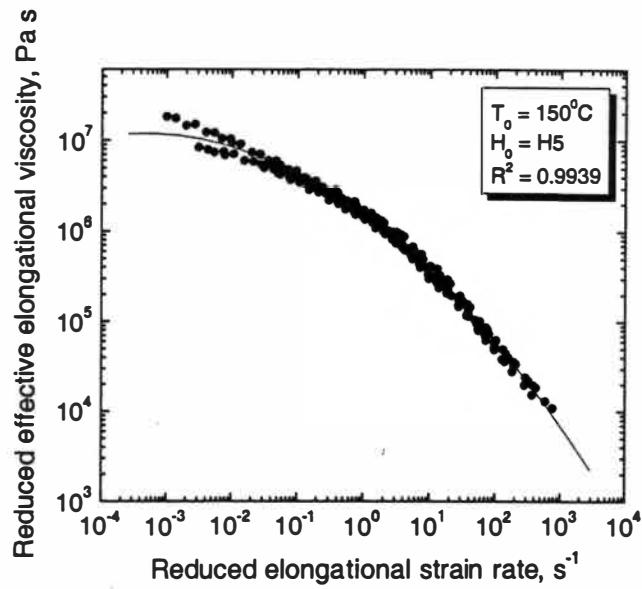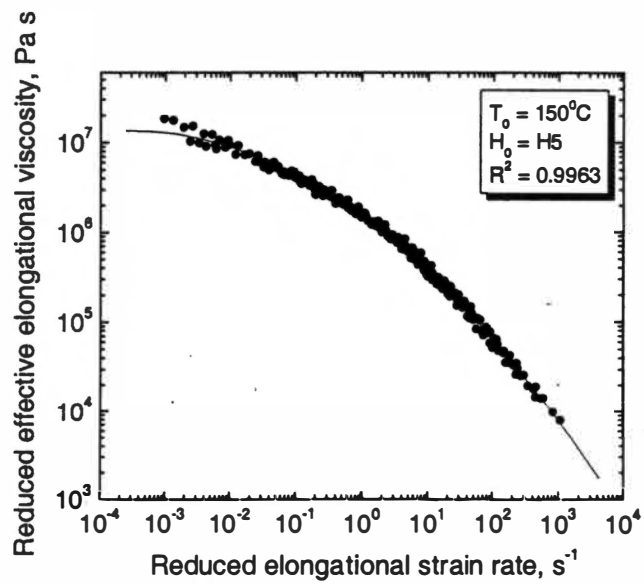
(a) Method 1

(b) Method 2

Figure 5.72. General master curves of effective elongational viscosity of PE-1 created by simultaneous temperature and Hencky strain shifting.
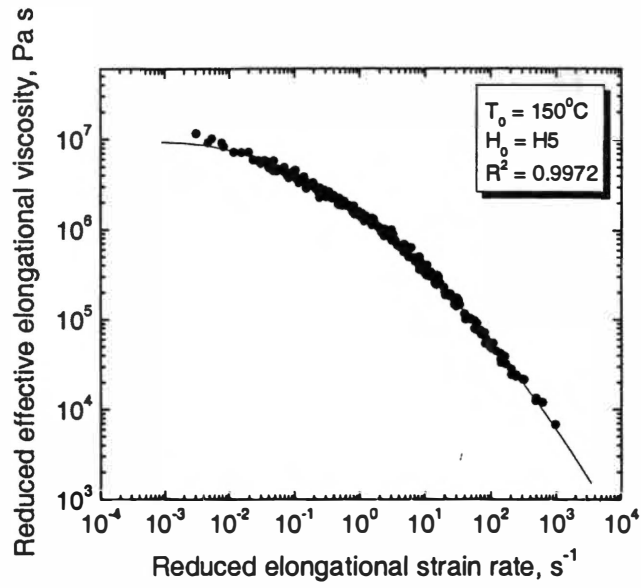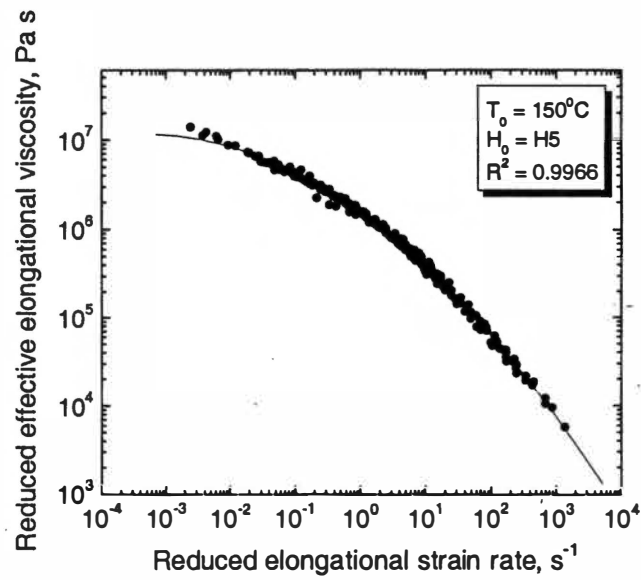
(a) Method 1

(b) Method 2

Figure 5.73. General master curves of effective elongational viscosity of PE-2 created by simultaneous temperature and Hencky strain shifting.

148
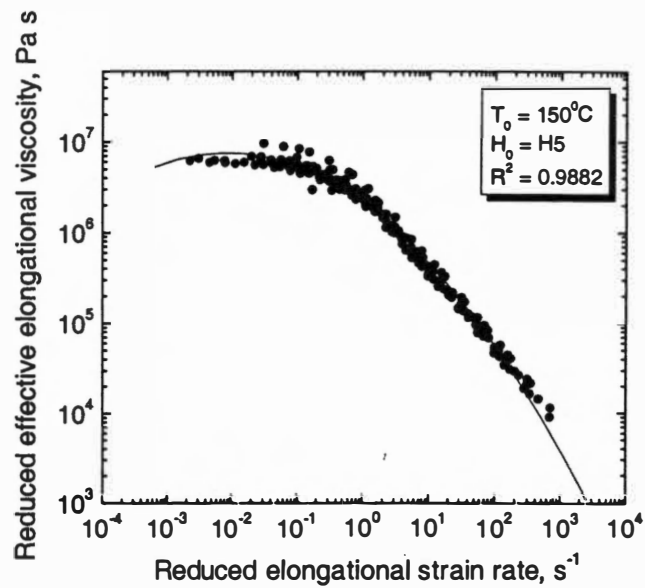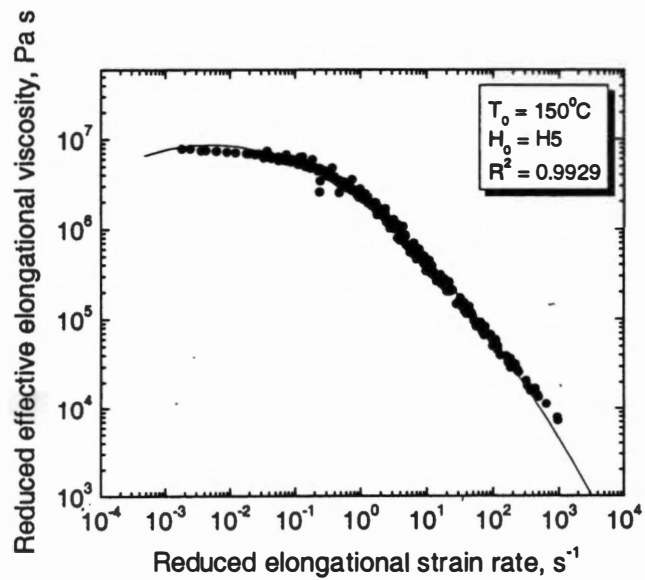
(a) Method 1

(b) Method 2

Figure 5.74. General master curves of effective elongational viscosity of PE-3 created by simultaneous temperature and Hencky strain shifting.
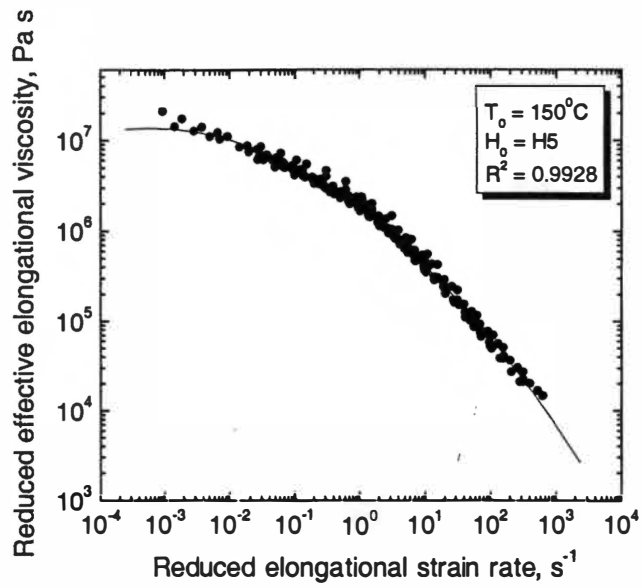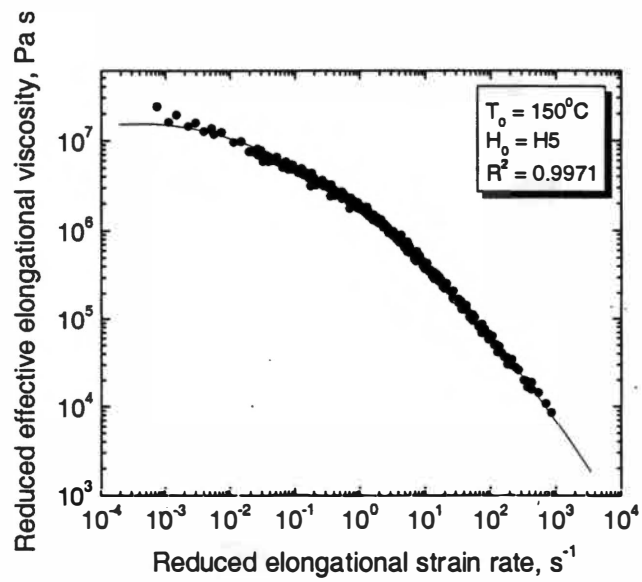
(a) Method 1

(b) Method 2

Figure 5.75. General master curves of effective elongational viscosity of PE-4 created by simultaneous temperature and Hencky strain shifting.

150
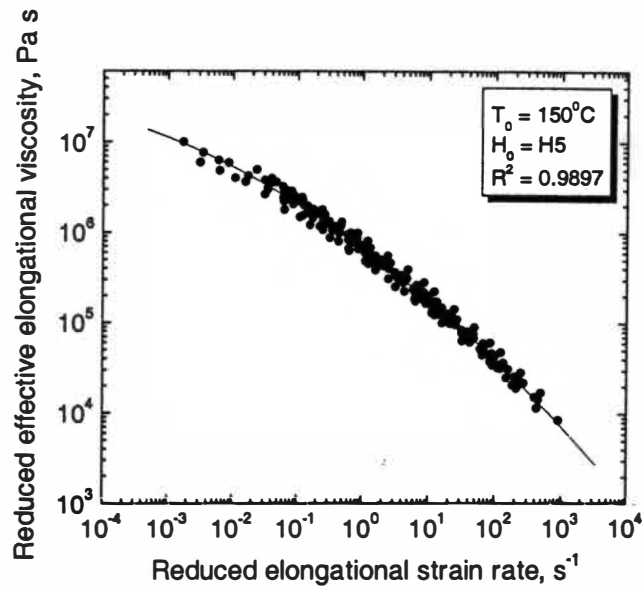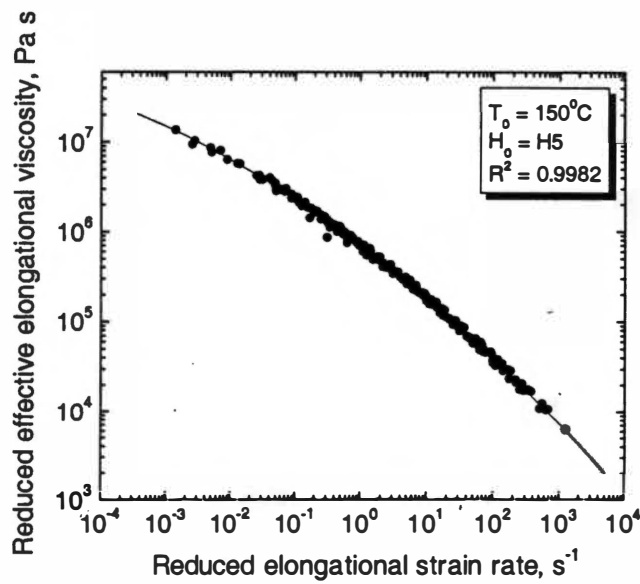
(a) Method 1

(b) Method 2

Figure 5.76. General master curves of effective elongational viscosity of PE-5 created by simultaneous temperature and Hencky strain shifting.
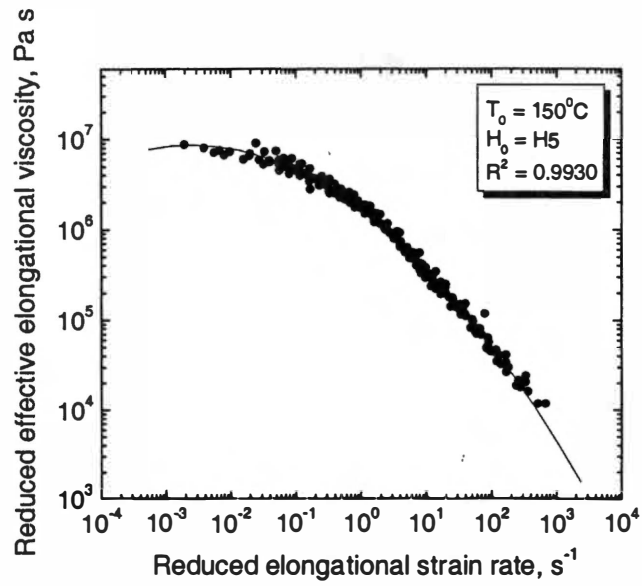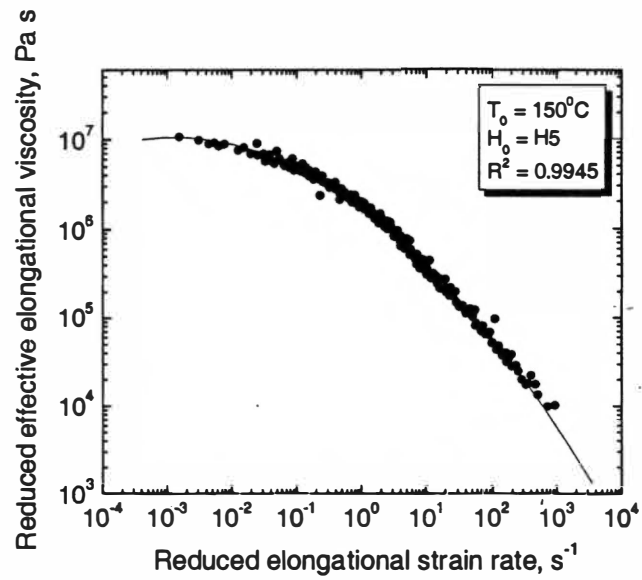
(a) Method 1

(b) Method 2

Figure 5.77. General master curves of effective elongational viscosity of PE-6 created by simultaneous temperature and Hencky strain shifting.

152
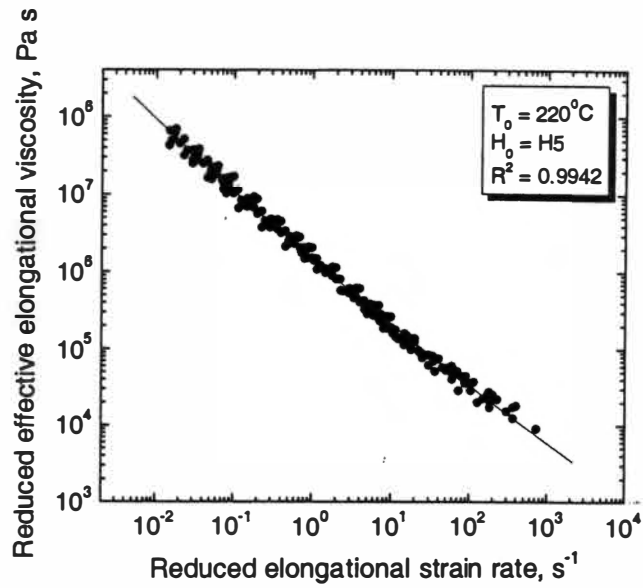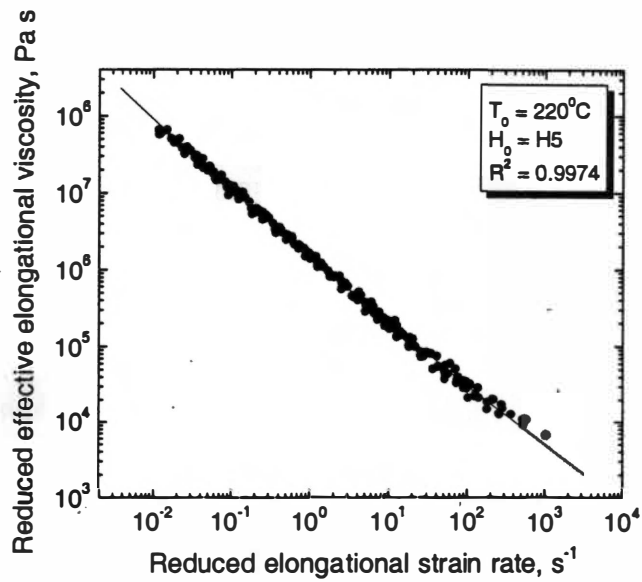
(a) Method 1

(b) Method 2

Figure 5.78. General master curves of effective elongational viscosity of PIB created by simultaneous temperature and Hencky strain shifting.

153

Table 5.5. Coefficient of determination, R^2, values for the polynomial fits of simultaneous temperature and Hencky strain master curves.

Sample	Method 1	Method 2
PE-1	0.9939	0.9963
PE-2	0.9972	0.9966
PE-3	0.9882	0.9929
PE-4	0.9928	0.9971
PE-5	0.9897	0.9982
PE-6	0.9930	0.9945
PIB	0.9942	0.9974

shown in Figures 5.79 to 5.92. From these figures we can see that the measured enthalpy and entropy changes increase in magnitude (become more negative) as the elongational strain rate increases for these four die geometries. Namely, the melt is increasingly transformed to a more ordered state corresponding to a lower entropy and greater magnitude latent heat of transformation with increasing elongational strain rate. Moreover, at comparable elongational strain rate, extruded melts exhibit larger enthalpy and entropy in magnitude for hyperbolic die with higher Hencky strain. These observations suggest that flow induced orientation occurs in the hyperbolic flow with the extent being dependent upon the elongational strain rate and die geometry.

It is also observed that conventional LDPE (PE-5), metallocene PE (PE-1, PE-2, PE-3, and PE-4) or conventional LLDPE (PE-6), and PIB have different shapes of enthalpy and entropy changes curves, indicating that the molecular

154
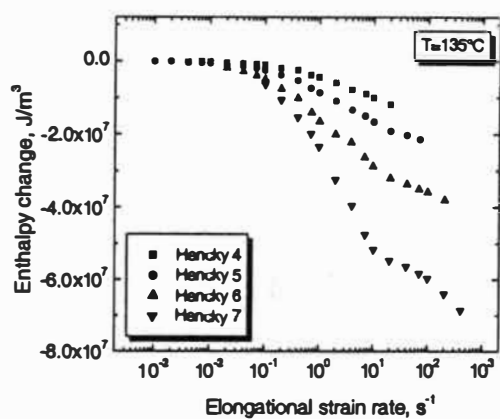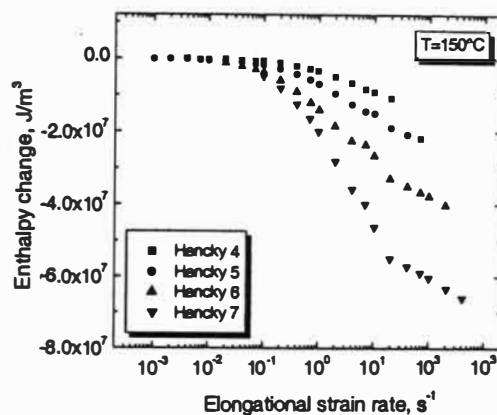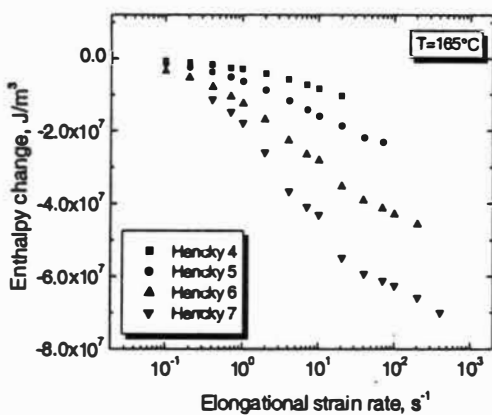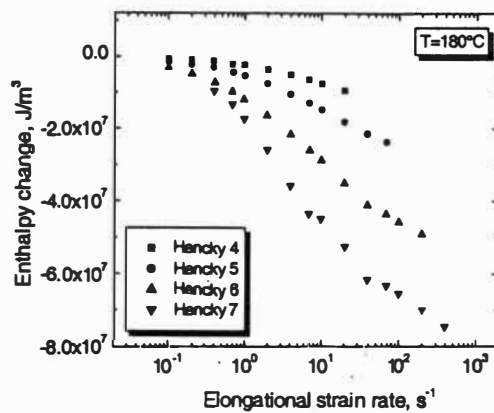
Figure 5.79. Enthalpy changes calculated from shear and elongational viscosities of PE-1 at different temperatures.

155
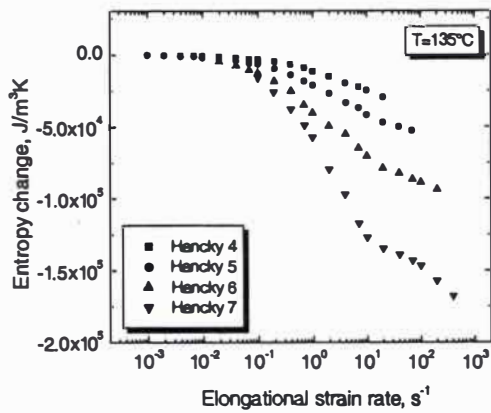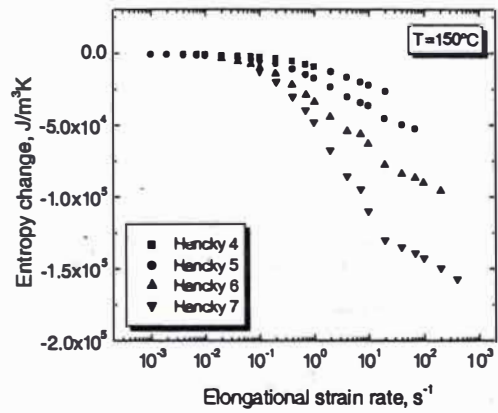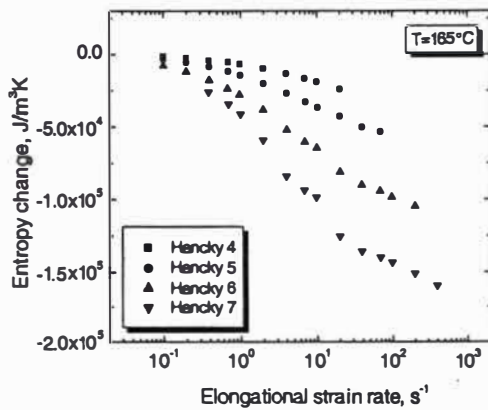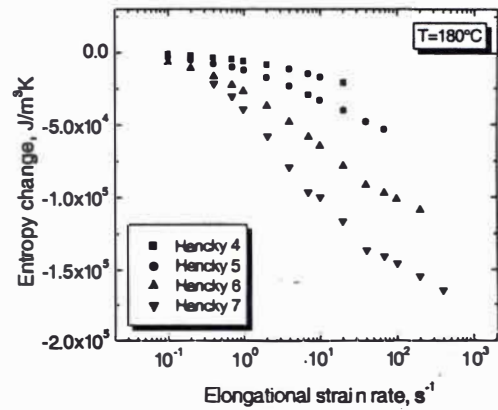
Figure 5.80. Entropy changes calculated from shear and elongational viscosities of PE-1 at different temperatures.
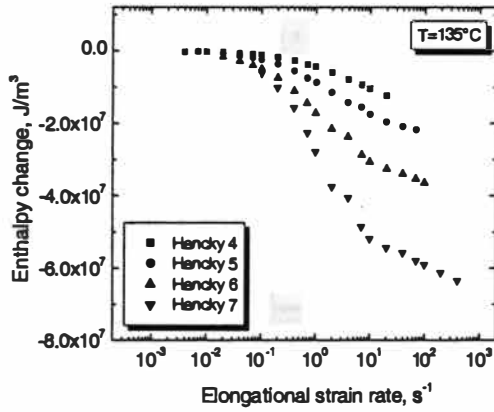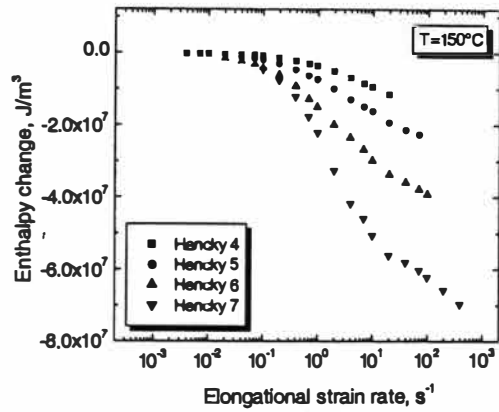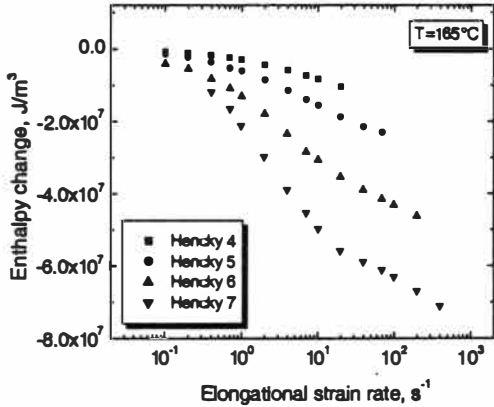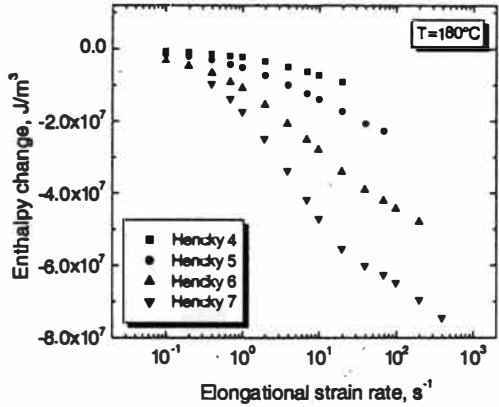
Figure 5.81. Enthalpy changes calculated from shear and elongational viscosities of PE-2 at different temperatures.

157
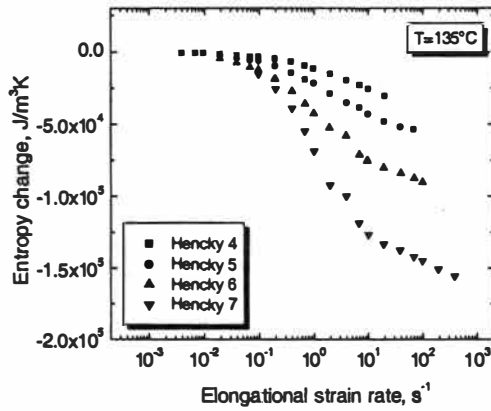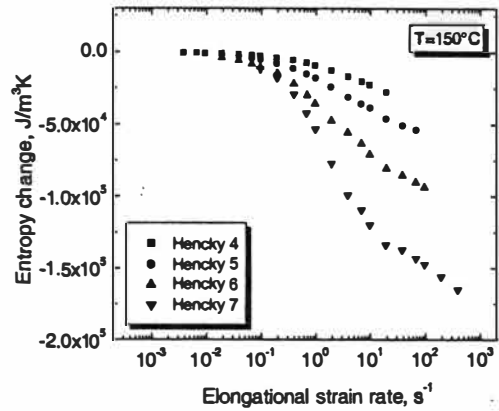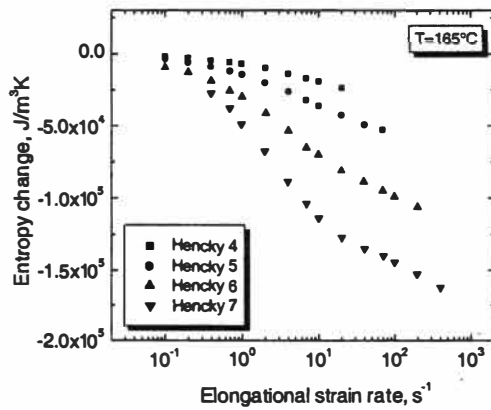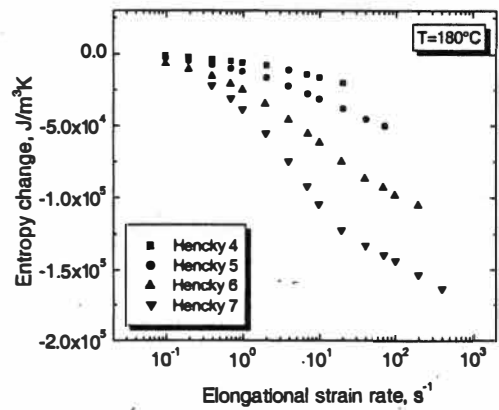
Figure 5.82. Entropy changes calculated from shear and elongational viscosities of PE-2 at different temperatures.
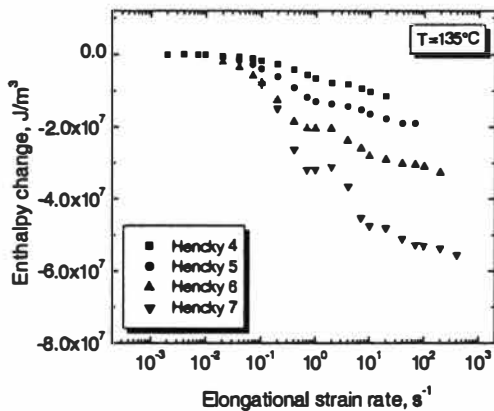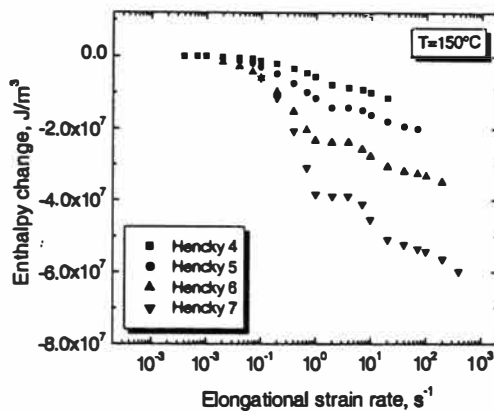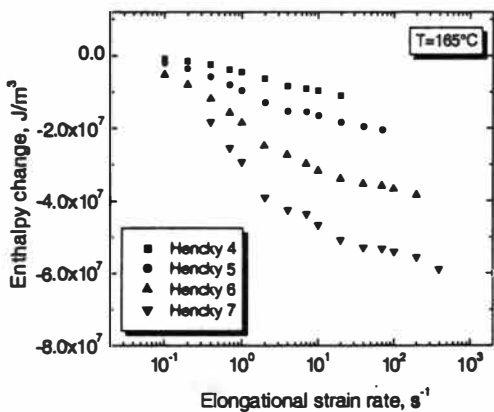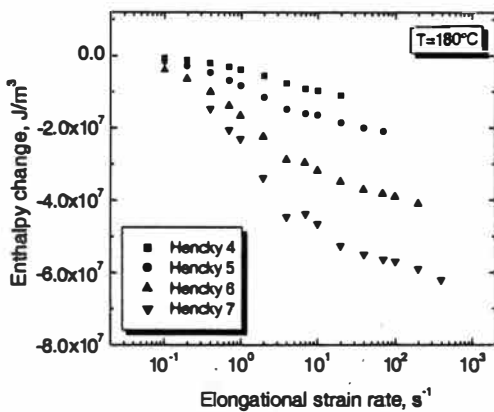
(a) 135°C

(b) 150°C

(c) 165°C

(d) 180°C

Figure 5.83. Enthalpy changes calculated from shear and elongational viscosities of PE-3 at different temperatures.
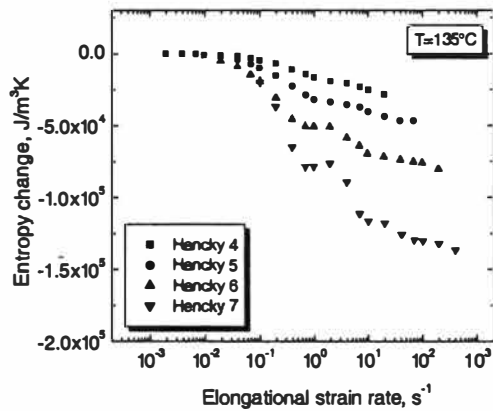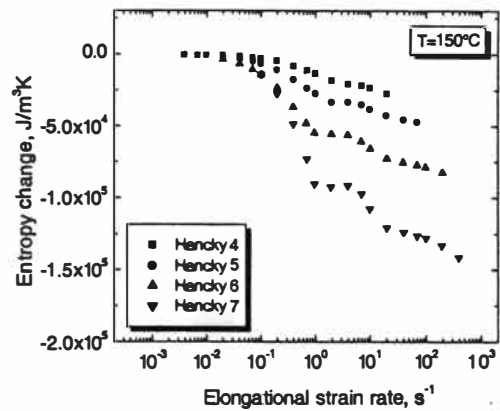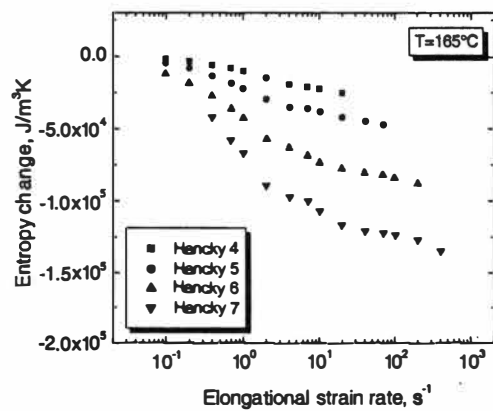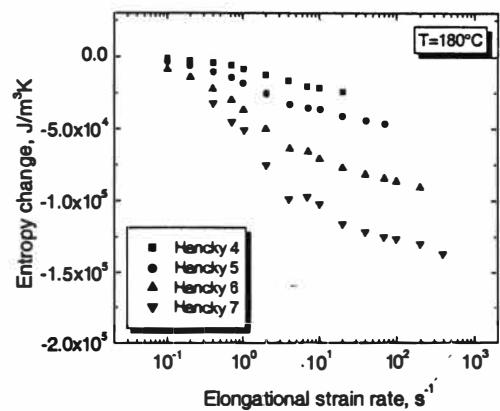
(a) 135°C

(b) 150°C

(c) 165°C

(d) 180°C

Figure 5.84. Entropy changes calculated from shear and elongational viscosities of PE-3 at different temperatures.

160
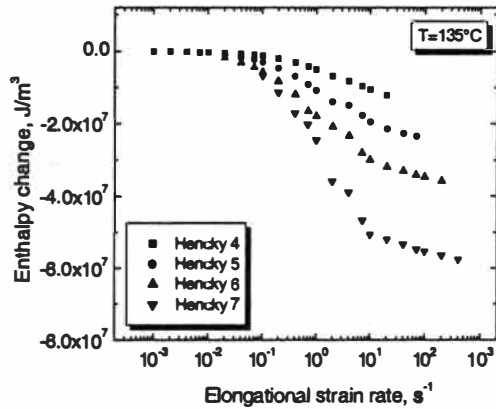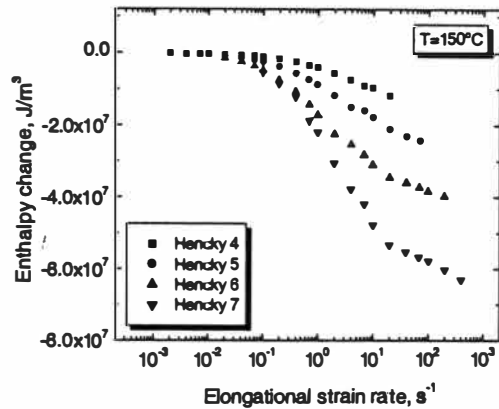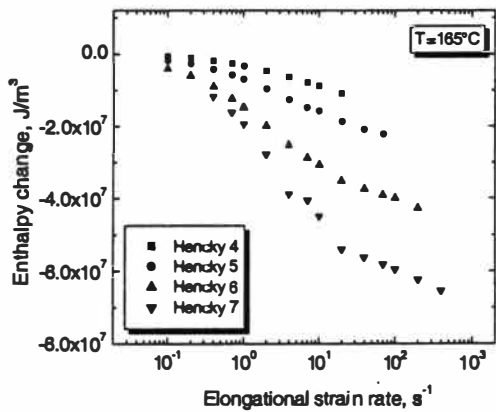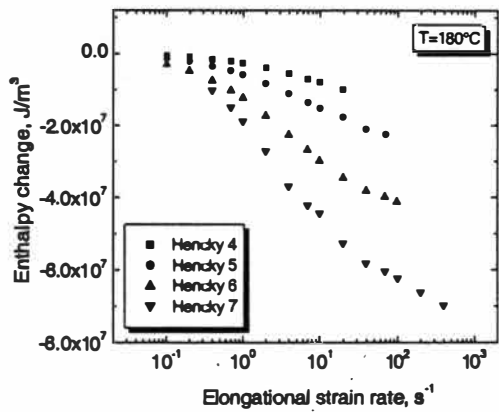
Figure 5.85. Enthalpy changes calculated from shear and elongational viscosities of PE-4 at different temperatures.

161
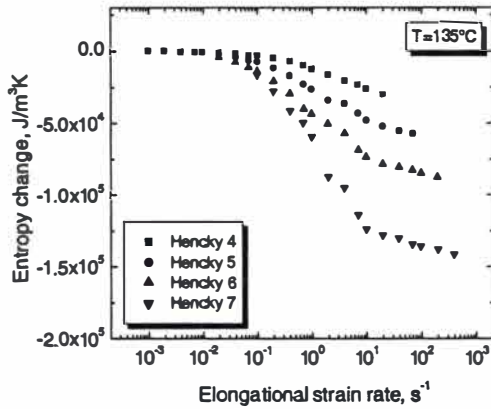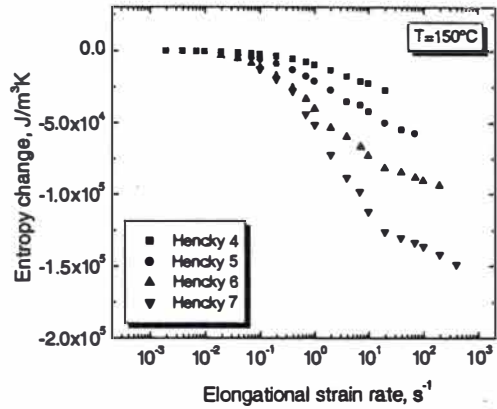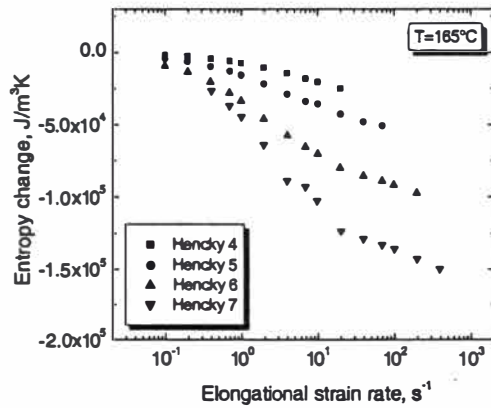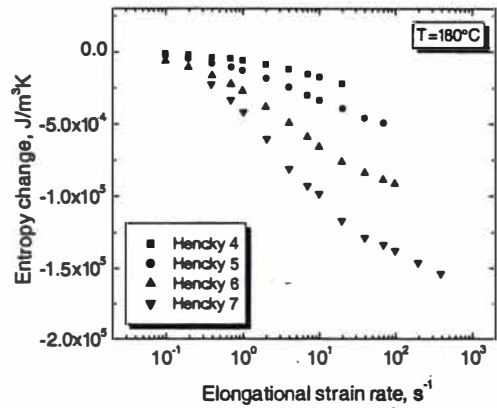
(a) 135°C

(b) 150°C

(c) 165°C

(d) 180°C

Figure 5.86. Entropy changes calculated from shear and elongational viscosities of PE-4 at different temperatures.

162
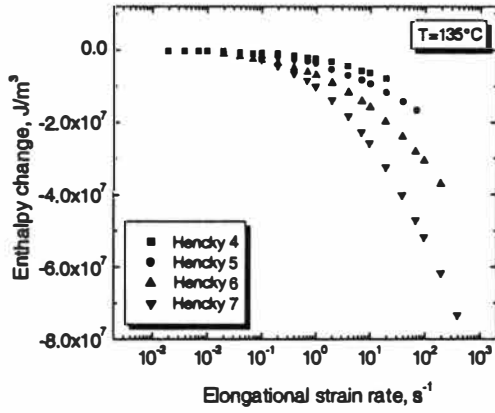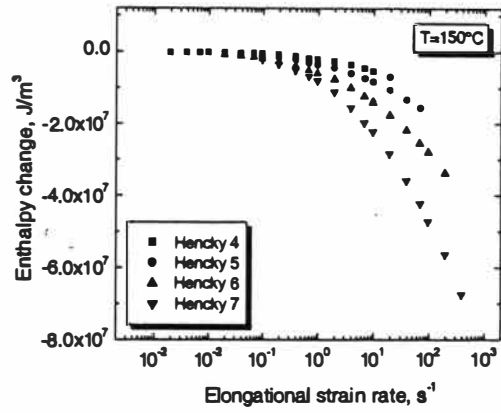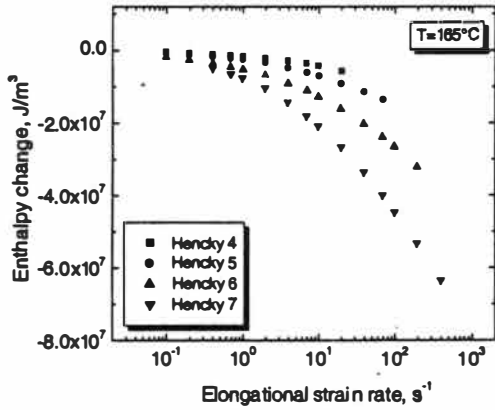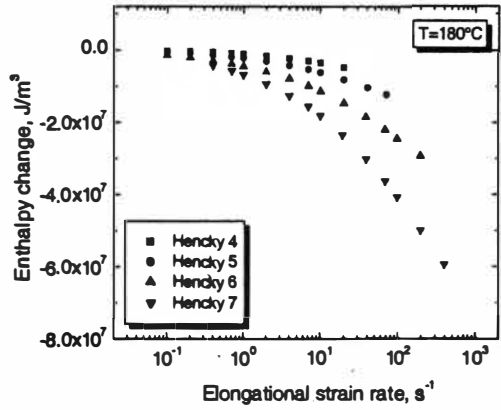
Figure 5.87. Enthalpy changes calculated from shear and elongational viscosities of PE-5 at different temperatures.

163
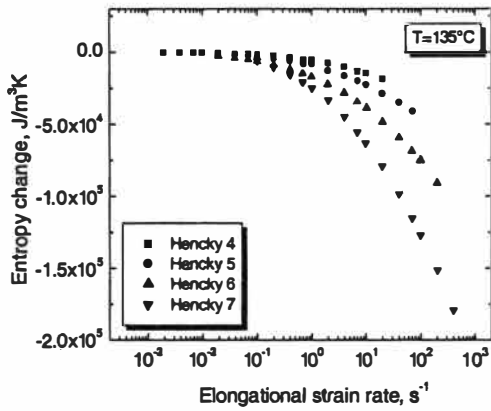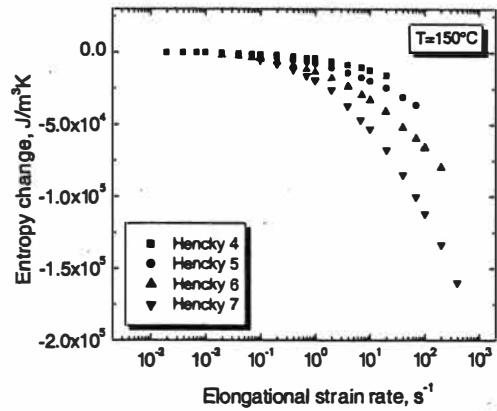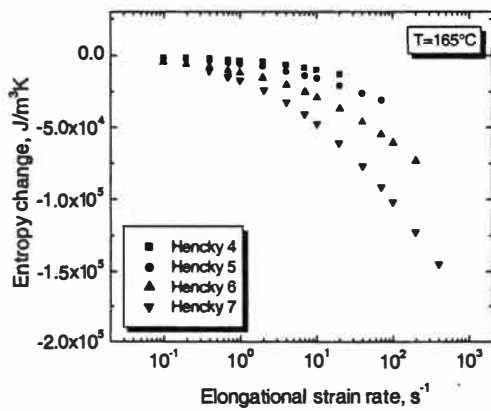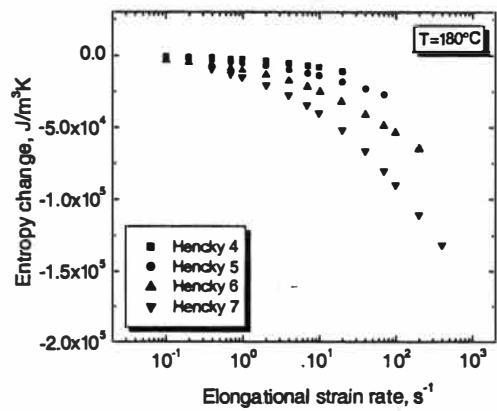
Figure 5.88. Entropy changes calculated from shear and elongational viscosities of PE-5 at different temperatures.
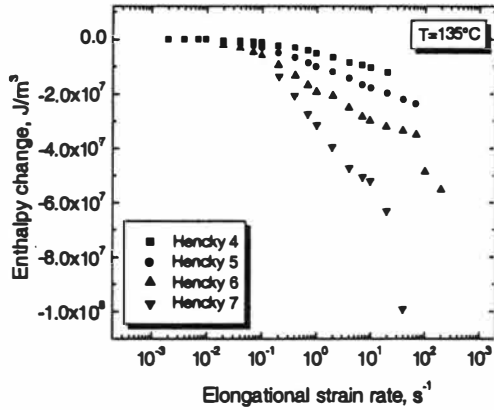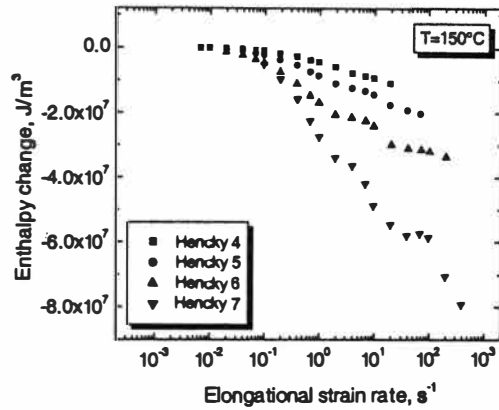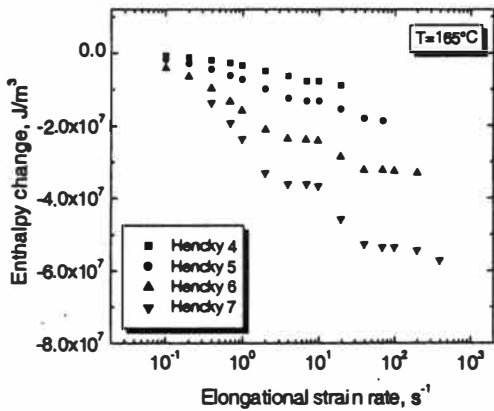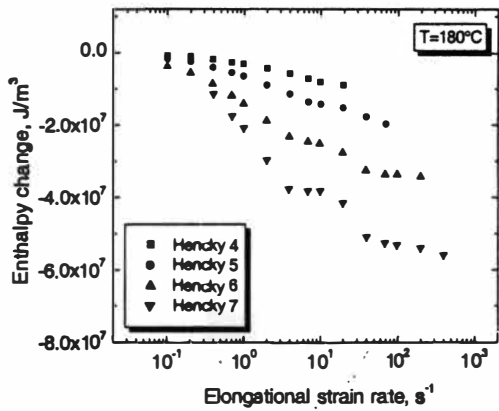
Figure 5.89. Enthalpy changes calculated from shear and elongational viscosities of PE-6 at different temperatures.

165
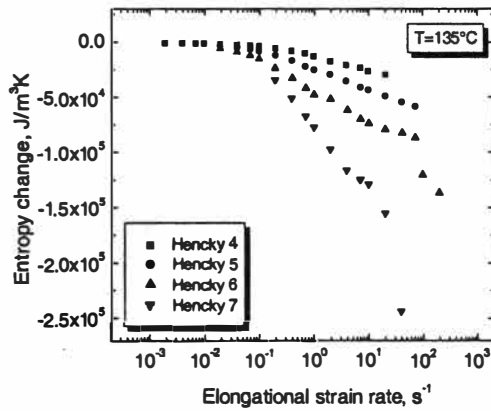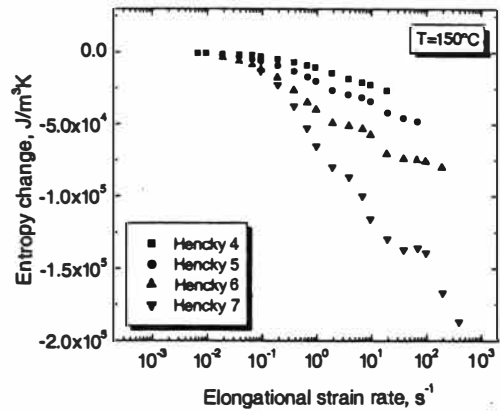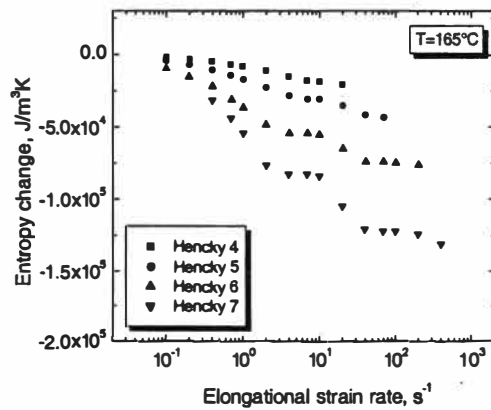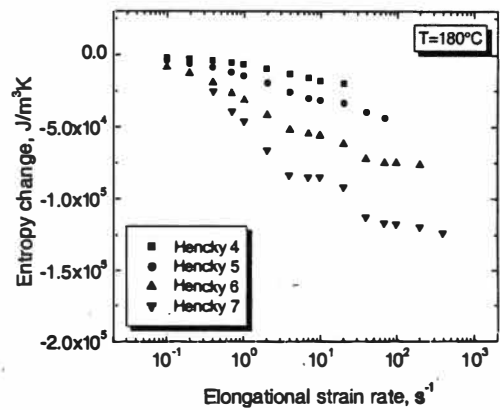
Figure 5.90. Entropy changes calculated from shear and elongational viscosities of PE-6 at different temperatures.
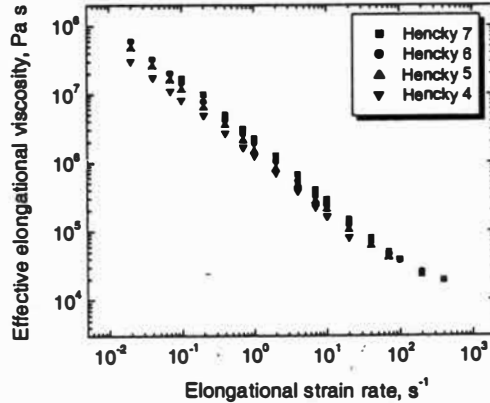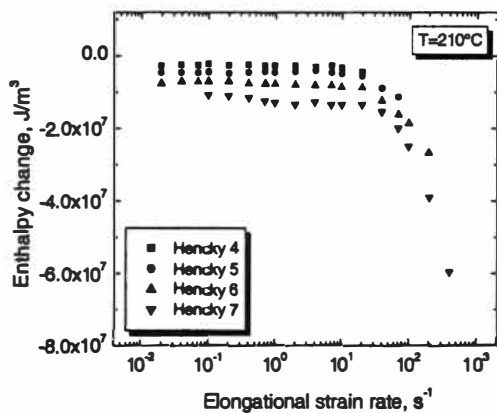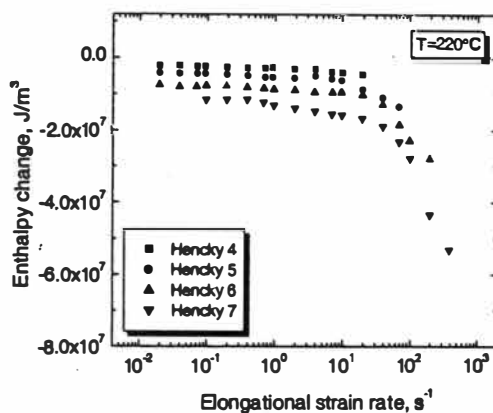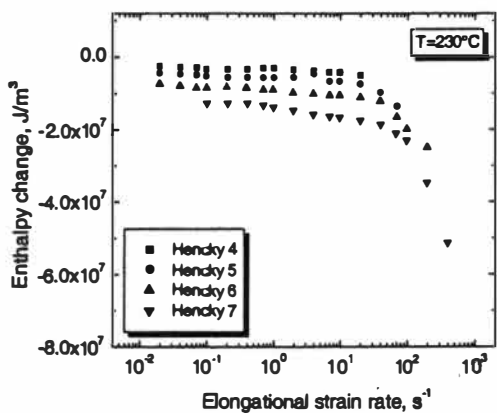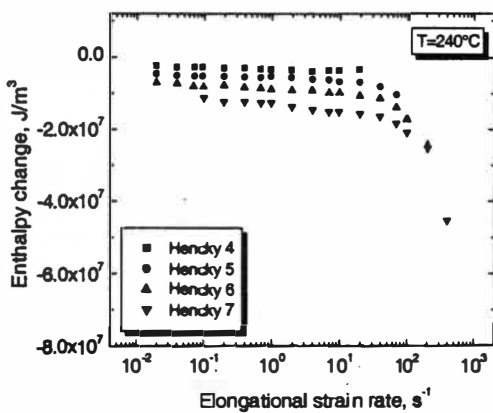
(a) 210°C
(b) 220°C
(c) 230°C
(d) 240°C

Figure 5.91. Enthalpy changes calculated from shear and elongational viscosities of PIB at different temperatures.
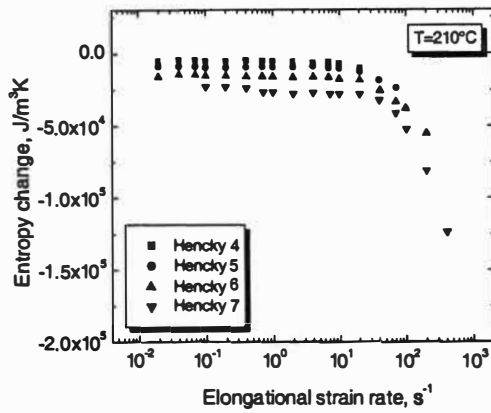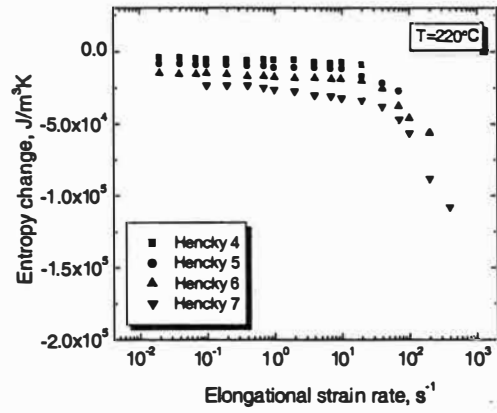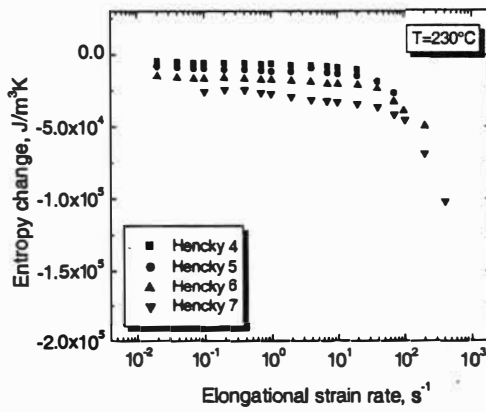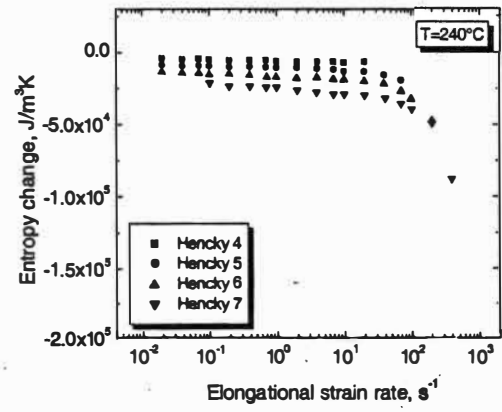
**Figure 5.92.** Entropy changes calculated from shear and elongational viscosities of PIB at different temperatures.

characteristics such as MWD and LCB affect the enthalpy and entropy changes curves. For PE-3 and PE-6, enthalpy and entropy changes curves show flat stages when the elongational strain rate is around $0.7 \ s^{-1}$ to $10 \ s^{-1}$. According to the decrease-and-increase pattern shown in the measured pressure profile for each rate, these flat stages could be related to the slippage that may occur in the hyperbolic dies. The slippage may be confirmed by the experimental observations of the extrudates which had alternate smooth and rough surfaces. At elongational strain rate lower than $100 \ s^{-1}$, extruded PE melts exhibit much larger enthalpy and entropy changes in magnitude than the PIB sample.

The effect of molecular characteristics on the enthalpy and entropy changes could also be studied using the shear and elongational data of the six PE samples. The results are shown in Figures 5.93 to 5.100. The molecular characteristics have similar effects on the effective elongational viscosity (discussed in the first section of this chapter) and the enthalpy and entropy changes. As shown in Figures 5.93(a) and 5.94(a), PE-5, which has larger PI and LCB, shows smaller enthalpy and entropy changes in magnitude when strain rate is larger than $0.07 \ s^{-1}$. Comparison of PE-3 and PE-6 having no LCB at strain rate between $0.2 \ s^{-1}$ and $2 \ s^{-1}$ shows that broadening the MWD seems to decrease the enthalpy and entropy changes in magnitude, because despite the fact that PE-3 has a lower MW, its enthalpy and entropy changes in magnitude are higher than those of PE-6 at the same elongational strain rate. PE-2 has higher MW and LCB but lower PI than PE-1. PE-1 and PE-2 have almost the same enthalpy and entropy changes in magnitude. Hence, the

169
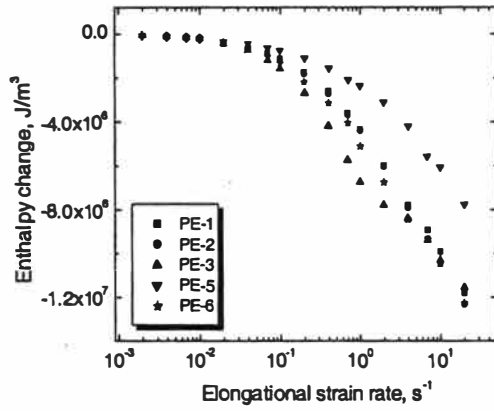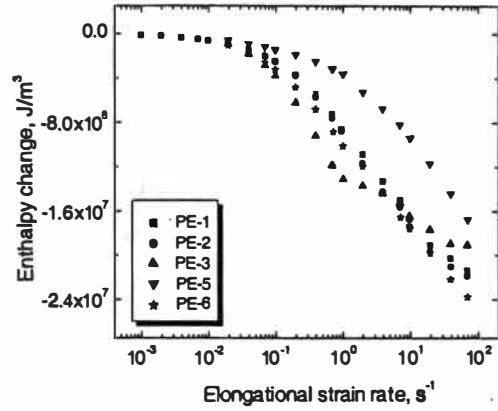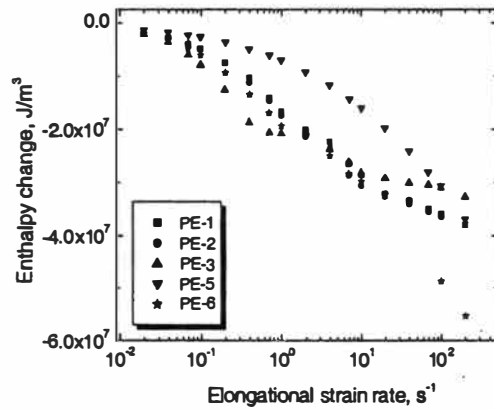
(a) Hencky 4
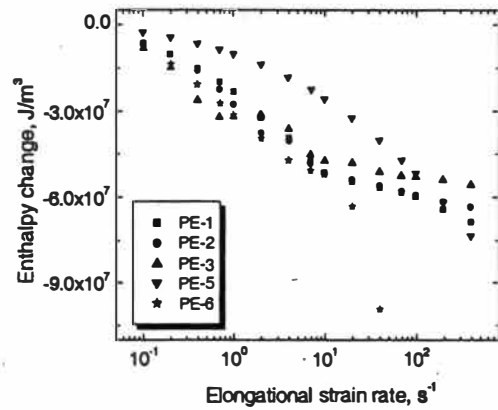
(b) Hencky 5

(c) Hencky 6

(d) Hencky 7

Figure 5.93. Enthalpy changes of different PE samples at 135°C.

170
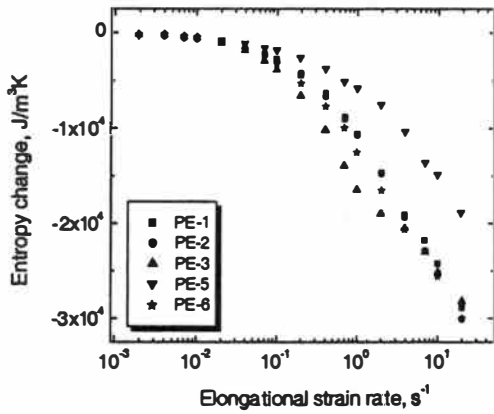
(a) Hencky 4

(b) Hencky 5

(c) Hencky 6

(d) Hencky 7

Figure 5.94. Entropy changes of different PE samples at 135°C.
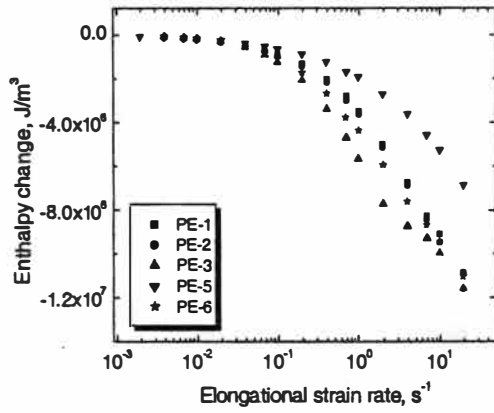
(a) Hencky 4
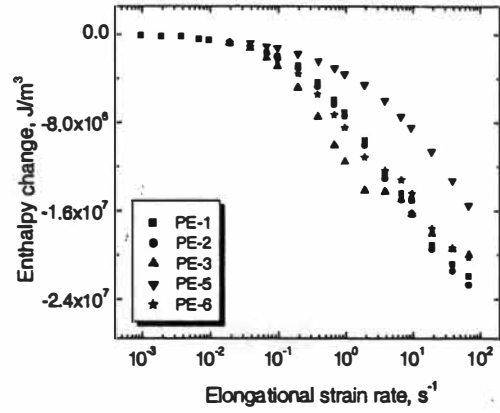
(b) Hencky 5
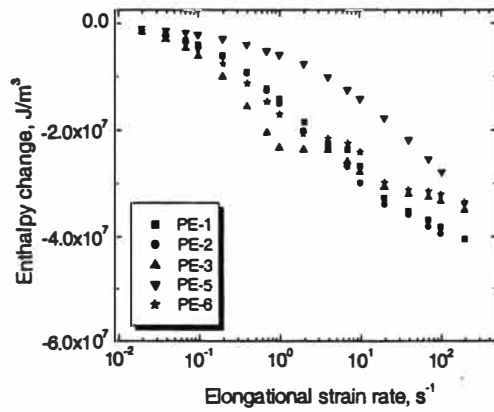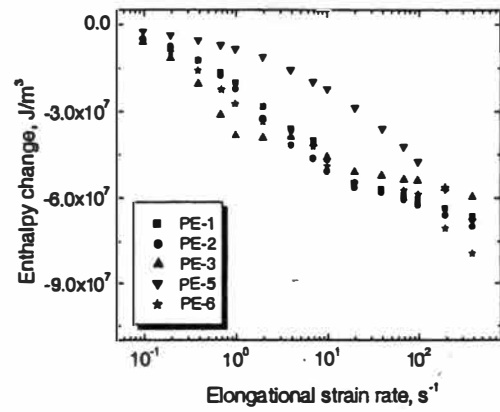
(c) Hencky 6

(d) Hencky 7

Figure 5.95. Enthalpy changes of different PE samples at 150°C.

172
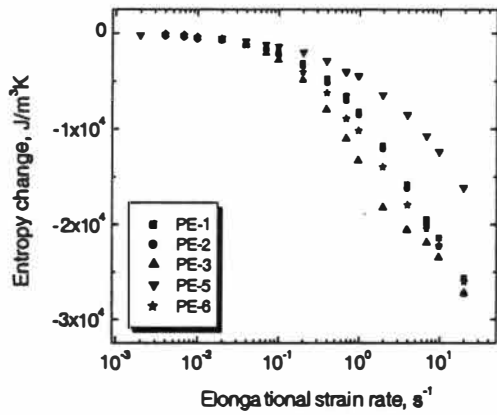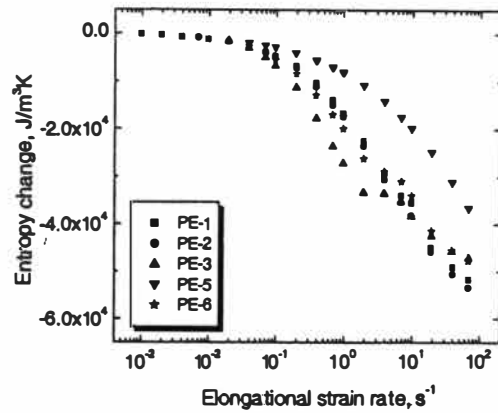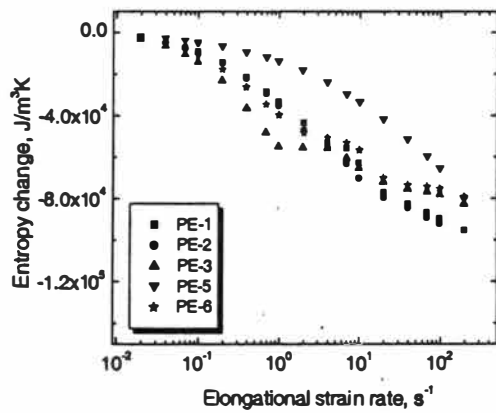
(a) Hencky 4
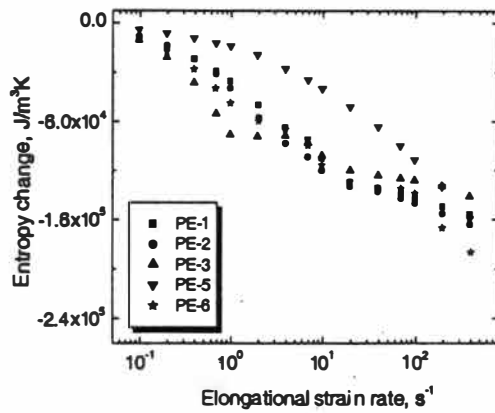
(b) Hencky 5

(c) Hencky 6

(d) Hencky 7

Figure 5.96. Entropy changes of different PE samples at 150°C.

173
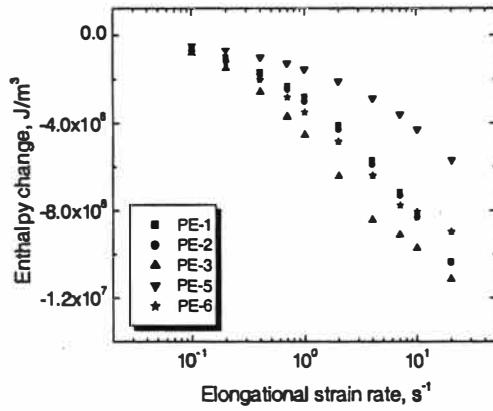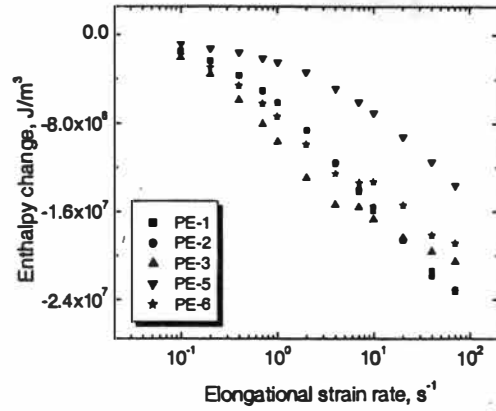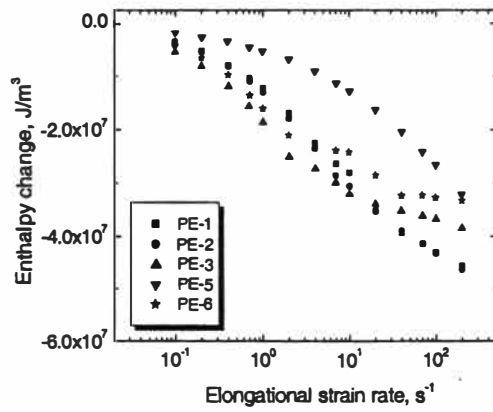
(a) Hencky 4
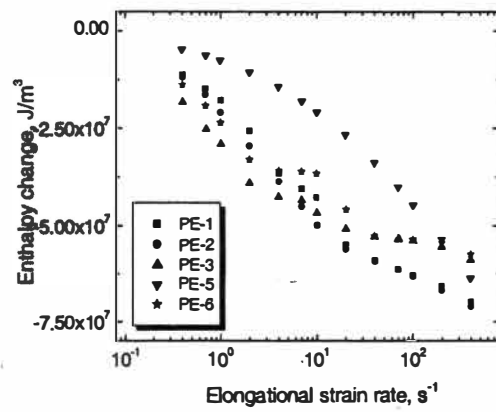
(b) Hencky 5

(c) Hencky 6

(d) Hencky 7

Figure 5.97. Enthalpy changes of different PE samples at 165°C.
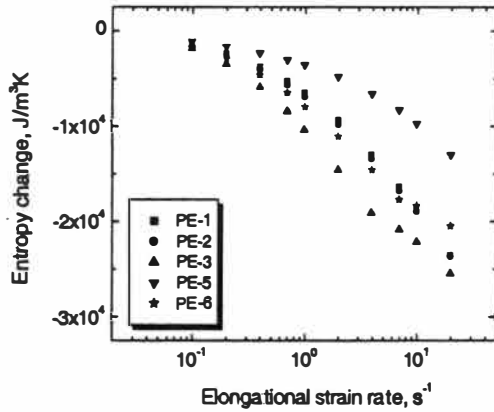
(a) Hencky 4
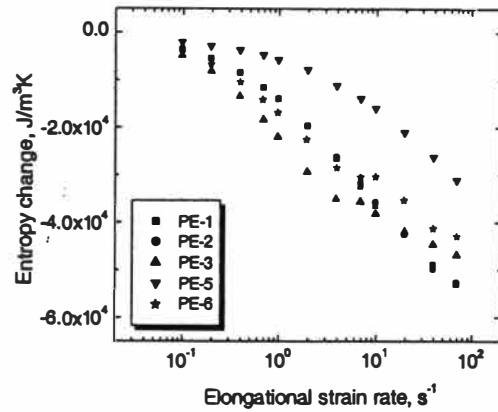
(b) Hencky 5
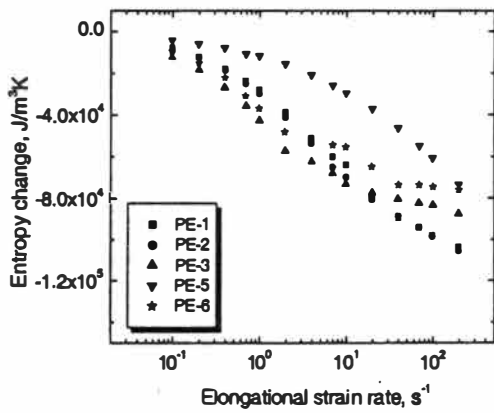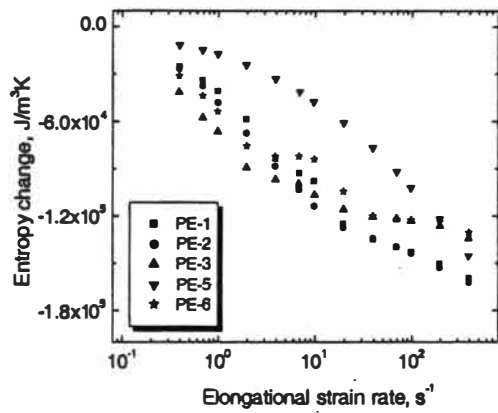
(c) Hencky 6

(d) Hencky 7

Figure 5.98. Entropy changes of different PE samples at 165°C.

175
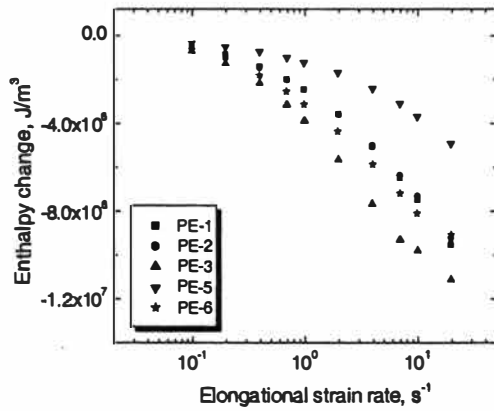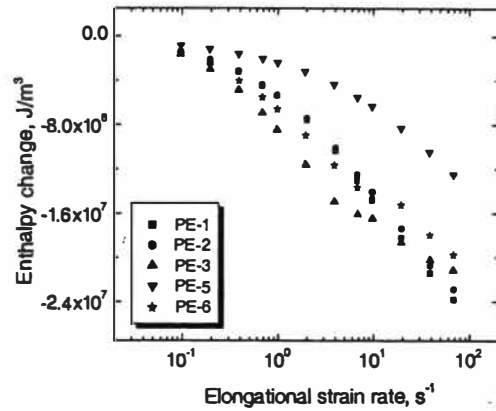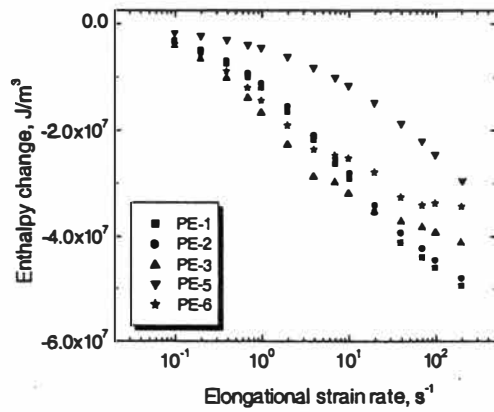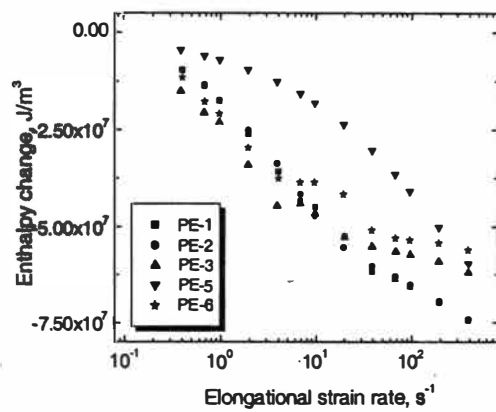
Figure 5.99. Enthalpy changes of different PE samples at 180°C.
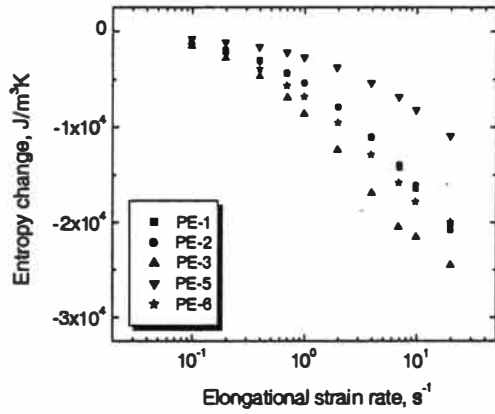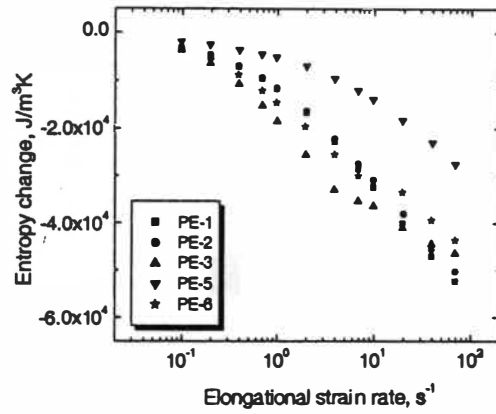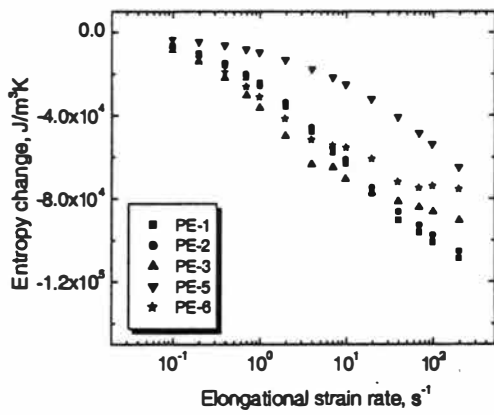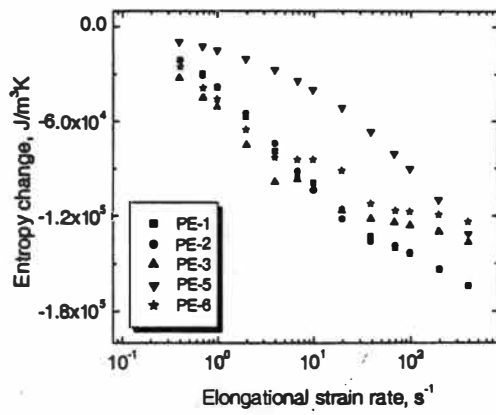
Figure 5.100. Entropy changes of different PE samples at 180°C.

effect of LCB seems to decrease the enthalpy and entropy changes in magnitude. All the rest figures show similar observations at different Hencky strains and temperatures.

The enthalpy change occurring in the hyperbolic flow can be compared with the heat of fusion from differential scanning calorimetry (DSC) measurement, which enables a comparison to the degree of orientation of a possible meta stable liquid form and of a solid crystalline state. A Mettler Toledo DSC 821^e was used for the DSC measurements where the heating was done followed by cooling. The heating was accomplished at a rate of 10°C/min for a temperature range of 20°C to 200°C. Then the temperature was held constant for 2 minutes. The cooling was done at a rate of 10°C/min from 200°C to 20°C. Table 5.6 shows the heats of fusion from DSC measurements and the maximum enthalpy changes in magnitude from the shear and elongational measurements at the rate of 400 s^{-1} for each sample. It can be seen that values are very comparable, indicating that the degrees of orientation of a possible meta stable liquid form and of a solid crystalline state are similar.

§5.4 DETERMINATION OF PARAMETERS NEEDED TO PREDICT MW AND MWD OF POLYMERS

§5.4.1 Theoretical Background

The behavior of storage modulus, G', vs. frequency, ω, for a typical linear amorphous polymer is illustrated in Figure 5.101 (86). There are two relaxation processes: the glass to rubber transition and the terminal cone relaxation. At low

178

Table 5.6. Heats of fusion from DSC and maximum enthalpy changes in magnitude from shear and elongational measurements of PE samples.

Sample	Density	DSC heat of fusion		Maximum enthalpy change in magnitude (J/m^3)
		(J/g)	(J/m^3)	
PE-1	0.909	87.53	7.96E+07	7.44E+07
PE-2	0.902	80.33	7.25E+07	7.43E+07
PE-3	0.900	81.69	7.35E+07	6.19E+07
PE-4	0.902	83.12	7.50E+07	6.97E+07
PE-5	0.919	90.91	8.35E+07	7.33E+07
PE-6	0.917	115.25	1.06E+08	9.92E+07
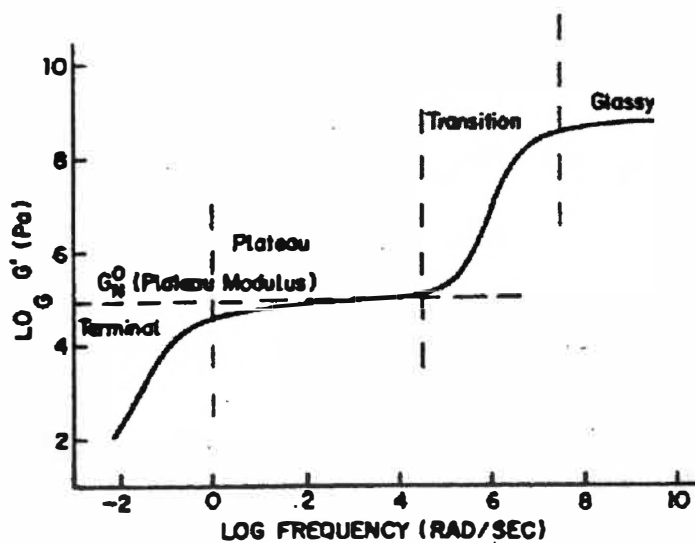
Figure 5.101. G' master curve for a typical linear amorphous polymer.
[Source: J.D.Ferry. *Viscoelastic Properties of Polymers.* Wiley, New York. 1980.]

179

frequencies, a plateau region is observed due to the presence of the transient entanglement network. The plateau modulus G_N can be defined as the constant G' value in the plateau region.

A mixing rule is a quantitative relationship relating the observed mechanical properties of a polydisperse melt and the underlying polymer structure. It is a relatively simple mathematical approximation to a more complex molecular theory of polydispersity. The double reptation model of des Cloizeaux (105-107) has achieved considerable success in modeling polydisperse systems (44, 125, 126). Mead (91) used the double-reptation mixing rule with a single exponential relaxation function to relate the relaxation modulus to the MWD.

This work uses Mead's approach (91) with the ^{RSI}Orchestrator^{TM} software to estimate the MW and MWD of PE and cellulose from dissolving pulp concentrated solution. The double-reptation mixing rule, used in the calculations here, is given as

$$G(t) = G_N (\int_0^\infty W(M)\sqrt{F(M,t)}dM)^2 \tag{5.18}$$

where $G(t)$ is the relaxation modulus, which can be determined from various linear viscoelastic experiments, G_N is the plateau modulus, $W(M)$ is the weight based MWD, and $W(M)dM$ represents the weight fraction of material with molecular weights between M and $M+dM$. The function $F(M,t)$ is the monodisperse relaxation function. It represents the time dependent fractional stress relaxation of monodisperse polymer following a small step strain. A single exponential form of this function (91) is

180

$$\sqrt{F(M,t)} = \exp\left(\frac{-t}{2\lambda(M)}\right) \tag{5.19}$$

where,

$$\lambda(M) = K_\lambda M^\alpha \tag{5.20}$$

where $\lambda(M)$ is the characteristic relaxation time for the monodisperse system and K_λ is a coefficient that depends on the precise chemical structure of the polymer and temperature. The relaxation time exponent α indicates how strongly the relaxation time of a polymer is related to its molecular weight.

The relaxation spectrum $H(\lambda)$ can be obtained from linear viscoelastic rheological data $G'(\omega)$ and $G''(\omega)$, using the following equations (116)

$$\frac{G'}{\omega^2} = \int_0^\infty \frac{\lambda(H(\lambda))d\lambda}{1+(\lambda\omega)^2} \tag{5.21}$$

$$\frac{G''}{\omega} = \int_0^\infty \frac{H(\lambda)d\lambda}{1+(\lambda\omega)^2} \tag{5.22}$$

The relaxation modulus $G(t)$ can be calculated from the following equation

$$G(t) = \int_{-\infty}^{+\infty} H(\lambda)e^{-t/\lambda}d\ln\lambda \tag{5.23}$$

Eq. (5.18) to Eq. (5.23) can be used to calculate the MW and MWD.

The "Synthesize Molecular Weight" function used by the ^{RSI}Orchestrator™ software is designed to calculate the MW and MWD of a material with given dynamic frequency sweep data ($G'(\omega)$ and $G''(\omega)$) by synthesizing a distribution based on material properties and an estimate for M_w and PI. Dynamic rheological

data are then calculated from this distribution and overlaid with the experimental data to determine how closely the two sets of data agree with each other. The M_w and PI parameters are then optimized to match the dynamic data. Figure 5.102 describes in a nutshell the procedure mentioned above.

§5.4.2 Results on Polyethylene Samples

§5.4.2.1 Material Parameters Determination

A close examination of Figure 5.102 reveals that three parameters are needed to convert the linear viscoelastic rheological data into MW and MWD curves, namely, the plateau modulus (G_N), the front factor (K_λ), and the relaxation time exponent (α). These parameters are dependent on the precise chemical structure and molecular architecture of the polymer. They are a function of the chemistry of the material and temperature, but generally do not vary with the MW or MWD of the polymer.

It can be assumed that PEs manufactured by the same process will have similar molecular architecture (i.e. type and degree of side chain branching), and hence, the same values of the mentioned parameters. However, PEs manufactured by different processes should in general have different values of the parameters. Keeping this in mind, the six PE samples mentioned in Table 4.1 are divided into three groups for data analysis: four metallocene catalyzed PEs (PE-1, PE-2, PE-3, and PE-4), two LLDPEs (PE-3 and PE-6), and one conventional LDPE (PE-5). Since
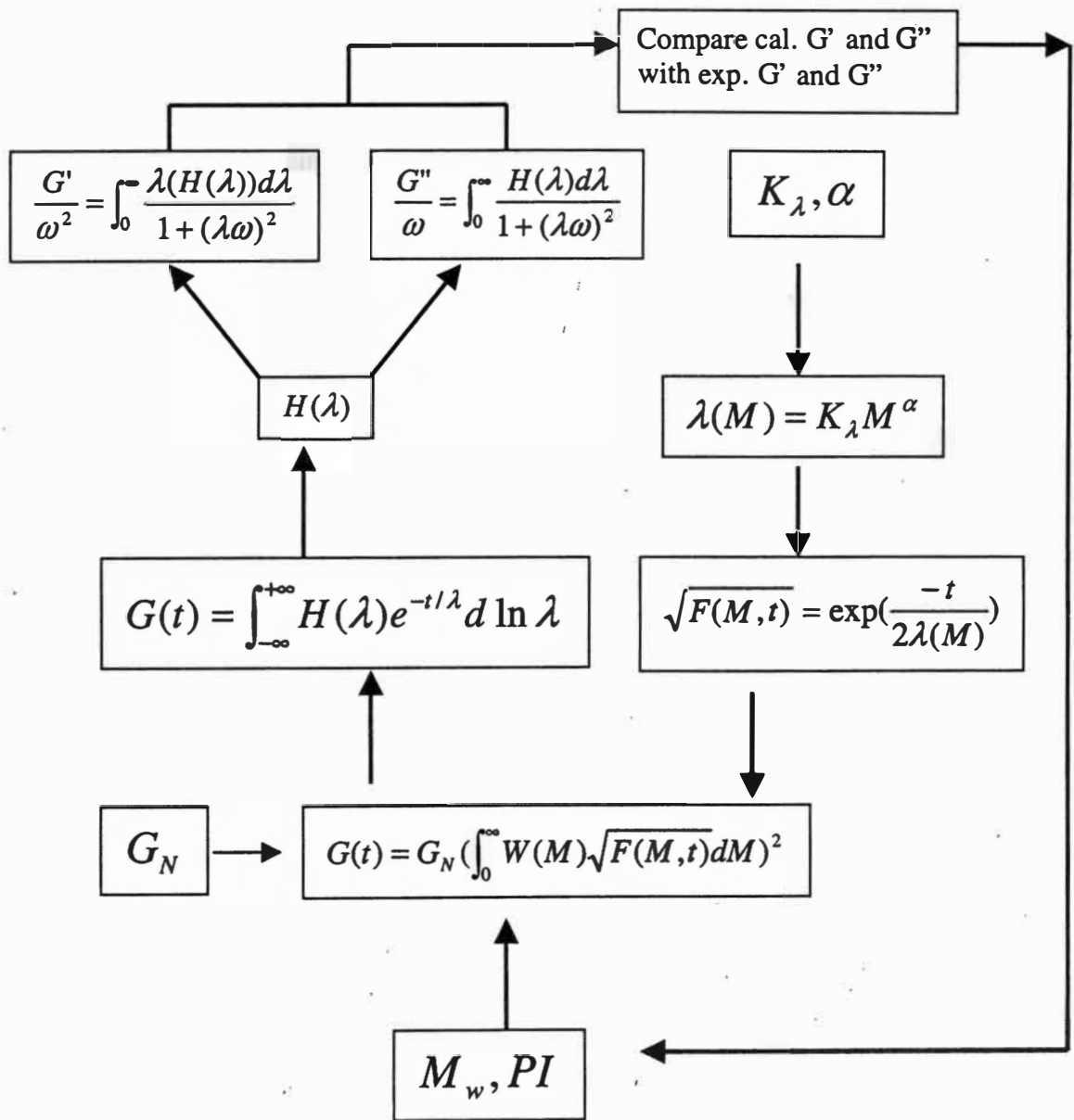
Figure 5.102. Summary of the calculation procedure to predict MW and MWD.

there is only one conventional LDPE in the PE sample set, two other conventional LDPEs (LDPE-D and E) are incorporated into analysis. These two LDPEs and their shear rheology data are from Dr. Parag Patil's dissertation (115). In each group, one sample is selected as a reference sample. The curve-fitting of the linear viscoelastic rheological data of this reference sample yields the required parameters for that particular group. Using these parameters, M_w and PI of the remaining samples in the group are then computed using the algorithm outlined in Figure 5.102 and are compared with the GPC measured M_w and PI. The procedure is repeated with each sample in the group and the sample that gives the best prediction results should be selected as the reference sample for that group.

Figures 5.103(a) and 5.103(b) show the plots of storage and loss moduli (G' and G'') vs. angular frequency (ω) at 175°C for metallocene PE and conventional LDPE samples, respectively. To accurately estimate the three unknown parameters (G_N, K_λ, and α), the dynamic moduli vs. frequency plot must satisfy three unique conditions. A scouting study reveals that the accuracy in fitting the moduli vs. frequency plot depends only on the value of G_N, and not on K_λ and α, i.e. a unique value of G_N exists for each sample that gives the minimum error in fitting the moduli vs. frequency curve. Once, the value of G_N is determined, K_λ and α can be estimated by equating the calculated M_w and PI with the GPC measured M_w and PI of the sample. Another scouting study reveals that the calculated M_w is much more sensitive to changes in K_λ than to changes in α, whereas, the calculated PI is much

184
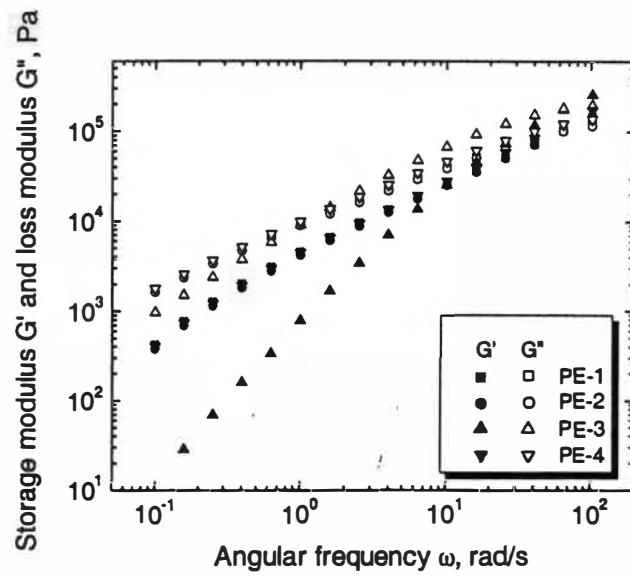
(a) Metallocene PE samples
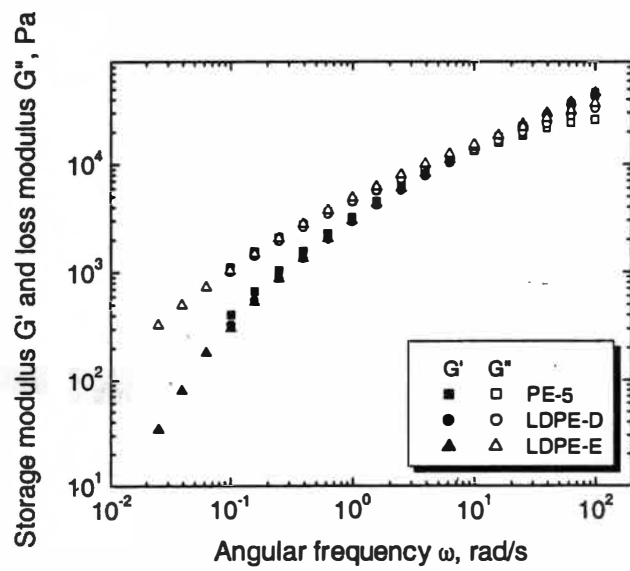
(b) Conventional LDPE samples

Figure 5.103. Storage and loss moduli curves for PE samples at 175°C.

185

more sensitive to changes in α than to changes in K_λ. Therefore, a best-fit value of α was first determined by comparing the calculated PI to the GPC measured PI followed by the determination of K_λ by comparing the calculated M_w to the GPC measured M_w. A log-normal distribution was assumed in these calculations to be consistent with the GPC measurements.

Figure 5.104 shows the excellent accuracy in fitting the moduli vs. frequency curves of PE-1. Similar analysis was performed on all PE samples and estimated values of parameters for each sample were obtained. Figure 5.105 shows the predicted MWD curves for PE-1 and PE-4. The values of parameters determined using each sample in the group were then used to calculate the M_w and PI of the remaining samples in the corresponding group, which were then compared with the M_w and PI measured by GPC. The average relative errors were calculated. Note that, only K_λ and α values are constant for the entire group of samples, whereas G_N value should be determined solely by minimizing the error in fitting the moduli vs. frequency curve for each sample. The prediction results were then compared to determine the best reference sample for each group.

Table 5.7 summarizes the accuracy in the estimation of M_w and PI of the PE samples at 175°C. However, this table shows that the predictions of MW and MWD of PE samples are not accurate. A good reference sample for the corresponding group cannot be found. To see whether this is due to the relatively short range of frequencies for the dynamic moduli data, master curves of dynamic moduli were

186
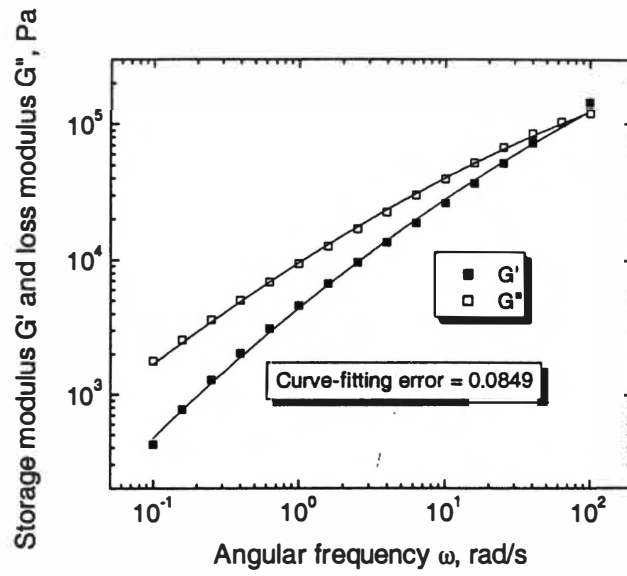
Figure 5.104. Experimental symbols and simulated solid lines storage and loss moduli curves for PE-1.
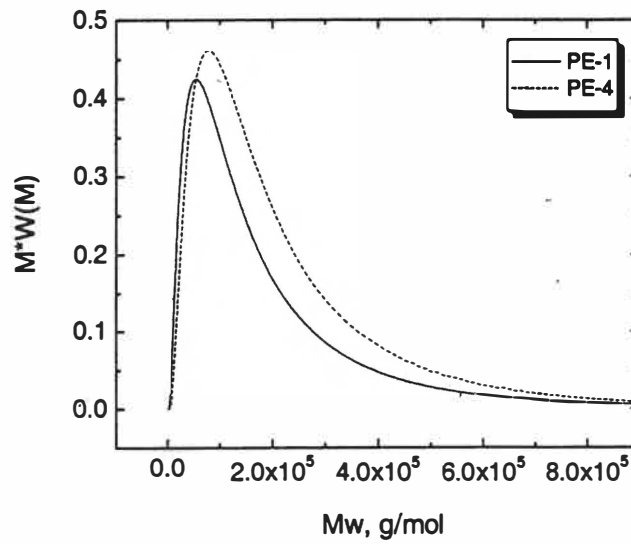
Figure 5.105. Predicted molecular weight distributions of PE-1 and PE-4.

187

Table 5.7. Accuracy of predictions of M_w and PI for PE samples at 175°C.

Sample type	Reference	Prediction	M_w (exp)	M_w (cal)	% error	PI (exp)	PI (cal)	% error
Metallocene	PE-1	PE-2	88700	87600	1.24	2.14	2.36	10.40
PE		PE-3	111000	143900	29.64	2.04	1.17	42.50
		PE-4	115800	79680	31.19	2.12	2.44	14.99
		Average			20.69			22.63
	PE-2	PE-1	87400	88500	1.26	2.43	2.19	9.95
		PE-3	111000	144300	30.00	2.04	1.15	43.55
		PE-4	115800	81140	29.93	2.12	2.20	3.54
		Average			20.40			19.01
	PE-3	PE-1	87400	91640	4.85	2.43	54.63	2148.27
		PE-2	88700	88960	0.29	2.14	47.78	2132.57
		PE-4	115800	75520	34.78	2.12	55.23	2505.00
		Average			13.31			2261.95
	PE-4	PE-1	87400	126100	44.28	2.43	2.11	13.02
		PE-2	88700	126400	42.50	2.14	2.07	3.49
		PE-3	111000	204800	84.50	2.04	1.14	43.92
		Average			57.10			20.14
LLDPE	PE-3	PE-6	122700	114200	6.93	3.44	5.33	55.06
	PE-6	PE-3	111000	126900	14.32	2.04	1.69	16.92
Conventional	PE-5	LDPE-D	86650	99740	15.11	6.85	9.32	36.09
LDPE		LDPE-E	80350	120100	49.47	5.15	4.10	20.43
		Average			32.29			28.26
	LDPE-D	PE-5	116000	99890	13.89	9.1	6.71	26.26
		LDPE-E	80350	105800	31.67	5.15	3.38	34.32
		Average			22.78			30.29
	LDPE-E	PE-5	116000	80180	30.88	9.1	12.89	41.59
		LDPE-D	86650	68110	21.40	6.85	13.25	93.46
		Average			26.14			67.53

obtained so that MW and MWD could be predicted in a wider frequency range. Dynamic moduli data at 135, 150, 165, and 180°C were shifted to the reference temperature of 150°C. These master curves are shown in Section 5.2. For comparison, dynamic moduli data at 150°C were also directly used to predict the MW and MWD.

Figures 5.106(a) and 5.106(b) show the resulted average relative errors from M_w and PI predictions for the metallocene PEs at 150°C, respectively. The x axis stands for the reference sample, where 1, 2, 3, and 4 are corresponding to PE-1, 2, 3, and 4, respectively. The relative errors from PI predictions using PE-3 as reference are not shown in Figure 5.106(b) since the errors are larger than 1000, too large compared with the others. Both Figures 5.106(a) and 5.106(b) show that the predictions of MW and MWD of metallocene PE samples are not accurate. By using master curves the relative errors from the M_w predictions decrease except for PE-3 while the relative errors from PI predictions increase. Therefore, the master curves do not increase the accuracy for the MW and MWD predictions for the metallocene PE samples.

A good reference sample for each group cannot be found using either the experimental dynamic moduli data or the master curves of these moduli data. This is probably due to the differences in the long chain branching or side chain branching of the PE samples. In the next sub-section, estimated values of parameters for each sample are compared at different temperatures.
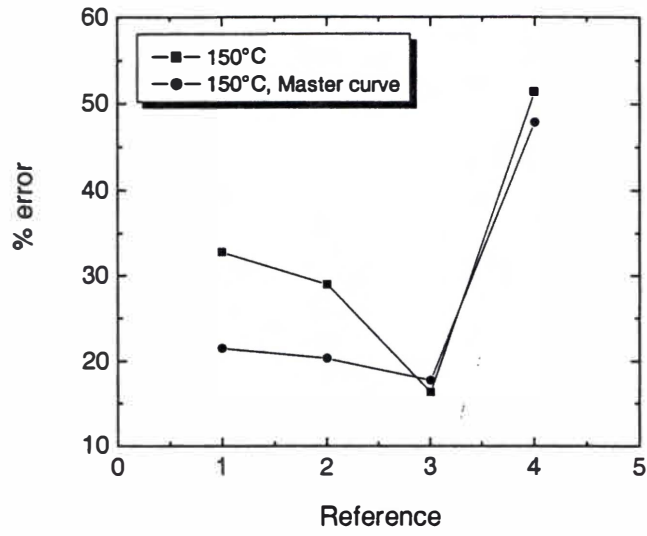
(a) M_w prediction
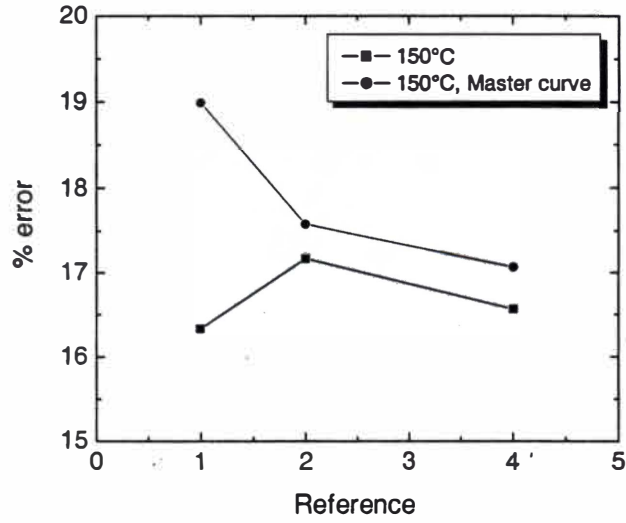
(b) PI prediction

Figure 5.106. Relative errors from M_w and PI predictions using moduli data at 150°C and from master curves shifted to 150°C.

§5.4.2.2 *Material Parameters Comparison*

Table 5.8 gives the estimated values of parameters for each PE sample except PE-3 at the temperatures of 135, 150, 165, 175, and 180°C. These parameters are also shown in Figures 5.107, 5.108, and 5.109. With the increase of temperature, the values of α and G_N decrease while the values of K_λ increase for all PE samples except for PE-6. For PE-6, the values of α and G_N increase while the values of K_λ decrease. The PE samples can be divided into two groups: the metallocene PE samples and conventional LDPE and LLDPE. The samples in each group have similar values of parameters. It is also observed that the metallocene samples have larger α and G_N values but much smaller K_λ values than the conventional LDPE or conventional LLDPE.

§5.4.3 Results on Cellulose Solution Samples

§5.4.3.1 *Linear Viscoelasticity*

The complex viscosity (η^*) data of 14% cellulose solutions from dissolving pulps of different DP_w as a function of strain are shown in Figure 5.110. It shows that the chosen strain of 1% for dynamic frequency sweep tests belongs to the linear viscoelastic range where η^* does not change with the strain. The η^* increases with the increase of DP_w at the same strain.

Figure 5.111 shows dynamic moduli curves for the cellulose solutions. Both G' and G'' increase with the increase of DP_w. In the range of experimental

Table 5.8. Results of curve-fitting of rheological data for parameter estimation.

Sample	T (°C)	α	G_N (Pa)	K_λ	M_w (cal)	PI (cal)	Curve-fitting error
PE-1	135	6.2030	8.00E+06	4.26E-35	87340	2.43	0.1139
	150	5.9000	7.00E+06	1.55E-33	87410	2.43	0.0865
	165	5.4675	4.60E+06	4.00E-31	87350	2.43	0.0730
	175	5.1081	3.22E+06	4.56E-29	87400	2.43	0.0849
	180	5.0223	3.00E+06	1.27E-28	87330	2.43	0.0750
PE-2	135	6.2012	5.00E+06	1.08E-34	88700	2.14	0.1259
	150	5.9955	4.50E+06	9.75E-34	88690	2.14	0.0966
	165	5.7050	3.86E+06	3.03E-32	88730	2.14	0.0759
	175	5.4303	3.10E+06	9.56E-31	88710	2.14	0.0786
	180	5.2804	2.80E+06	6.28E-30	88670	2.14	0.0799
PE-4	135	6.0680	5.90E+06	9.40E-35	115800	2.12	0.2022
	150	5.8870	5.60E+06	6.60E-34	115800	2.12	0.1462
	165	5.7181	5.20E+06	4.20E-33	115800	2.12	0.1105
	175	5.5610	4.85E+06	2.86E-32	115800	2.12	0.1023
	180	5.3654	3.80E+06	3.82E-31	115800	2.12	0.1028
PE-5	135	3.3870	3.20E+05	8.88E-19	116200	9.09	0.0184
	150	3.1011	2.50E+05	2.49E-17	116000	9.09	0.0389
	165	2.9817	2.28E+05	7.22E-17	115900	9.10	0.0248
	175	2.8955	2.15E+05	1.62E-16	116100	9.10	0.0342
	180	2.8850	2.00E+05	1.92E-16	116000	9.09	0.0327
PE-6	135	2.8000	1.00E+06	1.71E-16	122800	3.44	0.0880
	150	2.8016	1.12E+06	1.17E-16	122800	3.44	0.0700
	165	2.8330	1.18E+06	5.85E-17	122600	3.44	0.0880
	180	2.8830	1.20E+06	2.13E-17	122800	3.44	0.0764
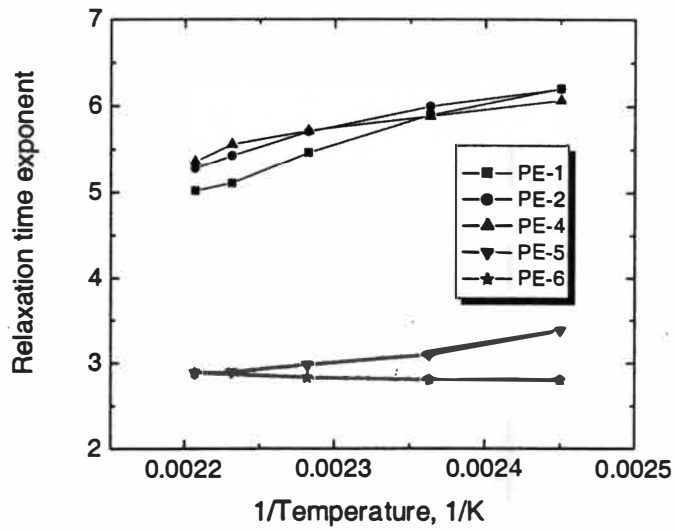
Figure 5.107. Relaxation time exponents of PE samples.
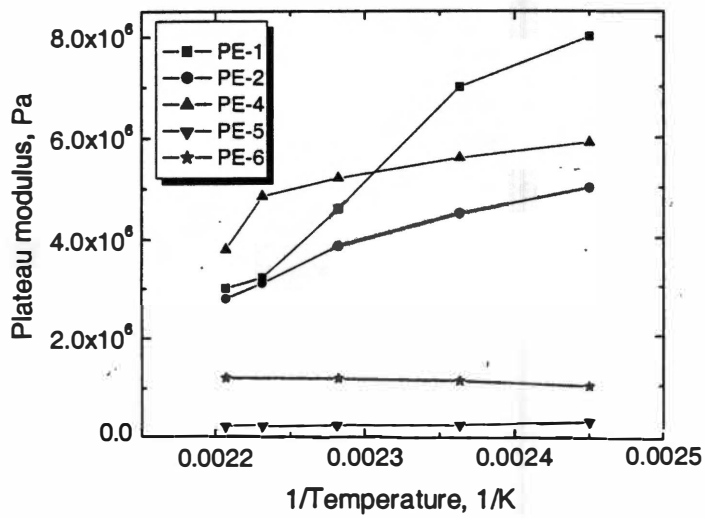
Figure 5.108. Plateau moduli of PE samples.

193
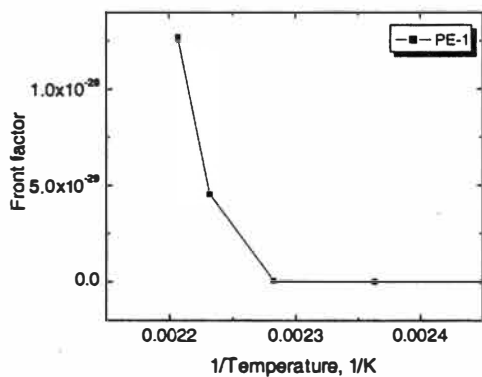
(a) PE-1
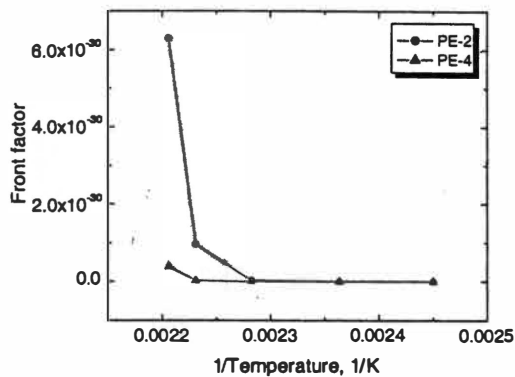
(b) PE-2 and PE-4
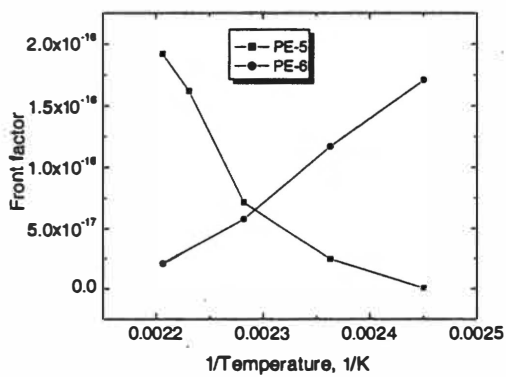
(c) PE-5 and PE-6

Figure 5.109. Front factor values of PE samples.

194
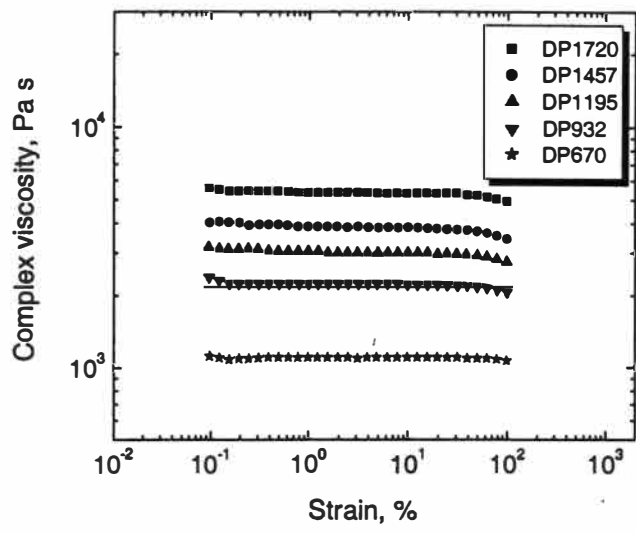
Figure 5.110. Complex viscosity vs. strain of 14% cellulose solutions at 90°C.
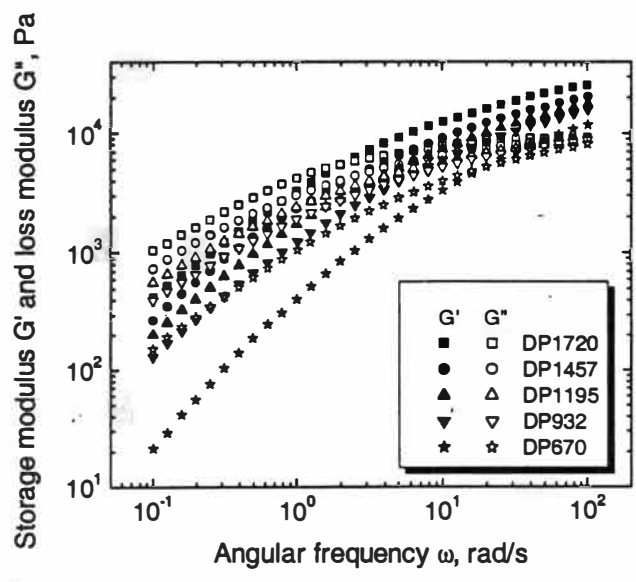
Figure 5.111. Storage and loss moduli curves of 14% cellulose solutions at 90°C.

195

frequencies, G' and G'' obviously increase with frequency. In the lower range of experimental frequencies, G'' are larger than G', showing the viscidity of cellulose solutions is relatively stronger than its elasticity. In the higher frequency region, $G' >$ G'', indicating the elasticity is relatively strong.

The complex viscosity data of cellulose solutions as a function of frequency are shown in Figure 5.112. For all the five solutions the complex viscosity data obviously decrease with the frequency. This is the shear thinning behavior of pseudoplastic fluids. At the same frequency, the viscosity increases with the increase of DP_w. But the differences between the complex viscosity data of five samples become smaller as the frequency increases.
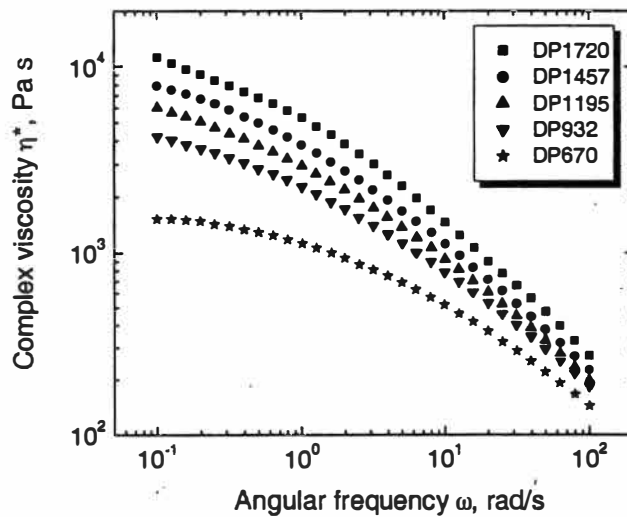
Figure 5.112. Complex viscosity of 14% cellulose solutions at 90°C.

§5.4.3.2 *Material Parameters Determination*

Since all the five cellulose solutions have the same concentration of 14% and were prepared from dissolving pulps, it is assumed that material parameters (G_N, K_λ, and α) to predict MW and MWD remain constant for these five pulps in the cellulose solutions.

For the dissolving pulps, the M_w can be calculated by multiplying the degree of polymerization by 162, the molecular weight of the monomer. However, PI data are not available unlike the PE samples. Therefore, a different calculation procedure was used to estimate the parameters required for the prediction of MW and MWD for the cellulose from these samples. Figure 5.111 shows the storage and loss moduli curves at 90°C for all samples. From these curves the frequency at which G' and G'' curves cross each other was calculated for each sample. If a Maxwell viscoelastic model is used, the reciprocal of the crossover frequency is the average relaxation time of the sample and therefore proportional to the weight-average MW for the cellulose from the solution. It is assumed that this is the characteristic relaxation time of the monodisperse system. The crossover frequencies and the average relaxation time for the cellulose solutions are given in Table 5.9. The average relaxation time increases with DP_w, showing that the molecular weight and interaction force between molecular chains increase with DP_w.

According to Eq. (5.20) the plot of $ln(\lambda)$ vs. $ln(M_w)$ should be a straight line with slope of α and intercept of $ln(K_\lambda)$. The plot of $ln(\lambda)$ vs. $ln(M_w)$ and its linear fit

Table 5.9. Crossover frequencies and average relaxation time of 14% cellulose solutions.

DP_w	Mw	Crossover frequency (s^{-1})	Average relaxation time (s)
670	108540	19.4640	0.0514
932	150984	5.8324	0.1715
1195	193590	3.5635	0.2806
1457	236034	2.5869	0.3866
1720	278640	2.0541	0.4868

are shown in Figure 5.113, from which K_λ and α were calculated as 1.00×10^{-13} and 2.3429, respectively. The value of G_N was estimated by minimizing the error in the fitting of moduli vs. frequency curves just as in the case of PE samples. A plot of predicted molecular weight distribution curves of the dissolving pulps is shown in Figure 5.114.

The comparison of the predicted and actual weight-average molecular weights of dissolving pulps is presented in Table 5.10, which shows good accuracy in the prediction of M_w. The predicted PI increases in the order of DP670 < DP1720 < DP932 < DP1195 < DP1457. The predicted PI data of blends are higher than those of neat materials, which is to be expected. Therefore, material properties K_λ, α, and G_N are determined as 1.00×10^{-13}, 2.3429, and 4.90×10^4 Pa. These material properties can be used to predict MW of cellulose from 14% dissolving pulps concentrated solutions by rheological method using the [RSI]Orchestrator[TM] software.

198
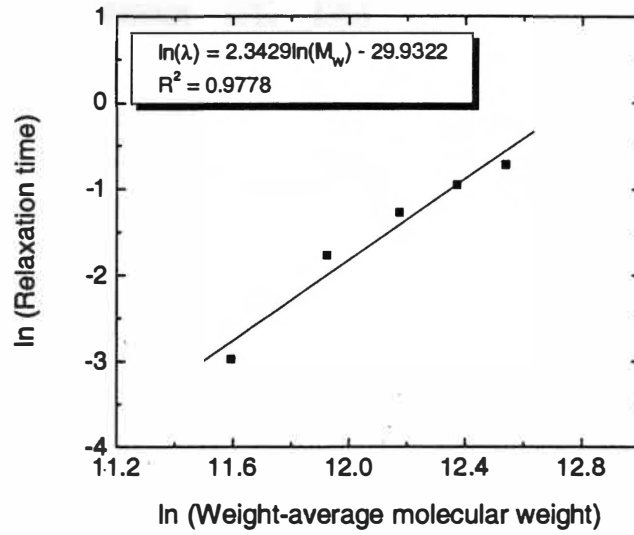
Figure 5.113. Plot of *ln(λ)* vs. *ln(M_W)* for dissolving pulps to estimate α and K_λ.
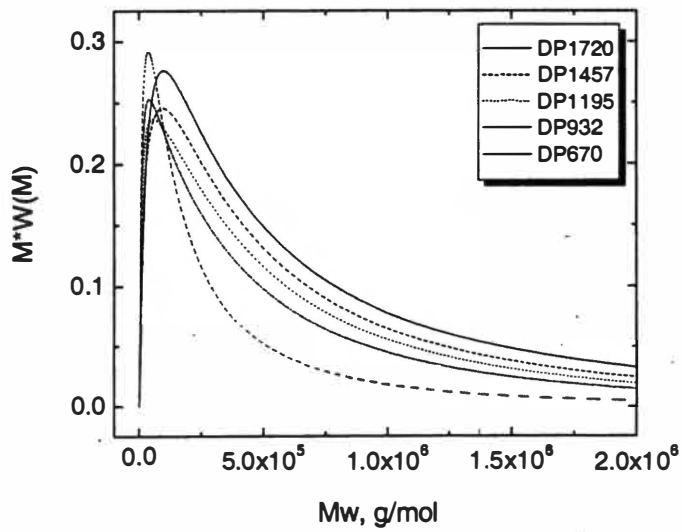
Figure 5.114. Predicted molecular weight distributions of dissolving pulps.

Table 5.10. Accuracy of prediction of M_w for dissolving pulps ($G_N = 4.90 \times 10^4$ Pa, $\alpha = 2.3429$, $K_\lambda = 1.00 \times 10^{-13}$).

DP	M_w (exp)	M_w (cal)	% error	PI (cal)	Curve-fitting error
670	108540	101000	7.04	6.4692	0.1789
932	150984	164000	8.82	8.7323	0.0071
1195	193590	193000	0.25	9.8832	0.0050
1457	236034	227000	3.74	11.7750	0.0240
1720	278640	287000	2.86	8.0605	0.2020
			Average: 4.54		**Average: 0.0834**

Chapter 6

Conclusions and
Future Work

§6.1 CONCLUSIONS

In this work, shear rheology of polyethylenes, polyisobutylene, and cellulose solutions was measured at different temperatures using a rotational rheometer (ARES). Elongational viscosity of polyethylenes and polyisobutylene was also measured at different Hencky strains and temperatures using a capillary rheometer (ACER) by replacing the capillary cylindrical die with a hyperbolic converging axisymmetric die. The hyperbolic shape of the dies enables a constant elongational strain rate throughout the die. The effects of both molecular characteristics and processing conditions on the elongational viscosity of polyethylenes and polyisobutylene were studied. The results from the hyperbolic dies were compared with results from other techniques, namely Rheometrics Extensional Rheometer (RER) and Elongational Rheometer for Melts (RME). Master curves from temperature and Hencky strain shifting, and general master curves by simultaneously shifting with respect to both temperature and Hencky strain were developed. The enthalpy and entropy changes were calculated from the shear and elongational viscosities and compared with the heats of fusion from DSC measurements. Methods to determine the parameters needed to predict the MW and MWD of polyethylene and cellulose (in dissolving pulp concentrated solution) samples from their shear rheological data were also presented.

The effective elongational viscosity of polymer melts is considerably affected by their molecular characteristics. The effective elongational viscosity of different

203

samples flattened out differently at low elongational strain rates. Both MWD and LCB seemed to promote the strain rate thinning. The onset of strain rate thinning occurred at a lower strain rate for the conventional LDPE so that the conventional LDPE showed a different shape of the viscosity curve and lower elongational viscosity. Moreover, both the PI and LCB seemed to decrease the elongational viscosity. All PE samples showed similar patterns of strain hardening, on which the temperature did not have considerable effect. All PE samples showed similar patterns when the effective elongational viscosity was plotted as a function of the residence time (defined as Hencky strain over strain rate) and compared with the shear viscosity. Strain hardening could be accessed from these plots according to the relationship between shear and elongational viscosities measured from Meissner-type extensional rheometer. PIB and PE samples had different patterns for the effective elongational viscosity as a function of the transient time. PE samples showed strain hardening, whereas PIB sample did not show strain hardening.

The elongational viscosity measured by using two techniques (the Rheometrics Extensional Rheometer and the hyperbolic converging die) showed good agreement for the conventional LDPE but not as good for other PE samples. The elongational viscosity of PIB measured by the hyperbolic dies and the Elongational Rheometer for Melts (RME) showed similar patterns to each other. The values obtained in our work are close to those from RME. The factorized Rivlin-Sawyers constitutive equation (116) had been used to calculate the elongational viscosity of some other PE samples by Dr. Brian Edwards' research group at The

University of Tennessee, Knoxville. Good agreement was found between the calculated values and the experimental data. The calculated results also showed the relationship between shear and elongational viscosities measured from Meissner-type extensional rheometer (117). Hence, the comparison of the measured elongational viscosity by different techniques and theory predictions indicates that the measured effective elongational viscosity is a good approximation to the material's true elongational viscosity.

Besides the molecular characteristics discussed above, rheological properties are considerably affected by the processing conditions such as temperature, Hencky strain, and strain rate. All samples showed strain rate thinning for the effective elongational viscosity. Furthermore, effective elongational viscosity of polymer melts increased with decreasing temperature and increasing Hencky strain. Both Cross and Carreau models yielded good master curves for the temperature shifting of effective elongational viscosity. The shift factors showed good Arrhenius dependence. Conventional LDPE have larger activation energy, whereas linear PEs have smaller activation energies. Hence, the presence of long chain branches increases the flow activation energy of PE.

Good master curves for the Hencky strain shifting of effective elongational viscosity were created using two methods to calculate the Hencky strain shift factors (124). But generally speaking, Method 2 gave slightly better results than Method 1, where Method 1 was based upon an orientation ratio being equal to the relaxation ratio while Method 2 was based upon an "orientational viscosity ratio". By

combining the shift factors from temperature and Hencky strain shifting, good general master curves were also generated for the simultaneous temperature and Hencky strain shifting. Hence, the elongational strain rate range of the experimental geometry extended. One of the long-term objectives of this research group is to design an on-line elongational rheology sensor for polymer processing processes involving elongational flow. Generalized master curves and the shift factors would be very useful in the development of such a sensor.

In an effort to investigate flow induced orientation of the polymer melts in hyperbolic dies, the enthalpy and entropy changes were calculated from the effective elongational and shear viscosities. The enthalpy and entropy changes increased in magnitude as the elongational strain rate increased. Namely, the melt was transformed to a more ordered state corresponding to a lower entropy and greater magnitude latent heat of transformation with increasing strain rate. Furthermore, extruded melts exhibited larger enthalpy and entropy changes in magnitude for hyperbolic die with higher Hencky strain. Thus, flow induced orientation occurred in the hyperbolic flow with the extent being dependent upon the elongational strain rate and die geometry. The molecular characteristics have similar effects on the effective elongational viscosity and the enthalpy and entropy changes. The conventional LDPE shows smaller enthalpy and entropy changes in magnitude. Both the PI and LCB seem to decrease the enthalpy and entropy changes. The heats of fusion from DSC measurements and the maximum enthalpy changes from the shear and

elongational measurements are comparable, indicating that the degrees of orientation of a possible meta stable liquid form and of a solid crystalline state are similar.

A new method was proposed to estimate the parameters required (the plateau modulus G_N, the front factor K_λ, and the relaxation time exponent α) for the rheology to MW and MWD conversions using Mead's approach based on the double-reptation model. These three parameters were determined by forcing the storage and loss moduli curves of PE samples to satisfy three unique conditions, namely, minimization of curve-fitting error, convergence of the calculated PI to the GPC measured PI, and convergence of the calculated M_w to the GPC measured M_w.

Assuming that PEs manufactured by the same process had similar molecular architecture, and hence, the same values of parameters, the PE samples were divided into three groups for data analysis: metallocene catalyzed PEs, LLDPEs, and conventional LDPEs. In each group, one sample was selected as a reference sample whose best-fit parameters (except G_N) were used for that particular group to calculate MW and MWD. A good reference sample for each group could not be found using either the experimental dynamic moduli data or the master curves of these moduli data. This is probably due to the differences in the long chain branching or side chain branching of the PE samples. With the increase of temperature, the values of α and G_N decrease while the values of K_λ increase for all PE samples except for the conventional LLDPE. The metallocene PE samples have similar values of parameters. So do the conventional LDPE and LLDPE. The metallocene samples

have larger α and G_N values but much smaller K_λ values than the conventional LDPE or conventional LLDPE.

For the dissolving pulps, PI data were not available through GPC. Hence, the parameters K_λ and α were determined from the plot of average relaxation time (the reciprocal of crossover frequency) vs. weight-average molecular weight. The value of G_N was estimated by minimizing the error in the fitting of moduli vs. frequency curves just as in the case of PE samples. This method predicted the MW very well. However, no experimental PI data were available to compare with the predicted values.

§6.2 FUTURE WORK

With the knowledge of the molecular characteristics of MW, MWD, and LCB, the six polyethylene samples studied in this work were very suitable to study the effects of molecular characteristics on the effective elongational viscosity, enthalpy and entropy changes associated with the orientation development in the melt in the hyperbolic dies. But this set of polyethylene samples could not give good general parameters for each PE group to predict the MW and MWD of polyethylene samples from their shear rheological data. Some other metallocene PEs and conventional LDPEs were previously studied in this research group. But only MW and PI are known for these samples. If the long chain branches are measured and obtained for these samples, and the MWD curves are obtained for all PE samples, the study of the effects of molecular characteristics on the effective elongational

viscosity, enthalpy and entropy changes could be complete and accurate. General parameters or methods to determine general parameters for each PE group might be found to predict the MW and MWD of polyethylene samples from their shear rheological data.

The comparison of the measured elongational viscosity by different techniques and theory predictions indicates that the measured effective elongational viscosity is an excellent approximation to the material's true elongational viscosity. If elongational viscosity of more PE samples would be measured and compared by different techniques, theoretically predicted and compared with the experimental data from the hyperbolic dies, then the relationship between the measured effective elongational viscosity from the hyperbolic dies and the material's true elongational viscosity would be better determined.

Good master curves were generated for the temperature and Hencky strain shifting, and simultaneous shifting with respect to both temperature and Hencky strain. Generalized master curves and the shift factors would be very useful in the modeling of an on-line elongational rheology sensor for polymer processing processes involving elongational flow. Work in this on-line sensor has been initiated in this group to measure either shear or elongational rheology by changing the shape of the die so that both shear and elongational rheology could be controlled simultaneously. Rheological measurements are quick, easy, and inexpensive. Knowing the parameters to predict the MW and MWD and incorporating the results of the effect of molecular characteristics on the shear and elongational rheology, and

incorporating the results of master curves, the on-line sensor would provide an opportunity to develop real time, on-line process and quality control analysis of polymer properties in industrial equipments.

Although the enthalpy and entropy changes were calculated from the effective elongational and shear viscosities, other methods need to be developed to quantitatively measure the flow induced orientation of the polymer melts in hyperbolic dies. Hence, the converging flow process in the hyperbolic die could be better understood.

REFERENCES

REFERENCES

1. B.Schlund and L.A.Utracki. *Polymer Engineering and Science* **27**, 380 (1987).

2. H.A.Barnes, J.F.Hutton, and K.Walters. *An Introduction to Rheology.* Elsevier Science Publishers B.V., Amsterdam. 1989.

3. J.Meissner. *Transactions of the Society of Rheology* **16**, 405 (1972).

4. F.N.Cogswell. *Plastics & Polymers* **36**, 109 (1968).

5. F.T.Trouton. *Proceedings of the Royal Society* **A77**, 426 (1906).

6. R.L.Ballman. *Rheologica Acta* **4**, 137 (1965).

7. J.Meissner. *Rheologica Acta* **8**, 78 (1969).

8. J.Meissner. *Rheologica Acta* **10**, 230 (1971).

9. Y.Ide and J.L.White. *Journal of Applied Polymer Science* **22**, 1061 (1978).

10. J.Meissner. *Journal of Applied Polymer Science* **16**, 2877 (1972).

11. B.Schlund and L.A.Utracki. *Polymer Engineering and Science* **27**, 1523 (1987).

12. S.E.Bin Wadud and D.G.Baird. *Society of Plastic Engineers Annual Technical Conference (ANTEC)* **1**, 1200 (1999).

13. O.Ishizuka and K.Koyama. *Polymer* **21**, 164 (1980).

14. R.Hingmann and B.L.Marczinke. *Journal of Rheology* **38**, 573 (1994).

15. H.Münstedt. *Journal of Rheology* **24**, 847 (1980).

16. H.Yamane and J.L.White. *Polymer Engineering Reviews* **2**, 167 (1983).

17. P.P.Kundu, D.K.Tripathy, and B.R.Gupta. *Journal of Applied Polymer Science* **63**, 187 (1997).

18. T.Takahashi, J.Takimoto, and K.Koyama. *Journal of Applied Polymer Science* **73**, 757 (1999).

19. P.P.Kundu, A.K.Bhattacharya, and D.K.Tripathy. *Journal of Applied Polymer Science* **66**, 1759 (1997).

20. H.M.Laun and H.Schuch. *Journal of Rheology* **33**, 119 (1989).

21. J.Meissner. *Chemical Engineering Communications* **33**, 159 (1985).

22. H.Münstedt and H.M.Laun. *Rheologica Acta* **20**, 211 (1981).

23. W.Minoshima and J.L.White. *Journal of Non-Newtonian Fluid Mechanics* **19**, 251 (1986).

24. H.Münstedt, S.Kurzbeck, and L.Egersdörfer. *Rheologica Acta* **37**, 21 (1998).

25. A.Santamaria. *Materials Chemistry and Physics* **12**, 1 (1985).

26. A.Valenza, F.P.La Mantia, and D.Acierno. *European Polymer Journal* **24**, 81 (1988).

27. H.Münstedt and S.Kurzbeck. In *Elongational Behaviour and Molecular Structure of Polymer Melts*. Darmstadt, Germany. 1998. p. 41.

28. H.Münstedt. *Rheologica Acta* **14**, 1077 (1975).

29. L.Berger and J.Meissner. *Rheologica Acta* **31**, 63 (1992).

30. J.Meissner and J.Hostettler. *Rheologica Acta* **33**, 21 (1994).

31. F.P.La Mantia, A.Valenza, and D.Acierno. *Polymer Bulletin* **15**, 381 (1986).

32. M.Kobayashi, T.Takahashi, J.Takimoto, and K.Koyama. *Polymer* **37**, 3745 (1996).

33. K.Walters. *Rheometry*. Chapman and Hill. 1975.

34. C.J.S.Petrie. *Elongational Flows*. Pitman. 1979.

35. *Handbook of Polymer Science and Technology*. Marcel Dekker, Inc., New York. 1989.

36. P.Micic and S.N.Bhattacharya. *Polymer Engineering and Science* **40**, 1571 (2000).

37. J.Meissner, T.Raible, and S.E.Stephenson. *Journal of Rheology* **25**, 1 (1981).

38. B.Zulle, J.J.Linster, J.Meissner, and H.P.Hurlimann. *Journal of Rheology* **31**, 583 (1987).

39. M.H.Wagner, H.Bastian, P.Ehrecke, P.Hachmann, and J.Meissner. In *A Constitutive Analysis of Uniaxial, Equibiaxial and Planar Extension of Linear and Branched Polyethylene Melts.* Darmstadt, Germany. 1998. p. 4.

40. H.C.Kim, A.Pendse, and J.R.Collier. *Journal of Rheology* **38**, 831 (1994).

41. J.R.Collier, O.Romanoschi, and S.Petrovan. *Journal of Applied Polymer Science* **69**, 2357 (1998).

42. J.R.Collier. *Lubricated Flow Elongational Rheometer.* [5,357,784]. 1994. U.S. Ref Type: Patent.

43. S.Petrovan, J.R.Collier, and G.H.Morton. *Journal of Applied Polymer Science* **77**, 1369 (2000).

44. C.Tsenoglou. *Macromolecules* **24**, 1762 (1991).

45. B.H.Shah and R.Darby. *Polymer Engineering and Science* **16**, 579 (1976).

46. E.Menefee. *Journal of Applied Polymer Science* **16**, 2215 (1972).

47. B.H.Bersted and J.D.Slee. *Journal of Applied Polymer Science* **21**, 2631 (1977).

48. S.Middleman. *Journal of Applied Polymer Science* **11**, 417 (1967).

49. D.Darwis, K.Nishimura, H.Mitomo, and F.Yoshii. *Journal of Applied Polymer Science* **74**, 1815 (1999).

50. C.W.Macosko. *Rheology: Principles, Measurements, and Applications.* VCH Publishers, Inc., New York. 1994.

51. H.Münstedt. *Journal of Rheology* **23**, 421 (1979).

52. A.E.Everage JR. and R.L.Ballman. *Journal of Applied Polymer Science* **20**, 1137 (1976).

53. H.M.Laun and H.Münstedt. *Rheologica Acta* **17**, 415 (1978).

54. P.Micic, S.N.Bhattacharya, and G.Field. *Polymer Engineering and Science* **38**, 1685 (1998).

55. P.Micic, S.N.Bhattacharya, and G.Field. *International Polymer Processing* **XIII**, 50 (1998).

56. T.S.Wilson and D.G.Baird. *Journal of Non-Newtonian Fluid Mechanics* **44**, 85 (1992).

57. W.A.Kernick III and N.J.Wagner. *Macromolecules* **32**, 1159 (1999).

58. A.D.Gotsis and M.A.Odriozola. In *Elongational Viscosity of a Thermotropic Liquid Crystalline Polymer*. Darmstadt, Germany. 1998. p. 222.

59. C.H.Suh and J.L.White. *Journal of Non-Newtonian Fluid Mechanics* **62**, 175 (1996).

60. H.Gramespacher and J.Meissner. *Journal of Rheology* **41**, 27 (1997).

61. N.E.Hudson and J.Ferguson. *Transactions of Society of Rheology* **20**, 265 (1976).

62. D.M.Jones, K.Walters, and P.R.Williams. *Rheologica Acta* **26**, 20 (1987).

63. J.Ferguson and M.K.H.El-Tawashi. In *Rheology Vol.2: Fluids*. Edited by G.Astartia. 1980. p. 257.

64. H.H.Winter, C.W.Macosko, and K.E.Bennett. *Rheologica Acta* **18**, 323 (1979).

65. A.B.Metzner and A.P.Metzner. *Rheologica Acta* **9**, 174 (1970).

66. F.N.Cogswell. *Polymer Engineering and Science* **12**, 64 (1972).

67. F.N.Cogswell. *Transactions of the Society of Rheology* **16**, 383 (1972).

68. D.M.Binding and K.Walters. *Journal of Non-Newtonian Fluid Mechanics* **30**, 233 (1988).

69. G.K.Batchelor. *An Introduction to Fluid Dynamics*. Cambridge University Press, Cambridge. 1967.

70. B.Tremblay. *Journal of Non-Newtonian Fluid Mechanics* **33**, 137 (1989).

71. G.G.Fuller, C.A.Cathey, B.Hubbard, and B.E.Zebrowski. *Journal of Rheology* **31**, 235 (1987).

72. S.L.Ng, R.P.Mun, D.V.Boger, and D.F.James. *Journal of Non-Newtonian Fluid Mechanics* **65**, 291 (1996).

73. M.E.Mackay, A.M.Dajan, H.Wippel, H.Janeschitz-Kriegl, and M.Lipp. *Journal of Rheology* **39**, 1 (1995).

74. S.A.McGlashan and M.E.Mackay. *Journal of Non-Newtonian Fluid Mechanics* **85**, 213 (1999).

75. R.H.Boyd and P.J.Phillips. *The Science of Polymer Molecules*. Cambridge University Press. 1990.

76. Y.R.Oh, Y.S.Lee, M.H.Kwon, and O.O.Park. *Journal of Polymer Science: Part B: Polymer Physics* **38**, 509 (2000).

77. H.Determann. *Gel Chromatography*. Springer-Verlag New York Inc. 1969.

78. T.R.Dargaville, F.N.Guerzoni, M.G. Looney, D.A.Shipp, D.H.Solomon, and X.Zhang. *Journal of Polymer Science Part A: Polymer Chemistry* **35**, 1399 (1997).

79. B.S.Paymond. *Introduction to Polymer Chemistry*. Mc Graw-Hill, Inc. 1971.

80. L.J.Porter. *Australian Journal of Chemistry* **39**, 557 (1986).

81. T.B.Macrury and M.L.Mcconnell. *Journal of Applied Polymer Science* **24**, 651 (1979).

82. M.L.Mcconnell. *American Laboratory* **10**, 63 (1978).

83. B.Folie, M.Kelchtermans, J.R.Shutt, H.Schonemann, and V.Krukonis. *Journal of Applied Polymer Science* **64**, 2015 (1997).

84. S.Shiga and Y.Sato. *Nippon Gomu Kyokaishi* **57**, 229 (1984).

85. T.Hjerberg, L.I.Kulin, and E.Soervik. *Polymer Testing* **3**, 267 (1983).

86. J.D.Ferry. *Viscoelastic Properties of Polymers*. Wiley, New York. 1980.

87. W.W.Graessley. *Advanced Polymer Science* **16**, 1 (1974).

88. D.S.Pearson. *Rubber Chemistry and Technology* **60**, 439 (1987).

89. W.H.Tuminello. *Society of Plastic Engineers Annual Technical Conference (ANTEC)*, 990 (1987).

90. M.T.Shaw and W.H.Tuminello. *Polymer Engineering and Science* **34**, 159 (1994).

91. D.W.Mead. *Journal of Rheology* **38**, 1797 (1994).

92. G.R.Zeichner and C.W.Macosko. *Society of Plastic Engineers Annual Technical Conference (ANTEC)* San Francisco. 1982.

93. E.J.Dormier, P.Tong, and R.R.Lagasse. *Society of Plastic Engineers Annual Technical Conference (ANTEC)* **30**, 421 (1984).

94. K.Nonomiya and H.Fujita. *Journal of Colloid Science* **12**, 204 (1957).

95. E.Menefee and W.L.Peticolas. *Journal of Chemical Physics* **35**, 946 (1961).

96. W.L.Peticolas. *Journal of Chemical Physics* **39**, 3392 (1963).

97. S.Wu. *Polymer Engineering and Science* **25**, 122 (1985).

98. M.Doi and S.F.Edwards. *Journal of the Chemical Society (Faraday Transaction II)* **74**, 1789 (1978).

99. P.G.de Gennes. *Journal of Chemical Physics* **55**, 572 (1971).

100. W.H.Tuminello. *Polymer Engineering and Science* **26**, 1339 (1986).

101. W.J.McGrory and W.H.Tuminello. *Journal of Rheology* **34**, 867 (1990).

102. W.H.Tuminello, T.A.Treat, and A.D.English. *Macromolecules* **21**, 2606 (1988).

103. W.H.Tuminello. *Polymer Engineering and Science* **29**, 645 (1989).

104. W.H.Tuminello. *Encyclopedia of Fluid Mechanics*. Gulf, Houston. 1990.

105. J.des Cloizeaux. *Europhysics Letter* **5**, 437 (1988).

106. J.des Cloizeaux. *Macromolecules* **23**, 4678 (1990).

107. J.des Cloizeaux. *Macromolecules* **25**, 835 (1992).

108. H.Braun, A.Eckstein, K.Fuchs, and C.Friedrich. *Applied Rheology,* 116 (1996).

109. Programm, PolySoft. 1996. Gebruder HAAKE GmbH. Ref Type: Computer Program.

110. J.P.Thelman, W.Meyer, L.Wang, and B.Jones. In *3rd International Symposium "Alternative cellulose - Manufacturing forming, properties".* 1998.

111. ^{RSI}Orchestrator^{TM}. [V.6.4.4]. 1998. Rheometric Scientific. Ref Type: Computer Program.

112. C.Schrempf, G.Schild, and H.Ruf. *Heft* **12**, 748 (1995).

113. C.Michels. *Papier* **52**, 3 (1998).

114. J.Ferguson and Z.Kemblowski. *Applied Fluid Rheology.* Elsevier applied science, New York. 1991.

115. P.Patil. *Measurement of Elongational Rheology of Polymer Melts Using Semi-hyperbolic Convergent Dies.* 2002. Ref Type: Thesis/Dissertation.

116. R.S.Rivlin and K.N.Sawyers. *Annual, Review of Fluid Mechanics* **3**, 117 (1971).

117. B.J.Edwards. 2002. Ref Type: Personal Communication.

118. R.B.Bird, C.F.Curtiss, R.C.Armstrong, and O.Hassager. *Dynamics of Polymeric liquids Volume I Fluid Mechanics.* John Wiley & Sons, New York. 1987.

119. P.J.Carreau, D.C.R.De Kee, and R.P.Chhabra. *Rheology of Polymeric Systems Principles and Applications.* Hanser Publishers, New York. 1997.

120. J.R.Collier, S.Petrovan, and P.Patil. *Journal of Applied Polymer Science* **87**, 1387 (2003).

121. S.E.Bin Wadud and D.G.Baird. *Journal of Rheology* **44**, 1151 (2000).

122. J.F.Vega and A.Santamaria. *Macromolecules* **31**, 3639 (1998).

123. P.Wood-Adams and S.Costeux. *Macromolecules* **34**, 6281 (2001).

124. J.R.Collier, S.Petrovan, and P.Patil. *Journal of Applied Polymer Science* **87**, 1397 (2003).

125. C.Tsenoglou. *Polymer Prepr. (American Chemical Society, Division of Polymer Chemistry)* **28**, 185 (1987).

126. S.H.Wasserman and W.W.Graessley. *Journal of Rheology* **36**, 543 (1992).

VITA

Xiaoling Wei was born in Fujian, China in 1973. She joined the Department of Materials Science and Engineering at Tongji University, China in 1991. Five years later, she received a Bachelor of Engineering degree in Polymer Materials. In September 1996, she joined the Institute of Chemistry, the Chinese Academy of Sciences and earned a Master of Science degree in Polymer Chemistry and Physics in 1999. In August of that year, she joined the Department of Materials Science and Engineering at The University of Tennessee, Knoxville and received a non-thesis Master of Science degree in Polymer Engineering in August 2001. She will receive her Doctor of Philosophy degree in Polymer Engineering in August 2003.